EFFECT OF PARTICLE SURFACE MODIFICATIONS ON DRY POWDER FORMULATION PERFORMANCES

A thesis submitted for the degree of Doctor of Philosophy

Laurent Bruno Schueller

Department of Pharmaceutics
The School of Pharmacy
University of London
29-39 Brunswick Square
London WC1N 1AX, UK

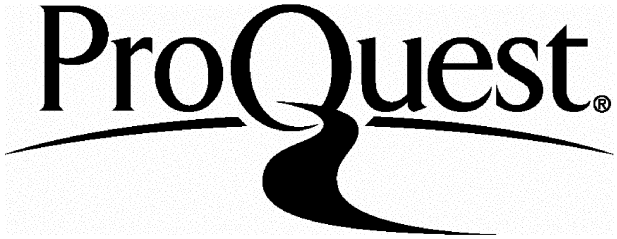

Abstract

Described in this dissertation are systematic studies designed to correlate the physico-chemical properties of dry powder inhalation formulations to the *in vitro* deposition patterns. Two model asthmatic drugs were selected for investigation: the hydrophilic β_2 adrenoreceptor agonist, salbutamol sulphate (SS) and the hydrophobic synthetic steroid, beclomethasone dipropionate (BDP).

To examine deposition differences between carrier particles from different sources, three different marketed grades of lactose were evaluated. *In vitro* assessment of the deposition using the Clickhaler®, as a device displayed significant differences depending on the carrier chosen. In particular BDP seemed to be positively influenced by the presence of fine lactose, whereas SS seemed to be more linked to the surface energetics of the coarse lactose.

The influence played by the fines was further evaluated by using crystalline lactose/polyethylene glycol 4000 (PEG 4000 g mol^{-1}) particles that were prepared by spray drying. Different parameters such as the chemical nature and the proportion of fines, the mixing sequence, and the drug to carrier ratio all influenced the deposition patterns of the drugs. Significant standardisation in the performances of BDP was achieved by modifying the surface of the coarse lactose.

Improvements in SS deposition were also achieved using a new type of carrier surface modification. Partially amorphous lactose/PEG 4000 fines were allowed to crystallise onto air-jet sieved lactose surfaces. Parameters such as particle morphology and surface energetics appeared to play a key role in the drug deposition. PEG 4000 [45-90] µm was also studied as a probe carrier using the Aerolizer®. This study also represented an opportunity to consider the device implication on the Twin Stage Impinger (TSI) deposition.

Finally, the possibility of modifying the surface properties of the drug substance was investigated by a spray drying process. It was found by inverse gas chromatography (IGC) that PEG modified the surface energy parameters of the drug. Different solutions and suspensions were studied in order to generate crystalline particles with suitable properties for pulmonary administration.

Acknowledgements

My first thanks are for my academic and industrial supervisors, Professor Graham Buckton, Dr Stephen Brocchini and Dr Dilraj Singh for their advice and support throughout this PhD.

I also would like to express my gratitude to Novartis Pharma for their financial sponsorship and their technical assistance, in supplying the Aerolizer® and Innovata Biomed for the Clickhaler®.

I should also acknowledge Dave Mc Carthy for imaging work, Keith Barnes for his endless technical help, Tony Silva for the long hours spent on deffective flow controllers, Rachel and Maria in the office and all my colleagues at the school.

Thanks are also due to Dr Catherine Tuleu, my "French colleague" for all the laugh in and outside SOP and to Juliette.

This thesis is dedicated to my parents whose emotional and financial support has allowed me to complete my studies. I am forever grateful.

Table of Contents

Chapter 1: Introduction

Chapter 2: Materials and Methods

Chapter 3: Influence of different grades of lactose on *in vitro* drug deposition

Chapter 4: Crystalline lactose/PEG 4000 co-spray-dried systems used as fines for DPI

Chapter 5: Partially amorphous lactose/PEG fines used as surface modifiers for DPI

Chapter 6: Surface modification of the drug substance

Chapter 7: Summary and conclusions

References

List of Figures

Chapter 1

Chapter 2

Chapter 3

Chapter 4

Chapter 5

Chapter 6

List of Tables

Chapter 1

Chapter 2

Chapter 3

Chapter 4

Chapter 5

Chapter 6

List of Abbreviations

A	Air-jet sieved
AFM	Atomic force microscopy
AN	Acceptor number
AN*	Acceptor number corrected
BDP	Beclomethasone dipropionate
BFMT	Bendroflumethiazide
BNF	British national Formulary
BUD	Budesonide
DN	Donor number
DPI	Dry powder inhaler
DSC	Differential scanning calorimetry
DVS	Dynamic vapour sorption
ECD	Effective cut-off diameter
ED	Emitted dose
FPF	Fine particle fraction
GSD	Geometric standard deviation
Hcl	Hydrochloric acid
IGC	Inverse gas chromatography
K_A	Acid contribution to the polar component of surface energy
K_D	Basic contribution to the polar component of surface energy
MMAD	Mass median aerodynamic diameter
MMD	Mass median diameter
N	Avogadro's number
PEG	Polyethylene glycol
PH	Pranlukast hydrate
PMDI	Pressurised metered dose inhaler
RH	Relative humidity
RD	Respirable dose
SEI	Surface energy interaction
SEM	Scanning electron microscopy
SS	Salbutamol sulphate
SSA	Specific surface area
T	Temperature

Tg	Glass transition temperature
Tr	Retention time
TSI	Twin stage impinger
UV	Ultraviolet
VMD	Volume mean diameter
V_N	Net retention volume
W_{adh}	Work of adhesion
W_{coh}	Work of cohesion
XRPD	X-ray powder diffraction
α	Alpha
β	Beta
Å	Ångstrom
γ_S^d	Dispersive component of surface energy of solid
γ_L^d	Dispersive component of surface energy of the liquid probes
µg	Microgram
µm	Micrometer
°C	Degrees Celius
®	Registered

Chapter 1

Introduction

1.1. Summary of chapter 1

For several decades, aerosol therapy has been accepted as a valuable tool in local treatment of pulmonary diseases. The emergence of new bioengineered proteins and peptides for new molecular targets led the pharmaceutical industry to consider the lungs as an alternative to more invasive routes such parenteral delivery. This chapter gives an introduction to the general principles of inhalation therapy and the major characteristics that should be considered for either local or systemic delivery of actives. Pulmonary delivery technology may be correlated to the devices employed to administer the aerosol, which is defined as biphasic system containing solid particles or liquid droplets suspended in air or another gaseous medium. After a brief description of the different inhalation delivery devices that are clinically available, emphasis is directed to dry powder inhalers (DPIs). Particle interactions affecting dry powder inhalation efficiency (i.e. capillary forces, electrostatic forces, solid bridge formation and van der Waals forces) are described in detail, with emphasis on the factors that influence these interactions.

1.2. Pulmonary delivery: advantages and applications

The administration of a medicine by inhalation has been clinically used for the treatment of many conditions in the lung, such as asthma, chronic obstructive bronchopneumopathy and cystic fibrosis (Clark, 1972; Neville *et al.*, 1977). To administer a medicine into the lungs the therapeutic agent must be aerosolised. An aerosol is typically defined as a two-phase system of solid particles or liquid droplets dispersed in air or another gaseous phase, having a sufficiently small size to display considerable stability as a suspension. The pulmonary route has several distinct advantages over other routes of administration. The direct delivery of medication to the tracheobronchial tree allows a rapid and predictable onset of action, which is particularly important for reliever therapy such as bronchodilators, and also avoids the first-pass effect (Zheng *et al.*, 1999). Furthermore, degradation within the gastrointestinal tract is avoided and lower dosages (Clarke and Newman, 1984) can be administered with similar efficacy. This means that fewer side effects will be induced which is particularly important for therapy with antibiotics and steroids.

In the past 20 years, DNA technologies have been refined, allowing "designer" biomaterials to be considered as candidates for new molecular targets. These promising developments do not come without new challenges: the use of traditional dosage routes such as oral or transdermal for these new entities (Agu *et al.*, 2001) is limited by the combination of their large molecular weight, hydrophilicity and lability both chemical and enzymatic. The only presently available route of administration is the injection route with its inherent compliance and cost issues. At present, the delivery of proteins and peptides such as insulin, calcitonin, α-interferon and genetic material in general is of particular interest (Smith, 1997; Courrier *et al.*, 2002).

1.3. Biophysical basis for pulmonary drug administration

The primary role of the pulmonary system is the oxygenation of the blood and the associated removal of carbon dioxide from the body. Breathing ventilates the respiratory tissue leading to gaseous exchange in the lungs. The two lungs of a human being are in slightly unequal proportions because of the asymmetric position of the heart (Figure 1.1). The right lung represents 56 percent of the total lung volume and is composed of three lobes separated by deep oblique fissures. On the other hand, the left lung has only two lobes separated by one oblique fissure.

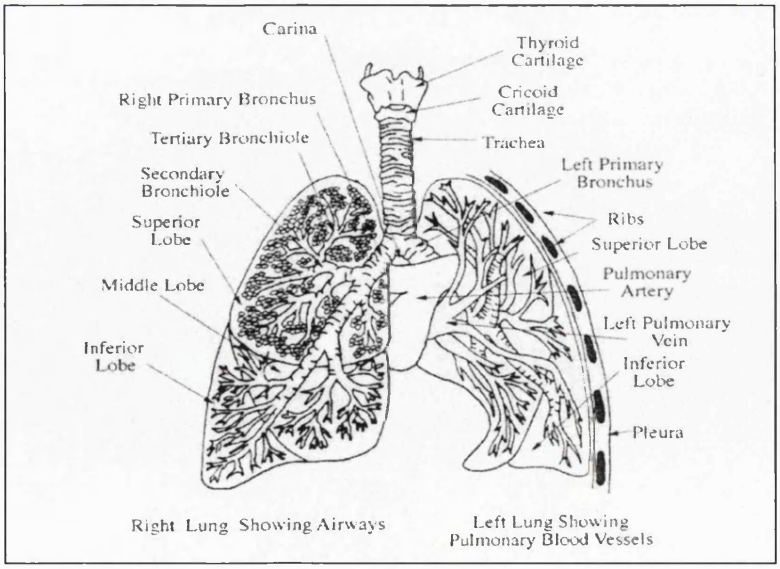

Figure 1.1. *Structure of the lungs (Washington et al., 2001).*

The respiratory tract is a strongly branched system designed to avoid penetration of particles into the lungs. It can be divided into two major domains: the conducting and the respiratory region. The conducting airways (comprising the basal cavity and associated sinuses, the nasopharynx, larynx, trachea, bronchi and the first 16 generations of airway bronchioles) are responsible for the filtration, humidification and warming of the inspired air. The respiratory region is composed of the bronchioles, alveolar ducts and alveolar sacs where rapid gas exchange with the venous blood occurs. The widely used morphologic model to describe the structures within the lungs given by Weibel (Weibel, 1963) is shown on Figure 1.2. In this tracheobronchial classification, the lungs are represented by a highly bifurcated system. Successive branching from the trachea (or generation 0) to the alveoli (or generation 23) reduces the diameters of the tubes but markedly increases the surface area of the airways (120-160m^2 in total); with a network of over 2000 km of capillaries. The conjunction of the large surface area, the thickness of the alveolar epithelium (approx. 0.1-0.5µm thick) and the extended capillary network makes the alveoli a target for systemic drug absorption.

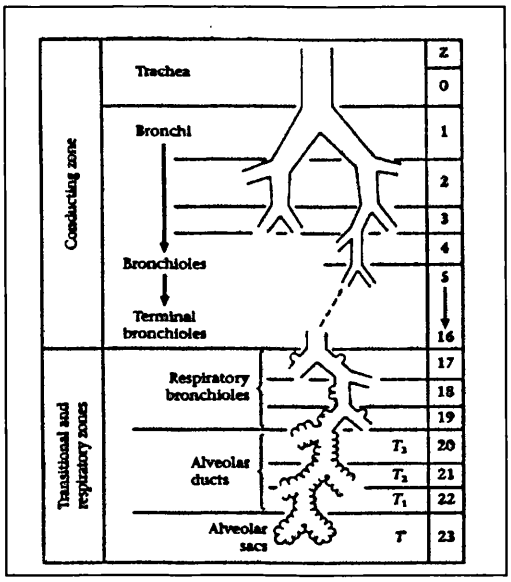

Figure 1.2. *Schematic of Weibel lung morphology model (Weibel 1963).*

At generation 17, the function of the tissue changes from conducting airways to gas exchange. The pulmonary parenchyma, consisting of approximately 130,000 lobules (each containing 2,200 alveoli), is the tissue responsible for the gas exchange. The alveoli are very small porous air sacs that use passive osmotic diffusion mechanisms. Once a drug aerosol deposits in the deep lung, the major barrier to entering the body is the 0.1 μm layer of type I alveolar cells that cover 95 % of the alveolar surface. These cells, also described as squamous epithelial cells, are covered by a thin layer of surfactant (produced by type II cells) whose role is to lower the surface tension at the air/alveolar interface. Lung surfactant consists of 90 % lipids (of which there are 70 % of saturated and non saturated phosphatidyl choline, 10 % of neutral lipids, 5 % of phosphatidyl glycerol, 3 % of phosphatidyl ethanol amines and 2% of other phospholipids), 8 % proteins and 2 % carbohydrates (Lopez-Vidriero, 1984). Alveolar cells have "tight junctions" acting as barriers to the absorption of macromolecules and as a way to prevent pulmonary oedema by keeping the oncotic pressure gradient constant. The type II pneumocytes differentiate into type I cells to maintain the type I cell population and to repair the alveolar surface after damage from a virus or chemical agent (Washington *et al.*, 2001). In addition to epithelial cells, the alveoli contain macrophages that phagocyte particles and migrate either in the ciliated airways where the particles are cleared by mucociliary clearance or into the interstitial space.

1.3.1. Aerosol deposition in the respiratory tract

1.3.1.1. Mechanism of deposition

An aerosolised medication is designed to be delivered through the airways within ventilated gas and then be deposited at sites in the lung through inertial impaction, gravitational sedimentation, and diffusion onto lung surfaces (Brain and Valberg, 1979) as shown in Figure 1.3.

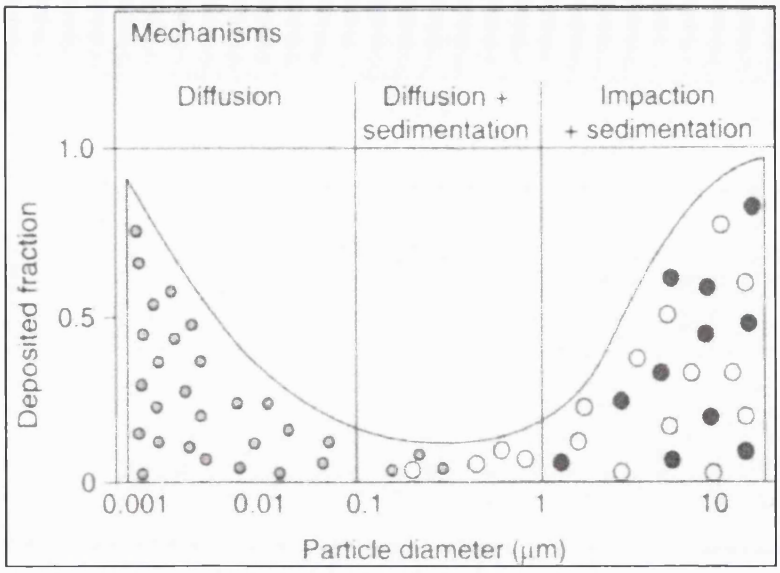

Figure 1.3. *Particle deposition mechanisms (Schulz, 1998).*

1.3.1.1.1. Inertial impaction

Impaction is the major mechanism of deposition in the upper airways: the probability of particle deposition is related to the mass and density of the individual particle. Deposition also depends on the velocity of the particle, which itself depends on the respiratory flow (Schlesinger, 1985). It is more likely to occur in the extrathoracic (i.e. naso-pharyngeal and oro-laryngeal) and large conducting airways in which flow velocities are high and airflow direction changes often. For a particle travelling in an airway, the probability of its deposition by impaction is a function of a dimensionless parameter involving the air velocity, known as Stokes' number (Stk), which may be calculated using the following equation:

$$Stk = \frac{\rho_\rho d^2 V}{8\eta R} \qquad \text{[Equation1.1]}$$

where ρ_ρ is the particle density, d the particle diameter, V the air velocity, η the air viscosity and R the airway radius.

The higher the value of Stokes' number, the more readily particles will deposit by impaction.

1.3.1.1.2. Sedimentation

Gravitational settling by sedimentation is the major deposition mechanism in the deeper airways where the airstream velocity is relatively low. The fraction of particles depositing by this mechanism is dependent upon their residence time. The distance at which a particle settles within a given time increases with its mass (i.e. with its density and with its diameter). For instance, a unit-density sphere of 1 μm diameter settles at a distance of 35 μm in 1s, whereas a unit-density sphere of 10 μm diameter settles at a distance of 3000 μm in the same time (Schulz, 1998).

The rate of sedimentation is governed by the particle density as expressed in the form of Stoke's law as Equation 1.2:

$$U_t = D^2 g \frac{\sigma\rho}{18\gamma} \qquad \text{[Equation 1.2]}$$

Where U_t is the terminal settling velocity, σ the particle density, ρ the density of air, g the gravitational constant, D the particle diameter and γ the viscosity of air.

1.3.1.1.3. Diffusion

For particles with a diameter less than 0.5μm, particle displacement is governed mainly by diffusional transport. The random displacement or Brownian motion that a particle will cover by diffusion increases with elapsed time and decreasing particle diameter. Hence the highest probability of particle deposition due to a diffusional displacement occurs for very small particles inhaled into the lung periphery with its small airways dimensions. It is thought that 80 % of particles with a Mass Median Aerodynamic Diameter equal or less than 0.5 μm are eliminated during exhalation (Courrier *et al.*, 2002).

1.3.1.2. Factors influencing the deposition

The amount of aerosolised medication that deposits via the above mentioned mechanisms in a given region of the lungs depends on the physical properties of the aerosol particles, the patient (i.e. ventilation factors) and the device used.

1.3.1.2.1. Physical properties of the aerosol

The variable most frequently used to describe the deposition of the aerosol in the respiratory tract is the aerodynamic diameter. The motion of dispersed particles in a gas stream depends on the size, shape and density of the aerosol particles. The aerodynamic diameter combining these three properties is given by Equation 1.3:

$$d_a = d\sqrt{\rho} \qquad \text{[Equation 1.3]}$$

Most aerosol devices available in respiratory medicine produce polydispersed aerosols, meaning that they contain particles that are of widely different sizes. Such an aerosol is frequently characterised by the Mass Median Diameter (MMD), the Geometric Standard Deviation (GSD) and the Mass Median Aerodynamic Diameter (MMAD).

- The MMD corresponds to the diameter of a particle such that 50 % of the mass lies below and 50 % above;

- The MMAD corresponds to the diameter of a sphere of unit density that has the same aerodynamic properties as a particle of median mass from the aerosol;

- The GSD in a log-normal distribution is defined as the square root size ratio of $d_{84\%}$ to the $d_{16\%}$ on the cumulative frequency curve; $d_{84\%}$ corresponding to the diameter for which 84 % of the particle mass lie below. A therapeutic aerosol typically exhibits a GSD of approximately 2. If the GSD is smaller than 1.2 then an aerosol is considered as monodispersed (Schulz, 1998).

Aerosol particles that can traverse the pharynx and upper airways are generally below 5 μm MMAD (Figure 1.4). Particles between 2 μm and 5 μm deposit in the central airways, and particles below 2 μm deposit at the peripheral airways. If there is a percentage of particles within the aerosol that is finer than 1 μm, a portion of these will be exhaled or will be trapped in the residual air and eventually deposit on the respiratory bronchioles and perhaps on alveolar surfaces. The fraction of the aerosol containing particles below 5 μm in diameter is termed the fine particle of respirable fraction (FPF). This parameter is widely used both to describe the characteristics of the aerosol and its potential for delivery to the lower respiratory tract and as a quality control parameter for inhalation product.

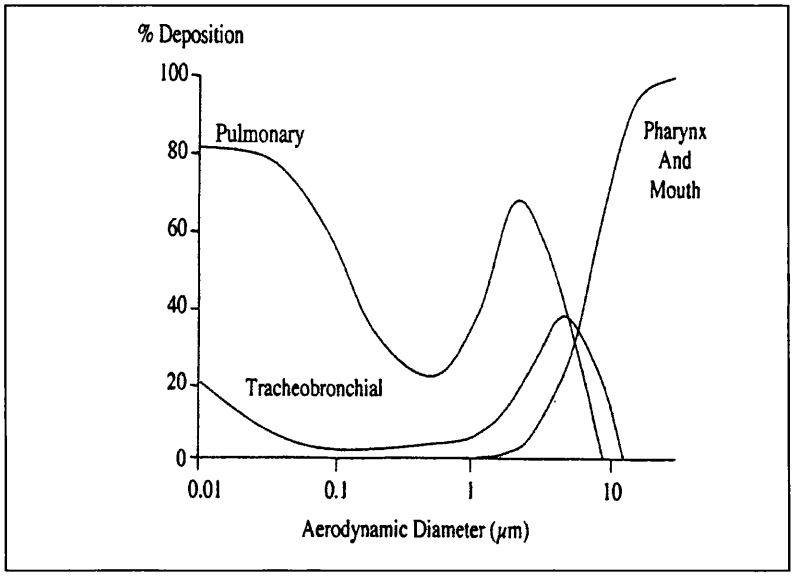

Figure 1.4. *Particle deposition mechanisms at an airway branching site (Washington et al., 2001).*

1.3.1.2.2. Ventilation factors

While particle size criteria must be met to ensure efficient lung delivery, other variables that influence deposition include ventilation factors. Particle velocity, inspired volume, inspiratory time, breath-holding duration and timing of aerosol delivery during inspiration all influence deposition. Particle velocity is determined by the aerosol generator and is influenced by the patient inspiratory flow of aerosol-laden air. Typical adult inspiratory flows during quiet tidal breathing are approximately 0.25-0.5 L/s.

Faster inspiratory flows increase oropharyngeal and upper airways deposition by inertial impaction, while slower inspiratory flows enhance more distal delivery and deposition through sedimentation and diffusion. Faster inspiratory flows (e.g. 0.5-2 L/s) may be necessary with some dry powder systems to disaggregate and disperse the dry powder. The size of the inspired volume influences deposition by affecting both the amount of aerosol that enters the lung and the depth of penetration of the aerosol into the lung. Breath-holding after inhalation enhances deposition by facilitating sedimentation and diffusion (Pavia *et al.*, 1977).

1.3.1.2.3. Device

Dry powder inhalation is a breath-actuated system requiring sufficient energy to be generated in order to effectively detach the adhesive therapeutical fine particles from their coarse carrier particles in the formulation (see point 1.4.1.3.) and disaggregate cohesive actives. If a patient inhales with a low flow, the efficacy of the separation process will therefore be reduced, the extent of which will be device and formulation dependent. One of the intrinsic characteristics of any DPI device is its resistance to airflow, which normally results in the flow through the DPI being restricted compared to that which is generated by the patient. Increasing resistance to airflow generally reduces the velocity of inhaled particles, reducing impaction and therefore increasing lung deposition. However, increasing the resistance of the device makes it more difficult for some patients to generate a sufficient airflow for an optimal aerosolisation. This is particularly true for children and geriatric patients who may be unable to generate high inhalation flows.

In pMDIs, a large proportion of the inhalable dose impacts and deposits in the oropharynx due to the velocity and the dispersion of the jet fired from the canister.

1.3.2. Absorption

The importance of lung clearance and absorption mechanisms relate to the action of the drug. For local therapy involving bronchodilators or anti-inflammatories, an extended residence time in the lung may be beneficial, whereas for systemic delivery (such as insulin for the treatment of diabetes) a rapid absorption is desirable. The alveolar epithelium and the capillary endothelium have a high permeability to water, gases and lipophilic substances. 90 % of the absorptive area of the lung is therefore attributed to the alveolar epithelium, which primarily consists of type I pneumocytes. Soluble macromolecules can be absorbed following two mechanisms: trancytosis (passage through the cells) or paracellular transport (between the cells). Two types of trancytosis are known: adsorptive or non specific (through the type I alveolar epithelial cells and capillary endothelial cells) and specific receptor mediated, for example in the case of albumin (Kim *et al.*, 2003). Three types of paracellular transport are known: bi and trijunctional transports, both occurring at the circumference of both endothelial and epithelial cells, and a transport through pores (Patton, 1996). The effects of the molecular weight, partition coefficient, pH and osmolarity on the kinetics of adsorption have been studied. Enna and Schanker (Enna and Schanker, 1972) showed that the adsorption of saccharides and urea was inversely proportional to the molecular weight. Effros and Mason (Effros and Mason, 1983), back in 1983 found a rough inverse relationship between the logarithm of the molecular weight and that of the clearance rate. It was also demonstrated that more lipophilic and non ionised drugs were absorbed better than their more hydrophilic and ionised counterparts (Schanker and Less, 1977).

1.3.3. Clearance

The clearance of inhaled particles deposited in the lower airways is accomplished by a self-cleaning mechanism known as the mucociliary escalator (in addition to coughing and alveolar clearance). The mucociliary clearance is a physiological function of the respiratory tract and is meant to remove dusts, excess of secretion and inhaled particles. It is one of the most important non-specific defence mechanisms of the airways.

The conducting airways, which in Weibel's model comprise airway generations 0 to 16 (trachea to terminal bronchioles), are lined with ciliated epithelium. The coordinated movement of the cilia propels the mucus lining (consisting of lower periciliary layer (sol) and upper mucus (gel)) and deposited foreign materials outwards towards the pharynx where they are swallowed (Wanner *et al.*, 1996) (Figure 1.5). Mucociliary transport in the conducting airways is thought to take approximately 24 hours from the lung periphery to the epiglottis.

For an optimal clearance the epithelial cells should be intact, the mucus rheology and the ciliary's activity normal. Limitations have been found for smokers (Foster *et al.*, 1985), patients with chronic bronchitis (Svartengren *et al.*, 1996) or with chronic asthma (Oberdorster, 1988).

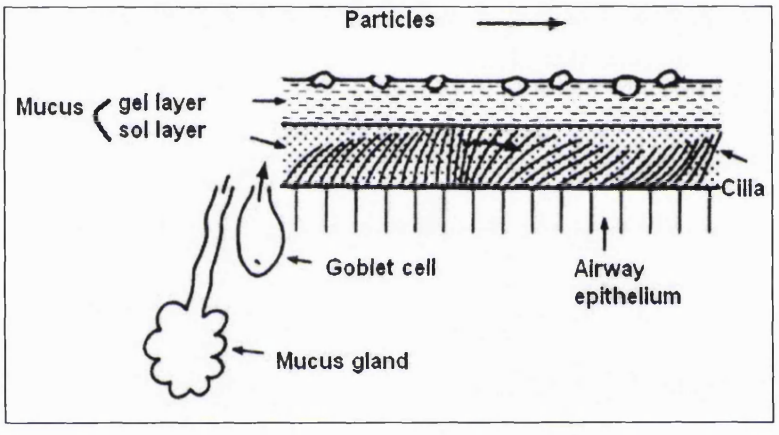

Figure 1.5. *Schematic representation of the mucociliary clearance.*

Particles deposited in the nonciliated region of the lung i.e. the terminal airways, will be subjected to alveolar clearance: the particles are phagocytosed by alveolar macrophages and subsequently transported to the ciliated bronchial airways (a non absorptive process) or into the alveolar interstitial space (an absorptive process). The absorptive process involves entering the alveolar wall. Once the particles leave the alveolar surface and penetrate below the epithelial barriers (type I and II cells), their removal occurs at a slower rate by both interstitial and intravascular macrophages. The rate of phagocytosis depends on the chemical composition, size and number of particles. Optimally the particle should be between 2 and 3 μm. The site of initial deposition of the drug particle is therefore an important parameter to consider in determining its resident time within the lung.

1.4. Aerosol therapy

1.4.1. Aerosol generators

Different devices generate therapeutic aerosols: nebulisers, pressurised metered-dose inhalers (pMDIs) and dry powder inhalers (DPIs). The available evidence supports the safety and efficacy of these devices at the recommended drug doses. Table1.1 summarises the advantages and disadvantages of these formats.

		Advantages	Disadvantages
Nebuliser	Jet	No patient coordination High dose possible NO CFC release Suitable for both solutions and suspensions	Expensive Not portable (bulky) Contamination possible Device preparation required before treatment
	Ultrasonic	+ Faster delivery than jet nebuliser	
MDIs	Conventional	Convenient Less expensive and more efficient than conventional nebulisers Portable Difficult to contaminate	Patient coordination and actuation required Cool feeling after actuation (Cold Freon effect) Large pharyngeal deposition CFC propellants
	With spacer	Less pharyngeal deposition Less patient coordination required	More expensive and less portable than conventional MDI
DPIs	Passive	Propellant free Less problem of drug stability Less contamination	Dependent on patient's inspiratory flow rate More expensive
	Active	Less dependent on patient breathing patterns	Not on the market

Table 1.1. *Advantages and disadvantages of the different inhaler devices, modified from Pierson (Pierson, 2000).*

1.4.1.1. Pressurised metered-dose Inhalers

Introduced in the mid-1950s pressurised metered-dose inhalers (pMDIs) are still the most commonly prescribed inhalation system for therapeutic aerosol delivery. A schematic representation of a pMDI is given in Figure 1.6. Eighty percent of the different inhaled medications (bronchodilators, anticholinergics, anti-inflammatory agents and steroids) are delivered in the US using this delivery system (International Pharmaceutical Aerosol Consortium, 1997). A pMDI contains the drug either as fine powder particles either dispersed or solubilized in propellants. Since propellants are poor solvents for most drugs and surface-active agents, co-solvents such as ethanol are required even if their low volatility may retard evaporation. The mixture contained in a pressurised canister is released upon actuation through a metering valve that is fitted into an actuator boot. After undergoing volume expansion in the passage within the valve, the droplets emerge into the air at high speed where the propellants evaporate, leaving free particles to be inhaled.

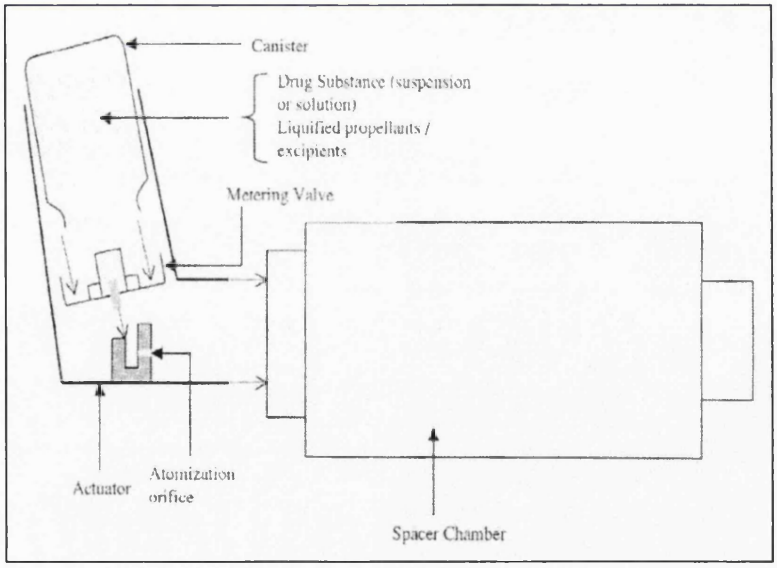

Figure 1.6. *Schematic representation of a pMDI (Smyth, 2003).*

Despite being the most commonly used device, there are inherent problems with this technique as shown in Table 1.1. Major drawbacks include large oropharyngeal deposition (Morén, 1981) and inefficient drug delivery stemming from lack of coordination between actuation and inspiration (Crompton, 1990). The introduction of large-volume spacers in the 1980s improved the efficiency by reducing both the importance of the inhalation/actuation coordination and the early deposition of large propellant droplets in the oropharyngeal areas, by allowing time for propellant evaporation and deceleration of the aerosol cloud. On the negative side, using a large-volume plastic spacer may be encumbering for the paediatric population.

Major challenges faced by pMDI technology are reformulation issues with the newly approved HFA propellants (McDonald and Martin, 2000) following the phase-out of the traditional chlorofluorocarbon (CFC) propellants as decided by the United Nations in 1987 (Montreal Protocol on substances that deplete the ozone layer). Even if specific exemptions for "essential uses" (metered dose inhalers (MDIs) used in the treatment of asthma and chronic obstructive pulmonary disease (COPD) were agreed for pharmaceutical aerosols, annual renewal is still required with decrease in allowances as alternatives become available (D'Souza, 1995). Much needed alternatives to CFCs may be found in the hydrofluoroalkanes (HFAs), especially tetrafluoroethane (HFA 134a) and heptafluoropropane (HFA 227), which do not contain chlorine and therefore have no ozone-depleting potential. Nevertheless, HFA and CFC propellants possess different physical and chemical properties leading to surfactant solubility problems in the new propellants (Byron *et al.*, 1994). The use of HFA propellants in pMDIs developed for CFC propellants may cause unwanted water uptake from valves (Williams and Tcherevatchenkoff, 1998).

1.4.1.2. Nebulisers

Although the first choice of aerosol generator for the delivery of bronchodilators and steroids is the pMDI (O'Donohue, 1996), this format has high innovative potential due to developments in liquid spray delivery systems. In nebulisers, the drug is solubilised or suspended in aqueous solutions and possibly with co-

solvents and surfactants. The active is inhaled during normal tidal breathing over several minutes through a mouthpiece or facemask.

Thus, nebulisers can be employed to deliver medications to populations such as children or elderly patients. Moreover, they are frequently used as an alternative to pMDIs or DPIs in patients who experience difficulties using these delivery devices.

There are two categories available depending on the energy type needed for the aerosol generation: the most commonly used jet nebuliser, relying on compressed air, and the ultrasonic nebuliser relying on a piezoelectric crystal (Figure 1.7). In a jet nebuliser, compressed air continuously enters the chamber through a narrow Venturi nozzle, creating an area of negative pressure at the outlet of the adjacent capillary feed system. This results in the fluid being drawn up into fine filaments according to the Bernoulli effect as shown in Equation 1.4.

$$P + \frac{\rho v^2}{2} + \rho g h = cons\tan t \qquad \text{[Equation 1.4]}$$

Where P is the pressure in the tube, ρ the gas or liquid density, v the gas or liquid velocity, g is the gravitational acceleration and h the height above some reference level.

These fine filaments collapse into droplets under the influence of surface tension. Small enough droplets are carried away by the inhaled airstream, whereas the large, non-respirable ones impact on the walls of the chamber and baffles. The impacted large droplets are hence returned for recycling to the bulk solution kept in the chamber. The droplet size is mainly governed by the rate of incoming gas flow. Clay *et al.* (Clay *et al.*, 1983) in a laser diffraction analysis of four jet nebulisers, showed a 50 % reduction in the MMAD when increasing the flow rate from 4 to 8 L/min. Droplets size was largely independent of the fill volume.

The ultrasonic nebulisers use a piezoelectric crystal vibrating at a frequency of 1-3 MHz to produce particles (Taylor and McCallion, 1997). The vibrations are transferred from the crystal to the surface of the solution, generating a "fountain"

from which large and small droplets are emitted. The droplet size is inversely proportional to the frequency and, as for the jet system, baffles remove large droplets by allowing them to fall again in solution. Most of energy is converted to heat as only a fraction is utilised in the formation of the aerosol droplets. This causes the temperature of the liquid within the nebuliser to increase, modifying the surface tension and viscosity of the liquid.

Despite the new developments including new designs, the use of nebulisers, traditionally a "hospital-focused therapy", to administer pharmaceutical agents has many important limitations such as a large amount of drug wastage (over 50 % with continuously operated ones (O'Callaghan and Barry, 1997), heterogeneous droplet population and dead volume (referring to the amount of solution trapped inside the device, usually in the range of 1 to 3 mL, that cannot be nebulised) (Dalby *et al.*, 1996).

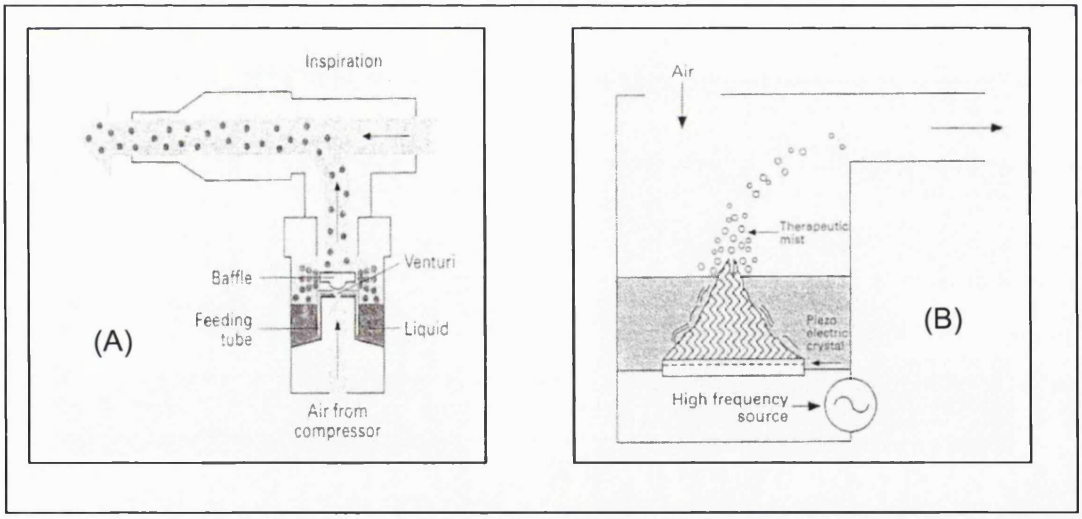

Figure 1.7. *Schematic representations of jet nebuliser (A) and ultrasonic nebuliser (B) (O'Callaghan and Barry, 1997).*

1.4.1.3. Dry Powder Inhalers

In the 1970s, the first single dose dry powder inhaler with a hard gelatine capsule technology (Fisons Spinhaler®) was initially developed for the inhalation of relatively large amounts of disodium cromoglycate, a low potency non-steroid used in the treatment of allergic asthma. Since then, this niche has been

extensively studied and the single-dose DPI technology expanded with the introduction of the Rotahaler® (GSK) for both salbutamol sulphate (SS) and beclomethasone dipropionate (BDP) and the Aerohaler® (Boehringer Ingelheim) for ipratropium bromide.

In 1987, the first multiple-dose DPI, the Turbuhaler® developed by Astra Zeneca was introduced on the market and quickly followed by the eight-blister Diskhaler® and later by its successor, the Acculaher® (GSK products). One of the strengths of the Turbuhaler system is it's ability to deliver drug particles in the absence of any excipients, except in the case of formoterol, a highly potent drug that is diluted using "microfine" lactose (Oxis® (formoterol) and Symbicort® (formoterol/budesonide). The loss of patent protection on some key drugs for the treatment of asthma (i.e. SS, terbutaline sulphate, BDP and budesonide (BUD) was concomitant with the emergence of generic DPIs (e.g. Clickhaler® and Easyhaler®). Most currently marketed DPIs rely on the patient's inspiratory effort to generate the aerosol. Difficulties can arise in producing sufficient a air flow, which has lead the industry to develop new "active devices" utilising an additional source of energy. The Spiros® DPI from Dura Pharmaceuticals, for example, applies electro-mechanical energy to disperse and aerosolise the formulation: battery-powered energy is converted into mechanical energy through a motor, which drives an impeller to create a high shear zone through which the powder must pass to exit the device. The patient's gentle inhalation through the mouthpiece triggers the impeller, which causes the drug powder to aerosolise.

1.4.2. Choice of the device

In general the pMDI is seen as the most convenient and cost effective way to deliver an aerosol (Clark, 1995). The very extensive spectrum of delivery formats particularly with the emergence of novel DPIs, may result in confusion for both the prescriber and the patient (Lenney *et al.*, 2000). In a study by Morice *et al.* (Morice *et al.*, 2002), it has been shown that patients may prefer the DPI to the conventional pMDI. The acceptability of the Clickhaler® (as a DPI model) and the Becotide® plus Volumatic® (as a pMDI device) for the delivery of BDP to adult and paediatric patients with asthma was studied: 67 % of the

patients found the DPI easier to use than the pMDI (22 %, $p<0.01$) and significantly more patients preferred the DPI (63 %) to the pMDI (28 %, $p<0.01$). An extensive review (Barry and O'Callaghan, 2003) compared the clinical efficiency of pMDI with or without spacers, DPIs and nebulisers. The available technology platforms should be chosen wisely, taking into consideration the characteristics of the different systems, the clinician and also the patient to ensure an optimal compliance and competence. For instance, young children and elderly patients may have difficulties coordinating pMDI actuation and inhalation, and devices requiring a high inspiratory flow rate may be not suitable for severe asthmatics. Table 1.2 summarises the device to be used for children with asthma.

Age (years)	First Choice	Second choice
0-3	pMDI + spacer + facemask	Nebuliser
3-5	pMDI + spacer	
5-12 (bronchodilators)	pMDI + spacer, or DPI	DPI
5-12 (steroids)	pMDI + spacer	
12+ (bronchodilators)	DPI or breath actuated pMDI	-
12+ (steroids)	pMDI + spacer	DPI or breath actuated pMDI
Acute asthma (all ages)	pMDI + spacer	Nebuliser

Table 1.2. *Choice of inhalation device for children with asthma, adapted from Barry et al. (Barry and O'Callaghan, 2003).*

1.5. Formulating dry powder inhalation systems

1.5.1. Production of micronised drugs

In dry powder inhalation, one of the first requirements is to use micronised drugs. There are classically three methods used to generate respirable particles: supercritical fluid precipitation, spray drying and milling.

Supercritical fluid precipitation (SCFP) is a relative newcomer in the production of micronised particles. One of the main methods used is termed Solution Enhanced Dispersion by Supercritical Fluids (SEDS). This one-step process involves the use of liquid carbon dioxide as a medium, which is being pumped at the required flow rate and being passed through a heat exchanger maintained at a constant temperature.
The drug is subsequently mixed and dispersed with the supercritical fluid in the nozzle before being precipitated in the particle formation vessel. This solvent free technology also enables the formation of uniform particles (with identical particle size, morphology and crystallinity). Velaga *et al.* (Velaga *et al.*, 2004) used this technique to produce particles of BUD and flunisolide with suitable characteristics for inhalation. In another study, Steckel *et al.* (Steckel *et al.*, 2004c) also showed the possibility of obtaining micronised BUD by precipitation in supercritical carbon dioxide. The authors also stressed the importance of the process conditions on the aerodynamic properties of the obtained particles.

Spray drying is a well established method for respirable particle production. This technique is fully described in chapter 3 and will therefore not be subjected to any further explanation here. Application of spray drying has been described in various reports, for instance disodium cromoglycate (Vidgren *et al.*, 1987; Chawla *et al.*, 1994; Steckel and Brandes, 2004); however, no spray-dried products are currently marketed for respiratory drug delivery.

Finally, air-jet milling (Figure 1.8) is the traditional method used to produce active particles in the micrometer region. High velocity compressed air is introduced as a high pressure jet through opposite nozzles at the bottom of the milling chamber. The high velocity creates zones of turbulence into which bulk crystals are fed. The mill contains no grinding parts so the particle fracture is due to the collision of one into another. The particles are retained in the mill and remain entrained in the airstream until sufficient particle size reduction is achieved (below 10µm). Upon completion of this step, the fine material is

removed by centrifugal flow into a collection vessel. Intense milling by fluid energy mill (also called air-jet mill) can induce particle changes such as variations in the surface area, crystallinity or polymorphic form, level of amorphous content and batch content uniformity. Those changes can lead to formulation problems in processing and redispersion, because of electrostatic (Byron *et al.*, 1999), van der Walls, capillary and mechanical forces that lead to increased energies of association.

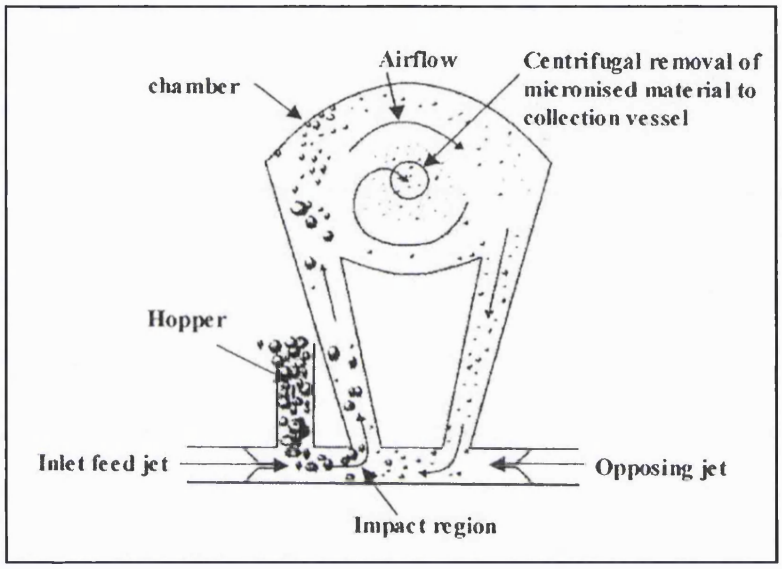

Figure 1.8. *Schematic of air-jet mill (adapted from Hickey, 2003).*

1.5.2. Examples of drugs administered via the pulmonary route

- Bronchodilators

Acute bronchospasm contributes to the characteristic wheezing of asthma. It is commonly treated by the utilisation of two different classes of drugs: β_2 agonist and anticholinergics. Mild to moderate symptoms of asthma respond rapidly to the inhalation of short acting β_2 agonists such as SS (Asmasal®, Ventodisks®) or terbutaline sulphate (Bricanyl®). These cause relaxation of bronchial smooth muscle through the activation of adenylate cyclase and thus allow the airway to dilate. Longer acting β_2 agonist such as salmeterol (Serevent®) or formoterol fumarate (Foradil®), useful in noctural asthma, should be intended for long-term prevention of asthma attacks and added to existing corticosteroid therapy. Muscarinic receptor antagonists block the action of acetylcholine released from

parasympathetic nerves and thus prevent bronchial muscles from being constricted. Anticholinergics do not therefore prevent all types of bronchospasm, but are effective against irritant-induced changes in respiratory function. Ipratropium bromide (Atrovent®) is used to provide short-term relief in chronic asthma.

- Corticosteroids

By reducing airway inflammation and subsequent excessive secretion of mucus, corticosteroids are very effective in asthma. They inhibit inflammatory cell infiltration into the airways. They are recommended for prophylactic treatment of asthma when a β_2 agonist is already administered more than once daily. BDP (Becodisks®, Asmabec®), BUD (symbicort®) and fluticasone propionate (Fixotide®) appear to be equally effective.

- Cromoglycate and related therapy

The asthmatic response triggered by an external allergen causes constriction of smooth muscle via the H1 receptors. This reaction can be prevented by using nedocromil sodium (Tilade®) and sodium cromoglycate (Spincaps®), which are the only non-steroid anti-inflammatory agents available for treating asthma.

- Mucolytics

Their role is to modify the rheological function of the mucus to aid in its clearance from the bronchi. It is particularly important in cystic fibrosis. A recombinant human deoxyribonuclease 1 is administered by inhalation using a jet nebuliser (Pulmozyme®).

1.5.3. Coarse carrier system

In most dry powder formulations, the micronised drug is blended with an inert excipient, usually α lactose monohydrate (in the size range of 70 to 120 μm) (Ganderton, 1992). The sugar is included in the formulation as a diluent and dispensing aid. The carrier's purpose is to convey surface-adhered drug particles into the air stream as controlled aggregates where they are stripped off as individual respirable particles. Lactose is a natural disaccharide of glucose

and galactose (as shown in its structural formula in Figure 1.9). It is obtained from the whey of cow's milk; whey being the residual liquid of the milk following cheese and casein production (Kibbe, 2000). It exists naturally as two optical isomeric forms, α and β, depending on the orientation of the hydroxyl group in position 1'.

It can also exist in a free aldehyde form qualifying lactose as a reducing sugar. This aldehyde form (open form) is observable during the interconversion of α and β lactose. For example, β-lactose mutarotates to α-lactose under the influence of water vapour.

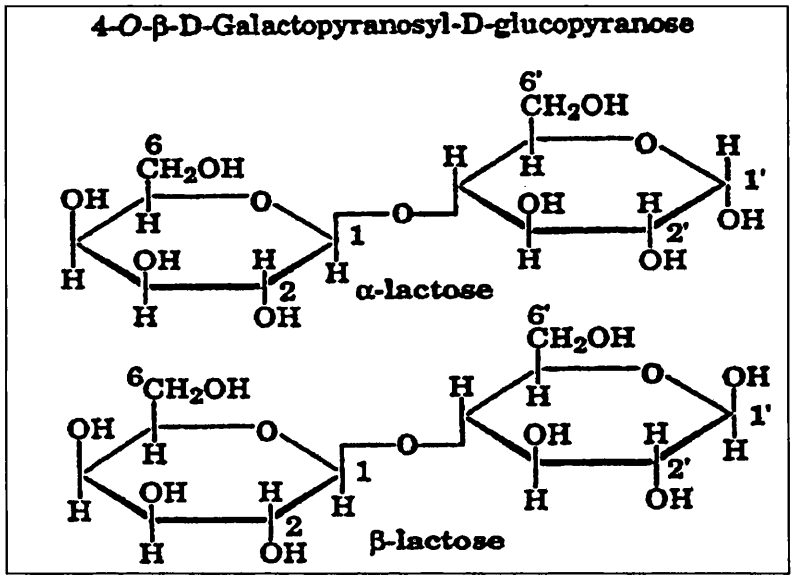

Figure 1.9. *Molecular structure of α and β lactose (Byron et al., 1996).*

The most commonly used form of lactose in industry is crystalline α-lactose monohydrate ($C_{12}H_{22}0_{11}.H_20$), which is prepared by crystallisation from a supersaturated solution below 93.5°C (Olano *et al.*, 1983), whereby each unstable α anhydrous molecule absorbs a molecule of water. Alpha lactose monohydrate is a white to off-white crystalline powder, practically insoluble in ethanol at room temperature and soluble 1 to 4 in water at 25°C. Various grades of lactose are commercially available which have different physical properties such as particle size distribution and flow characteristic (Kibbe, 2000). Adverse reactions to lactose are largely attributed to lactose intolerance, which occurs when intestinal enzyme lactase is deficient. The resulting indigestion of large quantities of lactose (over 12 g) may cause abdominal

cramps, flatulence or diarrhoea (Savaiano and Levitt, 1987). This is due to the increase in water and sodium following an osmotic effect in the lumen. At pharmaceutical dosage level, lactase deficient patients should feel no discomfort.

The advantages of lactose monohydrate reside in its large availability, low price, toxicity profile, smooth crystal surface and good flowability. Nevertheless, despite being overwhelmingly used as a carrier material, this disaccharide is not the ideal and universal carrier for all active materials. For example, its reducing sugar function may interact with peptide or protein functional groups. In addition, the possible presence of endotoxin (referring to the lipopolysaccharide complex associated with the outer membrane of Gram-negative bacteria) and additives of bovine source drove scientists to look for alternative carriers. Tee *et al.* (Tee *et al.*, 2000) investigated the dispersion and deaggregation of SS from mannitol and sorbitol carriers using a Rotahaler® coupled to a twin stage impinger (TSI). The authors showed that in binary systems, i.e. those without added fine sugars, formulations using mannitol as the carrier exhibited a higher fine particle dose (40.9 ± 4.4 µg) and higher fine particle fraction (9.0 ± 0.9 %) than those from a lactose based carrier (29.7 ± 4.3µg and 6.4 ± 1.0 % respectively). Using sorbitol as the carrier resulted in similar deposition pattern with a fine particle dose of 30.5 ± 3.0 µg and a fine particle fraction of 6.5 ± 0.6 %. It was concluded that both sugars might be employed as alternatives to lactose. In another study Steckel *et al.* (Steckel and Bolzen, 2004) confirmed the promising potential of mannitol as a drug carrier for DPI formulation. Other tested sugars including sorbitol, maltitol and xylitol were barred due to their sensitivity to humidity, which is likely to increase the drug-to-carrier adhesion and therefore show poor dispersibility.

1.6. Particle interactions in dry powder inhalation systems

The adhesion between two micronised particles or a micronised particle and a solid surface is complex to describe. Particulate interactions may result from a combination of physical forces including electrostatic or Coulombic forces, capillary forces, solid bridge formation, and van der Waals forces.

1.6.1. Electrostatic forces

In the gas phase, electrostatic forces can arise either from particle-charge interaction, image-charge effect, or electrostatic contact potential difference (Masuda and Gotoh, 1997).

- Particle-charge interaction

Particle-charge or Coulombic forces between two charged particles can be expressed mathematically by Coulomb's law:

$$F_{ec} = \frac{1}{4\pi\varepsilon_0}\frac{Q_1 Q_2}{R^2} \qquad \text{[Equation 1.5]}$$

Where Q_1 and Q_2 are the charges on the two particles, R the interparticle separation, and ε_0 the permittivity (or dielectric constant) of vacuum.

- Image-charge effect

When a negatively or positively charged spherical particle comes in contact with an uncharged surface, such as the walls of the container, an image charge results on the plane surface with the same magnitude but opposite sign as the particle charge. The resulting image force of attraction is given by the equation:

$$F_{ei} = \frac{1}{4\pi\varepsilon_0}\left[1 - \frac{H}{\sqrt{R^2 + H^2}}\right]\frac{Q^2}{(2H)^2} \qquad \text{[Equation 1.6]}$$

Where Q is the particle charge, R the particle radius, H the separation distance and ε_0 the permittivity of vacuum.

- Electrostatic contact potential difference

The contact between two uncharged, different solids results in an electrostatic contact potential difference being established. Electrons from the material with the lower work function are transferred to the material with the higher one.

The work function of a material can be defined as the difference in energy between the energy of an electron occupying the highest energy level (the Fermi level) and the energy of an electron at the vacuum level (point in space where the electron can no longer feel the potential of the surface). Thus it corresponds to the minimum energy required to remove the weakest bound electrons from a material. The two work functions will eventually be similar and equilibrium established (Stewart, 1986). This electrostatic force of attraction can be calculated using the following equation (Visser, 1989).

$$F_{ew} = \pi\varepsilon_0 \frac{R(\Delta U)^2}{H} \qquad \text{[Equation 1.7]}$$

Where R is the particle radius, H the separation distance, ΔU the potential difference arising from the difference in work functions, and ε_0 the permittivity of vacuum.

If one or both of the materials are poor conductors, static charges can accumulate on the surfaces for long periods of time (i.e. insulators prevent redistribution of electrical charge). As electrostatic forces dependent upon the physical and chemical states of each material, contact between varying materials will result in the generation of different electrostatic charges.

1.6.2. Capillary forces

Water is easily adsorbed to a wide range of surfaces. Adsorption of water molecules on dry powders results in the condensation of water vapour in the interstices between adjacent particles. If enough condensation occurs, the surface tension of the liquid may result in the formation of a liquid bridge or liquid annulus between adjoining particles. Capillary condensation normally occurs at high relative humidities, usually in excess of 60 % (Hiestand, 1966). The magnitude of the capillary forces will depend on the surface tension of the liquid, the particle size and the wettability of the particles. When a liquid bridge forms between two particles the magnitude of the van der Waals force is much less than what it would be for two particles separated by air. As a result, at high relative humidity, the overall force responsible for particle adhesion is

predominantly due to the capillary force and not the van der Waals force (Rabinovich *et al.*, 2002).

1.6.3. Solid bridge formation

Solid bridge interactions can occur between particles in a stationary particulate system in different ways. These includes mineral bridges between particles of the same material, direct chemical interactions between particles, partial melting of low melting point solids caused by friction, and shrinkage of the liquid film separating powder particles followed by crystallisation of the liquid bridge (Farber *et al.*, 2003).

1.6.4. Van der Waals forces

The principal attractive forces between neutral molecules, at a separation distance of the order of the molecule size, are named after the dutch physicist Van der Waals, who was the first to point out that deviations from the ideal gas law (PV=nRT) at high pressures were due to the gas molecules attracting each other, according to the following equation:

$$\left(P+\frac{an^2}{V^2}\right)(V-bn)=nRT \qquad \text{[Equation 1.8]}$$

Where P is the pressure, V the volume, n the number of molecules, R the gas constant, T the absolute temperature, a a constant whose value depends on the gas considered, and b the volume per mole occupied by the molecules.

Van der Waals forces are electromagnetic in nature, arising from the various interactions of the nuclei and electrons of one molecule or particle with the nuclei and electrons of another body. These low energy interactions, comprising the dispersion (London), orientation (Keesom) and the induction (Debye) interactions, are of greatest relevance to interfacial phenomena (Buckton, 1995). Higher energy short-range interactions, i.e. chemical bonding, are not important for the adhesion of aerosol particles, because water or other organic

molecules are usually adsorbed to the particles, thereby creating a physical shield or barrier to chemical bond formation.

- Keesom interaction (dipole-dipole interaction)

This type of van der Waals interaction occurs between polar molecules. These molecules possess a permanent dipole moment, because the centre of charge of the electrons does not correspond to the centre of charge of the nuclei. These interactions are due to the attraction between the negative and positive poles of nearby molecules combined with the repulsion between like-charged poles. Dipole-dipole interactions make, at most, a small contribution to surface and interfacial tension. One particular type of Keesom interaction is hydrogen bonding. This type of specific short-range interaction occurs between a hydrogen atom on one molecule and a more electronegative atom (usually oxygen, nitrogen, sulphur, or, less predominantly, a halogen atom) on a neighbouring molecule. The hydrogen atom acts as a proton donor (electron acceptor site), while the other atom has a lone pair and acts as a proton acceptor site (electron donor) (Zeegers-Huyskens and Huyskens, 1991).

- Debye interaction (dipole-induced dipole interaction)

This attractive interaction occurs when the permanent dipole (i.e. permanent electric field) on a molecule A induces a dipole moment on a neutral polarisable molecule B.

- London interaction (dispersion forces)

London interactions are the only van der Waals forces for molecules that have no permanent dipole or higher order moments. These are universally attractive and occur between all molecules. Of quantum mechanical origins, London interactions originate from correlation between instantaneous fluctuations in the charge distributions ρ^A and ρ^B of molecules A and B (due to rapid movement of their electrons).

Quantitatively, the van der Waals force can be determined by two theories, either the London-van der Waals or the Liftshitz-van der Waals theory (Fan and Zhu, 1998). The former is a microscopic theory, which takes as a starting point the interaction between two symmetrical molecules. The latter is a macroscopic theory that is better suited to the description of the interaction between two macrobodies (i.e. two particles), making this approach more appropriate in the case of dry powder formulations. In the London-van der Waals theory the approximated potential energy between two molecules is calculated using the following equation:

$$E = -\frac{\lambda_{12}}{r^6} \qquad \text{[Equation 1.9]}$$

Where λ_{12} is a constant that depends on the characteristics of the molecules and r is the separation between the centres of the molecules.

Based on the concept of additivity, Hamaker postulated that the van der Waals interaction between two solids could be taken as the integration of all the interactions between all pairs of molecules making up the solids. The resulting equation for the interaction of a spherical particle and a plane surface is:

$$F = \frac{A_{12} a_1}{6r^2} \qquad \text{[Equation 1.10]}$$

Where a_1 is the radius of the particle, r the separation distance, and A_{12} the Hamaker constant given by:

$$A_{12} = \pi^2 q_1 q_2 \lambda_{12} \qquad \text{[Equation 1.11]}$$

Where q_1 and q_2 are the atom/molecule density of the materials.
However, for closely packed atoms or molecules in a condensed body, the pairwise additivity approximation does not hold. The macroscopic Liftshitz-van der Waals approach solves this problem by modifying the expression of the Hamaker constant (Visser, 1989).

Instead of depending on the characteristics of the individual molecules, it depends on the bulk properties of the materials themselves:

$$A = \frac{3}{4\pi} h\varpi \qquad \text{[Equation 1.12]}$$

Where $h\omega$ is the Lifshitz constant, depending only on the material. For the interaction of two materials 1 and 2 separated by a medium 3, this constant is:

$$h\varpi_{123} = h\int_0^\infty \left(\frac{\varepsilon_1 - \varepsilon_3}{\varepsilon_1 + \varepsilon_3}\right)\left(\frac{\varepsilon_2 - \varepsilon_3}{\varepsilon_2 + \varepsilon_3}\right) d\zeta \qquad \text{[Equation 1.13]}$$

Where h is Planck's constant and ε_i the dielectric constant of material i along the imaginary frequency axis ζ.

1.7. Factors influencing particulate interactions

The performance of carrier-based and agglomerated dry powder aerosol formulations is predominantly influenced by drug and carrier properties such as size, shape, surface morphology, chemical composition, hygroscopicity, surface energy.

1.7.1. Particle size and the use of ternary components

It is easily understandable that van der Waals forces increase with particle size. Therefore it appears logical to decrease the particle size in order to decrease the particulate interaction. Staniforth *et al.* (Staniforth *et al.*, 1982) confirmed this theory by studying two size fractions, 250-500 and 500-710 µm of recrystallised lactose. Interparticle adhesion forces, measured using the ultracentrifuge method, were much higher in ordered mixes based on the larger carrier particles (10.6 10^{-3} N vs. 2.3 10^{-3} N). Indeed, increased drug deposition is generally observed with smaller carrier size (Steckel and Müller, 1997) and increased proportion of fine particles (Lucas *et al.*, 1998b; Zeng *et al.*, 1999; Zeng *et al.*, 2000b), as these factors may limit the adhesive forces occurring between the drug and carrier particles or the internal cohesive drug-drug

interactions. One of the possible explanations was given by Staniforth (Staniforth, 1996b) and was based on the theory of active and passive adhesion sites on particle surfaces (first proposed by Hersey (Hersey, 1975)). In this theory, there is a variable pattern of particle-particle adhesion forces at different surfaces sites. The fines would occupy the high-energy "active" adhesion sites before the carrier powder is exposed to the drug particle fraction. This leaves only the lowest energy sites available for the adhesion of drug particles (Figure 1.10). These are expected to be liberated from the carrier surface more completely upon application of a removal force.

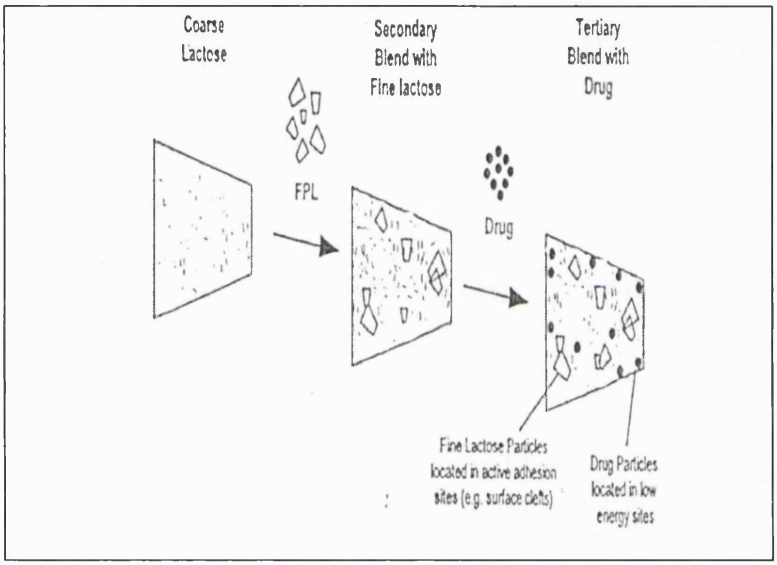

Figure 1.10. *Possible model for the action of fine particle lactose (FPL) (Lucas et al., 1998b).*

Another explanation might be that the lactose is intercalating between the drug particles, hence reducing the stability of the agglomerates. In the case of nedocromil sodium, which spontaneously exhibits agglomeration tendency, due to their high surface energy, high-shear mixing techniques physically disrupt drug-drug contact and promote deaggregation (Clarke *et al.*, 2001).

1.7.2. Particle shape-surface texture

Elongated carriers increase aerosol dispersibility and drug FPF, possibly because of the increased duration in the air stream drag forces. Manipulation of the shape and texture of the carrier can also improve the efficiency. Zeng *et al.* (Zeng *et al.*, 2000a) studied the influence of different morphological features (including shape and smoothness) with similar particle size on drug delivery. One of their conclusions was that increasing the surface smoothness of lactose crystals led to increased respirable fraction of SS. Clefs or pits on the surface of carrier particles provide areas within which drug particles are "hidden" from aerosolisation shear forces, whereas particles adhered to "flat" areas are more exposed. Higher rugosity of carrier and a more irregular drug particle shape can also reduce the flow and ease of dispersion by increasing the area of interparticle contact (Larhrib *et al.*, 1999).

1.7.3. Surface energy

Solid surfaces possess a net imbalance of surface forces and consequently have a surface energy. The surface energy is not evenly distributed over the solid surface: plane surfaces have lower surface energy than surface asperities for example. Surface free energy (γ_S^{TOT}) essentially refers to the attraction force between the surface solid molecules, which hold the molecular lattice together. It is usually described as the additive contribution from polar and non-polar forces as described in point 2.3.6. The minimum work necessary to separate two surfaces (and therefore the energy bonding them together) is equal to the difference in free energy before and after separation. The work of adhesion, W_a, between two different materials A and B is given by:

$$W_a = \gamma^A + \gamma^B - \gamma^{AB} \qquad \text{[Equation 1.14]}$$

Where γ^A and γ^B are the dispersive components of the two solids and γ^{AB} is the free energy of the interface.

Thus, for a single material C, the work of cohesion, W_c, is given by:

$$W_C = 2\gamma^C \qquad \text{[Equation 1.15]}$$

Where γ^c is the dispersive component of the solid.

It is now clear that both adhesion and cohesion of solids are related to the surface energies of the interacting objects. Since drug particle detachment from the carrier is only possible if the drag force overcomes the adhesion forces and the weight of the particles, the predominant role of surface energy is obvious. The most common ways of determining surface energy have been reviewed by Buckton (Buckton, 1997) and comprise contact angle techniques, isothermal microcalorimetry, gravimetric sorption and inverse gas chromatography. Contact angle techniques have been the traditional method of surface energy assessment, even if some difficulties persist. For example it has been shown that the solid surface free energy is dependent on the liquids used for its calculation. A difference in liquid contact of 1° modifies the solid surface energy value, the variation being dependent on the choice of the combination of liquids (Planinsek *et al.*, 2001). The method used in this study is inverse gas chromatography (IGC), which is described in detail in chapter 2. This technique provides important information about the surface chemistry of the substrate. This technique has been used to detect batch to batch variability both in term of excipients (α lactose monohydrate) (Ticehurst *et al.*, 1996) and active (SS) (Ticehurst *et al.*, 1994). It has also been used to assess differences in surface energy due to milling (Feeley *et al.*, 1998; Newell *et al.*, 2001a; Ohta and Buckton, 2004) and different relative humidities (Newell *et al.*, 2001b; Ohta and Buckton, 2004). Furthermore, differences of surface free energy for two isomers have been studied (Grimsey *et al.*, 1999). In 2002, a paper published by Cline and Dalby (Cline and Dalby, 2002) correlated the surface energy of active and carrier components (converted from mJ/m^2 to mJ/g by dividing by the surface area) to *in vitro* performance of a dry powder inhaler.

1.7.4. Relative humidity

Relative humidity has an impact on interparticulate forces. This can occur by two different mechanisms, causing an increase due to capillary forces at high humidities or a decrease due to an increase in the conductivity of both the particle and the surrounding atmosphere. Braun *et al.* (Braun *et al.*, 1996) studied the influence of storage humidity on the aerosol deposition of disodium cromoglycate (DSCG). Deposition (measured as fine particle fraction of DSCG from formulations containing either lactose or dextrose as carriers) was studied at 55 % RH and 33 % RH. After storage at 55 % RH only 47.2% of the DSCG that was delivered by the same mixture stored at 33 % RH was determined in the stage 2 of the TSI. In a humid environment, capillary condensation generates capillary forces that increase the total adhesion forces. Finot *et al.* (Finot *et al.*, 1996) determined that above 50 % RH the capillary forces dominate. In a study using the atomic force microscopy (AFM) (Berard *et al.*, 2002), adhesion between micronised zanamivir crystals and lactose monohydrate was measured at different RH. The authors concluded that from 0 to 32 % RH and from 32 to 85 % RH, the adhesion values were multiplied by two at each step. In another study, Young *et al.* (Young *et al.*, 2003) studied the effect of humidity (ranging from 15 to 75 %) on separation energies for SS using AFM. They claimed that the increase in particle cohesion at higher humidities (due to capillarity forces) led to an increase in energy required for deagglomeration. This may well result in a decrease in the aerosol efficiency. The effect of humidity should also be taken into account in the selection of a suitable salt for a drug. In two studies, Jashnani *et al.* (Jashnani *et al.*, 1995; Jashnani and Byron, 1996) investigated the dry powder aerosol performance of salbutamol and different related salts. In the first study, they showed that FPF of both salbutamol and salbutamol sulphate, at any temperature, decreased with increasing RH (FPF dropping from 59.4 % at 43 % RH to 35.8 % at 85 % RH for the salbutamol sulphate). In the second study, FPF for all compounds studied was humidity dependent at 45°C although the sulphate and the free base showed more drastic changes as RH increased compared to the other salts. Uncontrolled high humidities have been shown to decrease the FPF of BDP from a lactose based formulation (Geuns *et al.*, 1997). Harjunen *et al.* (Harjunen *et al.*, 2003) investigated how both the drug to carrier ratio and the storage

condition (40°C / 75 % RH) were affecting the deposition of both SS and BUD using different sugars as carriers: α lactose monohydrate, mannitol and glucose anhydrate. Irrespective of the chemical nature or the concentration of the carrier, the respirable fraction of SS decreased after storage. On the other hand, the effect of storage on the respirable fraction of BUD was dependent on the carrier and drug to carrier ratio. It has to be mentioned that ambient humidity can be particularly important as hygroscopic particles will increase in size as they flow through a high air stream (approximately 99 % relative humidity) due to condensation of water onto the particle surface (Ferron, 1977). Hygroscopic growth is therefore likely to increase the deposition in the upper airways.

1.7.5. Electrical properties - triboelectrification

During powder handling processes such as grinding, sieving, pneumatic conveying or mixing, electric charges arise from interparticulate friction and collision as well as collisions between the particles and the contact surface. The resulting effect is a net charge on the particle, which is either electronegative or electropositive. Charge accumulation is influenced by many factors including particle shape and size, nature and work function of the contacting surface, surface purity as well as atmospheric conditions (Bailey, 1984). Eilbeck *et al.* (Eilbeck *et al.*, 1992) charged a range of α lactose monohydrate particles (ranging from 125 to 1000 μm) against rough steel insert, and showed that the specific charge values increased in negativity with a decrease in particle size. Carter *et al.* (Carter *et al.*, 1992) investigated the triboelectrification process of α lactose monohydrate, SS and BDP. Different lactose size fractions were tested and their specific charge values (ratio of total charge to mass) were measured. This work showed that decreasing the particle size of the excipient led to an increase in the specific charge value due to an increase in particle number density of the smaller size fraction (resulting in a bigger surface area for charge transfer). Electrostatic interactions play a significant and important role in dry powder inhalation since they not only influence the stability of ordered mixes of drug and carrier particles but also the passage through the inhalation device and the particle separation upon actuation. In another study, Carter *et al.* (Carter *et al.*, 1998) studied the charge accumulation and decay on compacts of lactose, SS and polyvinyl chloride (used as a device material) using a Faraday

well method and a capacitive probe method. Using a corona electrode, SS retained a significant charge after 120 min. One possible way of modifying the charges within a binary system is by adding fine particles consisting of lactose (Bennet *et al.*, 1999), magnesium stearate (Staniforth, 1996a) or L-leucine (Staniforth, 2000). All additions resulted in a change in the attraction and detachment of the drug particles.

1.8. Aims of the thesis

In this study some factors influencing dry powder inhalation have been examined. Both the formulation and the device employed were investigated. Two model drugs: SS and BDP were chosen to represent a hydrophilic and hydrophobic active substance respectively. Two types of inhalers were also used: a metered reservoir device (Clickhaler®) and a capsule pre-metered inhaler device (Aerolizer®). The principal objective of this work was to rationalise the approach for dry powder inhalation systems and limit as much as possible the aerosol deposition variations induced by the different parameters.

Chapter 2

Materials and methods

2.1. Materials

2.1.1. Source of materials used

Lactose monohydrate from the following three sources were evaluated as carriers for DPIs in chapter 3: (1) Pharmatose 325M (B.N. 10007701) from DMV International (The Netherlands), (2) Aero Flo 65 (B.N. 8500122121) from Foremost Farms (USA), and (3) Lactohale LH 100 (B.N. 314039/S) from Borculo Domo Ingredients (The Netherlands).

In addition, crystalline α-lactose monohydrate (B.N. 23416) obtained from Borculo Whey Products (UK) was used as a reference material for the solution calorimetry study described in chapter 3. It was also used for the different spray drying experiments to produce either 100 % amorphous material or different lactose/PEG 4000 systems. PEG 4000 (B.N. 565220442049) was purchased from Prolabo (France). Microfine Pharma 201 (B.N. E949423) from Borculo Domo Ingredients (The Netherlands) was used for inverse gas chromatography analysis described in chapter 4. A mixture of 80 % β-lactose and 20 % α-lactose (B.N. A010045201) was obtained from Acros Organics (Belgium). This mixture was to be used as a reference material for the X-ray diffraction analysis in chapter 3.

Methanol used for the BDP analysis was HPLC grade and purchased from Fisher Scientific, UK. Analytical grades of ethanol (96 %) and hydrochloric acid solution (5 M) were provided by BDH and VWR respectively. Deionised water was obtained from a DV 25 water purification system (Elga Ltd, UK).

Materials used for inverse gas chromatography were all HPLC grade or 99 %+.

2.1.2. Drug models

2.1.2.1. Beclomethasone dipropionate

Beclomethasone dipropionate (BDP) was chosen as a representative hydrophobic drug model. This drug is a synthetic steroid used for the prophylaxis of asthma (British National Formulary, 2004). It reduces broncho-constriction by decreasing the airway hyper-response and mucus secretion. The high topical anti-inflammatory activity of BDP with a lower systemic activity, due to metabolic inactivation of the swallowed portion of the dose, appears to be the principal reason why beclomethasone controls asthma at doses that do not cause important glucocorticoid effects. Once inhaled, BDP is transformed in the lung to the monopropionate form through enzymatic hydrolysis. Due to its chemical structure (Figure 2.1), its solubility in acetone is high but sparing in alcohol. Three different forms of BDP are known: the anhydrate, the monohydrate and the organic solvate (Parmar, 1997). The crystal form of BDP used throughout was the anhydrous form used micronised (with a volume mean diameter of 1.7 μm) and supplied as a gift from Sicor (Italy, B.N. 6661/M1).

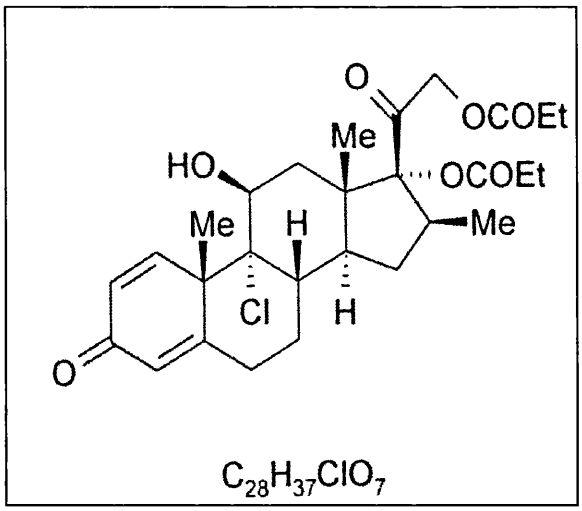

Figure 2.1. *Chemical structure of BDP.*

2.1.2.2. Salbutamol sulphate

Salbutamol sulphate (SS), also known as albuterol sulphate, was chosen as the hydrophilic drug model. This drug is a short acting β_2 adrenoceptor agonist, which is probably the most common medication group used in respiratory practice. It is generally used for its bronchodilator properties in the management of bronchospasm in bronchial asthma (reversible airways obstruction). The smooth muscle relaxation follows the stimulation of the β_2 receptor in the cell membrane (activating the adenylate cyclase). This leads to a decrease in intracellular calcium levels essential for actin-myosin cross linkage. SS is a white, crystalline powder, freely soluble in water and slightly soluble in alcohol or ether. No solvate or hydrate forms have been reported. The micronised form of SS (Figure 2.2) was supplied as a gift from Medeva Pharma Ltd (UK, BN 15732) with an average volume mean diameter of 2.3 μm.

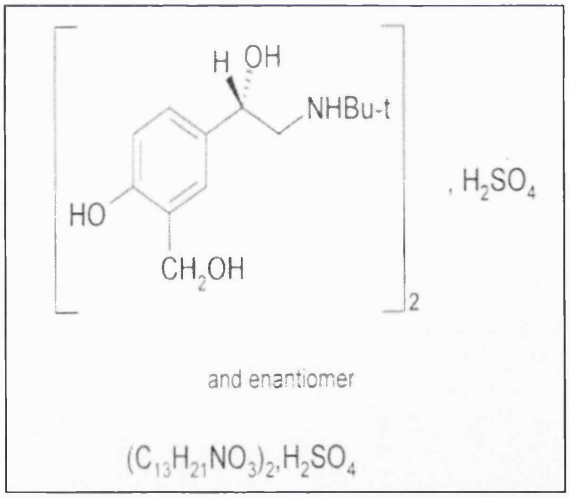

Figure 2.2. *Chemical structure of SS.*

2.1.3. Inhalation devices

2.1.3.1. The Clickhaler®

The Clickhaler® (Figure 2.3) is a multi-dose dry powder inhaler developed by Innovata Biomed Limited (St. Albans, UK) and is commercially available as Asmabec™ (BDP 50, 100 and 250 µg per dose) or Asmasal™ (SS 114 µg per dose) (British National Formulary, 2004). The Clickhaler® is a reservoir device metered inhaler containing a drug hopper and dose metering mechanism. Pressing the dosing push button causes the dosing cone to rotate and transports one metered dose into the inhalation channel, and allows the dose consisting of approximately 3 mg of the lactose blend to be presented for inhalation (Nantel and Newhouse, 1999).

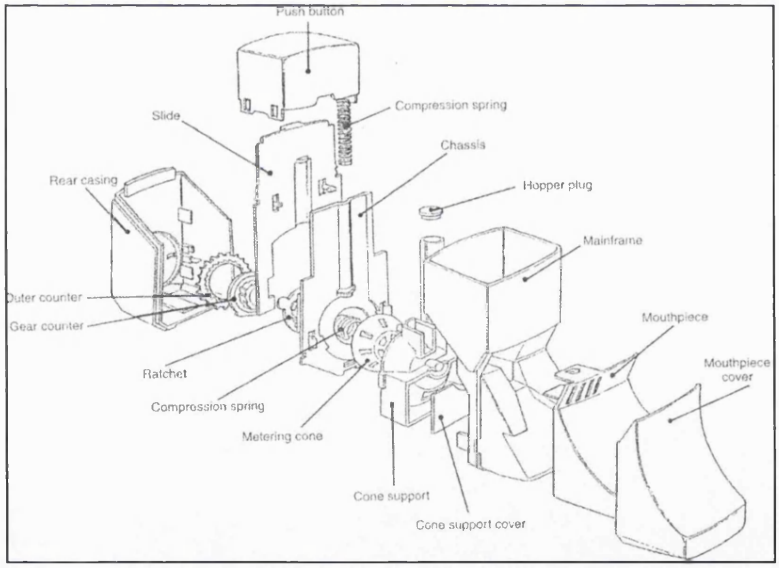

Figure 2.3. *Schematic view of the Clickhaler® (Parry-billings et al., 1999).*

The Clickhaler® device was selected because it has reported delivered dose uniformity, even at low nominal doses (Fukunaga *et al.*, 2000). It also produces efficient *in vitro* aerosol generation (30 to 60 % fine particle fraction (FPF) over a range of drug formulations and flow rates), whereas other recent passive DPI devices (Diskus® / Accuhaler®) have a lower efficiency (around 20 % *in vitro*). The performance of older DPIs may also be more flow rate sensitive.

Furthermore, the Clickhaler® is able to provide a comparable bronchodilator response in patients with moderate to severe asthma when compared to a pMDI used optimally (Newhouse *et al.*, 1999).

Empty devices were received as a gift from Innovata Biomed Ltd. The different formulations were introduced into the reservoirs of the empty Clickhaler® and plugged with caps. The reservoirs were filled to two thirds to allow enough headspace for device shaking prior to actuation. Each formulation was tested three times. Between two sets of experiments, the device was cleaned and ten waste shots fired. A new device was used for each separate formulation.

2.1.3.2. The Aerolizer®

The Aerolizer® (Figure 2.4) is a single-dose dry powder inhaler, developed by Novartis Pharmaceuticals Corporation (USA), commercialised to deliver the selective β_2 adrenergic drug formoterol fumarate. In the Aerolizer®, the capsule containing the single dose is pierced in the device by a set of four pins after depressing two buttons on each side of the capsule chamber. On inhalation, the capsule caused to lift out the capsule chamber into the inhalation spin chamber where it rotates. The device resistance is low (0.06 cm H_2O (L/min). Even if *in vivo* studies showed no impact of different flow rates on clinical effect using the similar device Cyclohaler® (Zanen *et al.*, 1992), *in vitro* studies pointed out the necessity to test DPIs at different flow rates depending on their resistance. Chew *et al.* (Chew and Chan, 2000) showed that the performance of the Aerolizer® was slightly dependent on the air flow rate, whereas there was no significant variability over a range of inspiratory flow rates (15, 30 and 60 L/min) observable with the Clickhaler®. All *in vitro* studies involving the Aerolizer® were performed at an airflow of 60 L/min.

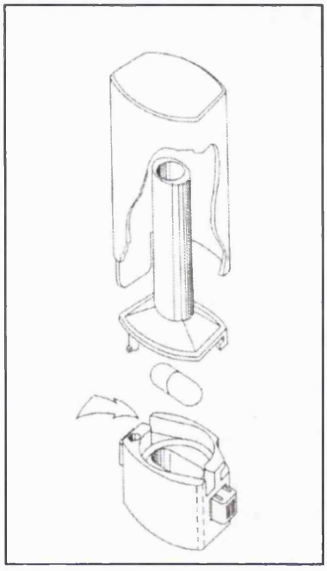

Figure 2.4. *Schematic view of the Aerolizer®.*

In order to load the Aerolizer® with a capsule containing the formulation to be tested, the body of a size 3 gelatine capsule was filled manually with 30 mg of powder accurately weighed using a micro-spatula. The capsule was then closed by placing and locking the cap and placed in the capsule chamber. The devices used were supplied by Novartis (Basel, Switzerland). Each device was used for only one measurement.

2.2. Methods

2.2.1. Production of particles by spray drying

Particles prepared by spray drying were examined throughout this dissertation. The production of particles by this process has gained considerable attention in recent years. By definition it is "the transformation of a given feed stock from a fluid state into a dried particulate form by spraying the feed into a hot drying medium" (Masters, 2002). The feed stock can be a solution, a suspension or an emulsion. One of the biggest advantages of spray drying over other drying techniques (such as tray-drying and freeze-drying) is the possible control over the final particle morphology, which is of the biggest importance within the pharmaceutical industry.

One of its biggest drawbacks, however, is the deposition of the product on the walls of the drying chamber and on the different ducts. This leads to poor yields and hence makes this technique quite costly, especially for expensive products. Four main stages are generally involved in this method: atomisation, spray-air contact, drying of feed material and separation of the dried product.

The formation of a spray (atomisation) and its contact with the drying medium are important characteristic features. Elversson *et al.* (Elversson *et al.*, 2003) studied the influence of spray drying parameters on the produced lactose particle characteristics. A higher atomisation airflow (at constant feed rate) resulted in smaller droplet size, whereas increasing the orifice diameter of the nozzle from 1.5 to 2.0 mm resulted in doubling the size of the particles. The feed solid content also influences the atomisation since an increase in feed concentration increases the feed viscosity, which in turn produces coarser sprays on atomisation. In the same study, the particle size distributions of lactose particles spray-dried from different feed solutions (1, 5, 10 and 20 % w/w) were investigated. Only a moderate size difference in particles was observed when lactose solutions of 5 to 20 % (w/w) were employed, whereas particles from 1 % solution appeared far smaller.

After atomisation, the second step is the spray-air contact. Three different types of contact can be encountered:

- Co-current flow where the feed and the drying air flow in the same direction;
- Counter-current flow where the material is sprayed in the opposite direction of the flow of hot air;
- Combined co/counter-current flow, combining the advantages of the two pre-mentioned methods.

The work described in this dissertation is focused on the operational characteristics of two laboratory scale spray dryers: the Büchi 191 mini spray dryer used for the production of lactose/PEG 4000 systems (see chapter 4 and 5) and the Niro SD MICRO™ for the production of SS/PEG 4000 systems (see chapter 6). Both spray dryers operate in a co-current manner.

Evaporation is rapid and the duration of exposure short. This is particularly important for heat sensitive materials such as proteins. Maa *et al.* (Maa *et al.*, 1997) investigated the effect of drying conditions and formulation variables on the morphology of spray-dried proteins. They stated that the droplets along the drying chamber were exposed to a temperature dominated by the outlet temperature rather than by the inlet temperature. They also showed that, based on the spray drying of water, an increase in the outlet temperature was directly proportional to an increase in the inlet temperature and/or the drying air flow rate. The outlet temperature decreased in a linear way with increasing liquid feed rate and/or atomizing airflow rate. Generally, particles reach a maximum temperature which is 15 to 20°C below the outlet temperature of the co-current dryer (Masters, 2002)

The drying of a wet droplet (Figure 2.5) corresponds to the double transfer of mass and heat after coming into contact with the drying air. The drying of a spherical droplet of liquid containing solid can be divided into 3 different stages.

- Stage 1 (sections A-B): In contact with the air, evaporation takes place from the saturated vapour film at the droplet surface. The temperature of the droplet surface approaches the wet-bulb temperature of the drying air. The wet-bulb temperature corresponds to the temperature at which evaporated water brings the air to saturation at the same temperature.

- Stage 2 (sections B-C): The drying rate is constant. There is sufficient moisture and molecular mobility within the droplet to replace lost moisture from the surface. The particle experiences shrinkage with a negligible temperature change.

- Stage 3 (sections C-E): At point C, the droplet moisture level is too low to compensate that which is lost. This results in the formation of a crust on the droplet surface (point D). The thickness of this crust increases with time, resulting in the slowing of the evaporation rate. Evaporation continues until the droplets or now the particles acquire a moisture content that is in equilibrium with the surrounding air.

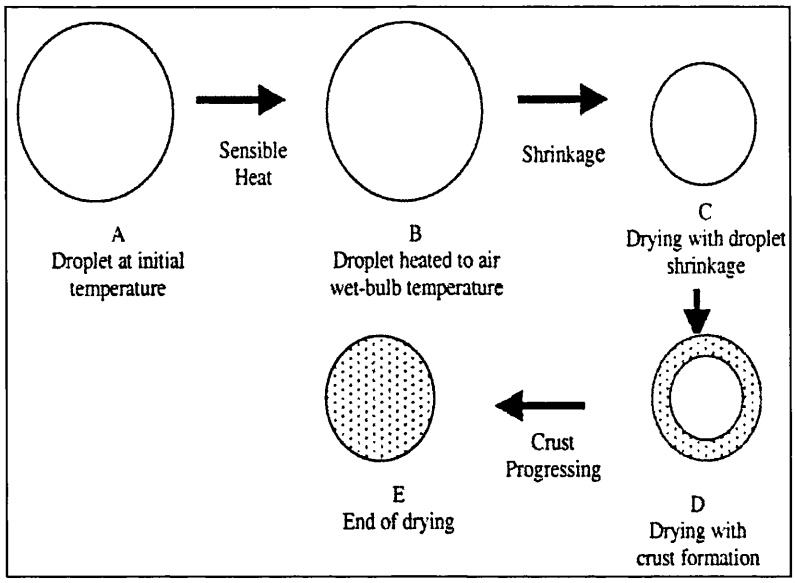

Figure 2.5. *Different drying stages involved in spray drying modified from Farid (Farid, 2003).*

The final stage involves the separation of the solid product from the air stream. A cyclone separator, through which product and air pass after exiting the drying chamber, enables a separation from the drying medium. The material accumulates in a collecting vessel at the base of the cyclone. It has to be mentioned that separation is not 100 % efficient and that some fines may be lost through the exhaust air. In the case of the Niro SD MICRO^{TM} some back filters ensure a full recovery of the product.

2.2.1.1. Spray drying using the Büchi 191

The Büchi 191 (Figure 2.6) uses a two-fluid pneumatic nozzle (0.5 mm diameter). The feed concentration is pumped to the nozzle by a peristaltic pump using silicon tubing and then atomized using compressed air from an in-house supply (100 psi).

- Production of amorphous lactose

In order to investigate the amorphous content of different batches of lactose using solution calorimetry, a calibration curve had to be established beforehand, requiring the production of amorphous lactose material. This was achieved by spray drying a 10 % (w/v) solution of α-lactose monohydrate following parameters shown in Table 2.1. The experiments were performed at constant process conditions and only the feed rate was slightly modified in order to minimise outlet temperature fluctuations.

Parameters	Settings
Inlet temperature (°C)	185-190
Outlet temperature (°C)	85-90
Aspirator dial	60 %
Pump	18 %
Atomiser airflow rate (Normliter/h)	400

Table 2.1. *Spray drying parameters used to obtain amorphous lactose and crystalline lactose/PEG 4000 particles.*

- Production of crystalline lactose/PEG 4000 systems

Three different 50.0 g blends consisting of lactose/PEG 4000 systems (containing 1, 5 and 10 % PEG 4000 by weight of solids) were dissolved at room temperature in 500 mL deionised water. This ensured full dissolution of lactose monohydrate in water (solubility at 25°C of 1 in 4.63 (Kibbe, 2000)). The spray drying parameters employed were identical to the ones set out in Table 2.1 above.

- Production of partially amorphous lactose/PEG 4000 system

A formulation comprised of 10 % PEG 4000 by weight of total solid, was spray-dried as a 10 % (w/v) aqueous solution using the parameters shown in Table 2.2.

Parameters	Settings
Outlet temperature (°C)	120-125
Inlet temperature (°C)	76-80
Aspirator	80 %
Pump	14 %
Atomiser airflow rate (Normliter/h)	600

Table 2.2. *Parameters used to obtain partially amorphous lactose/PEG 4000 co-spray-dried system.*

- SS/PEG 4000 and SS/lactose/PEG 4000 systems

For these systems involving a much larger number of experiments, the detailed methodology will be fully described in the relevant chapter.

All product powders were removed from the collecting vessel as soon as the spray drying process was over and stored in a desiccator over silica gel, at room temperature.

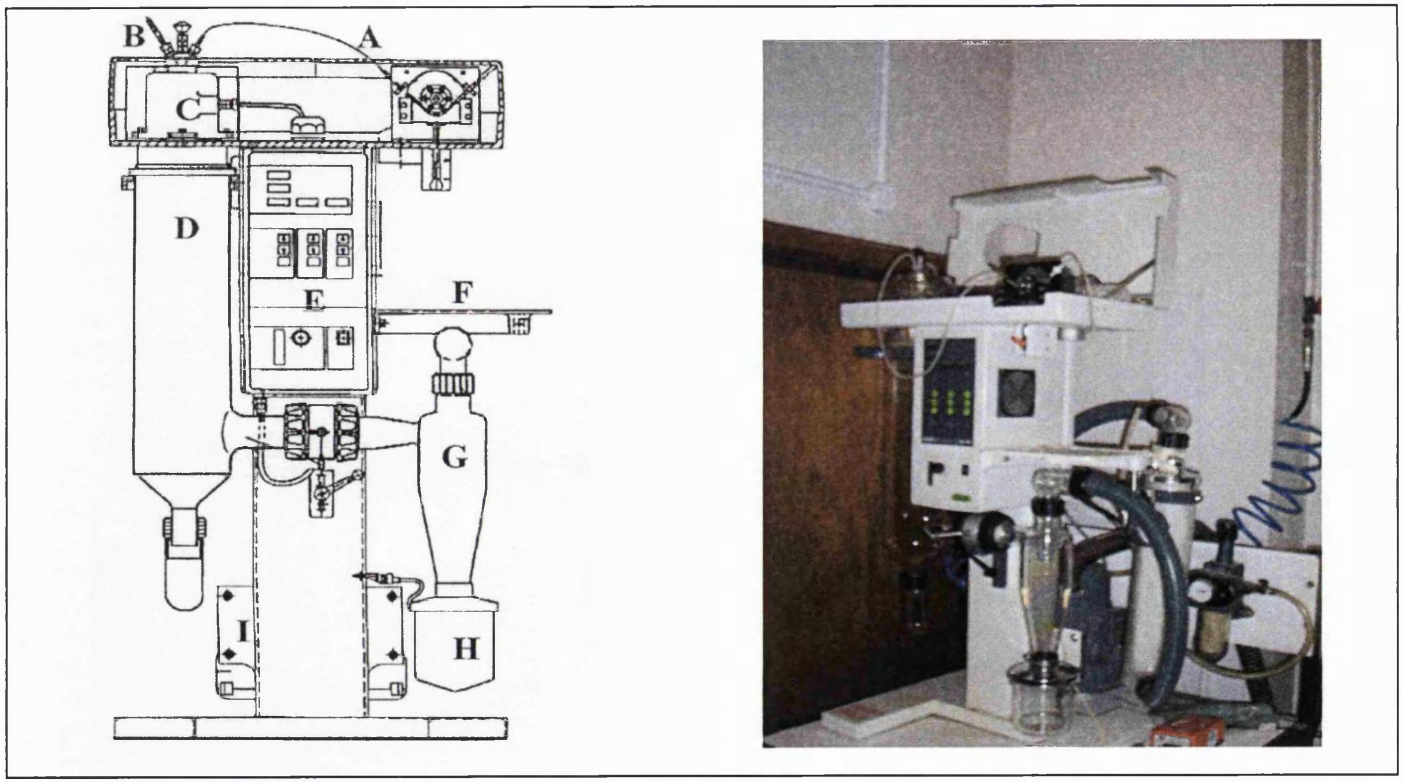

Figure 2.6. *Outline of the Büchi 191 spray dryer (left) and photograph of spray drying in operation (right): A=feed pump, B=compressed air inlet, C=pneumatic nozzle, D=primary drying chamber, E=control panel, F= sample feed holder, G=spray drying cyclone, H= collection vessel and I=aspirator.*

2.2.1.2. Spray drying using the Niro SD MICRO™

Unlike the Büchi, the process gas employed in the Niro SD MICRO™ (Figure 2.7) is compressed filtrated nitrogen, which is heated by means of an electrical air heater in order to evaporate the liquid contents of the feed solution. It enables the operator to use flammable solvents and, in our study, to spray dry organic suspensions consisting of SS suspended in an ethanolic solution containing PEG 4000. Prior to start up, it was important to determine and set the temperature safety class for the solvent employed. For ethanol a heater element surface temperature limit of 300°C was adopted since the auto-ignition temperature for this solvent was found to be 363°C (Niro Manual). The hot process gas enters the chamber through the process gas disperser and is immediately mixed with the atomized suspension coming from the two-fluid nozzle. The liquid is evaporated and the remaining dry particles leave the chamber through the outlet duct together with the process gas. The powder passes through the cyclone and is collected in a glass jar. Smaller fines accompanying the process gas may be collected within a bag filter. The process requires that gas flow and nozzle flow are obtained by opening the nitrogen main valve followed by adjustments with flow controllers. The inlet process gas temperature was set as shown in Table 2.3 and the heater switched on. When the inlet reached 10° C over the set value, the peristaltic pump controlling the feed rate of the ethanolic solution was turned on. The ethanolic solution was sprayed until the atomisation of liquid was constant. When all parameters were stabilised for ten minutes the hose of the pump was transferred to the feed suspension. Once finished, the hose from the peristaltic pump was transferred back to the clean solvent, and the jar containing the product was removed from the system and stored in a desiccator at room temperature.

Parameters	Setting
Chamber inlet gas flow (kg/h)	20
Atomiser gas flow (kg/h)	2.0
Inlet temperature (°C)	85-90
Outlet temperature (°C)	60-65
Feed pump	28 %

Table 2.3. *Spray drying parameters used on the Niro SD MICRO™.*

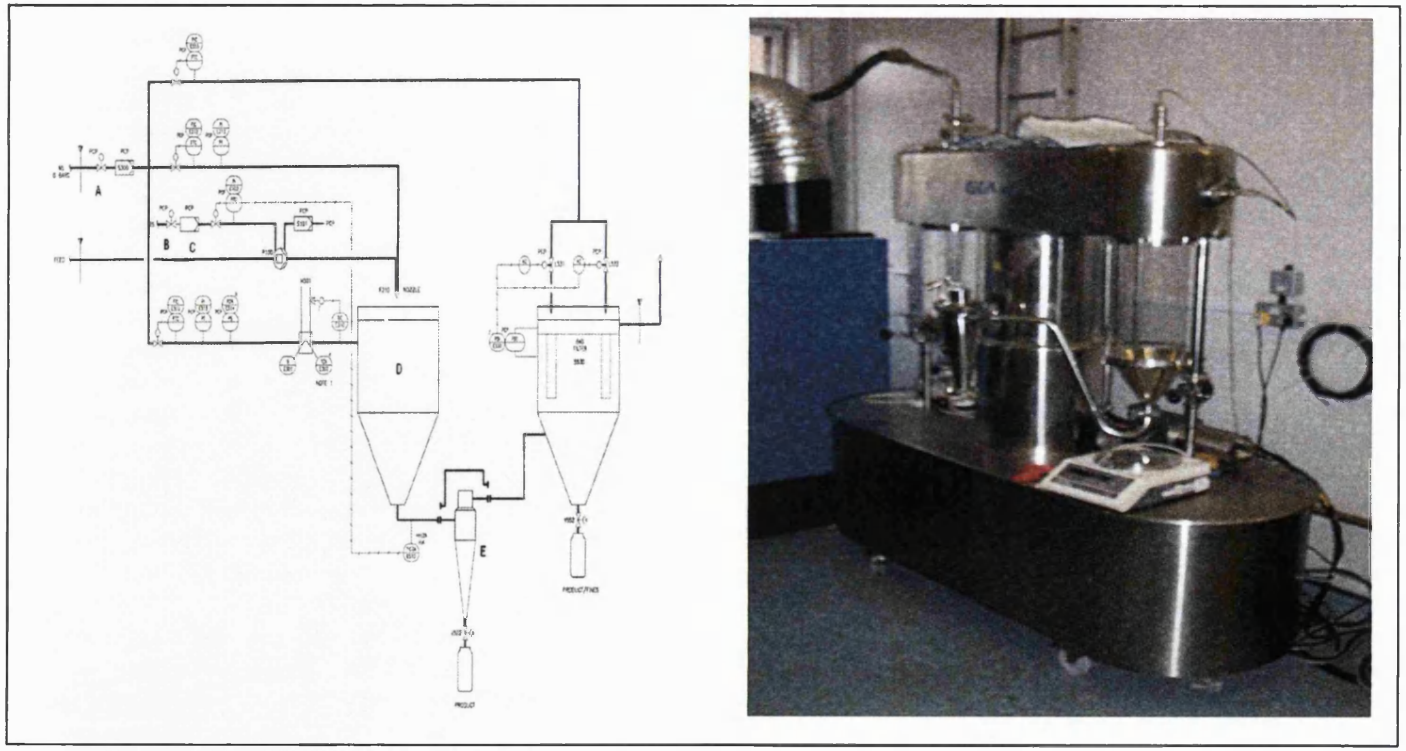

Figure 2.7. *Outline of the Niro SD MICRO™ spray dryer (left) and photograph of spray drying in operation (right): A=nitrogen main valve, B=feed pump main air valve, C=feed pump air filter, D=drying chamber,and E=spray drying cyclone. N.B. The schematic is a mirror image of the photograph.*

2.2.2. Preparation of powder blends

Mixing is an intermingling of two or more dissimilar fractions of material. The primary objective of powder mixing is to obtain dose uniformity. It is necessary for the active ingredient to be homogeneously mixed with the carrier excipient. Different factors influence the quality of a blend, including the order and length of time of mixing, type of mixer used, blender loading, and the physico-chemical properties of all active and excipients (size, shape, density and surface properties).

The best obtainable mixture would be one in which there was the least variation in composition for any given sample size. Two types of blend exist: random and ordered. Random mixes involve particles of equal size and weight with little or no surface effects, whereas ordered mixes do not require equally sized or weighted particles. Ordered mixes are therefore formed when a fine component has sufficient intrinsic cohesiveness to adhere to the surface of a coarser component. This involves the types of particle interaction, which were described in detail in chapter 1.

Experimentally, all blends were mixed in a 14 mL glass container with approximately 50 % of the blending vessel being filled. Lowering the fill volume would increase the space for powder movement and allow a greater degree of interaction, which in DPI formulation would be detrimental. On the other hand, increasing the powder volume would decrease the particle interaction, but also might decrease the mixing efficiency by decreasing the space for powder homogenisation. Blending was carried out in a three-dimensional Turbula T2C mixer (Glen creston UK). Adhesion to the vessel was regarded as insignificant by comparing the theoretical to the measured drug content in the sample. The drug powder was mixed with the carrier so that the final concentration of drug in the formulation ranged from 1.0 to 4.0 % (w/w). Each blend was prepared in 5.0 g quantities. A sieving process was required to deaggregate the raw materials. Due to the cohesive nature of SS and BDP, the deaggregation required manual pressure using a spatula for its passage through a 355 μm sieve screen.

When stated, an air-jet sieve (Alpine, Germany) was used to effectively remove any present particle below 45 μm in size. The air-jet method is a single-sieve system for dry powders. In this technique, the sieve is mounted in a sealed chamber and the air is drawn upwards through the sieve from a rotating slotted nozzle to fluidise the sample. Undersized particles are carried downward through the sieve to a collection canister. Each carrier was sieved for 15 minutes using a sieve aperture of 45 μm (Endecotts, UK).

2.2.3. Assessment of content uniformity

One of the issues in pharmaceutical formulation is to achieve a high drug content uniformity. Therefore, prior to the study of *in vitro* deposition patterns, the content uniformity must be assessed. Both SS and BDP were quantified by UV spectrometry.

Calibration curves for both drugs were determined by a procedure described in the British Pharmacopoeia (BP) under their respective monographs. A 0.008 % (w/v) solution of SS in 0.1M hydrochloric acid (HCl) was prepared following the method outlined in the BP. This solution was analysed over a range of 200 to 400 nm using a Cary 3E, UV/Vis spectrophotometer. A λ_{max} of 276 nm was obtained and all analyses conducted with SS were therefore performed at this wavelength. A range of concentrations varying from 0.0002 % (w/v) to 0.0010 % (w/v) was then prepared from a stock solution of 0.1 % (w/v) SS in 0.1M HCl. Samples were analysed using an Ultrospec 2000 spectrophotometer (Pharmacia Biotec, UK) at 276 nm. A good linear correlation between UV absorption and SS concentration was found within this region (r^2= 0.9987). The gradient of the solid line in Figure 2.8 was found to be equal to 61.5, with a y-axis intercept of 0.0003. BDP was also analysed over the range of 200 to 400 nm, using a Cary 3E, UV/Vis spectrophotometer. For this purpose, a 0.002 % (w/v) solution of BDP in methanol was prepared following the method outlined in the BP. A λ_{max} of 238 nm was obtained for the hydrophobic drug and all subsequent analyses were therefore performed at this wavelength. The same concentration range as that for SS was prepared and the calibration curve established.

A good linear correlation between UV absorption and BDP concentration was also found within this region (r^2= 1). The gradient of the dashed line was equal to 284, with a y-axis intercept of minus 0.0064.

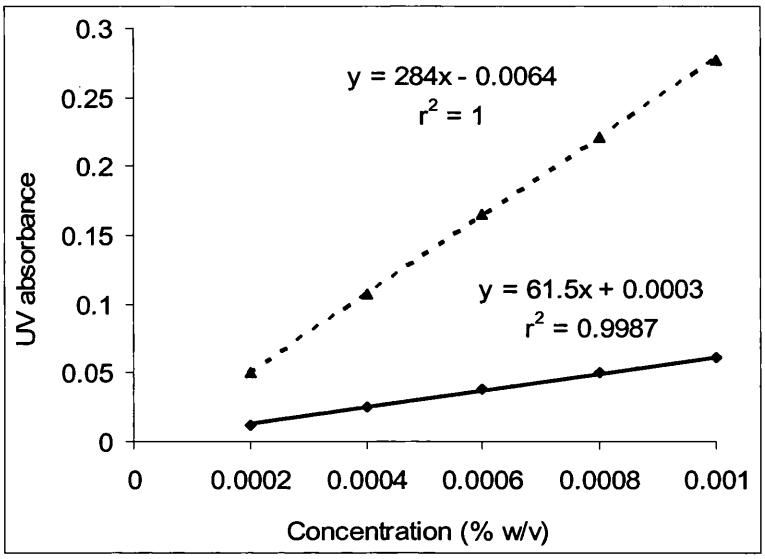

Figure 2.8. *UV calibration curves for SS(solid line) and BDP (dashed line).*

Neither PEG 4000 nor lactose interfered with the UV measurements since neither was absorbing alongside the drugs at these wavelengths.

Once the blending process was completed, ten samples of the powder bed (of approximately 10 mg each) were obtained and accurately weighed. Three samples were obtained from the top, four from the middle and three from the bottom of the powder bed, and each was finally transferred into a 100 mL volumetric flask. SS samples were dissolved in 0.1M HCl, while BDP samples were dissolved in a methanol-water mixture (70:30 (v/v)). The methanol-water mixture ensured that both lactose (hydrophilic) and BDP (hydrophobic) were fully dissolved. The solutions were subsequently analysed using UV spectroscopy. To eliminate the effect of weight variations between the individual samples, the drug content was normalised for each sample weight. The uniformity of the blend was characterised by the coefficient of variation of the samples. This parameter describes the standard deviation (σ) of the ten samples as a percentage of the mean drug content (M). A coefficient of variation (C.V.) below 5 % corresponded to good blends. Only these blends with a good homogeneity were taken to the next stage of the investigation.

2.2.4. Characterisation of aerodynamic properties of dry powder aerosols

A key pharmaceutical challenge for DPIs is to ensure that there is good dose uniformity. *In vitro* aerosol particle sizing methods have evolved in parallel to the increased interest in powders for inhalation. In all *in vitro* studies, the British Pharmacopoeia was followed, which adopts the TSI, Apparatus A, which was initially developed to assess pMDI performance (Hallworth *et al.*, 1978; Hallworth and Westmoreland, 1987). As illustrated in Figure 2.9, the aerosol cloud is introduced at the inlet (A) and passes through a glass tube containing a 90° turn (B), designed to mimic the oropharyngeal region. It then passes the upper impingement chamber (D), which is filled with 7 mL of a suitable solvent (0.1M HCl in distilled water for SS and a 70/30 mix (v/v) methanol/water for BDP). The particles passing to stage 2, corresponding to the lower impingement chamber, containing 30 mL of suitable solvent, are considered to be respirable and below 6.4 µm (Miller *et al.*, 1992). This value corresponds to the aerodynamic cut-off diameter at a flow rate of 60 L/min.

- *In vitro* study using the Clickhaler®

To operate the TSI (Copley instruments, UK), the primed Clickhaler® was placed into an appropriate mouthpiece adaptor specially moulded by Copley, ensuring that a good seal was obtained. An adjustable pump (model T12, Nr 65321, Erweka®, Germany) capable of maintaining an airflow of 60 L/min through the TSI, was connected to the outlet of the lower stage. A micro manometer ensured a 60 ± 5 L/min airflow during the entire process. The inhaler was then actuated for 5 seconds. The pump was then switched off, the inhaler removed and the mass change measured by comparing the initial and final weight of the inhaler. The procedure was repeated for a further nine discharges. Following these 10 actuations, the apparatus was dismantled.

Once completed, the mouthpiece and the different stages were rinsed with the suitable solvent for the drug to be assessed, and poured into volumetric flasks. The flasks made up to a volume of 100 mL each were then analysed using UV spectrometry as stated in Section 2.2.3. Each formulation was run at least three times. A new Clickhaler® device was used for each formulation tested.

- *In vitro* study using the Aerolizer®

A mouthpiece adaptor suitable for the Aerolizer® was obtained from Novartis Pharma and fitted to the glass part of the TSI. The pre-prepared capsule was placed into the capsule chamber. After checking that the capsule was correctly positioned, the inhaler was closed and the capsule perforated by pressing and releasing the two buttons simultaneously. The pump was switched on for 5 seconds and then turned off. The impactor was then dismantled and the different parts washed as described earlier on.

Following the calculation of the concentrations from the UV data in the different stages, three different aerosol parameters were obtained:

- The emitted dose (ED) corresponding to the amount of drug (in µg) in stage 1 (A to D) and 2 (E to H);
- The respirable dose (RD) corresponding to the amount of drug (in µg) in stage 2;
- The fine particle fraction (FPF) corresponding to the respirable dose as a percentage of the emitted dose.

Experimental data sets were statistically analysed by using either the student t-test (for two data sets) or the analysis of variance (One-Way ANOVA for more than two sets). A "p-value" of 0.05 was taken as indicative of statistical differences. Furthermore, the standard deviations of the different measurements are also presented in parentheses in this work. These statistical methods were also applied to the physico-chemical data sets of the different formulations.

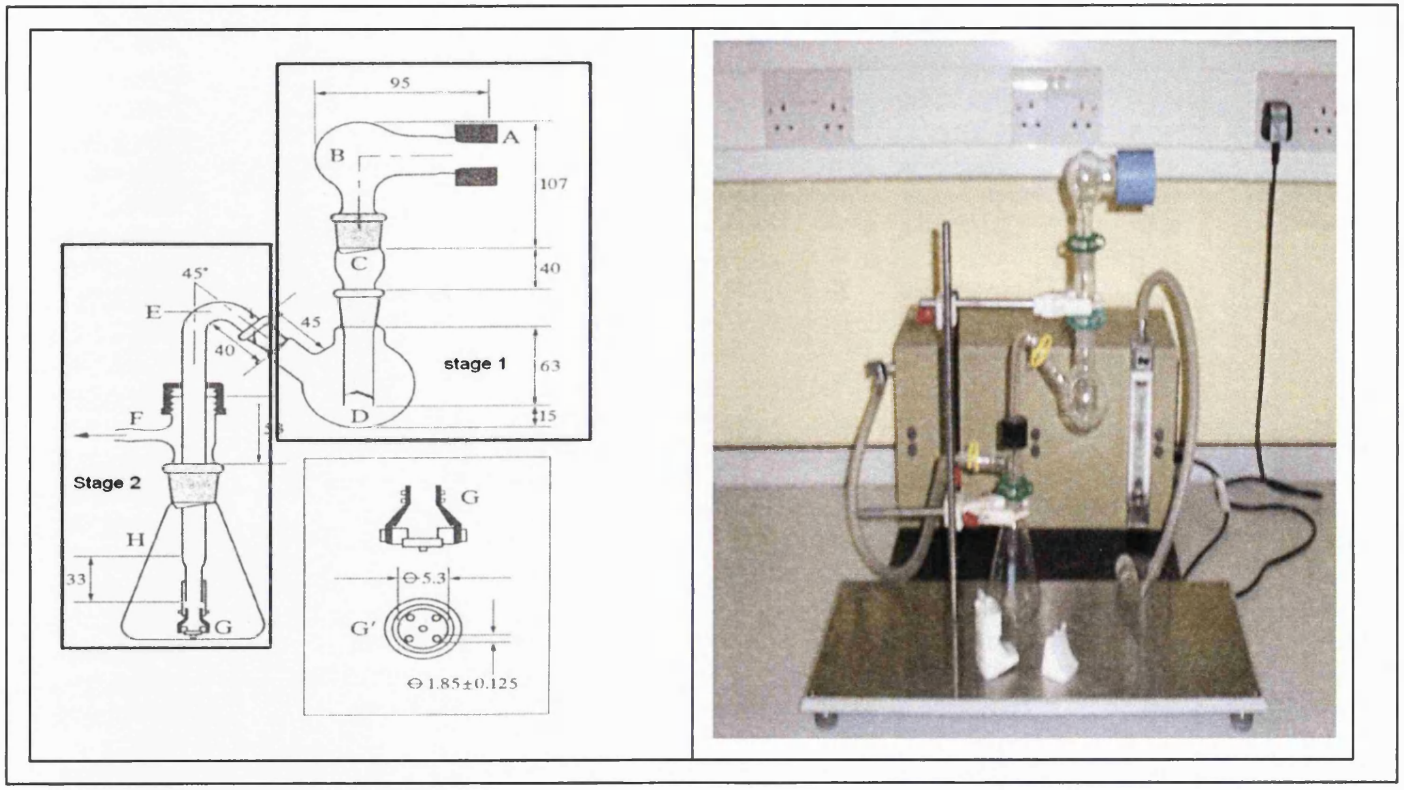

Figure 2.9. *Outline of the TSI (left) (modified from BP) and photograph of in vitro assessment in operation (right).*

2.3. Physico-chemical characterisation methods for the powder systems

2.3.1. Scanning electron microscopy

The morphology of the different carriers was studied using scanning electron microscopy (SEM). In this technique, a fine beam of medium energy electrons scans the sample in a series of parallel tracks. The interactions of these electrons with the sample generate different signals such as secondary electron emission, back-scattered electrons and X-rays. At magnification in the range of optical microscopy, a scanning electron microscope can give a depth focus several hundred times greater than that of an optical microscope. Particles generally greater than 1 μm can be imaged, making this technique particularly useful for the characterisation of dry powders.

SEM analysis was performed by Mr. McCarthy of the SEM department at the University of London, School of Pharmacy. The samples were mounted onto carbon disks attached to SEM stubs and coated with a thin layer (approximately 20 nm) of gold under vacuum in an argon atmosphere for 4 min at 30 mA using a sputter coater, to improve the conductivity. The micrographs were obtained using a Philips L20 SEM (Philips, the Netherlands).

2.3.2. Particle size measurements

Laser diffraction is a popular method for determining the size distribution of powders. Its widespread use is mainly due to its advantageous fast measurements, high reproducibility and good reliability (XU and Di Guida, 2003). A Mastersizer X (Malvern Instruments, UK) was used to measure the particle size distribution of the different samples. This technique is based on the interaction of laser light with particles that are suspended in an appropriate solvent. The determination of particle size by light scattering is based on the Mie theory. This theory results in a value for the volume of the particle, with the assumption that the particles are optically homogeneous, spherical and dilute in a random arrangement (to give independent, incoherent scattering) (Allen, 1997). The general diffraction principle relies on the fact that diffraction is inversely proportional to particle size.

When light is directed at particles that are much larger than the incoming wavelength, it is scattered with an angle that is linked mathematically to the dimension of the particles: the scattering power increases with the square of the particles diameter. In the simplest description, small particles scatter weakly and principally to large angles away from the incident light beam, while large particles scatter strongly to smaller angles.

The measurements performed are based on the concept of the equivalent sphere. In the case of Malvern measurements, which are volume based, the equivalent sphere is that which would produce the same scattering intensities as the particle. This corresponds approximately to a sphere of equal volume. When particles are introduced in the suspension medium, both the light scattered by the particles and the unscattered remainder are incident on the receiver lens. This lens, acting as a Fourier transform lens, focuses the diffracted and transmitted light onto a series of photo-detectors at fixed positions.

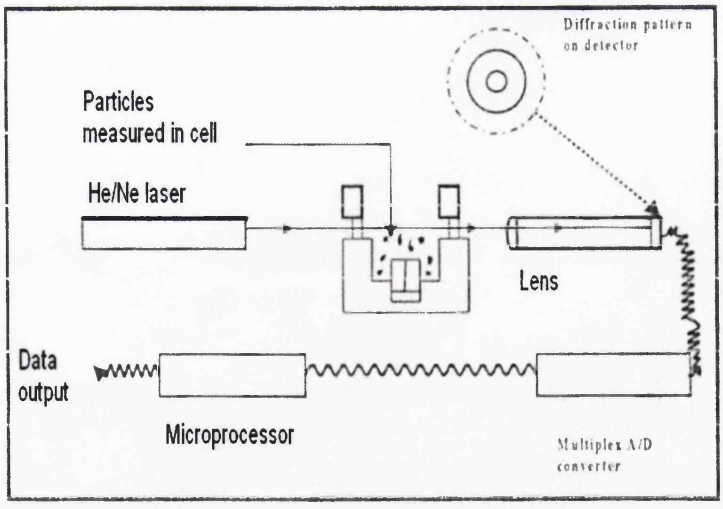

Figure 2.10. *Schematic diagram of laser light diffraction particle sizer (modified from Aulton (Aulton, 2002)).*

The apparatus schematised in Figure 2.10 consists of the following different modules:

- The transmitter module containing the laser, power supplies and beam collimation optics;
- The sample area;
- The collection optics;
- The receiver module (detector of scattered light);
- The computer (to transform scattered light data into particle size data).

The amount of light scattering signal recorded is a function of the scattering power of the particles, which itself depends on the refractive index of both the solid and the medium. The refractive index of a substance is defined as the ratio of the speed of light in vacuum to the speed of light in that substance. It is a complex spectral function with both real and imaginary (absorption) parts.

The instrument operated with a He-Ne 632.8 nm laser diffraction source, over a 0.5 – 900 μm particle size range. A Malvern MS7 magnetically stirred small volume (15 mL) diffraction cell was used. In order to avoid cross contamination, the cell was first washed with distilled water and then filled with propan-2-ol. Approximately 10 mg of lactose crystals were suspended in 5 mL of the same solvent. Collection from the powder bed was crucial since the data obtained from this small sample was meant to be representative of the entire batch. Thus it was always insured that the material was thoroughly stirred with a spatula before taking samples for measurement. Each specimen was then added dropwise with a pipette into the cell until a 10 to 15 % obscuration value (corresponding to the fraction of incident light intensity that is not detected at zero angle detector) was achieved. It is important to use dilute suspensions, since in concentrated suspensions possible multiple light scattering may modify the angular distribution of light intensity (Guardani *et al.*, 2002). The particle size distribution was generated from the diffraction data using a mathematical model or "presentation". The measurements were repeated three times for each material and both the mean and standard deviation were reported. Different parameters were defined: $d_{50\%}$, also known as the volume median diameter, indicates the median particle size distribution where 50 % of the volume of all

particles resides below and above this value. $d_{10\%}$ and $d_{90\%}$ indicate that 10 % and 90 % of particle volume lie below those values respectively. Calculating the coefficient of spread, called SPAN and corresponding to the ratio of d90% - d10% to d50%, assessed the width of the distribution.

2.3.3. Specific surface area

The surface topographies of the different lactose carriers can be further described quantitatively by the determination of the specific surface area (SSA). The measurement of the surface area is based on the fact that a solid, when exposed to a gas, adsorbs a proportion of the gas at its surface. The BET isotherm, derived by Brunauer, Emmett and Teller, is widely used to determine the surface area of solids. An adsorption isotherm can be defined as the relationship between the amounts of gas adsorbed on a solid at a constant temperature and the gas pressure. It was realised only in the 1930s that multilayer adsorption could occur at liquid nitrogen temperature (Sing, 2001). Assuming the formation of a multilayer of adsorbed molecules, the three scientists modified the Langmuir approach (type I isotherms, in which the core assumption is that adsorption stops at monolayer coverage) by balancing the rates of adsorption and desorption for the various molecular layers. With the BET approach, the determination of adsorption isotherms of nitrogen (which has an effective area per molecule of 0.162 nm^2) at the temperature of liquid nitrogen, approximately 77 K, is possible by a point-by-point procedure where successive amounts of nitrogen are introduced. At each stage the system is allowed sufficient time to reach equilibrium. The adsorbent surface is pictured as an array of equivalent sites on which nitrogen molecules are adsorbed in a random manner. The occupation probability of a site is assumed to be independent of the occupancy of neighbouring sites and the adsorbed molecules are assumed not to interact with each other (Sing, 2001). Since adsorption of gases onto pharmaceutical solids usually gives rise to type II isotherms, which may be considered as unrestricted monolayer/multilayer adsorption, the SSA of the different powders was calculated from the BET equation below:

$$\frac{1}{V}\left(\frac{P}{Po - P}\right) = \frac{1}{cVm} + \left(\frac{c-1}{cVm}\right)\left(\frac{P}{Po}\right) \qquad \text{[Equation 2.1]}$$

Where V corresponds to the volume of adsorbed vapour, V_m to the volume of gas adsorbed to form a monolayer, P to the partial pressure of the gas, P_o to the saturated vapour pressure of the gas and c to the BET constant.

If a plot of $P/V\ (P_o\text{-}P)$ is drawn as a function of P/P_o, the slope of the line is equal to $(c\text{-}1)/cV_m$ and the intercept is $1/cV_m$. Since the total volume of gas adsorbed by the sample (V) is measured, the volume of adsorbed gas required to form one complete monolayer on the solid (V_m) can thus be determined graphically. From this result, the total number of gas molecules adsorbed on the solid can be determined. Finally, knowing the area occupied by each nitrogen gas molecule, the totam surface area of the solid can be obtained.

Experimentally, an accurately weighed sample was transfered into a nitrogen BET surface area analyser tube fitted with a glass rod to minimise the overall free space. Each sample was then loaded in the outgas station of a SA 3100 surface area analyser (Beckman Coulter ^{TM}). The instrument included a sample port, three outgassing stations, a vacuum and a built in data processor. The outgas time ensured a removal of free particles from the surface which would be able to adsorb nitrogen molecules. Upon increase of the sample outgas time from 2 to 4 hours no apparent increase in the SSA was detectable. Therefore, after outgassing for 4 hours at 30°C, it was assumed that all surface contaminants such as physically adsorbed gas and moisture, had been successfully removed and the true specific surface area could then be measured. Upon completion of the outgas step, the sample was removed and sealed with a rubber cap to prevent any mixing of the backfilled nitrogen in the sample tube with the ambient air. The dry sample was reweighed and loaded in the analyser port of the analyser and the underlying Dewar-vessel was filled with liquid nitrogen.

Helium free-space calculation was conducted to account for the free volume in order to accurately measure the volume of gas adsorbed. After the free space measurement was completed, the isotherm measurements were made, from which the specific surface area was calculated. All samples were tested in

duplicate and then analysed using a Coulter® SA 3100 surface area and pore size analyser (Beckman Coulter ™), as shown in Figure 2.11.

Figure 2.11. *Photograph of a SA 3100 surface area analyser.*

2.3.4. X-ray powder diffraction

X-ray powder diffractometry (XRPD) has been used for decades for the measurement of crystallinity (Saleki-Gerhardt *et al.*, 1994). Moreover, the existence of drug polymorphism is well characterised by means of XRPD (Brittain *et al.*, 1991). X-rays are a type of electromagnetic radiation, with a wavelength ranging from about 10^{-5} to 10^{3} Å. They are a by-product of the sudden deceleration of electrons that had previously been accelerated to a high velocity. Within the X-ray tube, electrons emitted by the cathode are accelerated through a high-voltage field and a copper anode is bombarded at high potential (Figure 2.12). On impact, the electrons transfer their kinetic energy to the copper atoms, producing photon X-rays. As the target becomes very hot due to the collision of high-energy electrons, it must be cooled, typically by water.

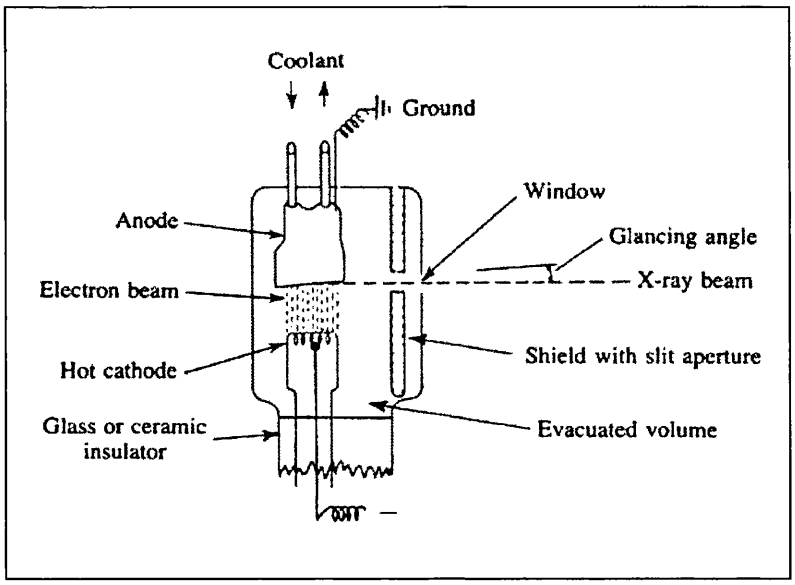

Figure 2.12. *Schematic of an X-ray tube (Willard et al., 1988).*

The X-rays pass out of the tube via a beryllium window. As illustrated in Figure 2.13, when the incident beam strikes a powder sample, diffraction occurs in every possible orientation of 2θ. Diffraction of an X-ray beam striking a crystal occurs because the wavelength of the beam is similar to the spacing of atoms in minerals (1-10 Å). When an X-ray beam encounters a crystal, most of the X-rays will destructively interfere with each other (i.e. cancel each other out), but under some specific conditions they constructively interfere and reinforce one another. Constructive interference only occurs when Bragg's law (Equation 2.2) is satisfied:

$$2d \sin \theta = n\lambda \qquad \text{[Equation 2.2]}$$

Where n is an integer, λ the wavelength of the incident beam, d the distance between atomic planes in the crystal, and θ the angle of incidence of the X-ray beam on the atomic planes.

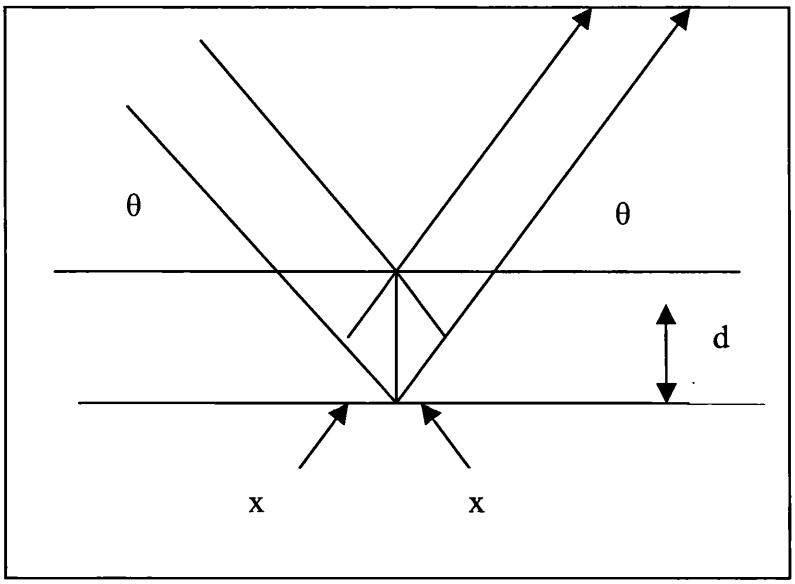

Figure 2.13. *Reflection of X-rays from two planes of atoms in a solid.*

In order to scan the emission spectrum of a sample, the analysing crystal is mounted on a goniometer (to measure angles) that slowly rotates through the desired angular region. The powder pattern consists of a series of peaks detected at various scattering angles. Characteristic peak intensities, or integrated peak intensities, can be measured.

XRPD measurements were performed on a Philips PW 3710 diffractometer. The Cu anode tube was operated at 45 kV and 30 mA in combination with a Ni filter to give monochromatic Cu K_α X-rays. This filter is needed in order to reduce the intensity of the line with the shorter wavelength (K_β). Experimentally, a sample of approximately 0.5 g was loaded in the sample holder, resulting in a powder bed of 2 mm thickness. The sample was scanned from 5 to 30° on the 2θ scale with a step size of 0.05° per second.

2.3.5. Solution calorimetry

Long-standing techniques such as XRPD but also differential scanning calorimetry (DSC) are known to quantify amorphous contents of 5 % and above (Saleki-Gerhardt *et al.*, 1994). It was established that solution calorimetry is useful for quantification of the amorphous content below this 5 % threshold

(Gao and Rytting, 1997; Hogan and Buckton, 2000). In this thermal analysis technique, the temperature change produced by chemical or physical interactions in a liquid due to dispersion or dissolution of the investigated material, in a constant environment, is monitored as a function of time. The software then converts the temperature to heat. Enthalpy of solution of any particular solute in one of its solvents can thus be measured, enabling the detection of slight changes in the physico-chemical properties of a material. The net measured response for the enthalpy of solution results from the addition of different components: wetting of the powder and dissolution following the disruption of the bonding between the solid molecules and the formation of bonds between the solute and the solvent. Moreover, some rearrangement of bonding within the solvent will also occur.

All experiments were carried out using a Thermometric 2225 Precision Calorimeter (Thermometric AB, Sweden) mounted in one channel of the Thermometric 2227 Thermal Activity Monitor (TAM) (Thermometric AB, Sweden). The TAM was used as a precise temperature water bath, having a stability of ± 0.0001°C over 24 hours. The Precision Calorimeter consists of three main components: the calorimetric unit itself (Figure 2.14), the calorimetric cylinder that holds the calorimetric unit, and the solution calorimeter module that houses the electronic components. The calorimetric unit consists of a 100 mL Pyrex glass vessel and a stirrer unit. The vessel is fitted with a heater for calibration and a thermistor for measuring the temperature change when the reaction takes place. The vessel also contains a sapphire-breaking tip mounted on a pin at the bottom, which enables the ampoule holding the sample to be broken. The vessel is attached to the holder by an interlocking nut, acting as a thermal insulator. The stirrer unit, also acting as the ampoule holder, ensures a good mixing of the sample with the dissolving solvent. Data was collected by the "Software for Solution Calorimeter", Version 1.2 (Thermometric AB, Sweden).

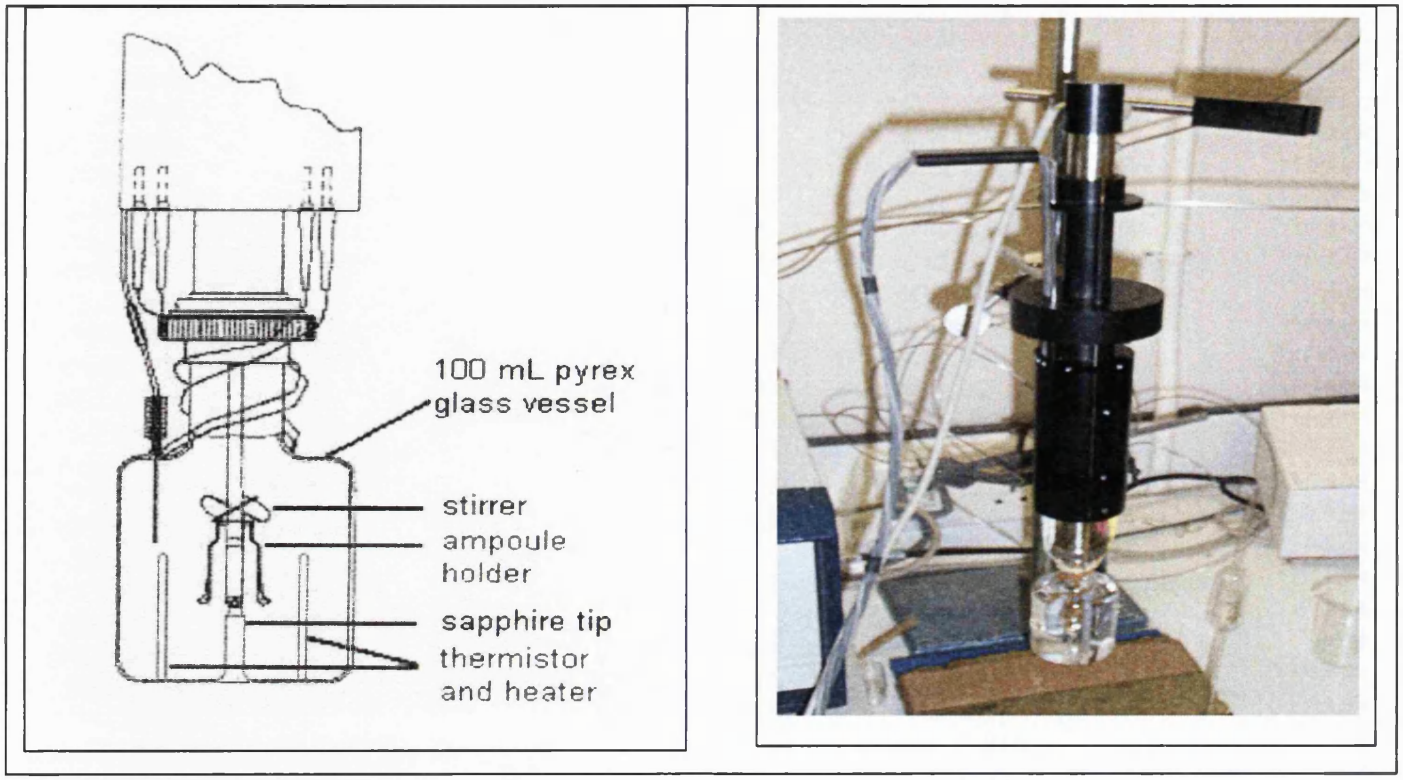

Figure 2.14. *Schematic diagram (Thermometric AB, 1997) and photograph of the calorimetric unit.*

All experiments were carried out with the TAM water bath set to 25.0000 ± 0.0001°C. A sample mass of approximately 200 mg was accurately weighed and filled into a 1.1 mL glass-crushing ampoule. The ampoule was then stored in a vacuum oven (Sanyo-Gallenkamp) between 40 and 50°C at -300 mbar, until complete dryness was achieved (no further weight loss recordable). It was subsequently plugged with a silicon bung before being sealed with molten bee's wax in order to avoid any water vapour contact (Hogan and Buckton, 2000). The glass-crushing ampoules were always handled wearing latex gloves to prevent deposition of dirt on the outer surface of the ampoule. The sealed ampoule was then placed in the ampoule holder, which was then inserted in the stirrer unit containing 100 mL of distilled water. The complete unit was lowered into the equilibrium position of the solution calorimeter channel of the TAM. The stirrer was operated at 600 rpm. After immersion and achievement of thermal equilibrium, the glass ampoule was pushed down by hand. On achieving a steady baseline (corresponding to a standard deviation of the experimental data points of less than 5 μK), the ampoule was broken to initiate the reaction and allow the enthalpy of solution to be measured. Following the break, a second electrical calibration was carried out. This supplied information about the background thermal energy (heat evolved from the stirrer action for example) upon which it could base its calculation through direct comparison of heat involved.

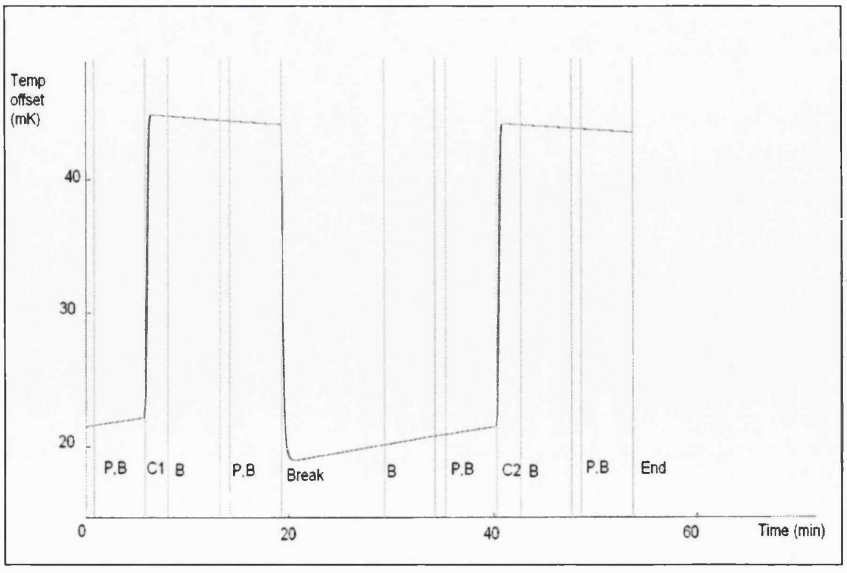

Figure 2.15. *Analysis example of a crystalline lactose sample by solution calorimetry (P=pause, B=baseline, C=calibration).*

An example of experimental raw data can be seen in Figure 2.15. The experiment sequence included the following sections:

- Pause (P): the different pauses allowed verification that both the reaction vessel and the water bath were in thermal equilibrium.

- Baseline (B): the different signals recorded resulted from stirring and noise. These baselines enabled the determination of parameters of the system such as the constant steady-state temperature (infinite temperature) and the calorimeter time constant.

- Calibration (C): calibrations consisting of a heating period followed by a waiting period were performed to calculate the calibration constant, which is an expression for the heat capacity of the reaction vessel (including the sample and detectors). The heat evolved by the experimental reaction is obtained by multiplying the change in temperature by this constant. A known amount of energy was supplied to the system by the heater to duplicate the thermal energy accompanying the reaction. Post-reaction calibration (C2) was regarded as more reliable than pre-reaction calibration (C1), since it reflected the presence of the solute and broken glass.

- Break: this section was automatically ended after 10 minutes and the instrument proceeded to the next section.

- End: the experiment concluded automatically when the End event in the experiment was reached.

2.3.6. Inverse gas chromatography

Inverse gas chromatography (IGC) is a direct extension of conventional gas chromatography. A common aim is to determine the composition of an unknown gaseous or liquid phase. In gas-solid chromatography, an unknown solute in a gas stream (corresponding to the mobile phase) passing over a known substrate (corresponding to the stationary phase) will adsorb and desorb repeatedly as it passes over the surface of the substrate. Gas separation occurs because of differences in the position of adsorption equilibriums between the gaseous components of the sample and the stationary phase. In recent years, IGC has been used in the study of batch to batch variability of both active and excipient (Ticehurst *et al.*, 1994; Ticehurst *et al.*, 1996; Feeley *et al.*, 1998; York *et al.*, 1998). The influence of milling (Ohta and Buckton, 2004) and that of humidity (Newell *et al.*, 2001b) on surface free energy was also investigated with this technique.

To conduct an IGC experiment, the solid material to be investigated is packed within a glass column. Well-characterised volatile probe molecules of known properties pass through the column under the flow of an inert gas. The simplest type of study that can be undertaken is at low solute concentration and is termed infinite dilution IGC. This technique allows determination of the substrate/solute interactions in the absence of solute/solute interactions. In this concentration region, chromatographic peaks are essentially Gaussian in shape and the retention volume V_n is independent of the solute concentration. Infinite dilution is verified by injecting smaller amounts of probe until the probe retention time does not change significantly with the amount of probe injected. A solute molecule, even without interacting with the adsorbent surface, requires time to pass through the column. This dead time t_0 is experimentally measured using a non-interacting standard such as methane.

From the retention time (t_r) of the probe, the net retention volume V_n can be determined according to Equation 2.3 developed by Schulz *et al.* (Schultz *et al.*, 1987):

$$V_n = JF(t_r - t_0) \qquad \text{[Equation 2.3]}$$

Where F is the carrier gas flow rate (in mL/min) and J the compressibility correction factor for the pressure drop over the column, taking account the compression of the gas.

This correction factor J is given by Equation 2.4 as follows:

$$J = \frac{3}{2}\frac{\left(P_{in}/P_{out}\right)^2 - 1}{\left(P_{in}/P_{out}\right)^3 - 1} \qquad \text{[Equation 2.4]}$$

where P_{in} is the pressure at the inlet and P_{out} the pressure at the outlet (normally equal to the ambient pressure).

2.3.6.1. Determination of the dispersive component of surface energy

The free energy of adsorption, resulting from polar and non-polar interactions, for a gaseous probe molecule under isothermal conditions is given by the following equation:

$$\Delta G°_A = \Delta G^D_A + \Delta G^{SP}_A \qquad \text{[Equation 2.5]}$$

Where ΔG^D_A is the non-polar free energy of adsorption and ΔG^{SP}_A the acid/base or specific free energy of adsorption.

$\Delta G°_A$ is also expressed by the equation:

$$\Delta G°_A = RT\,lnV_n + C \qquad \text{[Equation 2.6]}$$

Where R is the ideal gas constant, T the absolute temperature and C an empirical constant that takes into account the weight, the surface area and the vapour pressure of the probes in the gaseous state.

The work of adhesion W_{adh} per surface area between an adsorbate and an adsorbent is related to $\Delta G°_A$ by:

$$\Delta G°_A = N\, a\, W_{adh} \qquad \text{[Equation 2.7]}$$

where N is Avogadro's number and a the cross sectional area of the adsorbed molecule.

In the case of a non-polar liquid (L) adhering onto a solid (s), the work of adhesion, W_{adh}, is generally expressed as the geometric mean of the dispersive components of the solid (γ_S^d) and the liquid (γ_L^d) (Fowkes, 1964)

$$W_{adh} = 2\sqrt{\gamma_s^d \gamma_L^d} \qquad \text{[Equation 2.8]}$$

Thus by combining Equations 2.6, 2.7 and 2.8 we obtain:

$$RT \ln V_n = 2N\sqrt{\gamma_S^d}\, a\sqrt{\gamma_L^d} + C \qquad \text{[Equation 2.9]}$$

Typically, the free energy of adsorption of non-polar probes onto solid material is determined from a plot of RT ln V_n as a function of the dispersive component of alkanes (C_{10} to C_6), as shown in Figure 2.16. The slope of the line is equal to $2N\,(\gamma_S^d)^{1/2}$ from which the surface energy γ_S^d can be calculated. The values for a and γ_L^d were obtained from the literature (Schultz *et al.*, 1987; Nardin and Papirer, 1990).

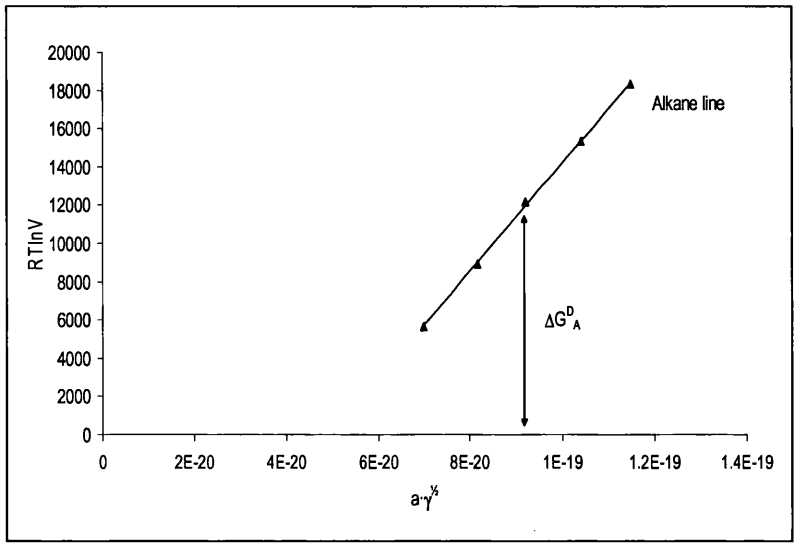

Figure 2.16. *Illustration of the free energy of adsorption of alkanes as a function of a* $(\gamma s^d)^{1/2}$.

2.3.6.2. Determination of specific polar interactions

The total free energy of adsorption is the result of non-polar and polar forces. Polar probes can interact with a polar surface by both dispersive and polar interactions. To calculate the specific interaction, polar probes are plotted with the alkanes on a graph of $RT\ ln\ V_N$ versus γL^d. Polar probes are located above the alkane line. The vertical difference between the polar probe and the alkane line gives the specific energy of interaction ($\Delta G°_A{}^{sp}$) (Figure 2.17). The difference in y-values between the polar probe and the x-axis is equal to the total free energy of adsorption.

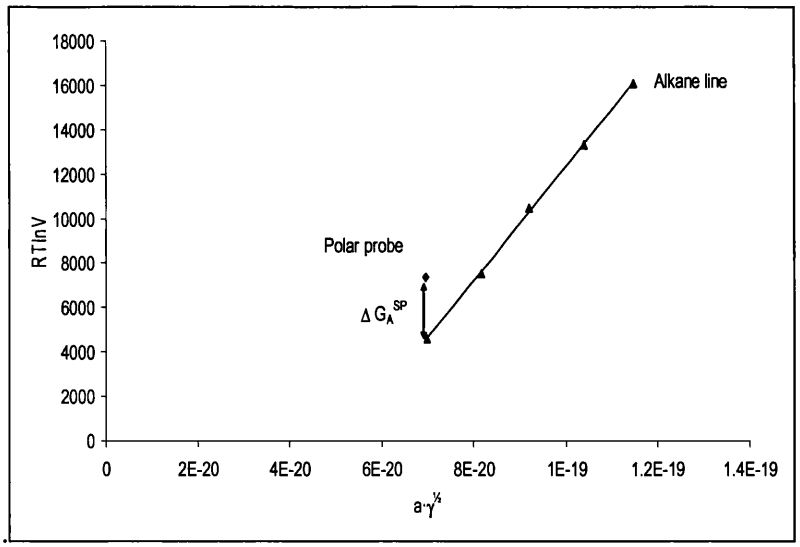

Figure 2.17. *Determination of specific polar interactions by IGC.*

The specific interactions of the polar molecules with the solid substrate can be used to determine the acid and basic constants. According to the Gutmann (Gutmann, 1978) acid-base concept, each probe is classified as either a Lewis acid (electron acceptor) characterised by a corrected acceptor number *AN,* or a Lewis base (electron donor) characterised by a donor number *DN*. Riddle and Fowkes (Riddle and Fowkes, 1990) corrected *AN* to *AN** by taking into account the van der Waals force contribution. The specific free energy of adsorption can then be used for the determination of the surface acceptor (K_A) and donor (K_B) parameters:

$$\Delta G°_A{}^{sp} = K_A DN + K_B AN^* \qquad \text{[Equation 2.10]}$$

Where *DN* and *AN** are Gutmann's numbers for the probes and K_A and K_B the acid and base parameters of the solid.

Plotting $\Delta G°_A{}^{sp}$ / AN* versus DN/AN* yields a straight line with a gradient of K_A and an intercept of K_B. Thus, the acid and basic parameters can be obtained from the slope and intercept respectively.

2.3.6.3. Column preparation

In all IGC experiments pre-treated columns (6 mm outer diameter, 3 mm inner diameter, and 30 cm long) were used. Treatment with dimethyldichlorosilane (Repelcote®, UK) was performed to ensure that the surface was hydrophobic and non interactive with any gaseous probe (Mohammad and Fell, 1982). Using a small funnel 300 to 500 mg of powder was poured into the column, whose bottom end had been previously plugged with DMCS silated wool (Chrompack). The powder within the column was packed by vertical tapping for 10 minutes (until no further settling was observable) using a tapping device supplied by Surface Measurement Systems. After completion, the top end of the column was plugged with more silated wool. The column was checked visually to ensure that no cracks or channels were present before being installed in the IGC.

2.3.6.4. Apparatus

Experiments were performed using an inverse gas chromatograph from Surface Measurement Systems (UK). It is comprised of three modules: a flow control module, a probe oven module and a column module, as illustrated in Figure 2.18. The flow control module consists of six flow controllers enabling the regulation of the relative composition of the different mixtures: a flow of dry helium as the reference and a mixture of helium and organic solvent vapours to produce the elutant gas mixture. The elution mixture (250 µL) is then injected by an automated valve into the reference gas flow and passes through the column to the two detectors, attached in series at the column outlet. A Hewlett Packard 6890 series gas chromatograph (GC) was used to control the solvent temperature. The GC data acquisition system was used to record data from both the flame ionization detector (FID) and the thermal conductivity detector (TCD). This combination of detectors allows differentiation between organic solvent and moisture. A separate column oven was used to control the sample temperature. Data was analysed using the SMS *i*GC Analysis Software, Version 1.6.

2.3.6.5. Experimental

After equilibrium in the column oven for 4 hours, probes were injected at a concentration of 4 % (v/v) using headspace sampling and each column was tested three times. This equilibrium time enabled any weakly adsorbed contaminant to be removed from the sample surface. No humidity program was used and all experiments were performed at 0 % RH. Both the column oven and solvent oven temperatures were kept at 30°C. Methane was injected as the non-interacting reference probe. Depending on the shape of the peaks and the pressure drop along the column, the helium gas flow rate was adjusted. In most cases, a rate of 10 mL/min was chosen.

The dispersive component and the specific interaction were determined using the different probes described in Table 2.4.

Vapour probe	Cross sectional molecular area *a* (m^2)	γ_L^d (mJ/m^2)	AN* (kcal/mol)	DN (kcal/mol)
Decane	7.5E-19	0.0234	0	0
Nonane	6.9E-19	0.0227	0	0
Octane	6.3E-19	0.0213	0	0
Heptane	5.73E-19	0.0203	0	0
Hexane	5.15E-19	0.0184	0	0
Acetone	3.4E-19	0.0165	2.5	17.0
Chloroform	4.4E-19	0.0250	5.4	0
Ethanol	3.53E-19	0.0211	10.3	19.6
Ethyl acetate	3.3E-19	0.0196	1.6	17.1

Table 2.4. *Properties of vapour probes required for IGC analysis.*

AN* is the corrected acceptor number (Mukhopadhyay and Schreiber, 1995), DN is the donor number (Schultz *et al.*, 1987), *a* is the cross sectional area (Schultz *et al.*, 1987; Nardin and Papirer, 1990) and γ_L^d is the dispersive component of surface energy of the liquid probes (Schultz *et al.*, 1987; Nardin and Papirer, 1990).

As previously described, IGC is gaining popularity as a method for assessing powder surface energy. Nevertheless, some points of caution should be noted in order to understand the results. Mukhopadhyay *et al.* (Mukhopadhyay and Schreiber, 1995) pointed out the dependence of the γ_s^d on the choice of the molecular cross sectional areas (*a*) for the alkanes. For a non-spherical molecule, the correct choice of the molecular area will depend on the orientation of the molecule. Moreover, "*a*" values are assumed to be constant regardless of the experimental temperature.

Probe conformation may change both due to changing kinetic aspects of the adsorbed molecule and temperature dependence of the force exerted by the adsorbing solid. At high temperatures the choice of "*a*" appears critical.

A second complication arises from the principle of operation: by injecting probes at infinite dilutions, it is assumed that adsorbate-adsorbate interactions can be ignored and only adsorbate-adsorbent interactions are involved. However, solid surfaces are known to be heterogeneous with broad site energy distribution. Vapour probes will therefore preferentially interact with the most energetic dispersive sites on the powder surface (Planinsek and Buckton, 2003). IGC determinations will therefore lead to higher values of γ_s^d than those obtained from conventional contact angle measurements. A relevant confirmation of this was given by Dove *et al.* (Dove *et al.*, 1996) who studied the surface energies of both caffeine and theophylline using IGC and two contact angle measurement methods.

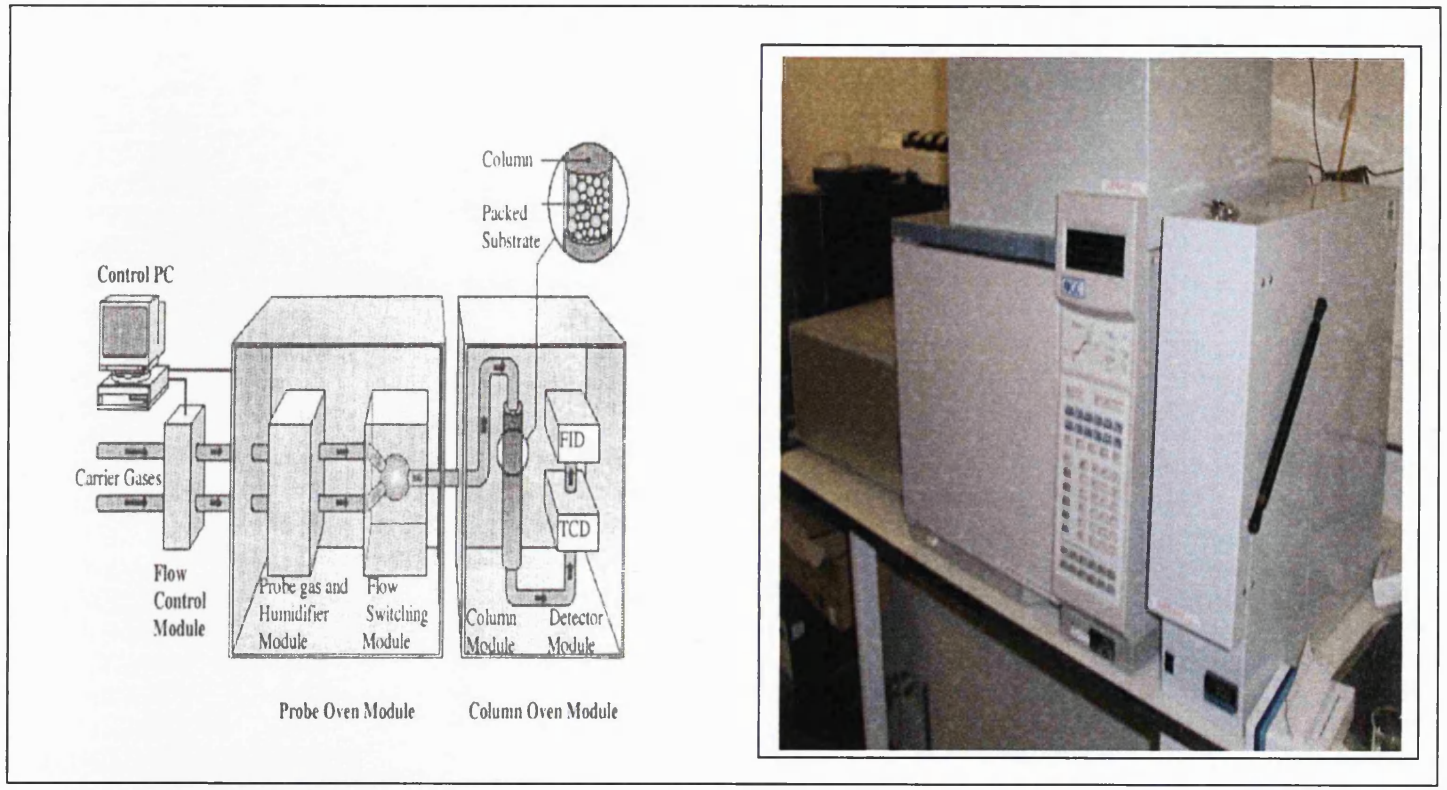

Figure 2.18. *Schematic diagram (Sing, 2001; Newell et al., 2001b) and photograph of the IGC apparatus.*

2.3.7. Dynamic vapour sorption (DVS)

Vapour sorption studies employing humidity controlled ultra-sensitive recording microbalance systems are often used to study the sorption/desorption of a solvent to a powder. Buckton *et al.* (Buckton and Darcy, 1995) studied gravimetrically the process of crystallisation of lactose, demonstrating the usefulness of this technique in detecting the presence of amorphous material at a concentration as low as 0.05 % (w/w). Columbano *et al.* (Columbano *et al.*, 2002), Hogan *et al.* (Hogan and Buckton, 2001) and Ticehurst *et al.* (Ticehurst *et al.*, 2000) respectively studied the recrystallisation of amorphous SS, amorphous raffinose and micronised revatropate hydrobromide using this technique. Many amorphous materials are plasticized by absorbed water, causing the glass transition temperature to drop below the experimental temperature. This newly acquired mobility allows rapid crystallisation. Upon crystallisation, the absorbed water is displaced and the resulting mass loss at elevated RH monitored.

The DVS system (Service Measurement Systems, UK) is based on a Cahn D-200 microbalance, which is able to detect weight variations of $\pm$ 1.10^{-4} mg. The sample and the reference empty glass pans are located on opposite sides and are attached to the microbalance by hand down wires. Each pan is enclosed in a glass tube and can be accessed by lowering the inferior part of the tube, after removing the metal clip holding the two parts in place. This microbalance is enclosed in an incubator in which the temperature (ranging from 25 to 80°C) and humidity (ranging from 0 to 98 %) are controlled. A schematic representation and a photograph are shown in Figure 2.19. Humidity is controlled by flow of dry nitrogen through switching valves, which regulate the total amount of gas passing through the humidification stage. This is enabled by the presence of two flow controllers that produce the required relative humidity. The sample and reference pans are exposed to a continuous gas flow set to 200 mL /min. The reference pan counteracts any effect on the sample pan and therefore any change in the weight of the sample, recorded as a function of time and humidity, represents the change due to the powder only.

Prior to an experimental run, the sample pan was cleaned using distilled water followed by absolute alcohol. To remove any residual solvent, the sample pan was allowed to dry at 0 % RH before being exposed to 90 % RH for 10 minutes to remove any static which may have developed during the cleaning process. The RH was then returned to 0 % and the balance zeroed until a steady baseline was observed. The criterion used to define the steady baseline was the % *dm/dt* value. The *dm/dt* value represents the rate of change of the sample mass as the percentage of the initial mass of the sample per 20-second time interval. The sample was considered dry when the *dm/dt* value was less then 0.0001.

Once this had been achieved, samples of 30 mg (± 10 %) were loaded onto the glass pan of the DVS. All experiments were performed at 25°C. The programme, which can be divided into three different sections, was then initiated.

- Initial drying step (0-6h) by exposing the sample to dry nitrogen (0 % RH);
- Exposition to 80 % RH to allow water uptake and crystallisation (6-16h);
- Final drying step (16-22h) by reexposing the sample to dry nitrogen (0 % RH).

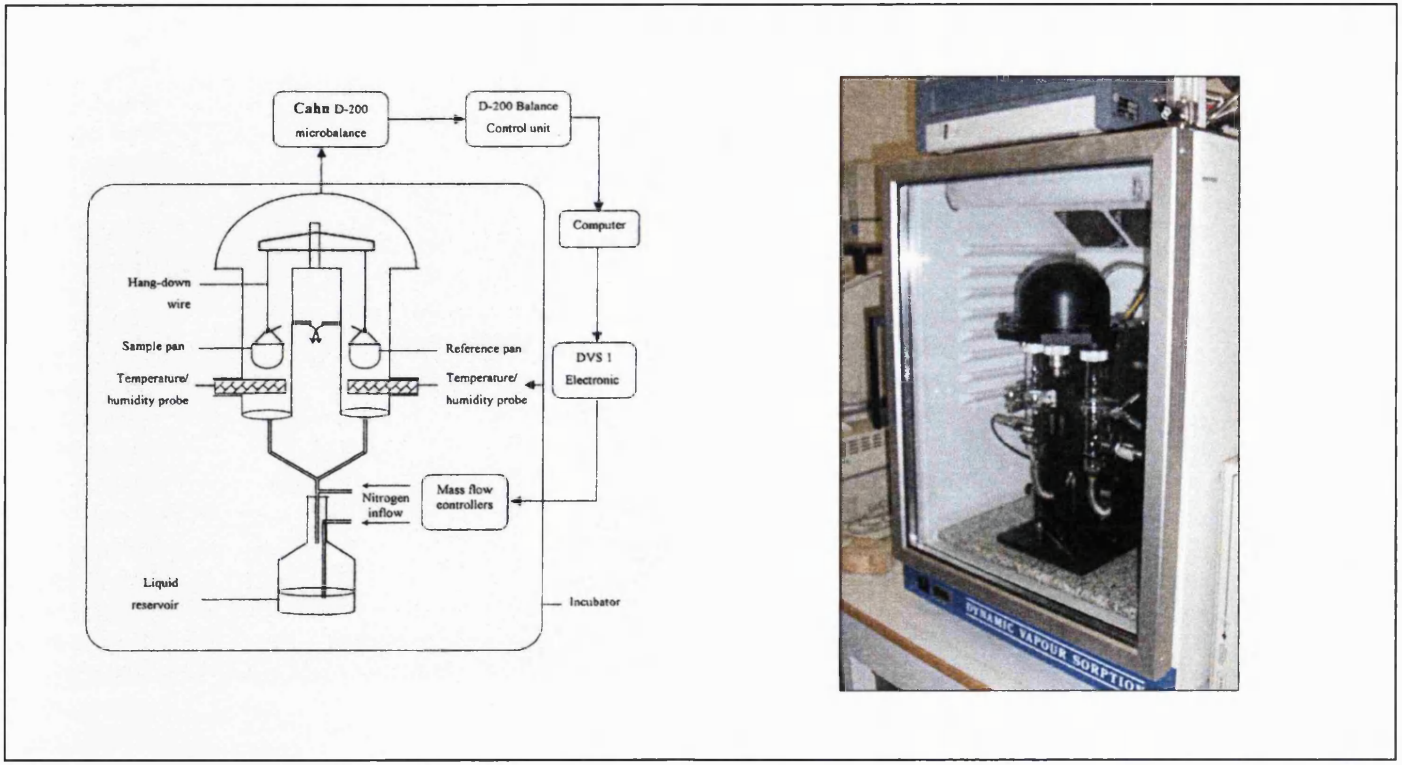

Figure 2.19. *Schematic diagram taken from Ahfat, 1998 and photograph of a DVS.*

Chapter 3

Influence of different grades of lactose on *in vitro* drug deposition

3.1. Summary

The source, quality and inter-batch control of lactose monohydrate is of utmost importance for the reproducibility of dose delivery performance of DPIs. Different qualities of lactose monohydrate are likely to influence the performance of a DPI (Steckel and Bolzen, 2004). This chapter describes first a blend homogeneity characterisation study for a formulation containing 4 % BDP using the Clickhaler® reservoir device, and then a comparative study of the influence of the surface characteristics of three different commercially available sources of α lactose monohydrate for inhalation purposes using the two selected drug models, SS and BDP. The first part of the study showed that the formulation complied with acceptance criteria according to compendial requirements. In the second part of the study, the measurements displayed a significant lactose dependence on the deposition of the BDP based formulations. In contrast, there was less variation in performance with the formulations using the hydrophilic drug model SS. Physico-chemical characterisation was undertaken in an attempt to correlate the *in vitro* performance with surface properties of the lactose. The findings of this study indicate that the presence of fine lactose particles on the carrier surface exerts a major influence on aerosol dispersion of BDP whereas deposition of SS is more dependent on the surface energy properties of the carrier surfaces.

3.2. Introduction

Steckel *et al.* (Steckel *et al.*, 2004a) investigated the aerosol behaviour from the Flowcaps® inhaler using five different batches of lactose monohydrate from three different manufacturers (Meggle, Borculo and DMV). BUD and SS were chosen as a hydrophobic and a hydrophilic drug respectively. Fine particle fractions were obtained using a multistage liquid impinger at an airflow of 30 L/min. They concluded that the average particle size of the different lactoses had a significant influence on the emptying behaviour of the capsules. For example, the gravitational force in the case of Pharmatose 110 or Inhalac 70, with an average particle size above 100 µm, was too high to obtain an optimal particle entrainment for this particular type of capsule-based DPI.

Reproducible delivery from the capsule was achieved using Lactohale LH 200 and Pharmatose 325M. Lactohale LH 200 was found to be more efficient than Pharmatose 325M for both drugs (43.6 vs. 14.6 % for SS and 20.8 vs. 12.3 % for BUD). The particle size distribution data revealed that the Lactohale LH 200 had a higher fine content ($d_{10\%}$=12 µm) compared to the Pharmatose 325 M ($d_{10\%}$=31 µm). Passivation by the fines of the high-energy sites of the lactose surface was put forward to explain those observations. In another study, Podczeck (Podczeck, 1998) examined ten batches of medium grade lactose monohydrate from three different manufacturers and salmeterol xinafoate as a drug substance. The author stated that a simple interchange of the carrier in terms of brand or grade appeared impossible due to the inherent physico-chemical properties of the different lactose used.

To obtain the required particle size distribution for the carrier, the crystals are fractionated by means of mechanical sieving procedures. This process may have an impact on the amorphous content on the surface of the lactose crystals, leading to performance differences. Processes such as drying and milling can induce disorder in the resulting apparent crystalline material (Buckton, 1997). The presence of a small amount of surface disorder may influence the product performance. The amorphous regions can take up more water than the crystalline regions. Ahlneck *et al.* (Ahlneck and Zografi, 1990) have shown that, assuming that essentially all water (e.g. 0.5 % (w/w)) is preferentially taken up by these amorphous regions (e.g. 0.5 % (w/w)), the associated water content would represent a huge amount of water for these small areas of the sample (i.e. 50 % (w/w)).
Prior to characterising the different carriers it is essential to describe briefly the different possible states of pharmaceutical materials.

- Crystalline state

A crystalline material can be characterised by repetitive spacing of constituent molecules in a regular three-dimensional array. Four main types of crystalline solids can be differentiated depending on the type of forces holding the crystals together: (1) ionic crystals (e.g. sodium chloride), composed of charged species held in place in the lattice by electrostatic forces; (2) covalent crystals (e.g.

diamond) in which atoms are connected by a framework of covalent bonds (atoms sharing their valence electrons); (3) metallic crystals (e.g. copper) comprising ordered arrays of identical cations and (4) molecular crystals (organic crystals), which are held together by non-covalent interactions including hydrogen bonds and non-covalent attractive forces. The latter depend on the polarisability, electronic distribution and dipole moments of the molecules.

Periodicity and symmetry characterise the crystalline state. Seven different types of crystal systems have been described: cubic, monoclinic, triclinic, orthorhombic, trigonal, hexagonal and tetragonal. During crystallisation, if the rate of growth is equal in all three directions, then a cubic shape will be formed. If the growth is limited to one or two directions, the crystal will be either a needle-shaped or a plate-shaped respectively. These differences in crystal morphologies will have large repercussions on dry powder inhalation systems. For example, most commercially available lactose crystals used as carriers in DPI formulations present irregularities on their surface (Tee *et al.*, 2000). In a recent study, Larhrib *et al.* (Larhrib *et al.*, 2003) investigated the potential use for DPI technology of engineered lactose crystals, using a one-step crystallisation process from acetone/water co-solvent mixtures. Depending on the water/acetone ratio, different crystal morphologies were obtained, from needle to tomahawk like shape, and different elongation ratios (defined as length expressed as a function of the width) calculated. The impact on the *in vitro* deposition of SS varied from 29.2 (2.2) % FPF to 5.1 (1.6) % FPF depending on the type of lactose crystals chosen.

The relative size of the faces of a particular crystal can vary considerably giving rise to different habits. Crystal habits are crystals with the same chemical composition and crystal structure but with different general shapes obtained during its growth. A substance capable of crystallising into different, but chemically identical, crystalline forms is said to exhibit polymorphism (e.g. graphite (hexagonal) and diamond (regular) forms of carbon). Polymorphism can be a result of different crystallisation conditions such as the crystallisation solvent, temperature and rate of cooling. Polymorphism is of utmost importance since different polymorphs will exhibit different fundamental characteristics (i.e. flowability, compression properties, solubility and solid-state stability). During crystallisation, solvent molecules may be entrapped with molecules of the given

sample into a unique structure. The solvent may be either in stoichiometric or non-stoichiometric proportion. If the solvent is organic, the crystals are called solvates; if the solvent is water, then the solvate is specifically called a hydrate. An interaction between the host molecule and the solvent molecule in the form of hydrogen bonding leads to the incorporation.

- Amorphous state

As in a crystalline solid, an amorphous solid may have short range molecular order (including hydrogen bonding) but no long range three dimensional order of molecular packing (Yu, 2001). As a result, amorphous solids have a lower energetic barrier to overcome in order to enter solution than a regularly structured crystalline solid. Amorphous materials have been therefore widely used to improve the dissolution of poorly soluble compounds and accelerate the dissolution of others. The amorphous material is usually described by the process of supercooling from the melt (Craig *et al.*, 1999) as seen in Figure 3.7. When the temperature is decreased from the liquid state to the melting point (T_m), an exothermic crystallisation occurs. This is followed by a sudden reduction in the free volume (defined as the difference between the total volume and the actual volume displaced by the constituent molecules) and in the enthalpy of the system. For a glass-forming material, the rapid cooling ($>10^5 K\ s^{-1}$) of the liquid below its melting point (T_m) creates a metastable state, also called "rubbery state", in which the molecules within the liquid do not have enough time to orientate themselves into the crystal lattice formation.
The typical viscosity of supercooled liquids is in the region of 10^{-3} to 10^{12} Pa.S. Upon further cooling, the viscosity of the liquid increases and a temperature is reached at which the molecular mobility is so low that the rearrangement to achieve equilibrium state before further cooling does not occur. This temperature is known as the glass transition temperature (T_g) and the dynamically relaxed solid ("rubbery state") undergoes a transition to the dynamically "kinetically frozen" solid ("glassy state"). The glassy state possesses an elevated amount of enthalpy, entropy and a higher specific volume than the rubbery state. The critical temperature at which the configurational entropy of a system is zero is called the Kauzmann temperature (T_K).

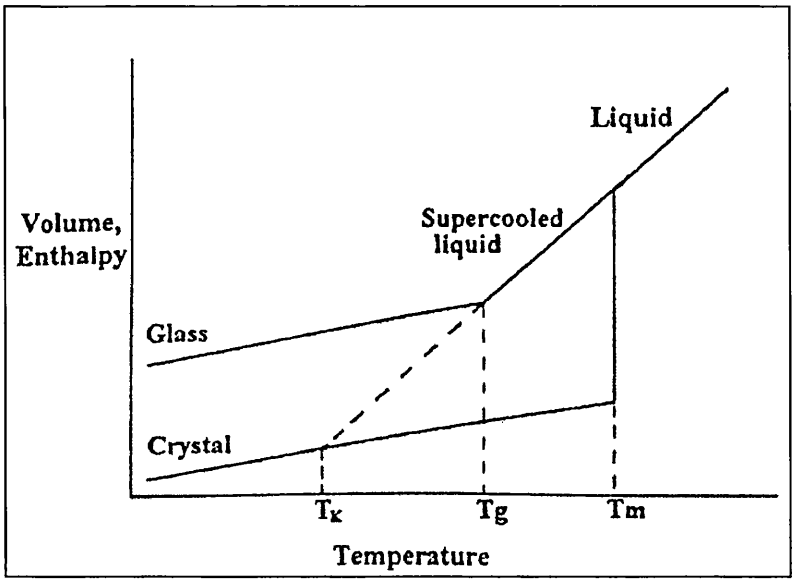

Figure 3.1. *The process of glass transition by cooling the liquid melt, reproduced from Ahneck (Ahlneck and Zografi, 1990).*

The glass transition temperature is characteristic of each system and its knowledge is really important since it can be used to predict the storage conditions. The addition of certain plasticizers (e.g. water) can lower the T_g. Plasticization at a molecular level increases the molecular space, leading to a change in apparent viscosity. Water with its very low T_g (-136°C) (Johari *et al.*, 1987), small molecular size and hydrogen bonding ability can be absorbed within the amorphous material. However, a recent paper (Yue and Angell, 2004) concluded that the glass transition of water could not be directly probed.

The effect of water plasticization on the T_g of an amorphous material can be predicted using the equation developed by Gordon and Taylor (Gordon and Taylor, 1952).

$$Tgmix = \frac{w_1 Tg_1 + kw_2 Tg_2}{w_1 + kw_2} \qquad \text{[Equation 3.1]}$$

Where T_{gmix} is the T_g of the mixture, T_{g1} and T_{g2} the glass transition temperatures of component 1 (solid) and component 2 (water), w_1 and w_2 the weight fractions of the solid and water respectively

k is a constant calculated from the density (ρ) and the T_g of the components according to:

$$k = \frac{Tg_1\rho_1}{Tg_2\rho_2} \qquad \text{[Equation 3.2]}$$

- Transition from amorphous to crystalline state

Amorphous forms are less thermodynamically stable than crystalline forms and, given the opportunity, will eventually recrystallise after nucleation and growth of crystals. Different factors can affect the rate of crystallisation such as temperature and the presence of plasticizers (Yu, 2001). For amorphous materials, this transition is only possible if the mobility of the molecules is sufficient to allow the rearrangements to take place. In fact, crystallisation occurs once the experimental temperature is above the T_g. Nucleation, which can be defined, as the formation of a small amount of crystalline material, may be either spontaneous or artificially induced. For spontaneous nucleation a group of constituent molecules must coagulate and orientate in a fixed lattice. Artificial nucleation occurs when seed crystals or impurities are included in a supersaturated system. The formation of these initial or primary nuclei is the first step that initiates the crystallisation process. Crystal growth takes place once stable nuclei are formed. Controlled crystallisation is a potential method for engineering carrier (Larhrib *et al.*, 2003) or drug microcrystals (Ikegami *et al.*, 2002) through manipulation of the crystallisation process.

3.3. Aims of the study

In the present study, the presence of a correlation between the *in vitro* deposition of DPI formulations and the physico-chemical properties of the chosen lactose carriers was investigated. The main objectives were to:

- Evaluate the Clickhaler® as a reservoir device;
- Compare the deposition performances of three different marketed grades of lactose blended with SS or BDP;
- Examine the physico-chemical properties of the lactose carrier particles to correlate to the aerosol deposition from the two drug models.

3.4. Materials and methods

Regarding the reproducibility study with the Aero Flo 65 as a carrier, this grade of lactose was blended with BDP so that the final concentration of the drug was 4 %. Typically, 4.8 g of lactose was mixed with 0.2 g BDP in a 14 mL glass container. This was carried out using a Turbula mixer for 30 minutes at 42 rpm. Figure 3.1 is an image of the binary mixture consisting of the coarse lactose and BDP. After content uniformity assessment, the formulation was tested in the Clickhaler® as previously described in chapter 2.
Ten consecutive runs were tested. In the second part of the work, three different lactose grades (Aero Flo 65, Pharmatose 325M and Lactohale LH 100) were blended with 4 % of the two model actives. The same blending conditions were used throughout.

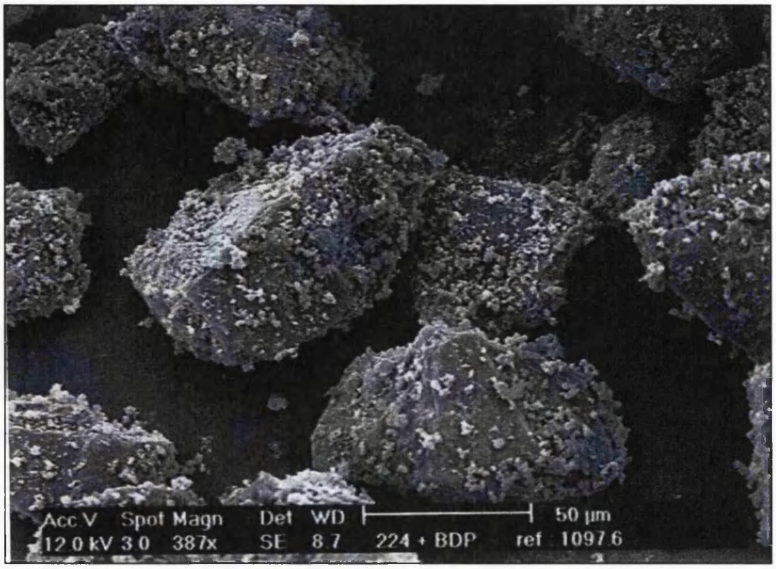

Figure 3.2. *Co-processed coarse carrier with an active.*

The physico-chemical properties of the different carriers and active compounds were characterised using the techniques described in chapter 2.

3.5. Results and discussion

3.5.1. Deposition study

3.5.1.1. Repetability study with BDP

A primary requirement for a dry powder formulation is the necessity for dose uniformity. Regulatory bodies have progressively increased the specifications for this requirement. In the European Pharmacopoeia (2002), test B is applied to the uniformity of pre-dispensed dose of powders for inhalation which states: " The preparation complies with the test if not more than one individual content is outside the limits 85 per cent to 115 per cent of the average content and none is outside the limits of 75 percent to 125 percent of the average content.

The preparation fails to comply with the test if more than three individual contents are outside the limits 85 percent to 115 percent of the average content or if one or more individual contents are outside the 75 per cent to 125 percent of the average content. If two or three individual contents are outside the limits 85 per cent to 125 per cent but within the limits of 75 per cent to 125 percent, a

second tier test is required where one determines the individual contents of another twenty dosage units taken at random. The preparation complies with the test if no more than three individual contents of the thirty units are outside the limits of 85 per cent to 115 percent of the average content."

The measured ED was normalised to the average of the 10 single delivered doses and the limits of ± 25 % of the average delivered dose were calculated. The data for the aerosol deposition study is listed in Table 3.1 and shown in Figure 3.2.

BDP deposition patterns from a Foremost Aero 65 carrier	ED (µg)	RD (µg)	FPF (%)
Run 1	1010	449	44.5
Run 2	910	342	37.59
Run 3	942	373	39.7
Run 4	707	218	30.92
Run 5	727	227	31.3
Run 6	874	335	38.3
Run 7	1097	433	39.5
Run 8	878	310	35.34
Run 9	980	328	33.45
Run 10	1014	367	36.2

Table 3.1. *In vitro BDP deposition patterns from ten repetitive actuation runs using Foremost Aero 65 as lactose carrier.*

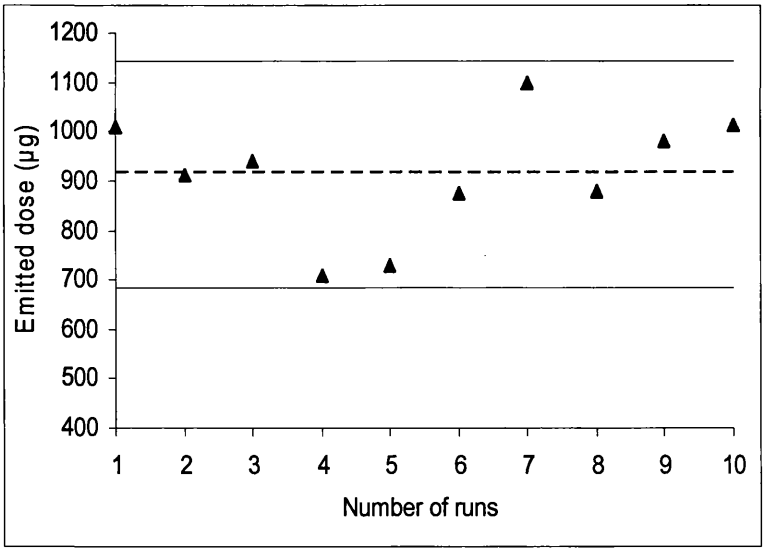

Figure 3.3. *Repetability assessment of the BDP emitted dose following 10 runs (each corresponding to 10 actuations).*

As shown in Figure 3.2, all actuations for this formulation complied with the set criteria for content uniformity, indicating that the flow properties of the carrier are suitable for the Clickhaler®. The doses were not delivered particularly consistently (especially run 4 and 5 which are both below the average) but still within the regulatory requirements. One possible explanation may be that the highly cohesive behaviour of BDP led to agglomeration, causing poorer flowability and increased variations in the delivered dose.

3.5.1.2. Results for aerosol deposition studies of SS and BDP formulations

The data for the evaluation of the influence of the lactose carrier on the deposition pattern of BDP and SS using the TSI are listed in Tables 3.2 and 3.3.

Material	ED (µg)	RD (µg)	FPF (%)
Aero Flo 65	954 (52)	388 (55)	40.6 (3.5)
Pharmatose 325M	1108 (35)	205 (35)	18.4 (2.7)
Lactohale LH 100	1292 (10)	201 (10)	15.6 (0.8)

Table 3.2. *Influence of the different lactose qualities on the BDP deposition patterns expressed as means (n=3).*

Different BPD deposition profiles were obtained depending on the grade of lactose chosen as the carrier (Table 3.2). It was found that the EDs of BDP of the different formulations were greatly influenced by the type of lactose carrier used. In particular, the ED for the Aero Flo 65 was 954 (52) μg, which was significantly lower than that for Pharmatose 325M, 1108 (35) μg, which was also lower than that for Lactohale LH 100, 1292 (10) μg. The differences in EDs may be attributed to one of many factors such as different densities or powder flow properties which could have resulted in different packing extents in the device reservoir and measuring cups. Changes in the grade of lactose chosen also influenced the mass of respirable BDP released from the different formulations. The RD was greater for the Aero Flo 65 (388 (55) μg) compared to both Pharmatose 325M (205 (35) μg) and Lactohale LH 100 (201 (10) μg). The differences between the carriers were further highlighted in the calculated FPF of BDP. The Aero Flo 65 displayed a FPF that was double that of the other grades of lactose (40.6 (3.5) % vs. 18.4 (2.7) % or 15.6 (0.8) %). The low fractions indicate that the drug does not separate well from those surfaces.

For SS formulations (Table 3.3), it was found that the EDs were less dependent than BDP on the type of lactose carrier used. The ED for the Aero Flo 65 was 1271 (61) μg, comparable to that of Pharmatose 325M, 1219 (125) μg, and slightly lower than that of Lactohale LH 100, 1477 (127) μg. The trend seen in the ED values for the SS formulations was also seen in the different RD values, with values ranging from 303 (53) μg for the Pharmatose 325M based formulation to 414 (37) μg for the Lactohale LH 100 based one. With respect to the FPF of SS deposited from the formulations under study, differences between grades are less marked with values ranging from 24.9 (3.2) % to 31.2 (0.9) %.

Material	ED (μg)	RD (μg)	FPF (%)
Aero Flo 65	1271 (61)	395 (12)	31.2 (0.9)
Pharmatose 325M	1219 (125)	303 (53)	24.9 (3.2)
Lactohale LH 100	1477(127)	414 (37)	28.1 (0.2)

Table 3.3. *Influence of the different lactose qualities on the SS deposition patterns expressed as means (n=3).*

This study highlighted the extreme importance of the lactose grade in DPI performance. It also showed clearly that a formulation performance is carrier and drug dependent. For example, using a cohesive drug such as BDP may affect the ED from Aero Flo 65 based formulation, whereas no apparent effect is noticeable when using SS. Such differences are not straightforward to explain and more thorough characterisation of the physico-chemical properties of the different lactose grades employed was needed to help in drawing hypotheses.

3.5.2. Physico-chemical properties of the different carriers

3.5.2.1. Particle morphology and size, and specific surface area of the different lactose carriers

The different lactose grades were characterised by SEM with a method identical to that described in Section 2.3.1. The individual crystalline coarse carrier particles adopted the characteristic tomahawk shape (Figure 3.3). The images are of carriers alone without the presence of the micronised drugs. The presence of clefts and fine particle lactose caused the surface to be regarded as rough. Close analysis of the SEMs suggested adherence of the small lactose particles on the coarse surface. The small particles were present to different extents in the samples used. Small differences in the surface texture and crystal form of the lactose particles could be seen: the Pharmatose 325M and the Aero Flo 65 appeared to be smaller than the Lactohale LH 100. Particle size measurements and specific surface area determination were performed to confirm these visual observations.

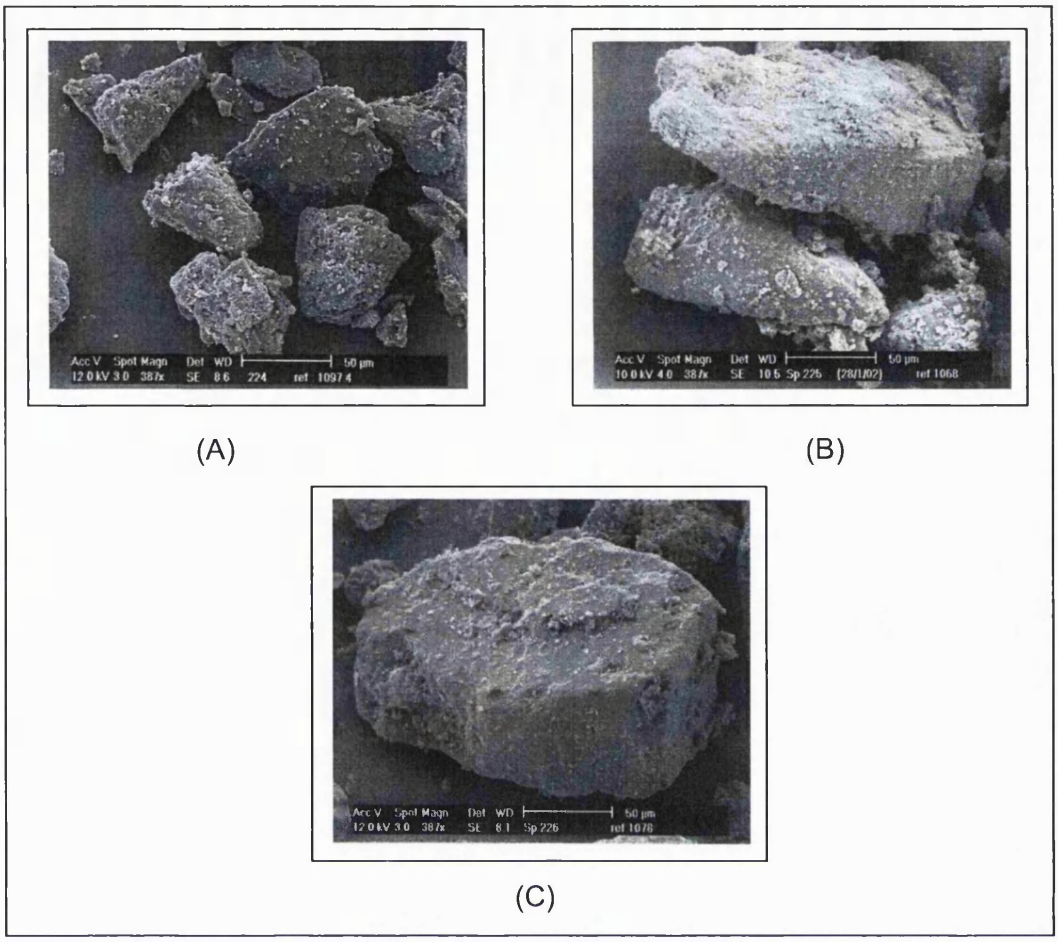

Figure 3.4. *Scanning electron micrographs of the different grades of lactose: Pharmatose 325M (A), Aero Flo 65 (B),and Lactohale LH 100 (C).*

The particles were sized by laser diffraction using a Mastersizer X (Malvern Instruments, UK). Particle sizing was carried out in accordance with Section 2.3.2. The results of particle size analysis of the lactose carriers are presented in Figure 3.4 and Table 3.4.

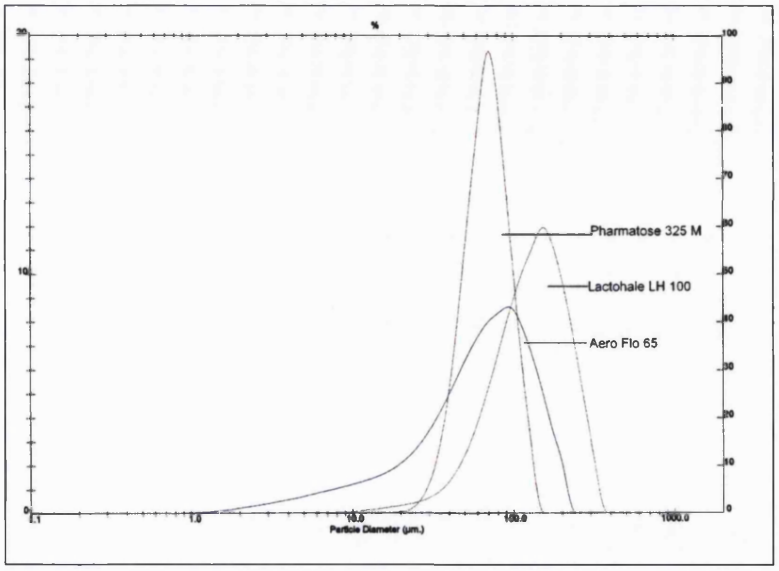

Figure 3.5. *Particle size distribution of the three different grades of lactose.*

Lactose grade	$d_{10\%}$	$d_{50\%}$	$d_{90\%}$	SPAN
Lactohale LH 100	57.8 (1.5)	134.8 (2.2)	238.4 (3.2)	1.35 (0.02)
Pharmatose 325M	44.1 (0.7)	68.3 (0.9)	100.0 (3.4)	0.82 (0.05)
Aero Flo 65	15.0 (3.1)	64.6 (1.8)	137.4 (2.6)	1.90 (0.1)

Table 3.4 *Particle size distribution parameters expressed as mean values (n=3).*

The lactose carriers all displayed bimodal distributions with narrow spans. Lactohale LH 100 had the largest volume median diameter (VMD 141 (2) μm). Pharmatose 325M and Aero Flo 65 exhibited the same VMD (70 (1) μm and 69 (1) μm). The wider particle size distribution of the Aero Flo 65 (SPAN of 1.90 (0.1)) compared to Pharmatose 325M (0.82 (0.05)) or Lactohale LH 100 (SPAN of 1.35 (0.02)) was mostly due to the large amount of fines in the Aero Flo 65 ($d_{10\%}$ =15 μm). Moreover the Aero Flo 65 had a large proportion of particles below 5 μm (4.8 %) whereas no such small particles were detectable in either Pharmatose 325M or Lactohale LH 100. Interestingly, this grade was also the most efficient in dispersing BDP particles, highlighting the role played by small fines. This type of effect of carrier on drug deposition efficiency in DPIs has been demonstrated previously (Zeng *et al.*, 1998; Louey *et al.*, 2003).

A trend was observed where the FPF of BDP increased as the carrier $d_{10\%}$ decreased (Figure 3.5 A) whereas SS deposition tended to be independent of the $d_{10\%}$ of the carriers (Figure 3.5 B). This confirmed that a carrier presenting a large amount of fine lactose particles was better at dispersing and deaggregating BDP than a carrier without fines. Such an improvement could not be confirmed with the hydrophilic drug model.

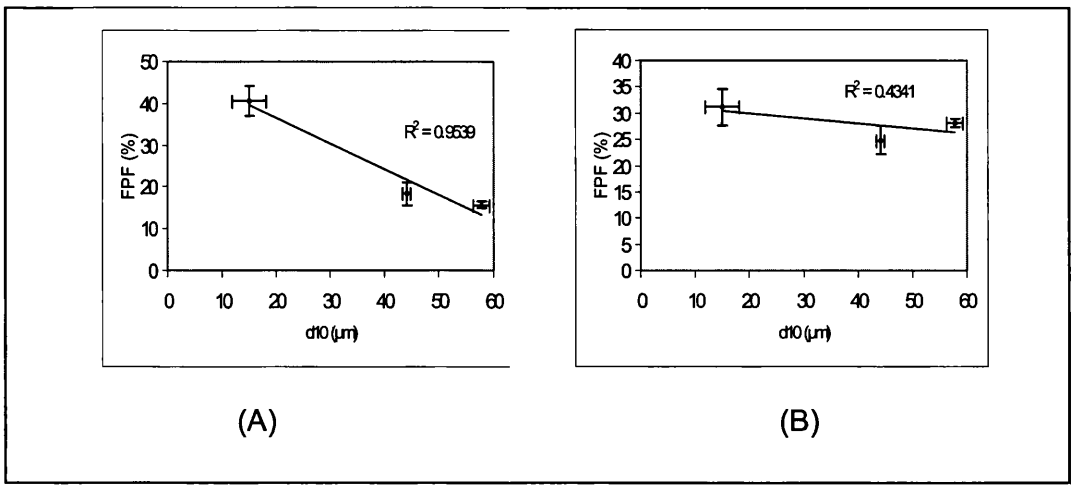

Figure 3.6. *Mean FPFs (n=3) of BDP (A) or SS (B) vs. mean $d_{10\%}$ values (n=3) of carrier.*

One possible explanation is that small Aero Flo 65 particles may, as well as possibly occupy the drug-binding sites on the coarse particle, disturb the BDP-BDP particle interactions and weaken the agglomerates, enabling more "single BDP particles" to be released from the carrier surface during inhalation.

The differences observed in the particle size measurements were supposed to be reflected in the specific surface areas (SSAs) of the different lactose carriers. This can be easily seen by considering both the area (A) (Equation 3.3) and the volume (V) of a sphere of diameter d (Equation 3.4).

$$A = \pi d^2 \qquad \text{[Equation 3.3]}$$

$$V = \pi d^3/6 \qquad \text{[Equation 3.4]}$$

Combining Equations 3.3 and 3.4 we obtain the surface area per volume [Equation 3.5]

$$A/V=6/d \qquad \text{[Equation 3.5]}$$

The SSAs of the different lactose grades were determined by the gas adsorption method based on the BET equation and performed on a Surface Area Analyser (SA 31000, Beckman Coulter UK) following the procedure described in chapter 2.

The results (Table 3.5) were in accordance with the particle size measurements: the Lactohale LH 100 displayed the largest VMD and therefore had the smallest surface area: 0.133 m^2/g. The Aero Flo 65 and Pharmatose 325M presented the same VMD but the Aero Flo 65 had the largest proportion of fines. Since those fines are likely to present a large surface area, the overall Aero Flo 65 surface exhibited a higher value (0.291 m^2/g) than Pharmatose 325M (0.218 m^2/g). The impact of SSA on the drug deposition is taken further into account in chapter 5.

Formulation	SSA (m^2/g)
Lactohale LH 100	0.133 (0.001)
Pharmatose 325M	0.218 (0.009)
Aero Flo 65	0.291 (0.001)

Table 3.5. *Specific surface areas of three different grades of lactose expressed as means (n=3).*

As already outlined in Figure 3.5 with the $d_{10\%}$ parameter, a correlation between BDP deposition and some characteristics of the carrier could be observed. A trend (r^2 = 0.7989) between SSA of the carrier particles and FPF of BDP can be seen in Figure 3.6 A. The correlation for SS was difficult to find with a r^2 value of 0.223 (Figure 3.6 B).

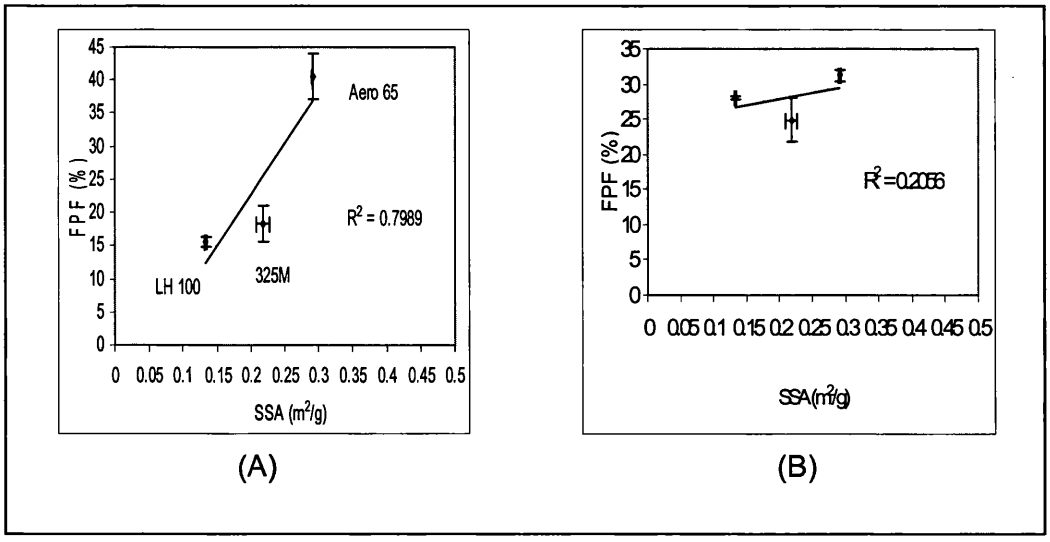

Figure 3.7. *Correlations FPFs of BDP (A) and SS (B) expressed as mean values (n=3) vs. SSAs (m^2/g) of carrier (n=3).*

3.5.2.2. Determination of crystallinity in the different materials

Pharmaceutical solids rarely exist as 100 % crystalline or 100 % amorphous states, so it was necessary to quantify the purity of the grade of lactose (e.g. traces of beta lactose) or the presence of amorphous material, generated during air-jet milling for example. X-ray diffraction was used in order to detect the presence of β-lactose, whereas solution calorimetry experiments were undertaken to measure the extent of crystallinity of the different carriers.

3.5.2.2.1. X-ray diffraction

Drapier-Beche *et al.* (Drapier-Beche *et al.*, 1997) recorded the X-ray peaks obtained by diffraction of two crystalline forms of lactose (α-lactose monohydrate and β-lactose). They located significant diagnostic peaks for each form. Presence of α-lactose monohydrate was characterised by intense peaks at diffraction angles 2θ of 12.5° and 16.4°, whereas β-lactose was characterised by such peaks at a diffraction angle 2θ of 10.6°.

The X-ray diffraction patterns of the three grades of lactose were measured at room temperature with an X-ray powder diffractometer as described in chapter 2. The XRPD scans (Figure 3.8) were all indicative of crystallinity and the peaks

at 12.6 were attributed to the presence of alpha lactose monohydrate. No traces of beta lactose were detectable in any grade of available lactose since no specific peaks at 10.6° were detectable. An X-ray diffraction scan of β-lactose is shown in Figure 3.9 as a reference control scan. All lactose grades used in this study were hence solely composed of α-lactose monohydrate.

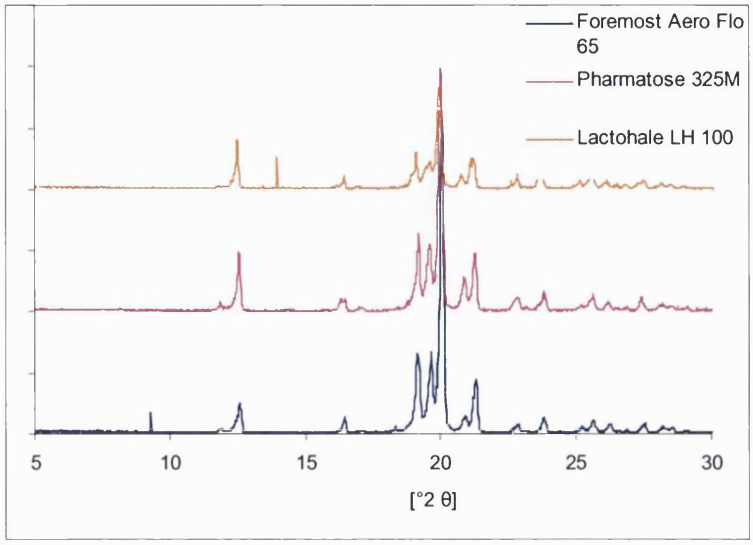

Figure 3.8. *X-ray diffractograms of the three different grades of lactose monohydrate.*

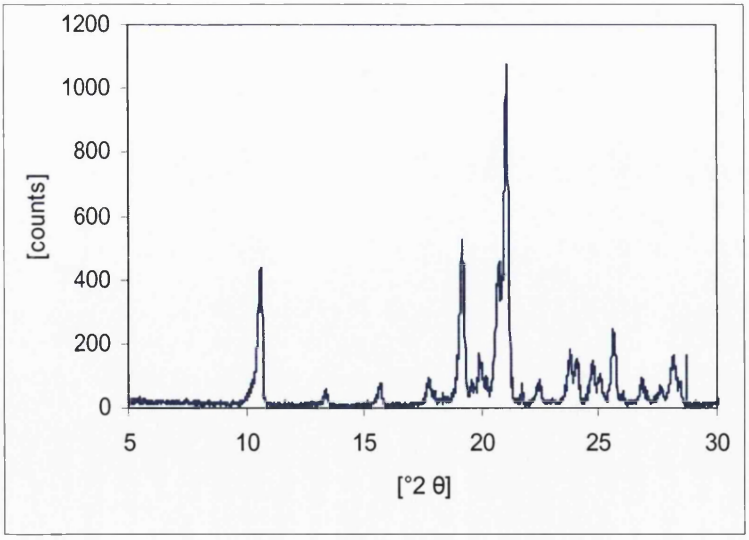

Figure 3.9. *X-ray diffractogram of β-lactose.*

3.5.2.2.2. Solution calorimetry

The enthalpy of solution for each lactose sample of approximately 200 mg was measured using the Thermometric 2225 Precision Solution Calorimeter (Thermometric AB, Sweden) and the water bath of the Thermometric 2227 TAM. Details of the experimental set-up are described in Section 2.3.5. All data here refers to the values calculated using the post-break calibration. A calibration curve had first to be established with 100 % pure amorphous and 100 % pure crystalline lactose standards. Crystalline α-lactose monohydrate was as supplied by Borculo Whey Products UK (B.N 23416). Production of amorphous lactose was prepared by spray drying, following the parameters outlined in Section 2.2.1.1. Confirmation of the amorphous nature of the yield was obtained by the XRPD pattern (Figure 3.10). Dried amorphous and crystalline lactose were accurately weighed and blended in 14 mL glass container to produce powder mixes of 1.0 %, 5.0 %, 10.0 %, and 20.0 % amorphous lactose (w/w). The samples were mixed for 20 minutes in a Turbula mixer at 42 rpm to ensure a homogeneous amorphous content. The sample mass (200 mg) was accurately weighed and filled into a 1.1 mL glass-crushing ampoule and the methodology explained in point 2.7.5.2 employed. The enthalpies of solution for lactose mixes of various amorphous contents (between 0 and 20 %) were calculated to provide the necessary calibration curve (Table 3.6 and Figure 3.11).

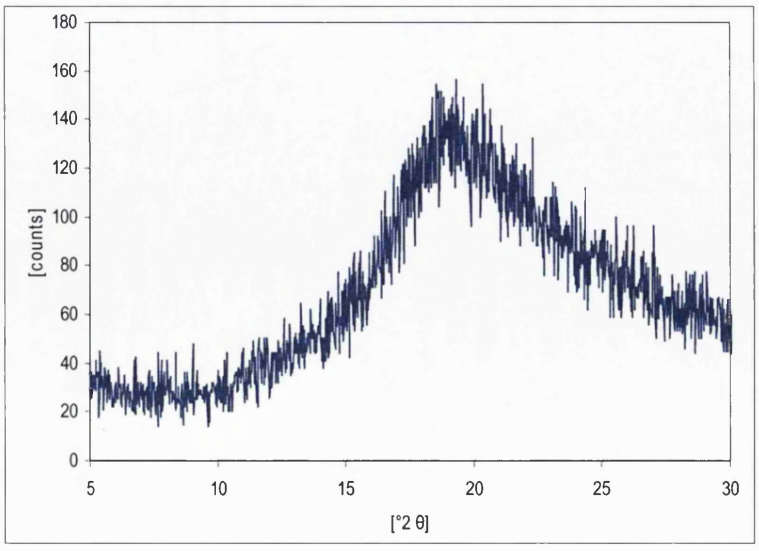

Figure 3.10. *X-ray diffractogram of spray-dried lactose.*

% of amorphous material	Enthalpy of solution (J/g)
0	55.99 (0.4)
1	55.67 (0.17)
5	52.43 (0.16)
10	44.62 (0.49)
20	34.41 (0.26)
100	- 48.26 (0.83)

Table 3.6. *Enthalpies of solution of different partially amorphous mixes expressed as mean values (n=3).*

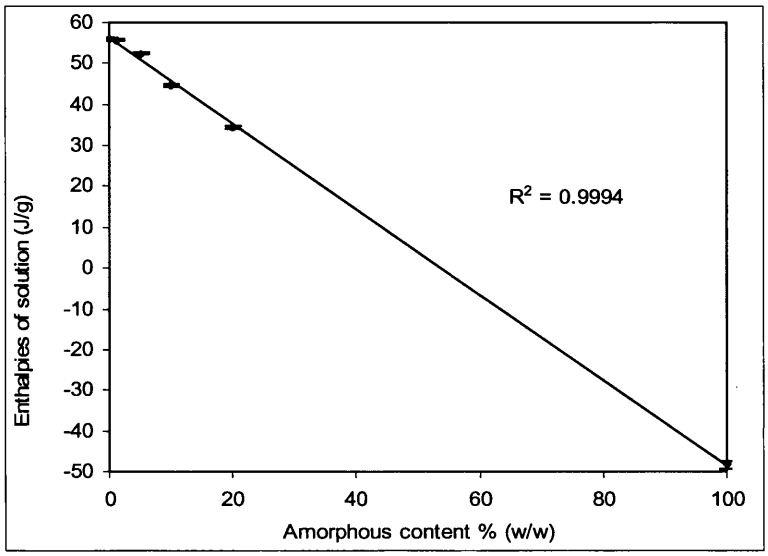

Figure 3.11. *Calibration curve for the determination of the lactose amorphous content by solution calorimetry (n=2)*

The enthalpy of solution decreased in a linear fashion with increasing amorphous content (Figure 3.11). As anticipated, the heat of solution of 100 % crystalline material was endothermic (55.99 J/g) whilst the heat of solution for 100 % amorphous lactose was exothermic (-48.26 J/g). This is due to the fact that amorphous lactose is more readily soluble in water than the crystalline form. For all blends, a net endothermic response was observed since the majority of the sample was crystalline in nature. The good linear correlation (r^2= 0.9994) proved that by using the technique with the sample parameters used, a quantification of about 1 % (w/w) amorphous content was possible. These findings were in agreement with a study by Hogan *et al.* (Hogan and Buckton, 2000) who investigated the use of solution calorimetry to quantify the amorphous content of lactose.

Differences in the amorphous content of the three grades of lactose under investigation were determined (Table 3.7) and the amorphous content calculated using the established calibration curve.

Grades of lactose	Enthalpy of solution (J/g) (mean ±
Pharmatose 325M	57.06 (0.22)
Aero Flo 65	56.48(0.55)
Lactohale LH 100	55.86 (0.09)

Table 3.7. *Enthalpies of solution of different grades of lactose. Values are mean and (standard deviation)*

Pharmatose 325M exhibited the largest enthalpy of solution, 57.06 (0.22) J/g, and Lactohale LH 100 the smallest, 55.86 (0.09) J/g. A fully crystalline sample used for establishing the calibration curve had an enthalpy of solution equal to 55.99 J/g. The values for the different grades are close to this value. Based on a sensitivity of 0.5 %, we can conclude that all three samples were totally crystalline. A possible explanation of the higher values obtained for Pharmatose 325M and the Aero Flo 65 may be due to accuracy problem in the ampoule weight or to sorption of water prior to enthalpy of solution measurement even though crystalline samples are not so hygroscopic and therefore not likely to have remaining absorbed water.

Another possibility is the possible contamination of the lactose used for the calibration curve. However, no β-lactose was detectable in the starting material (Figure 3.12). A more sentive method such as gas chromatography may have been employed to corroborate the findings of the XRPD.

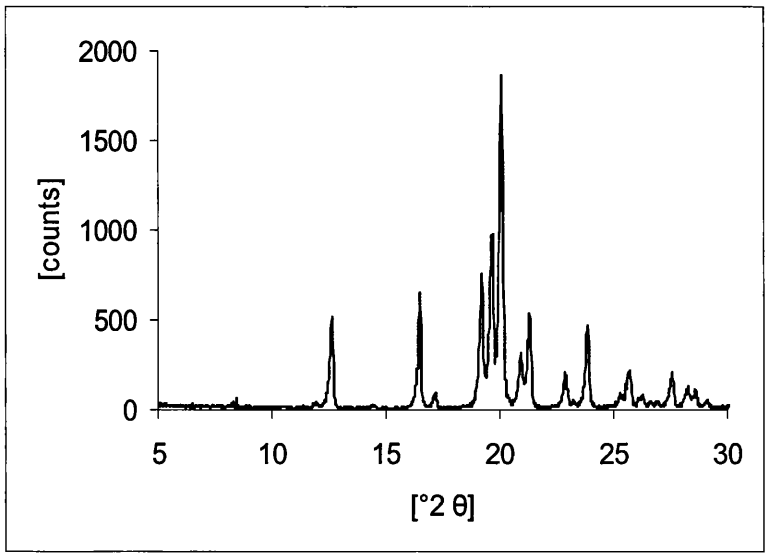

Figure 3.12. *X-ray diffractogram of starting lactose material used for the solution calorimetry calibration curve.*

3.5.2.3. Surface properties

To further evaluate the surface properties of the different lactose grades, IGC experiments were conducted. Columns were packed with the lactose samples and tested following the methodology described in Point 2.3.6. The dispersive components of the free energy and the specific polar interactions are presented in Tables 3.8 and 3.9.

Formulation	γ_s^d (mJ/m^2)
Aero Flo 65	42.9 (0.3)
Pharmatose 325M	40.1 (0.2)
Lactohale LH 100	42.5 (0.8)

Table 3.8. *Dispersive component of free energy for three different grades of lactose. Values are mean and (standard deviation).*

The γ_s^d of coarse Pharmatose 325M was found to be 40.1 (0.2) mJ/m^2, which is slightly lower that the γ_s^d of coarse crystalline Aero Flo 65 (42.9 (0.3) mJ/m^2) or that of Lactohale LH 100 (42.5 (0.8) mJ/m^2). Aero Flo 65 was expected to present a slightly higher γ_s^d due to the important presence of fines which are known to be more energetic. However, the size range under investigation may have been too narrow for changes in the dispersive component to be observed

and any straightforward conclusion was difficult to formulate. Consideration of a relationship between dispersive energy and SS FPF showed that an increase in the dispersive energy was associated with an increase in FPF. However, for BDP, the correlation between the two factors was limited. BDP tends to form cohesive aggregates whereas SS tends to bind to the lactose surface. It was therefore expected that BDP deposition data would be less linked to the surface properties of the lactose grade.

The probes that were used for the acid-base analysis of the different lactose grades were ethanol and chloroform, which are considered to be acidic probes, and acetone and ethyl acetate, which are considered to be basic probes. Using the method based on the Gutmann electron-donor acceptor numbers, K_A and K_D values were determined (see Table 3.9). The K_D value was found to be negative for Pharmatose 325M. This is a difficult concept to explain theoretically. Nevertheless, the determination of acid-base properties was clearly a better tool in investigating the different lactose batches compared to the dispersive nature. This was in accordance with the work of Ticehurst *et al.* (Ticehurst *et al.*, 1996) who found large differences in the specific interactions between four batches of α-lactose monohydrate with equivalent γ_s^d values.

Carrier	Specific polar interactions (J/mol)				Acid-base characteristics		
	Acetone	Chloroform	Ethanol	Ethyl acetate	K_A	K_D	K_D/K_A
Aero Flo 65	7830 (46)	1968 (52)	12478 (95)	10929 (59)	0.141	0.007	0.05
Pharmatose 325M	7134 (191)	-405 (109)	8188 (156)	7642 (203)	0.108	-0.108	-0.26
Lactohale LH 100	8088 (84)	1295 (82)	10781 (61)	9760 (65)	0.129	0.01	0.08

Table 3.9. *Specific polar interactions and acid-base properties of the different lactose carriers using a γ_s^d (mJ/m^2). Values are mean and (standard deviation).*

It was also difficult to interpret the experimental data below the alkane linear plot. In Figure 3.13, chloroform clearly lies below the non-polar line.

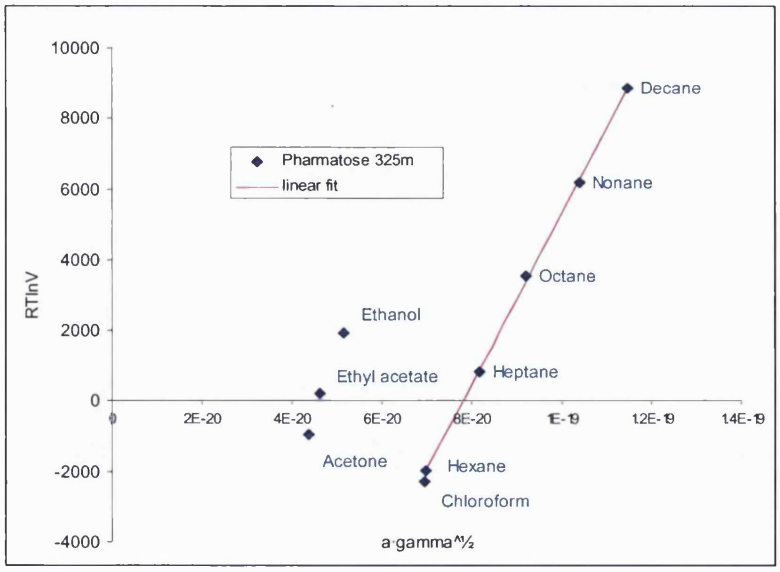

Figure 3.13. *Example of chloroform lying below the alkane line (obtained with Pharmatose 325M as the investigated carrier).*

Other physical criteria can be plotted against $RTlnV_n$ to determine the specific interaction. Chehimi *et al.* (Chehimi and Pigois-Landureau, 1994) assessed the acid-base properties of solid surfaces by using the dispersive contribution to the enthalpy of vaporisation (ΔH^d_{vap}). This method of analysis required values for (ΔH^d_{vap}) the test probes, taking into account the percentage of self-association of the probes. Unfortunately, no data for ΔH^d_{vap} of ethanol is available and therefore all calculations were based on three probes, i.e. acetone, chloroform and ethyl acetate. Plotting only three polar probes was considered insufficient to provide a confident reflection of the surface energetic properties of a powder surface. A third method was therefore used: the boiling point (T_b) of the liquid probes (Sawyer and Brookman, 1968). This approach might be the most convenient since T_b of most widely used probes are readily available in the literature. Table 3.10 summarises the different physical properties of the probes required for analysis.

	Boiling point (°C)	ΔH^d_{vap} (kJ/mol)
Decane	174.15	51.4
Nonane	150.82	46.4
Octane	125.67	41.5
Heptane	98.5	36.5
Hexane	68.73	31.5
Acetone	56.05	22.4
Chloroform	61.17	30.4
Ethanol	78.29	*
Ethyl acetate	77.11	29.3

Table 3.10. *Boiling point and heat of vaporisation data of the different vapour probes required for IGC analysis.*

* No literature data available

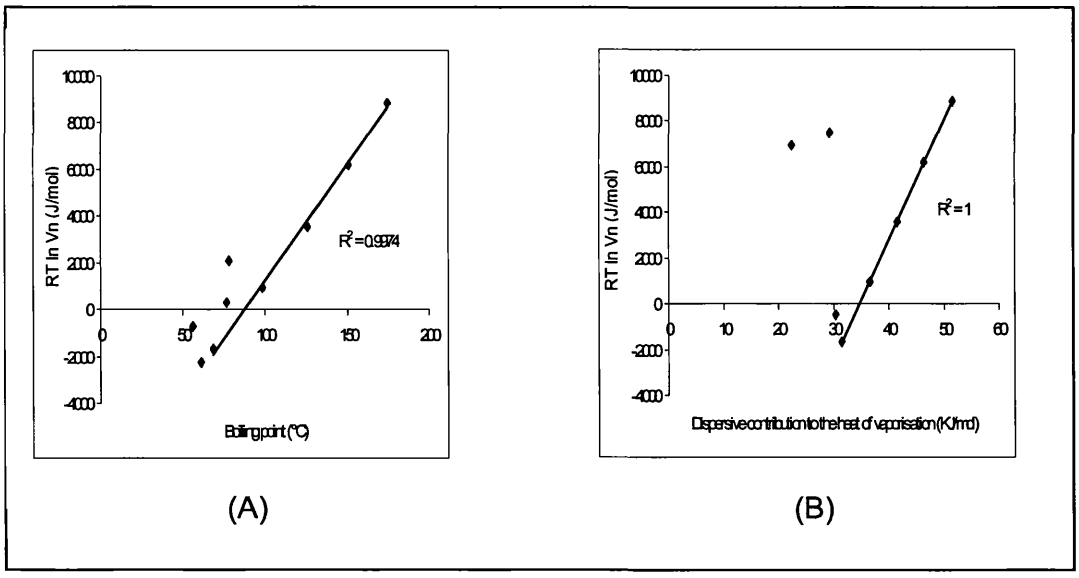

(A) (B)

Figure 3.14. *Plot of RT ln Vn against boiling point of the probes (A) and against* ΔH^d_{vap} *(B).*

The K_D/K_A ratios as determined by the enthalpy of vaporisation approach are presented in Table 3.11. From these values, the Aero Flo 65 and Pharmatose 325M surfaces were shown to have approximately as many basic as acidic sites. Lactohale LH 100 was found to have twice as many basic sites compared to acidic sited (K_D/K_A of 1.53). IGC was carried out at infinite dilution which relates to approximately 1 to 3 % coverage of the surface by the probe

molecules (Ticehurst *et al.*, 1996). It is therefore sensitive to high surface energy sites. Minor differences in the surface crystallinity of Lactohale LH 100 may be responsible for "hot spots" of high energy, which could be detected by IGC. This explanation would contrast with the conclusions obtained with the solution calorimetry measurements described earlier. It is more likely that K^D/K^A determination based on three probes was not entirely accurate.

Enthalpy of vaporisation approach			
	K_A	K_D	K_D/K_A
Aero Flo 65	0.18	0.209	1.16
Pharmatose 325M	0.146	0.154	1.057
Lactohale LH 100	0.185	0.284	1.53

Table 3.11. *Acid-base parameters based on $\Delta G°_A{}^{sp}$ values obtained using the ΔH^d_{vap} approach.*

The K_D/K_A ratios determined by the boiling point approach showed a different pattern, as presented in Table 3.12. Pharmatose 325M surface appeared to be nearly four times more acidic than basic, mainly due to the small K_D value. The Aero Flo 65 appeared to have more basic sites than acidic, whereas a more homogenous distribution appeared on Lactohale LH 100.

Boiling point approach			
	K_A	K_D	K_D/K_A
Aero Flo 65	0.047	0.07	1.57
Pharmatose 325M	0.018	0.039	2.12
Lactohale LH 100	0.036	0.07	1.97

Table 3.12. *Acid-base parameters based on $\Delta G°_A{}^{sp}$ values obtained using the boiling point approach.*

Attempts to correlate the acid-base properties to *in vitro* deposition patterns of both drugs are presented in Figure 3.15 and 3.16. The K_A and K_D values were chosen as obtained by the boiling point approach. Despite only three lactose carriers being examined, a correlation was found between an increase in K_A and K_D and an increase in the SS FPF (Figure 3.16). However, for BDP no obvious correlation could be found between the surface energy data and the deposition profiles.

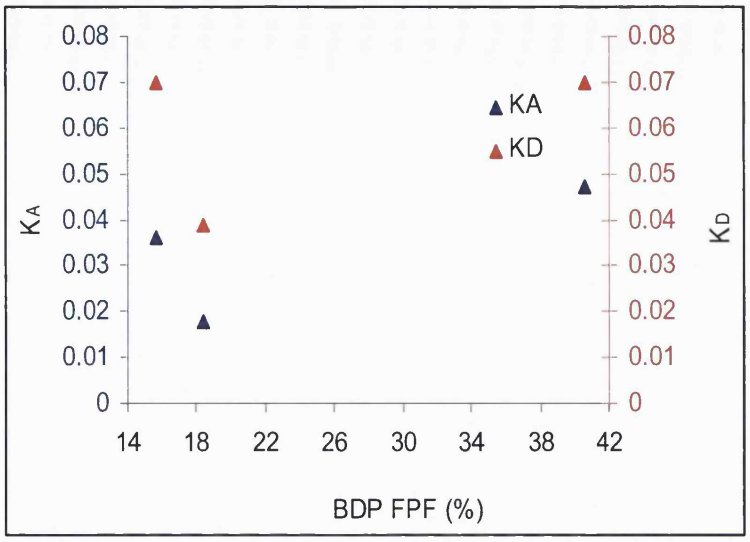

Figure 3.15. *Relationship between BDP FPF and acid-base properties of the different carriers.*

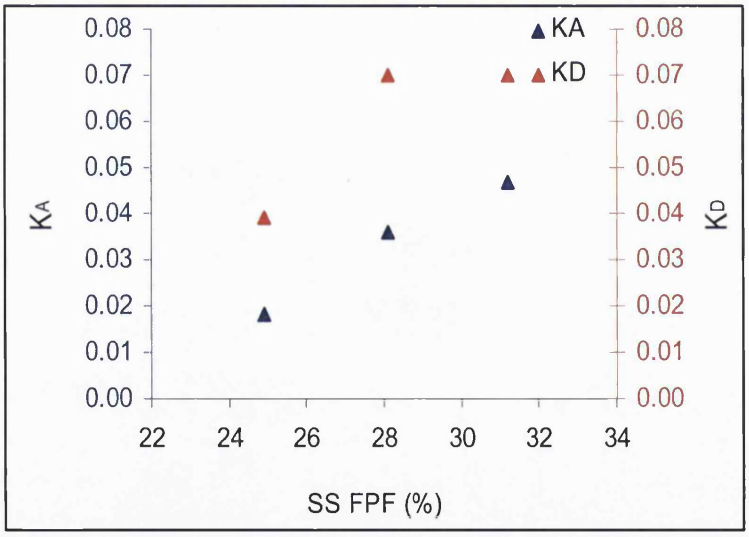

Figure 3.16. *Relationship between SS FPF and acid-base properties of the different carriers.*

An alternative representation of the data to illustrate the relationship between individual probe interaction and FPF for both drugs is shown in Figure 3.17. As previously mentioned, the individual polar probe interaction values displayed significant variance over the grades of lactose considered. Graphical representation of the specific free energy of adsorption (ΔG^{SP}_{A}) for all polar probes is presented in Figure 3.17.

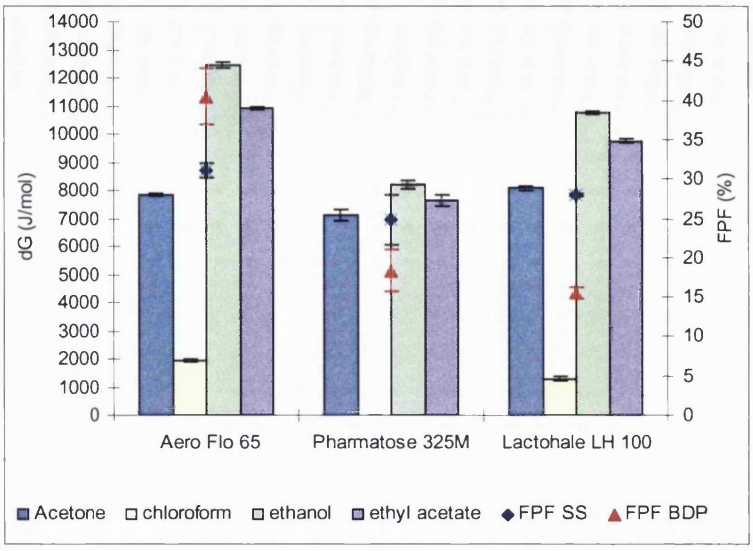

Figure 3.17. *Relationship between BDP FPF, SS FPF and the individual polar probe interactions (in J/mol) Values are mean and (standard deviation).*

Several observations based on the specific free energy of adsorptions as presented in Figure 3.17, can be drawn:

Basic probes interactions:

- Ethyl acetate: Aero Flo 65 > Lactohale LH 100 > Pharmatose 325M
- Acetone: Lactohale LH 100 > Pharmatose 325M > Aero Flo 65

Acidic probes interactions:

- Chloroform: Aero Flo 65 > Lactohale LH 100 > Pharmatose 325M
- Ethanol: Aero Flo 65 > Lactohale LH 100 > Pharmatose 325M

In vitro deposition:

- SS FPF: Aero Flo 65 > Lactohale LH 100 > Pharmatose 325M
- BDP FPF: Aero Flo 65 >Pharmatose 325M> Lactohale LH 100

The IGC data showed a correlation between the dispersive component of the surface energy and the FPF of SS. It also showed a relationship between the polar strength of interaction and the deposition patterns of both drugs. Aero Flo 65 may contain more acidic and basic sites at the highest energy states

responsible of the strong binding of polar probes to the surface. This could be associated with a greater interaction between this grade and the active, in comparison with other grades. Interestingly, the hydrophilic drug model SS deposition follows the same order as the interaction: the stronger the interaction the higher the FPF. This apparent contradiction was explained by the theory developed by Cline and Dalby (Cline and Dalby, 2002). The authors claimed that a minimum surface energy was required to pull highly cohesive drug particles apart during blending and aerosolisation. Any remaining agglomerates would not disperse upon actuation of the device, leading to poor deposition. IGC was also used to examine the surface properties of the two drug models. It became clear that the intrinsic characteristics of BDP and SS played a role in the deposition differences. The different drugs were packed into IGC columns (n=2) and analysed following the method described in Chapter 2. The examination of the dispersive component of the two materials did not explain directly the differences in deposition profiles. The γ_s^d of SS was found to be 50 (3.9) mJ/m^2, which was slightly lower that the γ_s^d of BDP (53.1 (3.0) mJ/m^2). The dispersive component was high compared to the γ_s^d of the coarse lactose carriers. This was expected since the micronised drugs present a high surface area to volume ratio. York *et al.* (York *et al.*, 1998) plotted γ_s^d of five batches of dl-propanolol against their median particle size. This study showed that as the particle size decreased during milling, the surface of the powder became increasingly more energetic. The acid and basic parameters of the drugs were also determined from the method involving the boiling point as previously described, since using the cross sectional method gave negative K_D/K_A values (Table 3.13).

Drug model	Specific polar interaction (J/mol)				Acid-base characteristics		
	Acetone	Chloroform	Ethanol	Ethyl acetate	K_A	K_D	K_D/K_A
SS	7980 (155)	1052 (58)	11506 (117)	10396 (112)	0.137 (0.002)	-0.011 (0.002)	-0.079 (0.011)
BDP	6610 (108)	826 (14)	9194 (34)	8476 (66)	0.114 (0.001)	-0.011 (0.001)	-0.091 (0.001)

Table 3.13. *Specific polar interactions and acid-base properties of SS and BDP determined using the cross sectional method. Values are mean and (standard deviation).*

The results, presented in Table 3.13, displayed a stronger interaction between the probes and the hydrophilic drug model compared to BDP. Here again, stronger interactions were associated with increased *in vitro* performances. Determination of the K_D/K_A using the boiling point approach (Table 3.14) indicated that BDP might contain more basic sites compared to acidic sites with a K_D/K_A ratio of 5.3. SS displayed a K_D/K_A ratio of 1.7. K_D/K_A ratios were chosen instead of either K_D or K_A as both parameters were found to be independent of each other. For example, SS exhibited a much larger K_A value (0.0352) compared to BDP (0.0116) but had identical K_D values.

Drug model	Specific polar interaction (J/mol)				Acid-base characteristics		
	Acetone	Chloroform	Ethanol	Ethyl acetate	K_A	K_D	K_D/K_A
SS	2430 (217)	1997 (79)	5545 (168)	3172 (173)	0.0352 (0.003)	0.060 (0.003)	1.7 (0.07)
BDP	1178 (75)	1787 (14)	3299 (27)	1331 (25)	0.0116 (0.001)	0.061 (0.001)	5.3 (0.23)

Table 3.14. *Specific polar interactions and acid-base properties of SS and BDP determined using the boiling point method. Values are mean and (standard deviation).*

Based on the strength of interaction between acidic and basic probes, a material possessing a greater amount of acidic sites on its surface would have a greater affinity for a material exhibiting a large amount of basic sites. Based on the results presented in Table 3.12, the Aero Flo 65 would therefore develop a better interaction with BDP compared to the other grades. Further studies are described in chapter 5 to assess the impact of surface energies on the deposition patterns of both drugs.

3.6. General conclusions

Lactose monohydrate is the most commonly used carrier in dry powder inhalation. A vast variety of suppliers and different grades leave the formulator with a large panel of possibilities. The main aim of this study was to assess the impact such a choice could have on the deposition of different model drugs. In addition, a great endeavour has been put on the characterisation of the physico-chemical properties of the three different lactose carriers under investigation, in an attempt to correlate the observed depositions to the carrier characteristics. The specific results of the different studies are summarised with respect to the original objectives.

Evaluation of the Clickhaler® as a reservoir device

In the first part of this chapter, aerosol deposition was carried out on a formulation containing Aero Flo 65 as a model carrier and BDP as a model drug. The device employed was the reservoir Clickhaler®. The results of ten actuations showed that reproducibility was obtained with this particular device and this particular formulation, so that the regulatory requirements were met.

Impact of the choice of the carrier on the deposition patterns of SS and BDP

Three different coarse lactose grades (Aero Flo 65, Pharmatose 325M and Lactohale LH 100), all commercially available as carriers for DPI formulations, were used for both SS and BDP using the Clickhaler® as a model device. The results showed that the hydrophobic drug deposition was profoundly affected by the type of lactose chosen. The formulation containing the Aero Flo 65 was found to emit a lesser amount of BDP than that which contained other lactose grades. However, more BDP particles were able to reach the lower stage of the impinger, resulting in a significantly greater FPF. For SS formulations, the selection of a lactose carrier over another did not seem to result, to the same extent as BDP, in major *in vitro* differences.

Overall, this study highlighted that the importance of the carrier was drug-related, the most noticeable effect being for the hydrophobic and cohesive BDP. This suggests that each drug requires different carrier properties for an optimal deaggregation and aerosol deposition.

Determination of correlations between the physico-chemical properties of the lactose carrier particles and the aerosol deposition of two drug models.

In order to correlate some solid state properties of the lactose used to the deposition patterns of the drugs, different methods and parameters were used. All samples under investigation were considered as fully crystalline α-lactose monohydrate following X-ray diffraction and solution calorimetry studies. Differences in particle size distribution and specific surface areas were linked to differences in the proportion of fine lactose particles present in the different samples. The presence of those fines seemed to play a vital role in the drug deposition profile of BDP, whereas SS appeared to be less sensitive to the fine concentration. Further evaluation of the exact role played by fine material and other factors governing the deposition patterns is presented in chapter 4.
Surface energy, being one of the most important factors governing adhesion between particles, was also considered. The surface energy data obtained by IGC enabled a better differentiation of the carrier materials. Despite similar dispersive components of free energy, the determination of the polar components gave more insight into the intrinsic differences of these lactose grades. Despite the limited number of carriers being tested (n=3), a correlation was found between an increase in K_A and K_D and an increase in the SS FPF. No obvious trend could be found between the surface energy data and the deposition profile of BDP. As previously stated, the hydrophobic drug model tends to form cohesive aggregates whereas SS tends to bind to the lactose surface. It was therefore predictable that SS deposition data would be linked to the surface energy of the lactose grades, whereas BDP would be more influenced by the presence of small particles, which may affect the stability of those aggregates.

Chapter 4

Crystalline lactose/PEG 4000 co-spray-dried systems used as fines for DPI

4.1. Summary

The previous chapter has focussed on the importance of lactose fines on the deposition pattern of micronised drugs. Numerous papers are related to the influence of adding a ternary component to improve DPI performances. Examples of adding different types of lactose fines, sugars, amino acids or lubricant are available in the literature. However, recent investigations conducted at the School of Pharmacy did not show any deposition improvement when adding crystalline lactose fines at 5, 10 or 15 % (w/w) to a coarse carrier (Al-Hadithi, 2004) Described in this chapter is a new type of fines consisting of crystalline lactose/polyethylene glycol (Corrigan *et al.*, 2002) co-spray-dried systems. Different such systems were produced by varying the lactose to PEG ratio. After characterisation of their physico-chemical properties, these systems were used as fines for DPI formulations. The impact of the nature of the fines and other formulation parameters, such as mixing sequence, fine concentration and drug concentration, were investigated.

4.2. Introduction

Chidavaenzi *et al.* (Chidavaenzi *et al.*, 2001) investigated the effect of spray drying lactose and a fixed proportion of PEG 4000 at levels of 12, 4, 2 and 1 % by weight of solid using different feed concentrations of solid (10 % (w/w) and higher). While lactose alone appeared to be completely amorphous after the process, all lactose/PEG 4000 systems were crystalline. This unexpected property for these systems to crystallise could be explained by the high affinity with which water binds to PEG, causing a reduction in water evaporation during spray drying. The slower solidification rate of lactose/PEG particles (compared to that of lactose alone) enables the organisation of the lactose molecules in a three-dimensional crystal structure. The crystallisation effect may also be associated with the low T_g of PEG 4000. PEGs exhibit a T_g which depends on the molecular weight of the sample (Craig, 1995). In the molecular weight range of 10^2 to 10^7, the T_g varies from approximately -98 to -17°C. The low T_g of PEG 4000 indicates that this material is likely to act as a pure plasticizer and therefore promote crystallisation.

Gilani *et al.* (Gilani *et al.*, 2004) studied the aerosol performance of binary mixtures composed of BDP and different lactose/PEG processed carriers. They used different molecular weights of this polymer (i.e. 400, 3000 and 6000 Da), which was mixed with lactose in aqueous media before being spray-dried using a Büchi 191. The resulting co-spray-dried products all appeared to be crystalline. These systems were used as carriers for BDP in a ratio of 67.5 to 1 (w/w). The deposition pattern was assessed using a Spinhaler® connected to a TS. Using these new lactose/PEG carriers showed a general improvement compared to conventional lactose carriers. For example, the FPF of BDP using spray-dried lactose/PEG 3000 was greater than for BDP using Pharmatose 325M (25.8 (5.3) % compared to 6.7 (1.1) %). The authors concluded that this improvement might result from the smaller asperities on the surface of the lactose/PEG particles compared to the bigger asperities on particles of conventional grades of lactose such as Pharmatose 325M. The larger asperities are likely to be responsible for the entrapment of the drug particles, which are dislodged, more difficultly, by the drag force generated by the inhaler, resulting in poor aerosol properties.

As described above, since the presence of PEG caused lactose to crystallise during the spray drying process, it is important to describe the characteristics of this polymer and in particular the molten state properties of PEG 4000, since the outlet temperature in the spray drying process was higher than the melting point of the polymer (T_m: 50-58°C)

PEG is a hydrophilic synthetic polymer, with the general structure HO-[-CH_2-CH_2-O]$_n$-H where n is the average number of oxyethylene groups (Kibbe, 2000). Depending on the molecular weight, these materials can exist at room temperature either as liquids (PEG 200-600 Da), semicrystalline solids (PEG 3000-20000 Da and above) and resinous solids for much higher molecular weights (>100000 Da). PEGs have a helical conformation consisting of seven monomers of repeat units and two turns in a fibre identity period of 20 (1.3) Å. It crystallises forming lamellae with chains fully extended or folded (once or twice) (Craig, 1995). In both cases the terminal hydroxyl groups protrude from the surface (Kovacs *et al.*, 1975).

The most stable form is the extended chain form, while the once or twice folded forms are the metastable ones. These metastable forms have been shown to unfold to form the extended chain form over a period of time (Chatham, 1985). As previously mentioned, the outlet drying temperature was higher than the melting point of the polymer (T_m 50-58°C). The crystallisation from a PEG melt can occur by one of two mechanisms: homogeneous or heterogeneous nucleation, as described in chapter 3. The polymer chains in the melt are randomly orientated and may experience spontaneous aggregation below the melting point. When a critical nucleus size is reached, the subsequent addition of chains is irreversible and growth occurs. This phenomenon is called homogeneous nucleation. Heterogeneous nucleation occurs from nuclei already present in the melt. However, the mechanism of crystallisation is not clearly understood, since the added material can also act as an inhibitor for crystallisation by limiting chain diffusion and packing.

PEG is widely used in pharmaceutical formulations including parenteral, topical, ophthalmic, oral and rectal preparations (Kibbe, 2000). Although PEGs have no special indications for use in the lungs, considerable attention has been put on their use for the controlled release of bioactive compounds within this organ. Fu *et al.* (Fu *et al.*, 2002) synthesised new polymeric carriers for controlled drug delivery following inhalation. The polymers were composed of sebacic acid and PEG monomers. PEG was incorporated into the polymer backbone in order to reduce the interparticulate adhesion forces and decrease the density of the subsequent polymer aerosol. This occurs because the polymer encourages water uptake and thus swelling of the particles, which are subsequently frozen and lyophylised. The authors stated that PEG may gain approval in pulmonary applications due its wide use and proven safety in other clinical applications. Other workers (Fiegel *et al.*, 2004) recently published *in vitro* deposition data of poly(ether-anhydride) microspheres from a Spinhaler® using an Andersen Mark II Cascade Impactor. Particles containing 10 % PEG 8000 into the polymer blackbone exhibited significantly higher FPF (16.1 %) than those made with 0 % PEG (9.1 % FPF).

French *et al.* (French *et al.*, 1996) used different florescently marked PEGs (obtained by rapid cooling of a solution containing calcein blue solubilised in molten PEG 6000 and 8000) directly as carriers to study the influence of formulation parameters (i.e. flow rate, active carrier mass ratio and carrier particle size) on the deposition of mannitol or mannitol with recombinant human granulocyte-colony stimulating factor (GM). The study emphasised the importance of the drug component properties in emission, deaggregation and deposition from the Spinhaler®. Besides being used as a coarse carrier, PEG has also been studied as microfine particles. Lucas *et al.* (Lucas *et al.*, 1998a) investigated the influence of PEG 6000 fines on the deposition of bovine serum albumin from a Rotahaler® attached to a TSI. Micronised PEG 6000 (VMD of 4.0 µm) was mixed with a coarse lactose carrier (63-90 µm size). The modified carrier containing 5.0 % (w/w) micronised PEG was blended with the drug (2 % (w/w)). The mean fine particle fraction was found to be 33.5 (4.5) % for the PEG-treated formulation, whereas formulations based on untreated lactose or treated lactose with 5 % fine lactose exhibited an FPF of 24.4 (4.1) % and 36.8 (6.9) % respectively. These results showed the possibility of using alternatives to lactose fines to improve the *in vitro* deposition of DPI formulations.

4.3. Aims and objectives

The main aim of the work described in this chapter was to examine different lactose/PEG 4000 co-spray-dried systems as a new type of ternary material for DPI formulations. The impact of such additives on the aerosol performance of modified carriers was evaluated.

The main objectives were to:

- Examine the fabrication of lactose/PEG fines by spray drying;
- Determine the physico-chemical properties of these systems to be used as fines for DPI formulations;
- Examine the influence of the lactose to PEG ratio in the spray-dried product on the deposition pattern of the drugs;

- Study the effect of the blending sequence on the performance of a DPI formulation;

- Examine the influence of varying the amount of fines and drug on the aerosol performance of different coarse lactose carriers.

4.4. Materials and methods

4.4.1. Preparation of the particles by spray drying

The different feed samples containing of the various desired α-lactose monohydrate to PEG 4000 ratios were prepared and spray-dried using the conditions described in Chapter 2. Solutions with 20 % PEG 4000 and above, produced particles, which appeared to be fused together (Figure 4.1), giving low yields. This was due to the powder sticking to the walls of the cyclone. Therefore PEG concentrations higher than 10 % were not evaluated any further.

Concerning the possible degradation of PEG during the different drying stages, Corrigan *et al.* (Corrigan *et al.*, 2002) examined the molecular weight characteristics of PEG 4000 upon spray drying by gel permeation chromatography. No significant differences were found in molecular weights before and after processing the PEG. The authors concluded that this technique did not result in polymer degradation. No degradation studies were therefore performed during this phase of research.

In addition to the crystalline lactose/PEG fines, crystalline lactose fines (B.N. E949423) and amorphous lactose fines (obtained by spray drying following the parameters described in Chapter 2) were also studied as references. PEG 4000 was also investigated for comparative surface energy studies. In order to obtain the desired particle size distribution, PEG 4000 flakes were ground manually and sieved to obtain particle size fraction of 45 to 90 µm. Adequate brass sieves were positioned in the sieve shaker (Copley, UK) and the system allowed to be shaken for 30 minutes.

4.4.2. Preparation of the different formulations

Due to the numerous formulation parameters investigated, all detailed preparation methods for the different carriers are described under the appropriate sections (Sections 4.5.2.1 to 4.5.2.4). All *in vitro* assessments were performed using the TSI and the Clickhaler®.

4.5. Results and discussion

4.5.1. Characterisation of the lactose/PEG 4000 fines

The methods of scanning electron microscopy, particle size determination by the Malvern Mastersizer X, X-ray diffraction, dynamic vapour sorption and inverse gas chromatography were employed here as described in chapter 2.

4.5.1.1. Scanning electron microscopy

Microscopic examinations were undertaken on the different types of fines obtained. The scanning electron micrographs are shown in Figure 4.1. The crystalline lactose fines (image A) appeared to be of irregular morphology with individual particles appearing to be less than 10 µm in diameter. Image B shows the smooth surface of amorphous lactose produced by spray drying. Images C, D and E show the different lactose/PEG 4000 co-spray-dried systems. The products consist of particles with a particle size of roughly 2 to 10 µm in diameter. This was consistent with the work of Chidavaenzi *et al.* (Chidavaenzi *et al.*, 2001). On the surface of the particles evidence of asperities could be seen at all lactose to PEG ratios employed. Asperities were present on these particles due to the crystallised PEG at the surface. Increasing the PEG concentration to 20 % (w/w) had an effect on the particle structure, with apparent loss of the integrity of the primary particles due to irreversible fusion of adjacent particles.

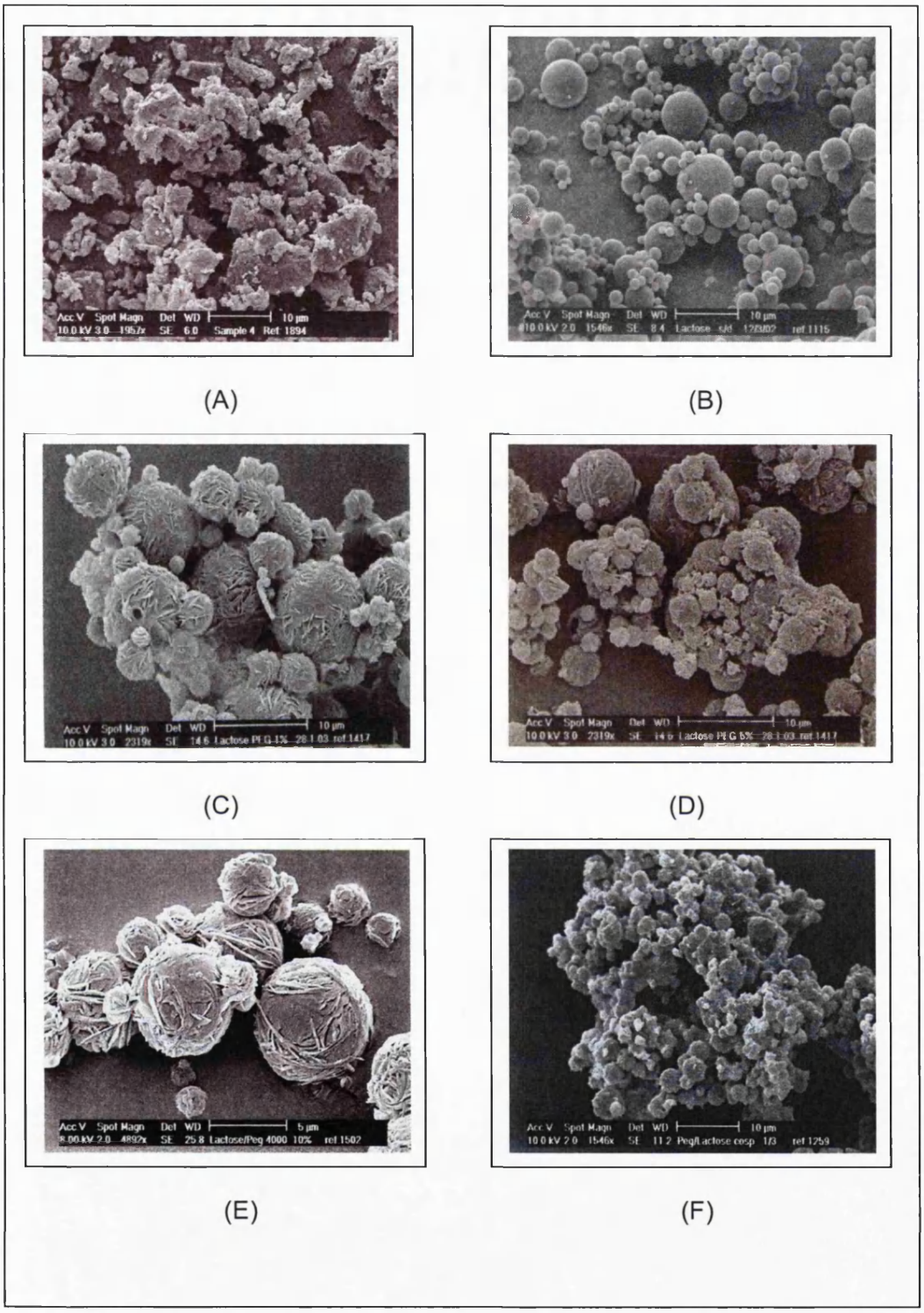

Figure 4.1. *Electron micrographs of (A) crystalline lactose, (B) amorphous lactose, (C) lactose/PEG 1 %, (D) lactose/PEG 5 %, (E) lactose/PEG 10 %,and (F) lactose/PEG 20 %.*

4.5.1.2. Particle sizing of the different co-spray-dried systems

The particle size of the different systems was measured using a laser diffraction particle analyser (Mastersizer X (Malvern Instruments, UK) as described in chapter 2. Propan-2-ol was used as the suspension medium. Each sample was analysed separately at least three times and the results are shown in Figure 4.2 and Table 4.1.

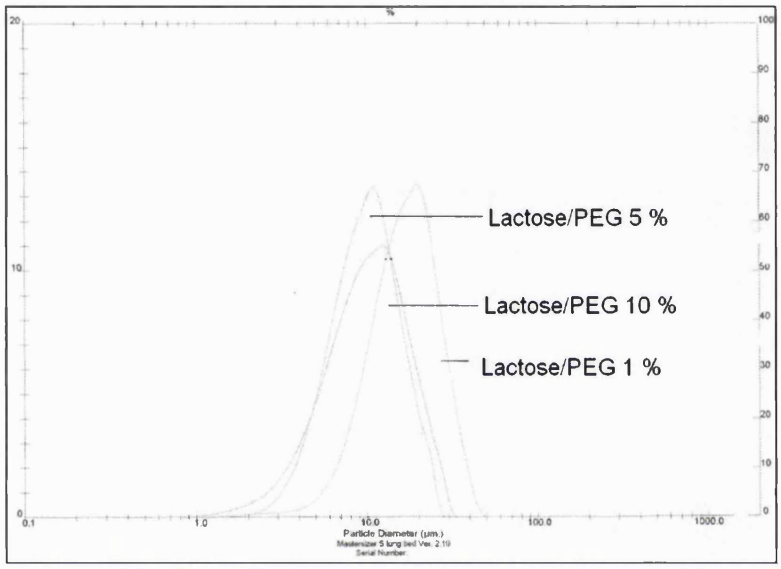

Figure 4.2. *Particle size distribution of the three different grades of lactose.*

Formulations	$d_{10\%}$	$d_{50\%}$	$d_{90\%}$	SPAN
1 % PEG 4000	7.4 (1.1)	15.7 (1.1)	28.0 (0.6)	1.30 (0.1)
5 % PEG 4000	5.0 (0.3)	9.4 (0.6)	15.9 (1.2)	1.16 (0.06)
10 % PEG 4000	4.6 (0.3)	10.6 (0.5)	20.5 (2.3)	1.49 (0.2)

Table 4.1. *Particle size distribution of the different co-spray-dried systems. Values are mean and (standard deviation).*

The spray drying process produced micronised particles with a volume median diameter (VMD) ranging between 9.4 and 15.7 µm (Table 4.1). Such a difference in particle size was interesting since all samples were spray-dried using similar conditions. The particle size analysis results indicated that the distribution of the particle was quite narrow whichever lactose to PEG ratio was considered.

The volume mean diameter of the lactose/PEG 4000 particles containing 1 % PEG was 15.7 (1.1) µm with a narrow span of 1.3 (0.1). This VMD appeared to be bigger than for particles containing a higher percentage of PEG. Particles containing 5 or 10 % (w/w) PEG appeared to have similar VMD (9.4 µm and 10.6 µm respectively). These systems were considered to be of intermediate size.

4.5.1.3. X-ray diffraction

The X-ray diffraction patterns of pure α-lactose monohydrate and pure PEG 4000 are shown in Figure 4.3 and 4.4. The diffraction spectrum shows the characteristic peaks corresponding to PEG 4000 (2θ = 19.2 and 23.4°).

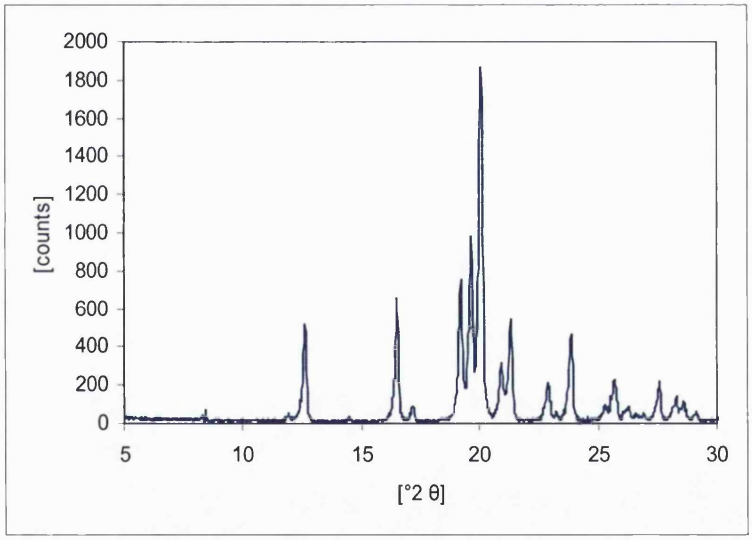

Figure 4.3. *X-ray diffractogram of the reference α-lactose monohydrate.*

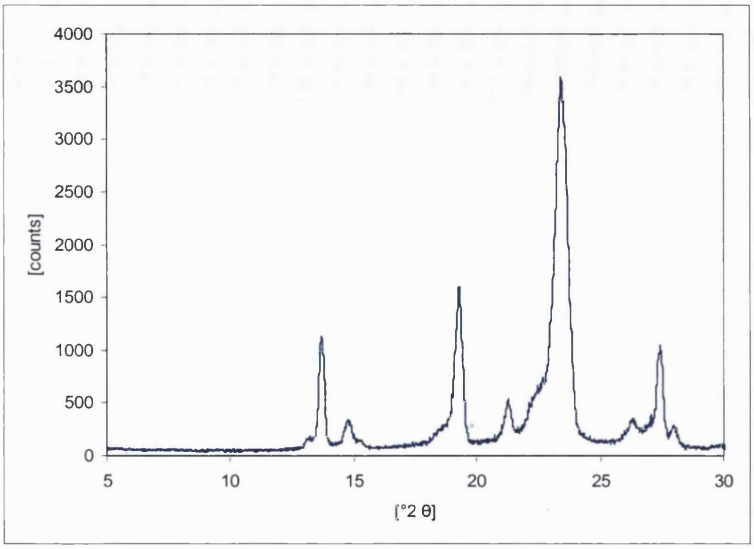

Figure 4.4. *X-ray diffractogram of the PEG 4000 reference material.*

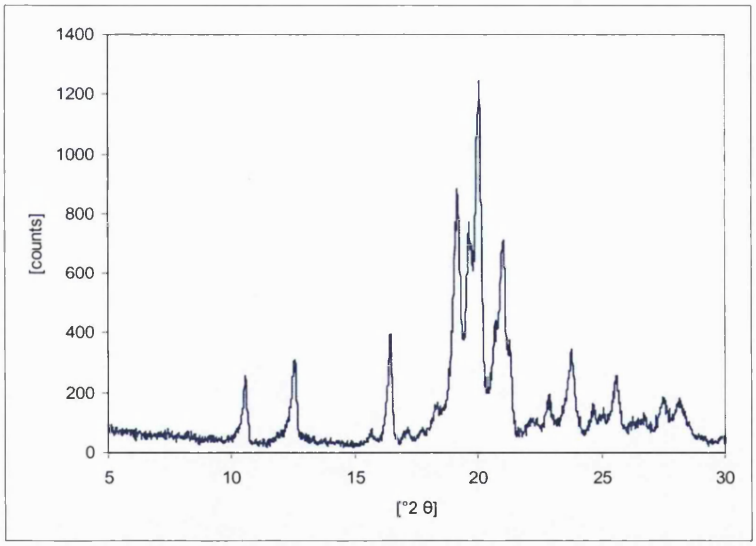

Figure 4.5. *X-ray diffractogram of the 10 % PEG/lactose spray-dried system.*

The X-ray diffraction data for the lactose/PEG co-spray-dried system containing 10 % PEG (Figure 4.5) showed composite diffraction peaks at 10.6° and 12.6°. These were attributed to the presence of β-lactose and α-lactose monohydrate respectively (Drapier-Beche *et al.*, 1997). The diffraction peaks for PEG were similar to that of the reference material, indicating that the sample presumably consisted of the extended chains. These findings were consistent with Chidavaenzi *et al.* (Chidavaenzi *et al.*, 2001). Regarding the 1 % and 5 % PEG systems (data not shown), the XRPD data were similar to the 10 % PEG. This was unexpected since the same workers showed that spray-drying solutions of

lactose/PEG consisting of a small amount of polymer resulted in the production of α-monohydrate, anhydrous α-lactose but no β-lactose. The mechanism by which lactose crystallises in the presence of PEG is not clearly understood.

4.5.1.4. Dynamic vapour sorption

Lactose monohydrate, despite being soluble in water, is not hygroscopic. Buckton *et al.* (Buckton and Darcy, 1995) showed as little as 0.02 % weight gain when subjecting the sample up to 80 % RH. Data for the water sorption of the different lactose grades under investigation (i.e. Lactohale LH 100, Aero Flo 65, and Pharmatose 325M) also confirmed this low affinity of the powder for water with weight gains varying from 0.039 % to 0.076 % at 80 % RH, making gravimetric sorption studies difficult to interpret. No DVS isotherm for the α-monohydrate is therefore presented here. Moisture sorption / desorption of PEG 4000 and the different co-spray-dried systems was studied in a dynamic vapour sorption apparatus. The method used was as described in chapter 2. Moisture uptake/loss (M) was calculated by Equation 4.1

$$M = (W-W_d)/W_d \, X \, 100 \qquad \text{[Equation 4.1]}$$

where W is the weight of the exposed sample and W_d the weight of the dry sample.

In the case of PEG 4000 and lactose/PEG 4000 system containing 1 % PEG (w/w), the humidity stage was increased from ten to fifteen hours for PEG on its own, and from ten to twenty hours for the co-spray-dried system since preliminary experiments showed that no equilibrium was reached within ten hours.

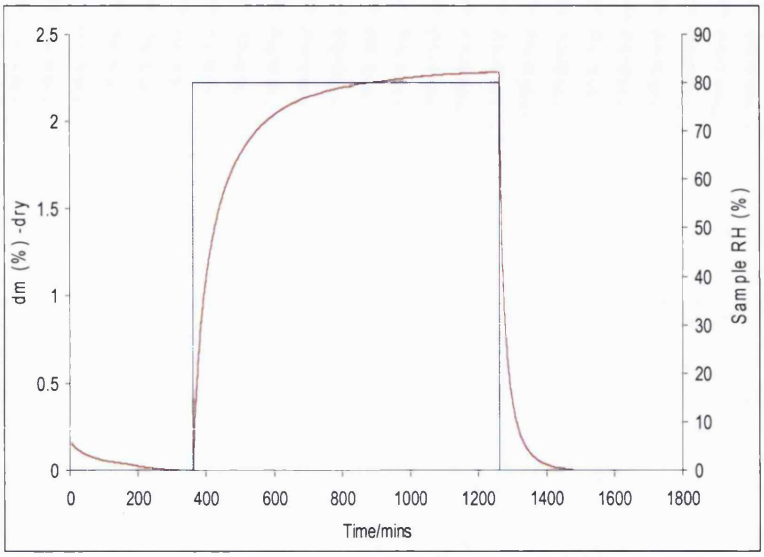

Figure 4.6. *DVS mass plot of PEG 4000 as a function of time and % RH.*

Gravimetric sorption data for a PEG 4000 sample is presented in Figure 4.6. The different relative humidities are illustrated by the blue line, whereas the corresponding changes in mass of the sample are represented by the red line. As the % RH was decreased to 0 %, water molecules evaporated from the sample surface, resulting in a recorded weight decrease. As the humidity of the system was raised to 80 % RH, no lag time was observed and the sample gained mass rapidly. The mass increase started to tail off after around 1000 minutes. This was indicative of saturation of the sample with sorbed water. At this point the mass had increased by 2.3 %. When the humidity of the system was reduced to 0 %, the mass of the sample was seen to decrease rapidly and then followed a slower rate of change. This mass loss took place within 220 minutes and returned to the original dry weight, indicating that reversible water sorption and desorption occurred with PEG 4000.

The water vapour sorption profile of lactose/PEG 4000 containing 10 % PEG (w/w) is presented in Figure 4.7. The mass gain reached a plateau (3.2 % mass increase). The result, showing the absence of mass loss during the humidification step, confirmed the initial XRPD data, indicating that no crystallisation occurred.

The mass increase can be attributed to the water uptake due to the PEG and also the transformation of anhydrous α-lactose, present in the initial product, as described by Chidavaenzi *et al.*, to the monohydrate form. During the final drying step, a quasi-instant loss in mass was observed with a residual mass gain of 0.8 % due to the expected formation of the hydrate.

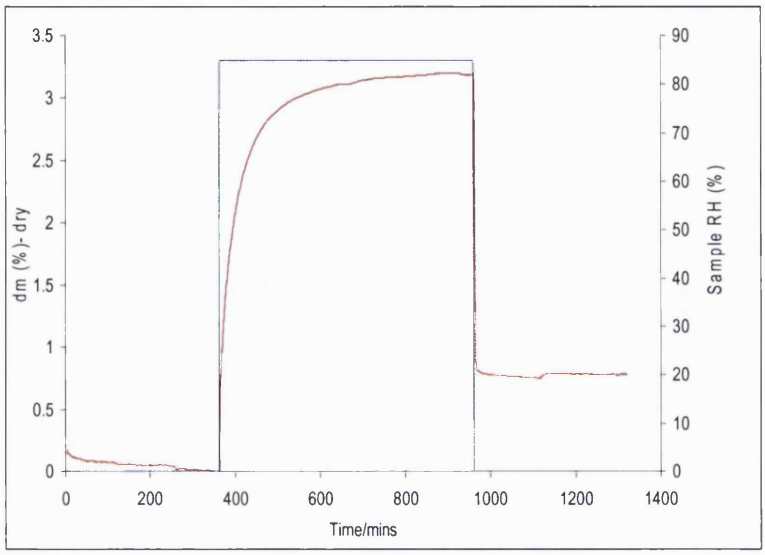

Figure 4.7. *Water sorption for lactose/PEG 4000 co-spray-dried system containing 10 % PEG (w/w).*

The water vapour sorption data of lactose /PEG 4000 product containing 5 % PEG is presented in Figure 4.8. The material was dried and subjected to the same RH as previously described. The sorption of water, illustrated by the increase in sample mass, was comparable to the one described for the 10 % PEG system shown in Figure 4.7. The increase in weight at the equilibrium corresponded to 2.9 % mass gain. The rate of desorption was also really fast with a final mass gain equal to 1.6 %.

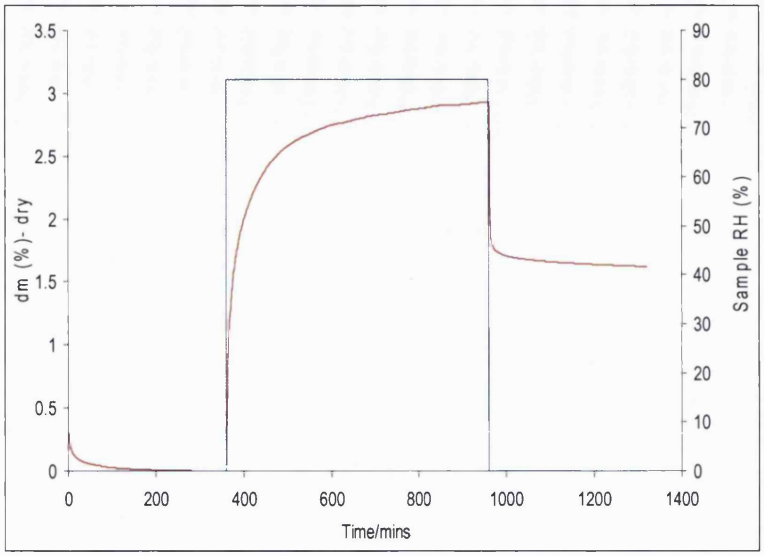

Figure 4.8. *Water sorption for lactose/PEG 4000 co-spray-dried system containing 5 % PEG (w/w).*

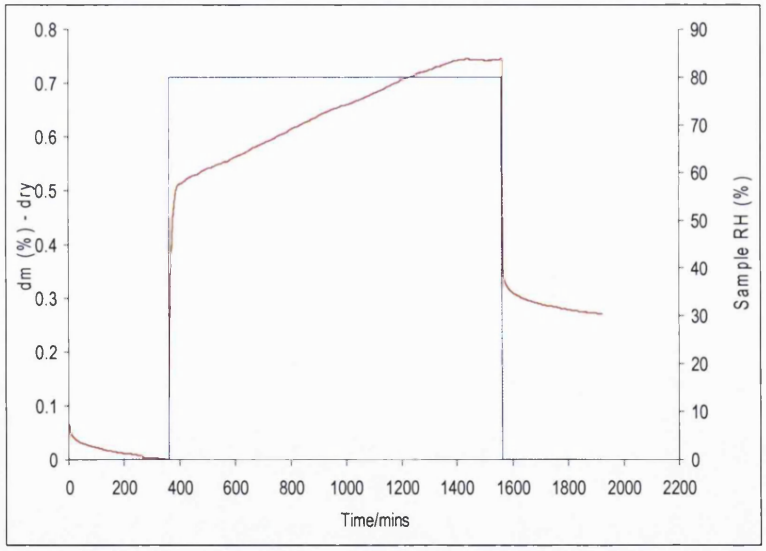

Figure 4.9. *Water sorption for lactose/PEG 4000 co-spray-dried system containing 1 % PEG (w/w).*

The sorption kinetic profile was different for the formulation containing 1% PEG (Figure 4.9) in comparison to the other lactose/PEG formulations (Figure 4.7 and 4.8). Following a rapid water uptake for 40 minutes, a far slower rate of sorption occur for 980 min before reaching equilibrium with a water level peaked at 0.74 % mass gain. The final drying step resulted in a 0.27 % mass increase. This was attributed to the formation of some α-lactose monohydrate.

4.5.1.4. Inverse gas chromatography

In addition to the different lactose/PEG systems, PEG 4000 and crystalline lactose (Microfine) were also studied as reference materials. The influence of different powder masses of PEG 4000 was also studied as Planinsek *et al.* (Planinsek and Buckton, 2003), had shown a dependence of the acid/base terms on the sample mass. The authors investigated the acid and base properties of different excipients including Methocel K4M and Pharmacoat 606. The K_D/K_A ratio of these two materials was seen to be influenced by the powder mass. Increasing the sample mass from 250 mg to 500 mg resulted in an increase in K_D/K_A value (1.02 to 1.36 for the Methocel and 1.66 to 2.14 for the Pharmacoat sample). Access to more of the material or an artefact of the retention of vapours was presented as a possible explanation for this observation. Three silanized columns were packed with three different masses of PEG and the surface energies determined using the parameters described in chapter 2. The K_A and K_D were determined using the cross section method. Linear regression between the data values for the acid-base analysis is critical. The coefficient of correlation indicated a poor fit with the boiling point method (r^2 below 0.6). The acid-base values obtained with this method were disregarded and are not shown here. The dispersive component of free energy, the specific surface energies of adsorption and the resulting K_A and K_D are listed in Table 4.2.

Mass (mg)	Specific polar interaction (J/mol)				Acid-base characteristics			γ_s^d (mJ/m^2)
	Acetone	Chloroform	Ethanol	Ethyl acetate	K_A	K_D	K_D/K_A	
319.6	9536 (109)	7608 (165)	12904 (168)	10115 (173)	0.118	0.197	1.68	32.9 (0.9)
402.6	10042 (68)	8069 (46)	13639 (67)	10509 (52)	0.122	0.214	1.75	33.3 (0.4)
494.6	9885 (21)	8017 (42)	13315 (28)	10435 (34)	0.121	0.208	1.72	33.2 (0.3)

Table 4.2. *Influence of the sample mass on the IGC measurements. Values are mean and (standard deviation).*

The dispersive component of surface energy was not affected by the sample mass. The specific interactions of the four vapours were found to be statistically different (ANOVA $P<0.05$), the lowest values being observed with the lowest sample mass. The resulting K_D/K_A ratios were nevertheless very comparable, with values varying from 1.68 to 1.75. Overall, the sample mass did not affect significantly the determination of the acid-base nature of PEG 4000. The PEG data presented below corresponds to the average of the measurements undertaken with three different sample masses.

Materials	Specific polar interaction (KJ/mol)				Acid-base characteristics			γ_s^d (mJ/m^2)
	Acetone	Chloroform	Ethanol	Ethyl acetate	K_A	K_D	K_D/K_A	
Lactose fines	8060 (53)	1135 (26)	12728 (65)	10885 (53)	0.143	-0.007	-0.05	42.8 (0.16)
Lactose/PEG (1 %) fines	6081 (132)	2992 (68)	8834 (99)	7614 (137)	0.094	0.055	0.59	34.7 (0.7)
Lactose/PEG (5 %) fines	6532 (32)	3500 (33)	9191 (15)	8014 (26)	0.096	0.101	1.06	38.4 (0.3)
Lactose/PEG (10 %) fines	6942 (68)	3809 (173)	9767 (175)	8153 (241)	0.097	0.121	1.25	35.4 (0.6)
PEG 4000	9821 (259)	7898 (252)	13286 (368)	10353 (209)	0.12	0.206	1.71	33.1 (0.2)

Table 4.3. *IGC measurements for the different lactose/PEG systems and lactose fines. Values are mean and (standard deviation).*

The surface energies of the different systems were first examined in terms of their dispersive surface energies (γ_s^d) (Figure 4.10). PEG 4000 with a size distribution of 45 to 90 µm, exhibited a relatively low dispersive surface energy (33.1(0.2 mJ/m^2) compared to lactose monohydrate (chapter 3). The crystalline lactose was found to have a surface energy of 42.8 (0.2) mJ/m^2. This relatively high value may be due to the relatively small size of these particles as shown by SEM. The surfaces of the co-spray-dried systems were less energetic than those of pure lactose. The γ_s^d of fines consisting of 5 % PEG was found to be higher (38.4 (0.3) mJ/m^2) compared to that of the systems containing either 1 % PEG (34.7 (0.7) mJ/m^2) or 10 % PEG (35.4 (0.6) mJ/m^2). Overall, the γ_s^d decreased when incorporating PEG, demonstrating that PEG incorporation increased the hydrophilicity of the spray-dried systems. Moreover, the γ_s^d of the different co-spray-dried systems were closer to the γ_s^d of the PEG than the

lactose, indicating the presence of PEG at the surface of the particles (as already seen on SEM). Those particles may be mimicking the PEG 4000 surface, as their dispersive surface energies were comparable. Low surface energy materials exhibit low van der Waals forces and therefore systems containing those particles may be seen as good candidates due to the reduction of thestrong drug to carrier adhesion forces.

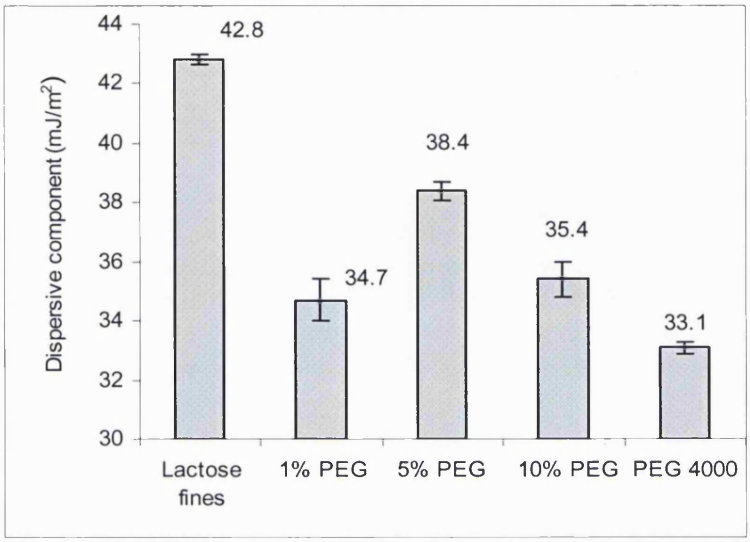

Figure 4.10. *Dispersive components of the crystalline lactose, the different lactose/PEG systems and PEG 4000. Values are mean (n=3).*

In polar terms, there were also significant differences between the different systems studied. The K_D/K_A ratios, determined by the cross sectional approach, are shown in Figure 4.11. Values of K_D/K_A greater than 1 suggest a basic nature on a solid surface, whereas values less than 1 imply an acidic nature. Accordingly, the crystalline lactose fines had a negligible K_D, which was close to zero and an acidic surface. This was in agreement with the values obtained for the coarse lactose described in Chapter 3. PEG 4000 gave a greater K_D value, indicative of its predominantly basic surface. This material was found to have nearly twice as many basic sites compared to acidic sites with a K_D/K_A ratio of 1.71. In general, most oxygen-containing organic compounds are Lewis bases because of their lone pairs of electrons. Based on its general chemical structure, PEG can be regarded as an electron pair donor and therefore the IGC results were in accordance with the theoretical approach. The K_D values of the different co-spray-dried systems increased with increasing PEG concentration (K_D increasing from 0.055 for a 1 % PEG system to 0.121 for a 10 % PEG

system), whereas the K_A values remained constant. As a result, the K_D/K_A ratios increased indicating that the surface basicity was also increasing.
This may also indicate that more PEG crystals were present on the lactose/PEG surface and therefore that the amount of asperities due to those PEG crystals was higher.

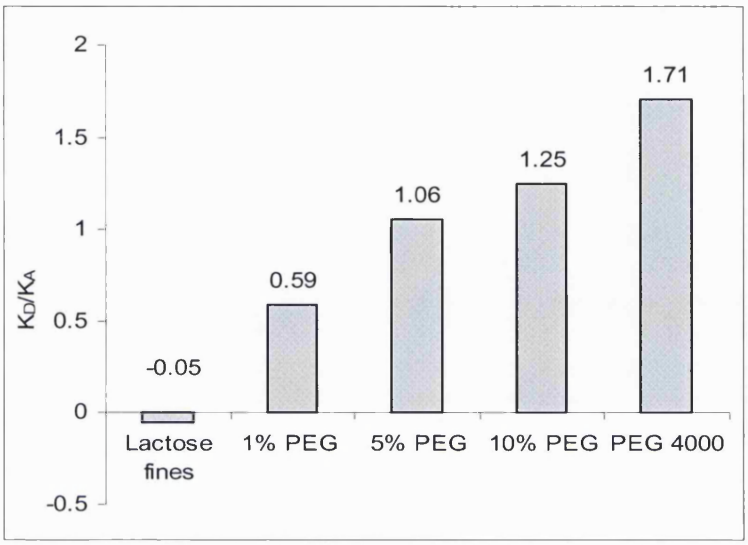

Figure 4.11. *Acid-base characteristics of the crystalline lactose, different lactose/PEG systems and PEG 4000. Values are mean (n=3).*

4.5.2. Different factors affecting drug deposition

4.5.2.1. Influence of the lactose/PEG ratio

The role of fine lactose in dry powder excipients has been widely addressed (Louey and Stewart, 2002; Louey *et al.*, 2003; Islam *et al.*, 2004). Additionally, the use of L-leucine as a ternary component has also been reported (Lucas *et al.*, 1999). The use of other amino acids, methionine, phenylalanine and valine, was also investigated with varying results (Staniforth, 2000). Tee *et al.* (Tee *et al.*, 2000) have used different sugars (mannitol and sorbitol) as coarse and fine carriers. They concluded that the chemical nature of the coarse carrier was more important in the resulting FPF of SS than that of the fines. All these studies have in common the use of ternary components that had reasonably smooth surfaces. Since the lactose/PEG particles may display different levels of asperities, as suggested by surface energy data, it was anticipated that the

deposition properties could be correlated with differences in surface energies. Two grades of carrier lactose (Aero Flo 65 and Pharmatose 325M) were selected and air-jet sieved. The air-jet method is a single-sieve system for dry powders. In this technique, the sieve is mounted in a sealed chamber and the air is drawn upwards through the sieve from a rotating slotted nozzle to fluidise the sample. Undersized particles are carried downward through the sieve to a collection canister. Each lactose grade was sieved for 15 minutes using a sieve aperture of 45 μm (Endecotts, UK). This was done to remove particles that were less than 45 μm in size. In all following tables, the presence of an air-jet sieved material will be indicated by a preceding (A) in the formulation name.

Experiments were conducted with the hydrophobic drug model, since preliminary studies described in chapter 3 showed that higher respirable fractions of BDP were obtained using a lactose carrier with a high proportion of lactose fine particles. The role of fine lactose in the dispersion of the hydrophilic drug model from lactose mixtures was also studied in the previous chapter. SS deposition patterns appeared to be less related to the fine concentration.

Different binary mixtures consisting of air-jet sieved lactose and lactose/PEG fines (containing 1, 5 or 10 % (w/w) PEG 4000) were prepared in 5 g batches. The powders were mixed for 30 minutes at 42 rpm. To each of these binary mixtures, micronised BDP was added so that the final drug concentration was equal to 4 % (w/w). The final mixing step was carried out using a Turbula Mixer at a speed of 42 rpm for 20 minutes. After conclusive content uniformity assessment (varying from 3.6 to 4.6 %), the reservoir of a Clickhaler® was filled with the final mix and measurements undertaken using a TSI as described in chapter 2.

Aerosol deposition studies were first conducted with blends of BDP and the Aero Flo 65 based formulations (Table 4.4). The different EDs and RDs are represented in Figure 4.12 by the grey columns, whereas the FPFs are represented by the black points. Significant differences in the deposition of the micronised drug were observed after removing the fines from the carrier surface. In fact, formulation 2 produced a RD of 69 (23) μg, over 5 times less than the values obtained for the untreated formulation (RD of 388 (55) μg).

The ED remained constant: 959 (51) µg vs. 929 (114) µg. Overall, this resulted in a dramatic decrease in FPF (7.3 (1.5) %) vs. 40.6 (3.5) %). When assessing the effect of incorporating 10 % (w/w) of crystalline lactose/PEG fines containing 1, 5, 10 % (w/w) PEG 4000, it appeared that no significant improvement in the ED was observed for the 1 and 5 % PEG systems (Formulations 4 and 5) compared to the original Aero Flo 65 (Formulation 1). Adding 10 % fines containing 10 % PEG (Formulation 5) however had a detrimental effect on the ED when compared to the two other co-spray-dried systems. The ED dropped from the similar values of 1007 (151) µg when using fines containing 1 % PEG and 954 (74) µg for the 5 % PEG, to the lower value of 799 (84) µg for the 10 % PEG. On comparison to the air-jet sieved Aero Flo 65, the data indicated that there was a significant improvement in both the RD and the FPF of BDP whichever lactose to PEG ratio was used. All formulations delivered similar RD, indicating that the nature of the fines did not seem to have a significant impact on the deposition properties of the formulations. The FPF of the different formulations containing lactose/PEG fines ranged from 22.8 (4.3) to 31.6 (5.8) %.

Formulation	Carrier	ED (µg)	RD (µg)	FPF (%)
1	Aero Flo 65	954 (51)	388 (55)	40.6 (3.5)
2	A Aero Flo 65	929 (114)	69 (23)	7.3 (1.5)
3	A Aero Flo 65 +fines Containing 1 % PEG	1007 (151)	229 (58)	22.8 (4.3)
4	A Aero Flo 65 +fines Containing 5 % PEG	954 (74)	227 (61)	23.7 (5.3)
5	A Aero Flo 65 +fines Containing 10 % PEG	738 (77)	234 (88)	31.6 (5.8)

Table 4.4. *Influence of the nature of the fines on BDP deposition from the Aero Flo 65 based carriers. Values are mean and (standard deviation).*

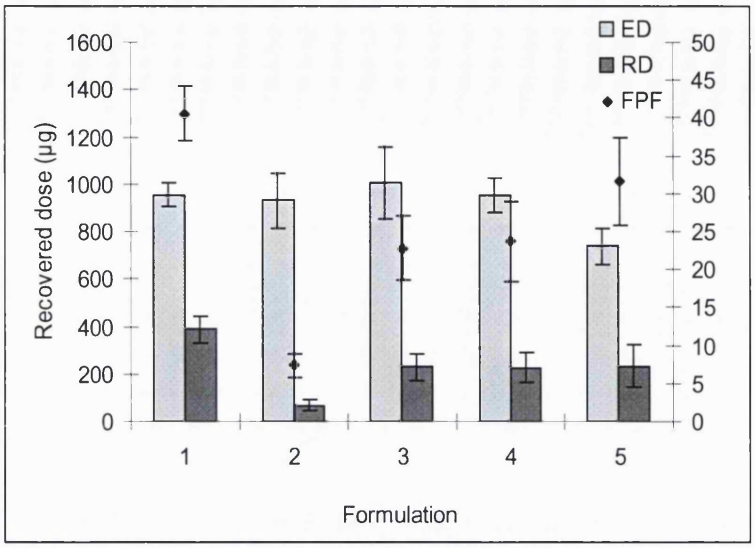

Figure 4.12. *In vitro deposition of the different Aero Flo 65 based formulations with BDP as drug model. Values are mean (n=3).*

The results of adding lactose/PEG systems used as fines to an air-jet sieved Pharmatose 325M are presented in Table 4.5 and Figure 4.13. Removing the majority of lactose fines also had a detrimental effect on the performance of this particular grade of lactose. The air-jet sieved grade (Formulation 2) produced a RD of 91 (13) µg and an FPF of 10.6 (1.2) %, compared to 204 (33) µg and 18.4 (2.7) % for the untreated Pharmatose 325M (Formulation 1). Adding crystalline lactose/PEG systems had a beneficial effect on the RD not only compared to the air-jet sieved grade but also compared to the original lactose. Here again, the RD for the different formulations was similar with RD varying from 263 (11) µg to 347 (105) µg depending on the lactose to PEG ratio in the added fines (Formulations 3 to 5). When the level of PEG 4000 in the fines was increased to 10 %, the ED, as observed in the case of the Aero Flo 65 based formulations, decreased (860 (84) µg). This may be related to poor packing and poor flowability of the formulation containing 10 % fines consisting of 10 % PEG. The ED was not affected with the other types of fines that were prepared.

Formulation	Carrier	ED (µg)	RD (µg)	FPF (%)
1	Pharmatose 325M	1110 (35)	204 (33)	18.4 (2.7)
2	A Pharmatose 325M	927 (23)	91 (13)	10.6 (1.2)
3	A Pharmatose 325M + fines containing 1 % PEG	1209 (169)	347 (105)	28.3 (5.1)
4	A Pharmatose 325M + fines containing 5 % PEG	1277 (184)	307 (18)	24.6 (5.3)
5	A Pharmatose 325M + fines containing 10 % PEG	860 (84)	263 (11)	30.9 (3.4)

Table 4.5. *Influence of the nature of the fines on BDP deposition from Pharmatose 325M based carriers. Values are mean and (standard deviation).*

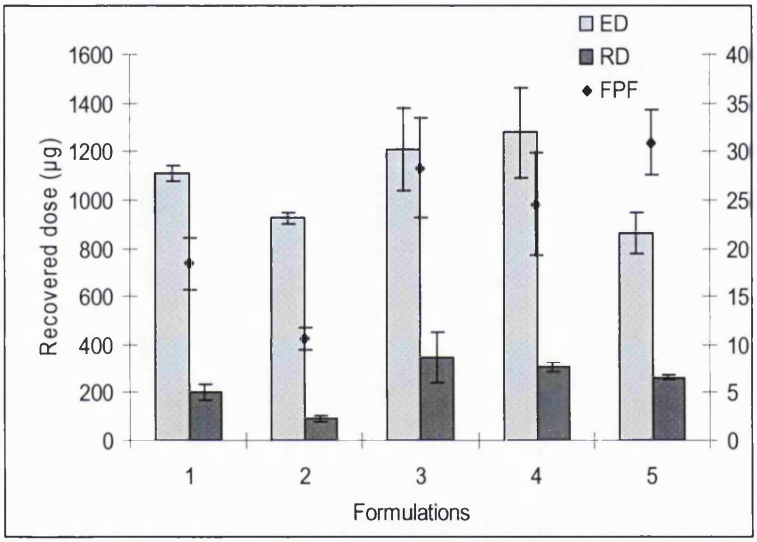

Figure 4.13. *In vitro deposition of the different Pharmatose 325 M based formulations with BDP as drug model. Values are mean (n=3).*

When comparing the delivery of respirable BDP particles using different carriers, the FPF was the most useful parameter to consider, since the amount of emitted drug differed. The highest FPFs were obtained in both cases with the highest proportion of the polymer in the fines. The greater PEG concentration was thought to be associated with a higher amount of small asperities on the surface of the lactose/PEG fines. The presence of those asperities is likely to result in a reduction in the van der Waals attractive forces, due to an increased separation distance between the surface and the associating drug particles. The differences in performance observed between the two lactose grades decreased when the 10 % PEG fines were introduced in the formulation.

Without modifications the Aero Flo 65 displayed a FPF and a RD, which were about double that of untreated Pharmatose 325M. After adding 10 % crystalline fines consisting of 10 % PEG, the modified carriers exhibited comparable performances for the three *in vitro* parameters. This may represent a significant advantage for the formulator, in that differences between marketed lactose grades from different sources can be removed.

To further examine the effect of adding 10 % fines containing 10 % PEG, experiments were conducted with the hydrophilic drug model. The data for the deposition of SS is shown in Table 4.6 and Figure 4.14.

Formulations	Carrier	E.D (µg)	R.D (µg)	FPF (%)
1	Aero Flo 65	1271 (61)	395 (12)	31.2 (0.9)
2	Pharmatose 325 M	1219 (125)	303 (53)	24.9 (3.2)
3	A Aero Flo 65 + fines containing 10 % PEG	691 (14)	292 (16)	42.4 (1.7)
4	A Pharmatose 325 M + fines containing 10 % PEG	1065 (50)	487 (21)	45.8 (0.9)

Table 4.6. *SS aerosol deposition from different lactose carriers. Values are mean and (standard deviation).*

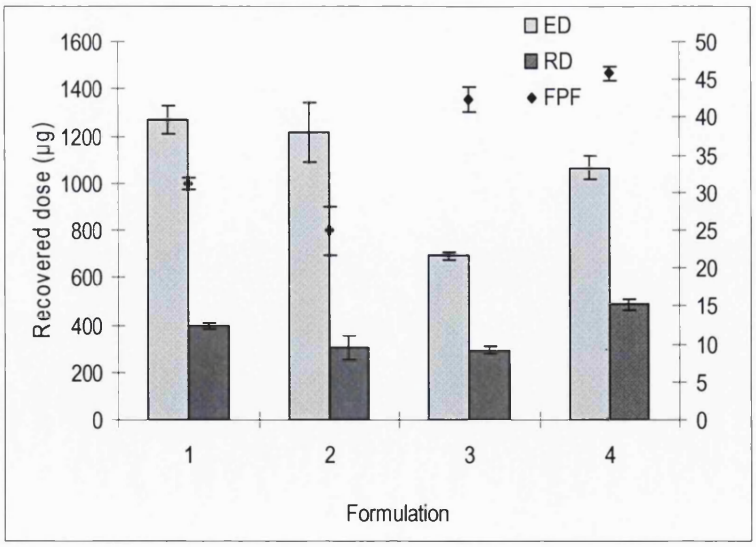

Figure 4.14. *In vitro deposition of the different lactose modified carriers with SS as drug model. Values are mean (n=3).*

The addition of 10 % lactose/PEG (containing 10 % PEG) had a detrimental effect on the ED of the hydrophilic drug whichever grade of lactose was chosen. This was in accordance with the results obtained with BDP where decreased EDs were also found with this particular formulation. Both modified formulations gave rise to improved FPFs: 42.4 (1.7 % for the Aero Flo 65 based formulation and 45.8 (0.9) % for the Pharmatose based formulation. Modifying the surface of the carriers did not result in a standardisation of the performances of the hydrophilic drug model due to differences in EDs.

4.5.2.2. Mixing sequence

Preliminary studies have shown the importance of the mixing sequence on the deposition of different drugs from dry powder formulations. Zeng *et al.* (Zeng *et al.*, 1999) investigated the effect of particle size and the addition sequence of the different components on the deposition of SS from a Rotahaler® coupled to a TSI. Ternary mixtures composed of coarse lactose (63-90 µm), lactose fines of two different volume mean diameters (5 µm or 15.9 µm) and SS were prepared using different mixing sequences. They reported an improvement in both RD and FPF for the formulations containing fines compared to that for the control.

Mixing the coarse lactose with the smaller-sized fines prior to adding the drug led to the highest dispersion efficiency. Larger-sized fines also have a positive impact on the efficiency of the formulation, even if the mixing sequence appeared to be less significant. The least efficient formulations were obtained by mixing SS and coarse lactose prior to adding the fines. These results were confirmed in another study by the same author (Zeng *et al.*, 2000b), in which the content homogeneity and dispersibility of BDP from different lactose carriers were evaluated. The effect of the chosen sequence of powder component addition confirmed the previous study: all ternary formulations exhibited a higher dispersibility of BDP than the binary mixtures (coarse lactose and drug). It also confirmed that pre-blending coarse lactose and fine lactose prior to adding BDP led to a higher RD and FPF (21.7 (4.8) µg and 4.9 (0.8) %) compared to the values obtained when mixing the drug and the coarse lactose prior to adding the fines (13.6 (4.4) µg and 3.1 (1.0) %). The authors attributed such an effect to the coverage of high energy binding sites on the coarse particles by the fines,

leaving the drug particles to adhere to less energetic alternative binding sites. This in turn resulted in higher efficiency. However, in another study by Lucas *et al.* (Lucas *et al.*, 1998a), the order of addition of lactose fines did not affect *in vitro* deposition of either SS or albumin, from a Diskhaler®, leading the authors to suggest another possible mechanism involving the presence of small drug-fine aggregates. This was indicative of a redistribution of the drug from the coarse carrier to the ternary component. Louey *et al.* (Louey and Stewart, 2002) also concluded that the dispersion of ternary mixtures comprising SS, coarse lactose and fine lactose were independent on the order of mixing.

Acknowledging the existence of these conflicting results, the purpose of this section was to assess whether the mixing sequence involving the lactose/PEG fines had an impact on the deposition patterns of both BDP and SS. In addition to the data already described and used as controls, the impact of mixing the drug with the coarse carrier prior to adding the fines had to be assessed. The Aero Flo 65 was designated as the control carrier as it was the most efficient in delivering the hydrophobic drug. The air-jet sieved Aero Flo 65 was mixed with BDP for 30 minutes using a Turbula mixer at 42 rpm before adding the lactose/PEG fines and blending for a further 20 minutes. Each time, the overall drug and fine concentrations were 4 % (w/w) and 10 % (w/w) respectively.

The results of experiments conducted to study the effect of the mixing sequence on drug deposition from the Clickhaler® are summarised in Table 4.7 and shown in Figure 4.15. In the following table, the notation "fines" refers to lactose/PEG crystalline fines containing 10 % (w/w) PEG 4000.

Formulation	Carrier	ED (µg)	RD (µg)	FPF (%)
1	A Aero Flo 65 + BDP	929 (114)	69 (23)	7.3 (1.5)
2	A Aero Flo 65 + fines +BDP	799 (84)	256 (72)	31.6 (5.8)
3	A Aero Flo 65 + BDP + fines	960 (80)	139 (24)	14.6 (2.5)
4	A Aero Flo 65 + SS	1114 (37)	358 (14)	31.7 (1.2)
5	A Aero Flo 65 + fines +SS	690 (14)	292 (16)	42.3 (1.7)
6	A Aero Flo 65 + SS + fines	1200 (49)	406 (41)	33.8 (2.9)

Table 4.7. *Influence of the mixing sequence on the performances of SS and BDP. Values are mean and (standard deviation).*

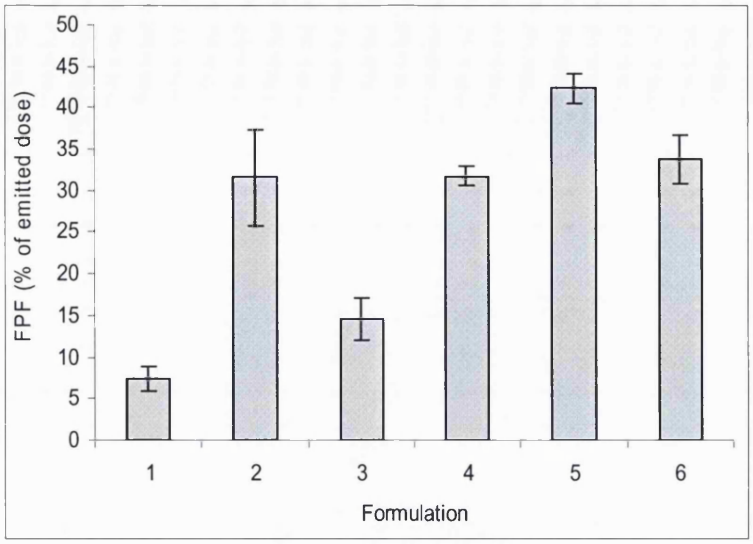

Figure 4.15. *Influence of the mixing sequence on the FPF of SS and BDP formulations. Values are mean, n=3..*

Regardless of the mixing sequence, ternary ordered mixes (Formulations 2, 3, 5 and 6) exhibited higher FPFs than the corresponding binary mixes (Formulations 1 and 4). As previously described, adding a ternary component (here, crystalline lactose/PEG fines) to an air-jet sieved lactose had an impact on the RD and FPF for both drugs. This effect may be partly due to the coverage of active binding sites on the coarse lactose by the fines, affecting the particulate interaction between the drug and the coarse carrier. Only more passive sites would remain available for adhesion during the second stage of blending. When BDP was mixed with the coarse carrier prior to adding the fines, the RD was found to be equal to 139 (24) µg and the FPF to 14.6 (2.5) % (Formulation 3). Those values were significantly higher than those obtained with the binary mixture consisting of the air-jet sieved grade and the drug (Formulation 1). Therefore, if the fines were only acting by occupying the high energy binding sites, then their addition to a binary ordered mix would have had no effect on the FPF. The improved deposition observed with Formulation 3 may be due to some redistribution of BDP and fines between active and passive adhesion sites on the surface of the coarse carrier occurring during the powder mixing. Another possibility is the existence of small aggregates or individual particles free within the mix, acting as an alternative carrier as previously described by Clarke *et al.* (Clarke *et al.*, 2001). An example is in Figure 4.16.

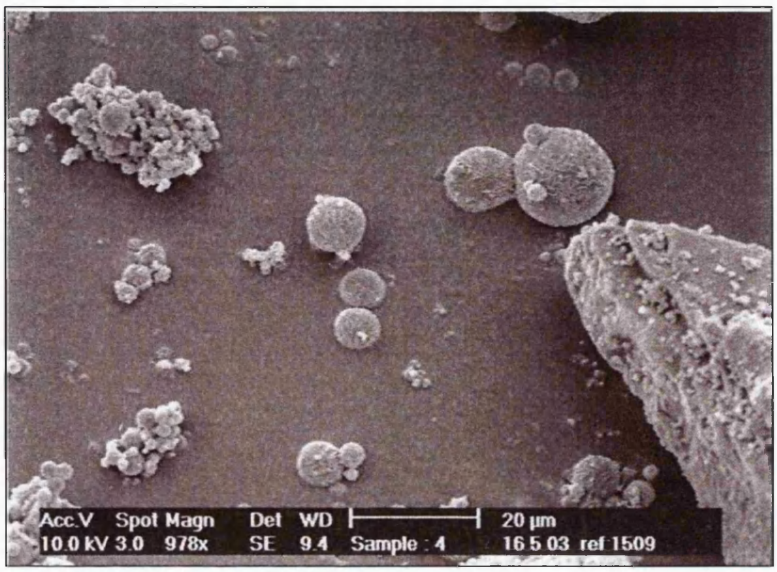

Figure 4.16. *Scanning electron micrograph of a ternary mixture consisting of A Aero Flo 65, lactose/PEG 10 % fines and BDP.*

The ED was also influenced by the blending process, the lowest being observed for Formulation 2 (799 (84) µg). The dramatic increase in both the RD and FPF for BDP for Formulation 2 compared to Formulations 1 and 3 corroborated the observations of Zeng *et al.* (Zeng *et al.*, 2000b), who had previously shown an improvement in the dispersion and deaggregation of BDP particles. The addition sequence during the formulation had a different impact on SS deposition. The performances of SS were similar for the binary mixture (Formulation 4) and the ternary mixture where the fines were added last (Formulation 6). Adding the fines to a carrier prior to adding SS (Formulation 5) led to the highest FPF with a value of 42.3 (1.7) %, compared to 31.7(1.2) % for Formulations 4 and 33.8 (2.9) % for Formulation 6. Although the ED for Formulation 5 dropped dramatically compared to the control (Formulation 4), it was in accordance with the ED of Formulation 2 with the same mixing sequence but containing BDP (690 (14) µg vs. 799 (84) µg). The RD of Formulations 5 and 2 were also comparable (292 (16) µg vs. 256 (72) µg).

In conclusion, the addition of fines and the mixing order do not have the same effects with different drug models. As previously described, these results indicate that BDP is much more sensitive to the presence of fines than SS.

4.5.2.3. Effect of the fine concentration

Lucas *et al.* (Lucas *et al.*, 1998b) investigated the role of fine particle lactose on aerosol performances of albumin based dry powder formulations using the Diskhaler® device. They pre-mixed fine particle lactose (Sorbolac 400; VMD = 5.4 µm) with a coarse lactose (63-90 µm) carrier. The concentration of fines used varied from 2.5 % to 10 % (w/w). The active was then blended with this binary mixture. The performance modifying effect of fine lactose was demonstrated by the improvement in albumin FPF, which increased from 31.7 (2.4) % for a coarse lactose to 49.8 (5.1) % in the case of carrier lactose pre-treated with 10 % (w/w) fines. The role of the concentration of the ternary component in the dispersion of SS from a Rotahaler® coupled to a TSI was examined by Louey *et al.* (Louey and Stewart, 2002). Batches containing 5 % w/w drug and 0-10 % (w/w) fines were prepared. Two types of materials were used as fines: micronised lactose (VMD = 4.0 µm) and micronised glucose (VMD = 4.4 µm). The authors found that increasing ternary concentration increased the FPF to a maximum level of around 40 %. In another study, Islam *et al.* (Islam *et al.*, 2004) demonstrated the relationship between the fine lactose concentration and the dispersion of salmeterol xinafoate. They found a reasonably good linear relationship and significant regression between the FPF of the active and the concentration of fine lactose (less than 5 µm) (r^2= 0.908 and r^2= 0.972) for Aero Flo 65 and Aero Flo 95 respectively). Other research by Al-Hadithi (Al-Hadithi, 2004) showed no beneficial effect of adding crystalline lactose fines (5 to 15 % (w/w)) to an air-jet sieved Pharmatose 325M in term of SS deposition.

Modifying lactose grades by adding lactose/PEG fines influenced the deposition profiles for the two model drugs studied. This section aims to define the level of added fines needed for optimum deposition.

Different percentages of fine lactose/PEG 4000 particles were added (0, 2.5, 5, 7.5 and 10 % (w/w)) to the air-jet sieved Aero Flo 65. The effect of ternary concentration in excess of 10 % (w/w) was not determined since the ED appeared to be affected by 10 % fines due to possible poor flowability of the blend. The PEG to lactose ratio in the spray-dried particles was 10 % (w/w).

The effect of the fine concentration was studied for both SS and BDP. The drugs were added last to reach a 4 % (w/w) concentration. The blending process was the same as presented in Section 4.6.1.

The relationship between FPF of the active (BDP or SS) and the concentration of lactose/PEG fines is shown in Figure 4.17. Good linear relationships between FPF and fine content were found for both drugs (r^2= 0.76 for BDP and 0.75 for SS). Moreover, the steeper gradient for BDP compared to SS points out again that BDP is more likely to be influenced by the surface carrier than SS. When considering the hydrophobic drug model, it appeared that the greatest stepped-increase in the fine particle fraction was obtained with the addition of 5 % (w/w) of lactose/PEG fines. While the ED was maintained (929 (114) µg vs. 999 (32) µg), the RD increased from 69 (23) µg to 225 (16) µg. This improvement was also demonstrated by an increase in FPF, rising from 7.4 (1.6) % to 22.5 (1.2) %. Adding 7.5 % fines did not have an effect on the ED either, with a valur of 970 (12) µg. However, this formulation resulted in a significant lower RD (150 (12 µg)), which was linked to a lower FPF (15.5 (1.3) %). Adding 10 % fines, as previously described, had a detrimental effect on the ED. Regarding the hydrophilic drug model, the addition of fines up to a level of 7.5 % does not seem to impact to the same extent on the performance of the carriers. Both the RDs and the FPFs were comparables with values ranging from 306 (10) µg to 58 (14) µg and 31.0 (2.2) % to 34.5 (1.1) % depending on the formulation considered. The higher FPF observed with the 10 % fines (42.3 (1.7) %) was mainly due to the decrease in the ED (690 (14) µg). These findings were in accordance with the work previously carried out in our laboratory. Adding lactose/PEG crystalline fines at these specified levels did not improve the efficiency of the carrier in delivering SS.

	BDP			SS		
% of fines	ED (µg)	RD (µg)	FPF (%)	ED (µg)	RD (µg)	FPF (%)
0 %	929 (114)	69 (23)	7.4 (1.6)	1114 (37)	358 (14)	31.7 (1.2)
2.5 %	990 (29)	110 (31)	10.8 (3.3)	995 (53)	309 (29)	31.0 (2.2)
5 %	999 (32)	225 (16)	22.5 (1.2)	886 (12)	306 (10)	34.5 (1.1)
7.5 %	970 (12)	150 (12)	15.5 (1.3)	990 (18)	339 (19)	34.2 (1.8)
10 %	799 (84)	256 (72)	31.6 (5.8)	690 (14)	292 (17)	42.3 (1.7)

Table 4.8. *Influence of the fine concentration on both BDP and SS deposition. Values are mean and (standard deviation).*

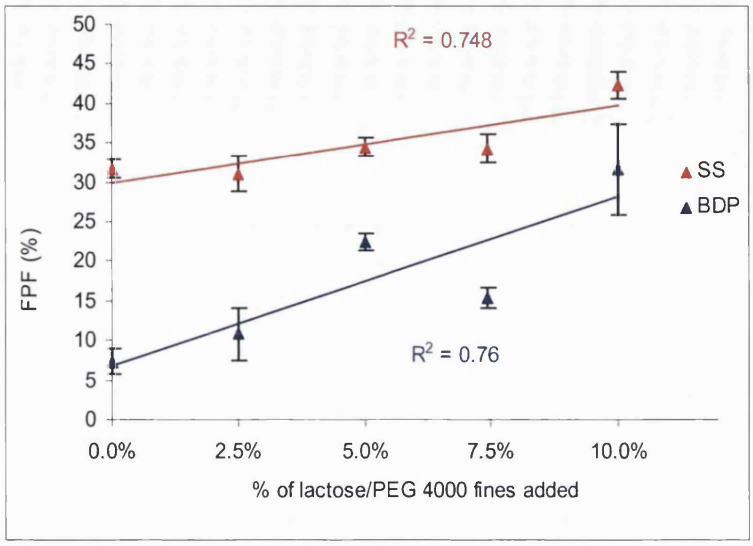

Figure 4.17. *Relationship between FPF of SS and BDP and the concentration of lactose/PEG fines. Values are mean (n=3)).*

4.5.2.4. Effect of the drug concentration

The concentration of micronised drug in the powder formulation is usually low with a typical drug to carrier ratio of 1 to 67.5 (Zeng *et al.*, 2000a). All experiments that have been described were conducted with a drug concentration of 4.0 % (w/w), in accordance with the ratio employed in the commercial Asmasal™ formulation. In this section the effect of SS and BDP concentrations was evaluated. It is known that the drug to carrier ratio may influence the deposition profiles. Lucas (Lucas *et al.*, 1999) studied the deposition of SS-coarse lactose carrier formulations with different drug loadings. Formulations with 0.96 and 3.2 % (w/w) drug were prepared and tested using a Diskhaler® and a modified TSI with a cut-off diameter of 5.3 µm. An increase in drug concentration led to a higher drug deposition (FPF of 11.1 % and 16.5 % respectively). This was in accordance with the earlier observations of Ganderton (Ganderton, 1992; Steckel and Müller, 1997). However, the effect of the drug to carrier ratio is not always straightforward. Steckel *et al.* (Steckel and Müller, 1997) investigated the influence of the percentage of BUD (1, 5 and 9 % (w/w)) in the interactive mixtures containing a coarse lactose carrier on the deposition from the single-unit dose Spinhaler® and the multiple-unit dose Easyhaler®. Three different lactose sieve fractions were studied: below 32 µm, between 63 and 90 µm, and between 125 and 180 µm.

For the 63-90 µm fraction, it was found that increasing the drug to carrier ratio resulted in a signifiant decrease in FPF, independent of which sieve fraction or device was used. For example the FPF dropped from 28.40 (0.74) % using a 1 % drug loading to 23.69 (0.46) % using a 9 % drug loading. Those values dropped from 37.25 (0.41) % to 25.96 (2.19) % using the same conditions and the Easyhaler®.

The aim of this section was to aerosolize formulations containing different ratios of drug to lactose carrier. Formulations were prepared by mixing the Aero Flo 65 with a range of active concentrations (1, 2 and 4 % (w/w)) using either BDP or SS. This was carried out using a Turbula mixer for 30 minutes at 42 rpm. The aerosol deposition data obtained from these formulations are summarised in Table 4.9.

	BDP			SS		
Drug loading	ED (µg)	RD (µg)	FPF (%)	ED (µg)	RD (µg)	FPF (%)
4 %	954 (52)	388 (55)	40.6 (3.5)	1271 (61)	395 (12)	31.2 (0.9)
2 %	487 (55)	122 (23)	25 (2.2)	636 (128)	214 (38)	33.7 (1)
1 %	233 (33)	59 (12)	25.1 (1.7)	357 (32)	108 (12)	30.5 (4.8)

Table 4.9. *Effect of the drug to carrier ratio on the deposition profiles of BDP and SS. Values are mean and (standard deviation).*

Increasing the percentage of drug in the formulation led to an increase in the ED. As expected, positive correlations between the drug loading and the EDs for the two drugs were observed. For the hydrophobic drug model, a 1 % (w/w) drug loading resulted in an ED of 233 (33) µg. Doubling the drug loading to 2 % (w/w) increased the ED to 487 (55) µg, twice that of 1 % drug loading. The RDs followed the same trend with an increase from 59 (12) µg to 122 (23) µg. This resulted in similar FPF of BDP for these two drug loadings: 25.1 (1.7) % vs. 25.0 (2.2) % for 1 and 2 % drug loading respectively. Further doubling the concentration to 4 % was seen to raise the ED to 954 (52) µg and the RD to 388 (55) µg, leading to a 40.6 (3.5) % FPF. This more effective dispersion of the

powder at high coverage of drug has been already described by Ganderton (Ganderton, 1992). He stated that at high drug loading, more drug particles may be adhering with less strong binding affinities to the surface of the lactose carrier, leading to higher FPF.

For the hydrophilic drug model, the ED and the RD increased in parallel with increasing drug loading. As a result of this, similar FPFs were obtained for the different formulations. The FPF for the 1 % blend was 30.5 (4.8) %, 33.7 (1) % for the 2 % blend and 31.2 (0.9) % for the 4 % blend. In conclusion, *in vitro* deposition appeared to be independent of the SS concentration.

4.6. General conclusions

The aim of the work described in this chapter was to study some of the factors influencing the performance of dry powder formulations for inhalation using two drug models, SS and BDP. A new type of crystalline fines consisting of lactose/PEG co-spray-dried system was evaluated as a ternary component for DPI technology. The major findings are summarised below associated with the original objectives of the work carried out.

Investigating the suitability of different lactose/PEG 4000 systems as fines for DPI formulations:

Lactose/PEG 4000 particles were produced by spray drying, the concentration of PEG varying from 1 to 10 % (w/w). The different polymer to lactose ratios were not seen to affect either the general morphology or the particle size distribution of the particles. Physico-chemical characterisation of these systems by dynamic vapour sorption and inverse gas chromatography highlighted the major differences in the particles produced. Visual examination by SEM and surface energy data generated by IGC confirmed the presence of crystalline PEG at the surface of the particles. The presence of those crystals at the surface of the particles may play in important role in decreasing the van der Waals attraction forces responsible for the adhesion of particles.

Examination of the influence of the lactose to PEG ratio in the spray-dried product on the performance of a coarse carrier:

Two different coarse lactose grades were used in this study (i.e. Pharmatose 325M and Aero Flo 65). The influence of adding fines containing different amounts of PEG to a coarse carrier was dependent on the carrier type. The addition of fines did not improve the performances of the original Aero Flo 65, which was found to perform well on its own. Moreover, the RDs for the formulations based on this carrier were independent of the nature of the fines added. However, higher RDs and FPFs were obtained in ternary mixtures for the Pharmatose 325M carrier.

Overall, blending 10 % fines containing 10 % PEG 4000 to air-jet sieved lactose grades prior to adding the BDP seemed to standardise the *in vitro* performances. To assess the robustness of this specific formulation, SS was also tested. Although the FPFs were improved, the EDs varied from one grade to the other, hence limiting the practical use of this approach.

Examination of the effect of the blending sequence on the deposition patterns:

The mechanism by which the addition of fine modifies the drug deposition in these dry powder formulations was not fully understood. Observations from the mixing sequence study were not fully consistent with the theory of the active sites saturation. A competitive adhesion was more likely to have occurred, with the drug being distributed between the large carrier particles and the fine lactose/PEG particles to produce an equilibrium mixture as stated by Louey *et al.* (Louey and Stewart, 2002). Moreover, the high drug loading (4 %) and the high concentration of fines added are likely to involve aggregation and multilayer formation, leading to more complex adhesion processes.

Examination of the influence of varying the concentration of fines and drug on the aerosol performance of different coarse lactose carriers:

When the added fines were increased from 0 % to 10 % in the air-jet sieved Aero Flo 65, the FPF increased from 7.4 % to 31.6 % for the hydrophobic drug model. The optimal level of added fines was found to be 5 % (w/w), at which there was a balance between the effect of the flow properties of the powder (i.e. affecting the release of the dose from the inhaler) and the optimum BDP deposition. The introduction of fines to the coarse lactose did not result in any improvement in the ability of the carrier to liberate SS from its surface.
The drug to carrier ratio also appeared to influence the FPF of the hydrophobic drug model with an increase in the detachment from the carrier particles at high drug loading. This study highlighted once again the differences between the drugs, with the hydrophilic drug model deposition not being affected by the drug loading.

Chapter 5

Partially amorphous lactose/PEG fines used as surface modifiers for DPI

5.1. Summary

In chapters 3 and 4 the importance of fine particles on the aerosol performance of the carrier had been confirmed. The effect of adding different types of crystalline fines had also been extensively studied in the literature. The controlled addition of crystalline lactose/PEG fines into the mixes had varying results on the deposition pattern of the two drug models. A consequence of adding a large amount of fines was the apparent reduction in the powder flow, which had significant implications on the obtained RDs. This chapter evaluates the use of partially amorphous lactose/PEG fines to be recrystallised onto two coarse lactose surfaces. Based on the early surface energy measurements presented in chapter 4, it appeared that adding lactose/PEG fines resulted in an apparent "PEG like" surface. This current chapter also aims to compare the performances of these new systems with the performance of a PEG 4000 carrier. In the second part of this chapter, the overall applications of surface energy data in predicting DPI performances were investigated.

5.2. Introduction

In a recent work, Al-Hadithi (Al-Hadithi, 2004) introduced amorphous lactose fines onto a crystalline carrier surface. The amorphous fines were allowed to crystallise onto the coarse surface by controlled crystallisation at 53 % RH using a "specially built" conditioning chamber. The crystallisation time varied from 0.5 to 5 hours. The modified carriers were then blended with one of the two model drugs (SS or BDP). *In vitro* assessment was performed using a Clickhaler® coupled to a TSI. Significant improvement in the SS deposition was observed when the crystallisation time was 2 hours. Following these 2 hours of crystallisation, the RD of SS was found to be equal to 499 (169) µg, with an ED of 1250 (320) µg. However, this improvement was not maintained for systems that underwent crystallisation for upwards of 2 hours. Furthermore, the deposition from the hydrophobic model employed (BDP) did not follow this trend and the efficiency of those treated surfaces appeared to be inferior compared to their SS analogs.

5.3. Aims and objectives

The principle aims of the work described in this chapter were to modify the physical characteristics of two coarse lactose surfaces and to correlate the surface free energy of the different systems to the deposition of both hydrophilic and hydrophobic drug models.

The objectives were to:

- Fuse partially amorphous lactose/PEG fines onto the surface of air-jet sieved coarse lactose and to assess their influence on the performance (section A);
- Determine different surface energy parameters by IGC in order to examine how the surface energy of the carriers was affected by physical changes (section A);
- Compare the deposition profiles of these modified carriers with a PEG carrier (section A);
- Determine the correlations between IGC data and deposition patterns (section B).

5.4. Materials and methods

5.4.1. Production of the fines

Alpha-lactose monohydrate and PEG 4000 were added to purified water to give a 10 % (w/v) solution. PEG was added so that the polymer concentration was equal to 10 % by weight of lactose. The raw materials used were identical to the ones used to generate crystalline lactose/PEG 4000 co-spray-dried systems (investigated in chapter 3). The Büchi 191 was used to spray dry the solution at constant process conditions, following the parameters described in chapter 2, Section 2.2.1. The physico-chemical properties of the spray-dried material were analysed using SEM, X-ray diffraction and dynamic vapour sorption. The conditions and instruments used in this study were as reported in chapter 2.

5.4.2. Surface treatment of lactose crystals

Two different grades of α-lactose monohydrate (Pharmatose 325M and Aero Flo 65) were air-jet sieved over a 45 μm mesh sieve, as previously described in chapter 4. As soon as the spray drying process was over, the fines were collected and blended with the air-jet sieved coarse carrier for 30 minutes at 42 rpm using a Turbula mixer. The fines were left to recrystallise for 24 hours at room temperature. BDP or SS were then added at a concentration of 4.0 % (w/w) and mixed for 30 more minutes at 42 rpm. Content uniformity assessment and *in vitro* deposition studies were conducted as previously described.

5.4.3. Investigation of PEG 4000 as a control probe carrier

It was necessary to evaluate the use of PEG 4000 directly as drug carrier. This was a way to assess the importance of the chemical nature of a surface. PEG 4000 flakes were ground manually and sieved to obtain a particle size fraction of 45 to 90 μm. This size fraction was then blended with each micronised drug

(4 % (w/w)). The Aerolizer® was used instead of the Clickhaler® as a device since the reservoir device was inefficient in delivering this formulation (see section 5.5.4)

5.5. Results and discussion

5.5.1. Characterisation of the partially amorphous lactose/PEG fines

A scanning electron micrograph (Figure 5.1) of the spray-dried product showed particles with an apparently smoother surface than that observed for crystalline lactose/PEG fines (Figure 4.1). The particle shape is governed by the relatively low presence of asperities, which are due to the presence of surface crystalline PEG.

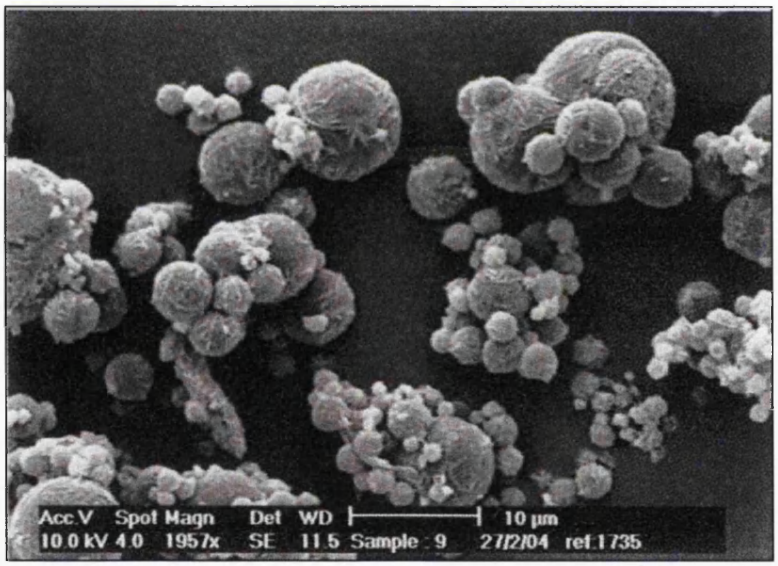

Figure 5.1. *Electron micrograph of partially amorphous lactose/PEG system.*

X-ray diffraction along with DVS was used to characterise the co-spray-dried product. A sample of the spray-dried product was analysed as soon as the run was finished. Corrigan *et al.* (Corrigan *et al.*, 2002) stressed the importance of the timing of the first analysis due to the rapid crystallisation of these systems.

The XRPD diffractogram (Figure 5.2) displayed a partially amorphous lactose/PEG system with some peaks indicative of some crystallisation having already taken place. Figure 5.3 showed the same sample after 24 hours, which is consistent with a recrystallised sample.

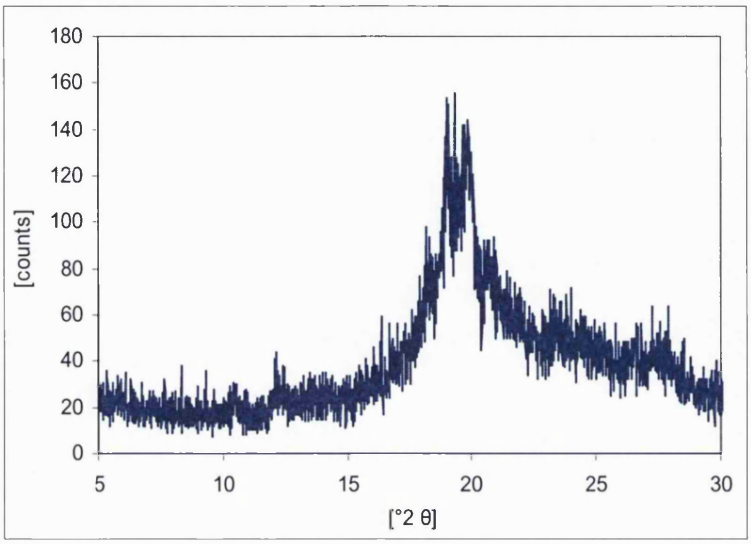

Figure 5.2. *X- ray diffraction data of lactose/PEG 4000 (10 %) showing the partially amorphous compound.*

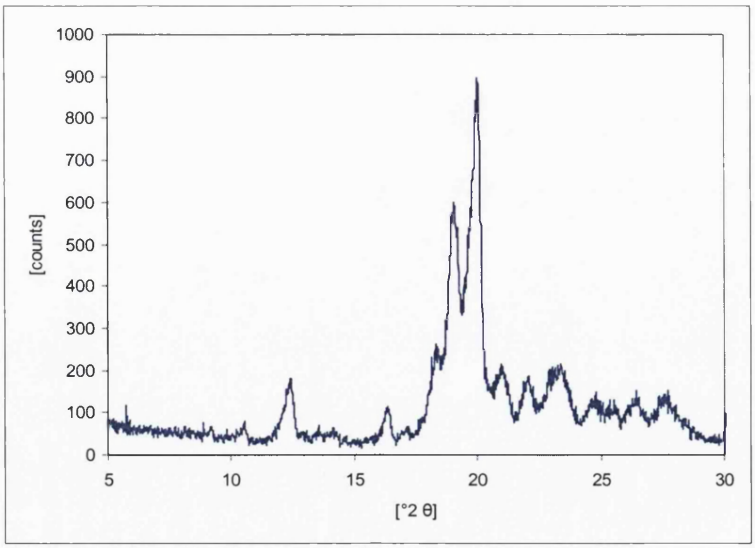

Figure 5.3. *X-ray diffraction data of lactose/PEG 4000 (10 %) after 24 hours showing crystallisation of the partially amorphous compound.*

The water vapour sorption properties of partially amorphous lactose/PEG were analysed using a DVS-1 (Figure 5.4). A three-step experiment was set up. After the initial drying phase (0 % RH for 360 minutes), the powder was exposed to 80 % RH. A swift mass uptake of water was observed due to vapour sorption at this elevated RH. The maximum water absorption was found to be equal to 6.6 %. This uptake was followed by a nearly instant mass loss whilst the sample remained at 80 % RH. This mass loss was due to the crystallisation of the amorphous sample, which is a consequence of the sorbed water. The sorbed water induced plasticization of the amorphous phase, lowering the glass transition temperature below the experimental temperature (25°C). The newly acquired mobility of the molecules enabled the rapid crystallisation and the displacement of the water. The expulsion of the plasticizing water was not complete and even after the final drying step, some of the water (approximately 1.4 %) is retained as a partial monohydrate.

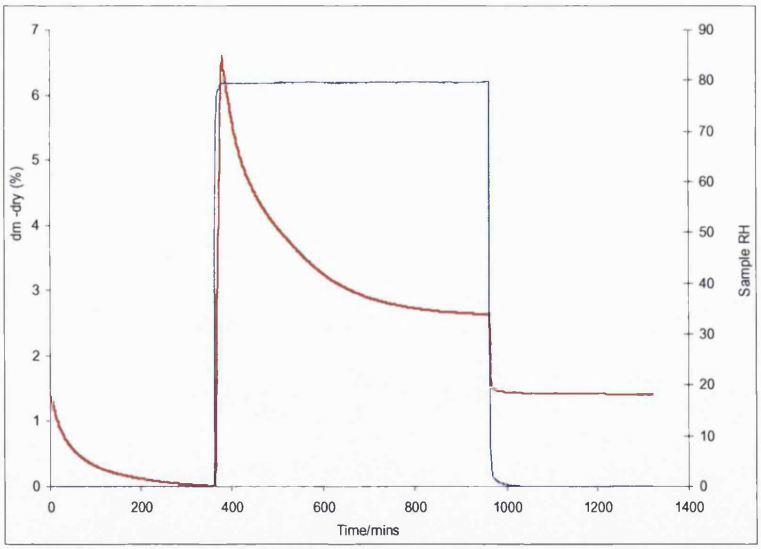

Figure 5.4. *Water sorption for partially amorphous lactose/PEG 4000.*

5.5.2. Characterisation of the modified carriers

Figure 5.5 shows a micrograph of a modified lactose surface with small spherical lactose/PEG fines associated with the coarse carrier.

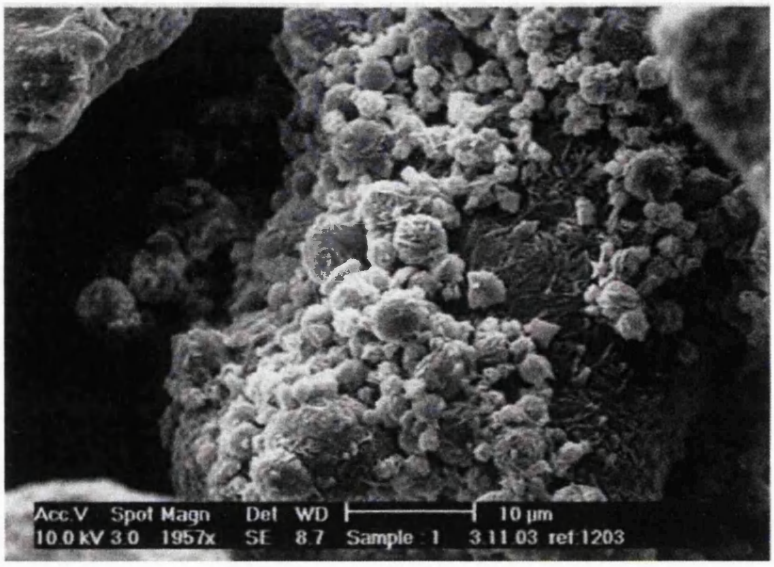

Figure 5.5. *Scanning electron micrograph of the" fused system".*

Surface energy measurements by IGC were obtained as described in chapter 2. Two different batches of surface modified lactose carriers were analysed and the different parameters measured are summarised in Tables 5.1 and 5.2.

	Run 1	Run 2	Run 3	Run 4	Run 5	Run 6	Average
γ_s^d (mJ/m^2)	35.7	37.5	36.4	34.7	35.6	35.1	35.8 (1.0)
Acetone (J/mol)	5456	5642	5637	5550	5787	5982	5676 (186)
Chloroform (J/mol)	2514	2722	2522	2635	2713	2729	2639 (100)
Ethanol (J/mol)	8094	8298	8067	8181	8256	8203	8183 (90)
Ethyl acetate (J/mol)	7115	7507	7268	7304	7446	7499	7357 (155)

Table 5.1. *Surface energy parameters of the modified Aero Flo 65 obtained with 2 different columns and three repeats for each column.*

The modified Aero Flo 65 (Table 5.1) exhibited on average a relatively low dispersive surface energy, with a γ_s^d of 35.8 (1.0) mJ/m^2 compared to that of the original grade (42.9 (0.3) mJ/m^2). This may anticipate a lower binding tendency of the drug and increased aerosolisation efficiency. The K_A and K_D were determined using the cross-section method, because the linear fit with the boiling point method was seen to be poor (r^2 below 0.4). The calculated K_D/K_A ratio was found to be equal to 0.44 (0.02) with a K_A value of 0.0922 (0.001) and a K_D value of 0.0411 (0.002). These acid-base properties were very similar to

the ones of the Pharmatose 325M based formulation (Table 5.2), which had a calculated K_D/K_A ratio of 0.47 (0.02). The corresponding K_A value of the latter formulation was equal to 0.0921 (0.002) and the K_D value was 0.0435 (0.003). The γ_s^d was also similar with an average value of 34.4 (1.2) mJ/m^2.

	Run 1	Run 2	Run 3	Run 4	Run 5	Run 6	Average
γ_s^d (mJ/m^2)	36.7	34.1	34.0	34.5	33.1	34.2	34.4 (1.2)
Acetone (J/mol)	5859	5789	5753	5671	5592	5795	5743 (96)
Chloroform (J/mol)	2915	2700	2742	2701	2540	2713	2718 (120)
Ethanol (J/mol)	8615	8237	8217	8006	7783	7977	8139 (287)
Ethyl acetate (J/mol)	7710	7266	7422	7342	7072	7320	7355 (209)

Table 5.2. *Surface energy parametersof the modified Pharmatose 325M surface obtained with 2 different columns and three repeats for each column.*

Having examined the surface energy parameters of the different formulations in chapters 3, 4 and 5, it appeared important to plot some of the results that were described fully in these previous chapters. Figure 5.6 presents the dispersive component determinations and Figure 5.7 summarises the individual probe interactions with each powder surface.

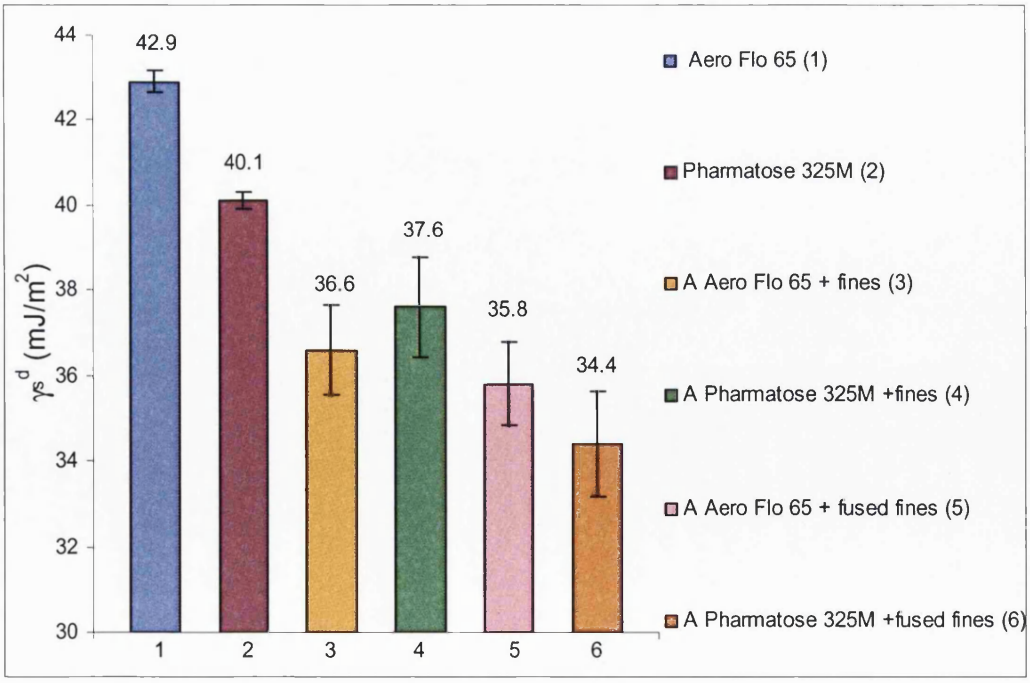

Figure 5.6. *Effect of powder modification on the resulting dispersive energy. Values are mean and based on at least three measurements.*

Compared to the dispersive surface energies of the different grade of lactose alone (Formulations 1 and 2), those of mixtures containing lactose/PEG fines (Formulations 3 to 6) were generally lower with a γ_s^d comparable to that of lactose/PEG fines alone. Interestingly, the variations observed between the two α-lactose monohydrate samples diminished after the surface treatment. Moreover, the differences in specific interactions were also affected by the addition of lactose/PEG fines. Examination of the specific free energy of adsorption (dG) for each probe also showed a "standardisation" of the surface properties, especially for the fused systems. Previous work detailed in chapter 4 showed that modified carriers, consisting of air-jet sieved grades of lactose mixed with 10 % lactose/PEG fines, exhibited comparable aerosol performances for the hydrophobic drug model. The idea that surfaces with similar energies would result in similar deposition patterns was further tested with the fused system.

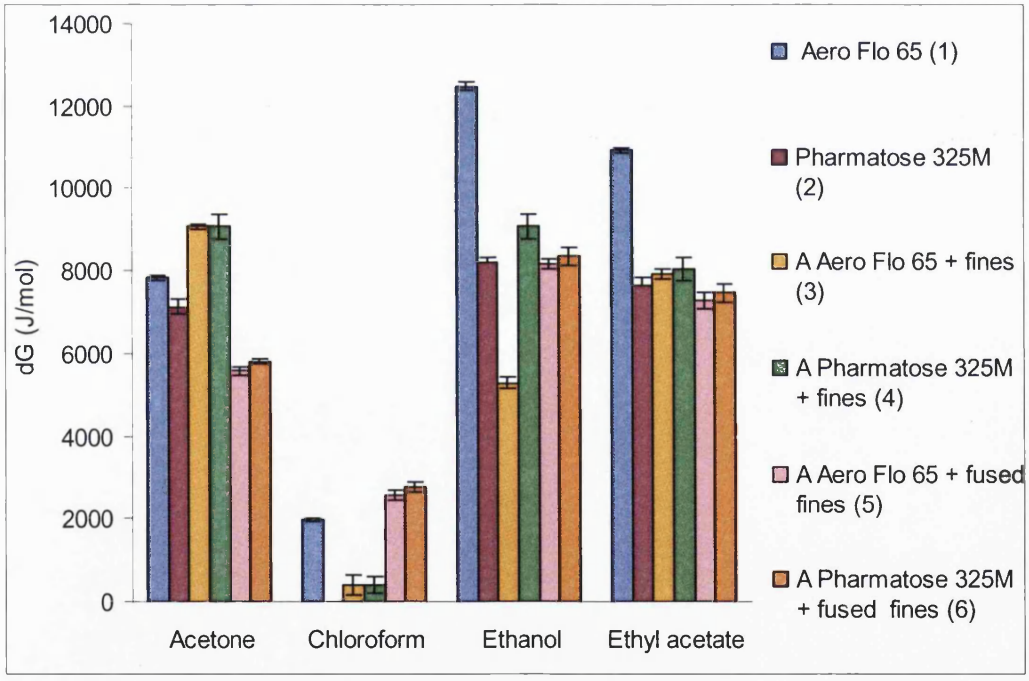

Figure 5.7. *Effect of powder modification on the specific interactions of polar probes. Values are mean and based on at least three measurements.*

5.5.3. Deposition studies

The deposition data of SS and BDP in the TSI via the Clikhaler® is summarised in Table 5.3.

	SS			BDP		
	ED (µg)	RD (µg)	FPF (%)	ED (µg)	RD (µg)	FPF (%)
A Aero Flo 65 + lactose/PEG fused fines	1024 (37)	358 (21)	34.9 (0.9)	955 (172)	119 (7)	12.8 (2.8)
A Pharmatose 325M + lactose/PEG fused fines	1065 (53)	349 (21)	32.8 (0.5)	945 (96)	191 (51)	20.2 (4.3)

Table 5.3. *SS and BDP aerosol deposition from modified lactose carriers. Values are mean and (standard deviation).*

The data in Table 5.3 showed that there were signicant differences in the deposition of SS and BDP. Comparing the performance of the two carriers, the EDs of SS (1024 (37) µg and 1065 (53) µg) were comparable for both carriers. The RDs of the drug were also similar, with values varying from 358 (21) µg to 349 (21) µg. As a result, the modified carriers gave rise to statistically ($p=0.05$) similar FPFs of SS (34.9 (0.9) % vs. 32.8 (0.5) %). In contrast, for BDP, the modified carriers gave poor RDs, ranging from 119 (7) µg for an Aero Flo 65 based carrier to 191 (51) µg for the Pharmatose 325 M based carrier. Overall, the resulting FPF of BDP from the two carriers was low, with values ranging from 12.8 (2.8) % to 20.2 (4.3) %.

As a conclusion, fusing lactose/PEG fines on the surface of air-jet sieved lactose had a mixed effect on the aerosol performances of the resulting carrier, depending on the drug model evaluated. Adding crystalline fines dispersed and deaggregated the hydrophobic drug better than using a fused system. This confirms the importance of free fines in weakening the drug agglomerates.

5.5.4. Deposition studies using PEG 4000 as a model carrier

The individual crystalline PEG 4000 particles (Figure 5.8) adopted the usual tomahawk shape. As previously mentioned, this size fraction (45-90 µm) was then blended with each micronised drug.

The blend coefficient of variation was higher than 5 % due to the difficulty to disperse the drug particles efficiently (C.V. of 7.4 for SS and 9.3 for BDP). Despite these poor blend homogeneities, evaluation for drug deposition was still carried out.

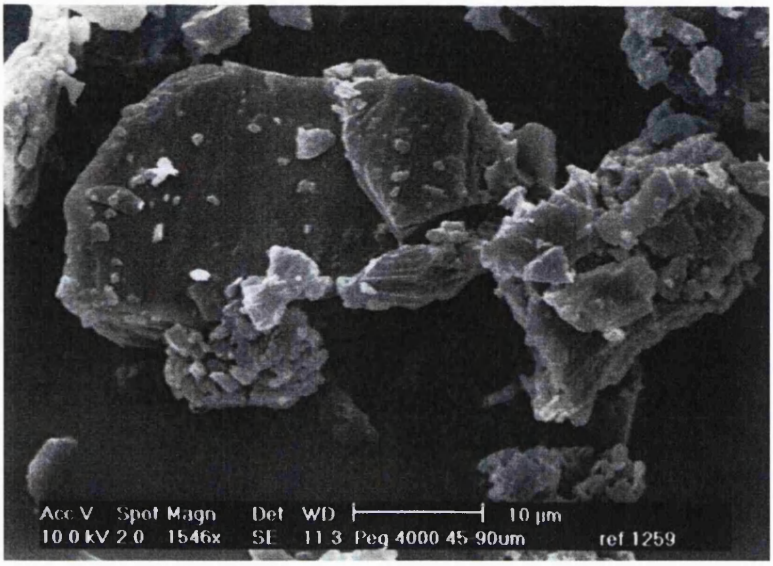

Figure 5.8. *Scanning electron micrograph of PEG 4000 [45-90] µm.*

Difficulties in aerosol generation were also encountered with PEG 4000 (45-90 µm) using the Clickhaler®. The total inhaler weight loss was lower than that of the lactose carrier, with the amount of powder leaving the device varying from 15.4 mg to 16.2 mg for runs comprising ten actuations. This may be due to sub-optimal flow properties or density. A unit dose device, the Aerolizer®, was therefore used as an alternative device. This study also provided a good opportunity to investigate the influence of the device on the deposition.

The loss of patent protection for many of the key drugs in asthma therapy (i.e. SS, terbutaline sulphate, BDP and BUD) has resulted in an increased prescribtion of generic products. As a result of this, the number of newly developed DPI devices also increased (Smith and Parry-billings, 2003). For example, SS could be administered in 2002 in the European Union using 8 different devices (Clickhaler®, Easyhaler®, Pulvinal® and Turbuhaler® as multiple-dose reservoirs; Cyclohaler® and Rotahaler® as single-dose capsules; Diskhaler® as a small multiple-dose replaceable cartridge; and Diskus/Accuhaler® as a multiple unit-dose strip). Drug-carrier formulations can

produce significantly different performances depending on the device that is used (Srichana *et al.*, 1998).

The Aerolizer® and Clickhaler® differ in the aerosol production and also in the device resistance to air flow. The flow (F) through an inhaler device follows the equation:

$$F = \frac{\sqrt{\Delta P}}{R} \qquad \text{[Equation 5.1]}$$

Where $\sqrt{\Delta P}$ is the pressure gradient developed across the device and R the device resistance.

Both devices are of medium resistance, approximately 0.1 cm of H_2O at a rate of 0.5L/min for the Clickhaler® and 0.06 cm of H_2O at a rate of 1L/min for the Aerolizer®. A TSI operating at 60 L/min for 5 seconds was employed to detect the FPF from the firing of a single dose from the Aerolizer®.

Three capsules with the same fill weight (30 mg) were tested for each formulation. Aerosol deposition studies were performed with the two drug models at a concentration of 4 % (w/w). The results are summarised in Table 5.4

	ED (µg)	RD (µg)	FPF (%)
SS deposition	1407 (171)	556 (96)	39.6 (4.9)
BDP deposition	993 (65)	337 (32)	33.9 (1.2)

Table 5.4. *Evaluation of PEG 4000 as a carrier for DPI formulation. Values are mean and (standard deviation).*

As previously mentioned, three 30 mg capsules with 4 % (w/w) drug blends were tested. Based on a uniform blend, the total amount of drug in the impactor and the device should not exceed 1200 µg. However, SS data showed a higher amount of drug recovered (1407 (171) µg). Nevertheless, the calculated FPF was still indicative of the ability of the carrier to disperse both drugs efficiently. In both cases, the percentage of respirable particles was high, with a FPF ranging from 33.9 (1.2) % for BDP to 39.6 (4.9) % for SS. It was surprising to find that PEG was performing so well with the two drug models. One possible

explanation may be found in the surface energy properties of this material: its γ_s^d of 33.1 (0.2) mJ/m^2 suggests lower van der Waals interactions compared to other materials such as lactose. The aerosol generation mechanism of the inhaler being different, it was also important to carry out a comparative study between the Clickhaler® and the Aerolizer®.

5.5.5. Comparative study between the Clickhaler® and the Aerolizer®

5.5.5.1. BDP deposition obtained using the Aerolizer®

All formulations previously tested with the reservoir device were reaerosolised using the capsule-based device following the method described in chapter 2. Results are presented in the following tables and figures.

Formulation	Carrier	ED (µg)	RD (µg)	FPF (%)
1	Lactohale LH 100	814 (68)	220 (14)	27.1 (2.9)
2	Pharmatose 325M	831 (78)	178 (14)	21.6 (2.8)
3	A Pharmatose 325M	773 (47)	178 (23)	23.1 (3.6)
4	Aero Flo 65	916 (92)	292 (46)	31.9 (2.7)
5	A Aero Flo 65	870 (65)	175 (52)	19.9 (4.5)
6	A Pharmatose 325M+ fines	1093 (261)	428 (107)	39.1 (0.6)
7	A Aero Flo 65 + fines	883 (16)	242 (39)	27.5 (4.7)
8	A Pharmatose 325M + fused fines	869 (52)	137 (36)	15.7 (0.4)
9	A Aero Flo 65 + fused fines	941 (38)	186 (9)	19.8 (1.1)

Table 5.5. *Aerosolisation of BDP from different lactose carriersusing the Aerolizer® Values are mean and (standard deviation).*

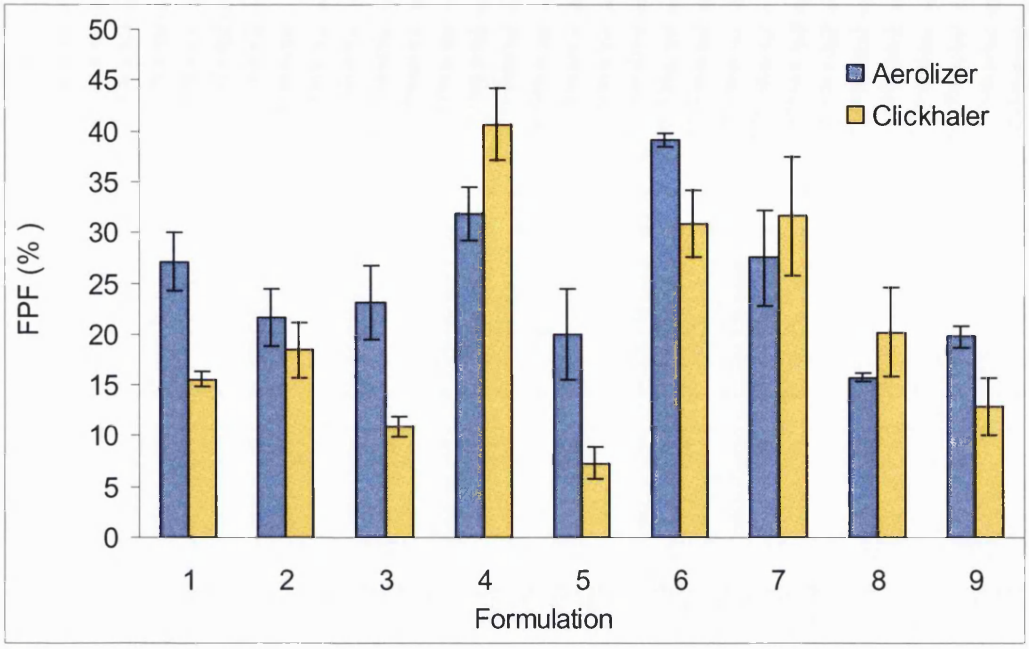

Figure 5.9. *BDP deposition obtained from nine DPI formulations using two different inhaler types. Values are mean (n=3).*

The importance of developing a BDP formulation in combination with the design of the device is illustrated by the data presented in Figure 5.9. The differences in deagglomeration efficiency for these two inhalers were highlighted by the different FPFs obtained from the same powder formulation, using the same inspiratory manoeuvre. The FPFs ranged from 15.7 to 39.1 % with the Aerolizer® device and from 7.3 to 40.6 % with the Clickhaler® device. As an example, with the Aerolizer®, Lactohale LH 100 showed a larger FPF (27.1 (2.9) %) compared to the same formulation in the Clickhaler® (15.6 (0.8) % FPF). The regular-shaped lactose batches (Formulations 1 to 5) showed a high capsule retention, in that the powder emissions were quite low. This observation was in accordance with previously published work on the evaluation of five different batches of Lactohale using the Aerolizer® or the Easyhaler® (Steckel *et al.*, 2004b). Different adhesion tendencies of the lactose/BDP blend to the inner wall of the capsule may be responsible for the decreased emission. The FPF obtained with the different formulations containing lactose/PEG fines (Formulations 6 to 9) generally appeared to be less dependent on the device chosen. Overall, the FPFs obtained with the Aerolizer® appeared higher than with the reservoir device.

5.5.5.2. SS deposition obtained using the Aerolizer®

Formulation	Carrier	ED (µg)	RD (µg)	FPF (%)
1	Lactohale LH 100	889 (25)	306 (25)	34.4 (2.5)
2	Pharmatose 325M	897 (126)	350 (53)	38.9 (0.8)
3	A Pharmatose 325M	997 (33)	379 (23)	38.0 (1.3)
4	Aero Flo 65	1019 (29)	431 (16)	42.3 (2.4)
5	A Aero Flo 65	911 (28)	279 (13)	30.6 (0.6)
6	A Pharmatose 325M+ fines	1005 (57)	390 (42)	38.8 (2.3)
7	A Aero Flo 65 + fines	1130 (77)	452 (40)	39.9 (1.9)
8	A Pharmatose 325M + fused fines	1136 (158)	322 (69)	28.3 (3.4)
9	A Aero Flo 65 + fused fines	1111 (21)	309 (14)	27.8 (0.9)

Table 5.6. *In vitro SS deposition using the Aerolizer®. Values are mean and (standard deviation).*

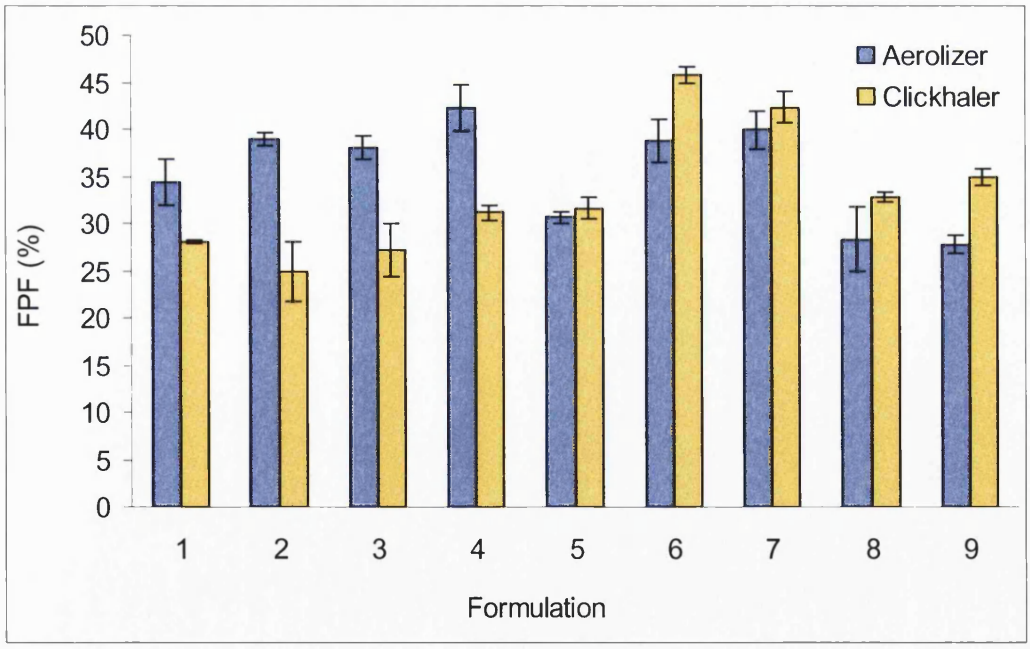

Figure 5.10. *SS deposition obtained from nine DPI formulations using two different inhaler types. Values are mean and n=3.*

Here the FPFs ranged from 27.8 to 42.3 % with the Aerolizer® device and from 24.9 to 45.8 % with the Clickhaler® device. Again, as a general trend, the capsule-based device showed better results than the reservoir one with respect to the SS FPF for the non-modified grades of lactose. This device was also more efficient in aerosolising SS (average ED of 1010 (98) µg) than BDP (average ED of 887 (92) µg). Those two values corresponded to 84 % and 74 % of the targeted dose respectively. Furthermore, the device retentions were noticeably lower in the Aerolizer® for the irregularly-shaped lactose (Formulations 6 to 9). The Clickhaler® gave marginally higher FPFs for PEG modified formulations than the Aerolizer®.

These results confirmed the hypothesis that a given formulation would perform differently, in terms of FPF, depending on the device chosen. A possible explanation for these differences may be linked to the variations in pressure drop across the inhalers. The flow rate being kept constant at 60 L/min and the devices having a different resistance to airflow, the pressure drop was likely to be different and hence resulted in a different fluidization process. This could have been assessed by modifying the flow rate so that the pressure drop across the device stayed constant (4 kPa).

SECTION B: Applications of surface energy data to predicting DPI performances

IGC was found to be useful in highlighting small differences in surface energy for surfaces of different grades of lactose (chapter 3). Those differences, which should affect the performance of the BDP deposition, could not have been detected using any other physical technique employed in this thesis. In chapter 4, measurements of surface energetics proved to be useful in the characterisation of the different lactose/PEG co-spray-dried systems. The surface modification of the air-jet sieved grades of lactose by fusing partially amorphous fines on the surface was also evaluated by this technique. All IGC data was compiled here to correlate with the DPI performances of all produced formulations.

5.5.6. Relationship between dispersive free energy and deposition

Formulation	Carrier	γ_s^d (mJ/m^2)
1	A Pharmatose 325M	31.8 (0.4)
2	A Pharmatose 325M + fused fines	34.4 (1.2)
3	A Aero Flo 65 + fused fines	35.8 (0.9)
4	A Aero Flo 65 + fines	36.6 (1.0)
5	A Aero Flo 65	37.4 (0.5)
6	A Pharmatose 325M + fines	37.6 (1.2)
7	Pharmatose 325M	40.1 (0.2)
8	Lactohale LH 100	42.5 (0.8)
9	Aero Flo 65	42.9 (0.3)

Table 5.7. *Dispersive component of the surface energy of the different lactose based carriers. Values are mean and (standard deviation).*

Attempts to correlate the dispersive component of free energy and the FPF of SS and BDP determined using the Clickhaler® and the Aerolizer® are presented in Figures 5.11 to 5.14. The different γ_s^d are represented by the grey columns, whereas the FPFs are represented by the black points.

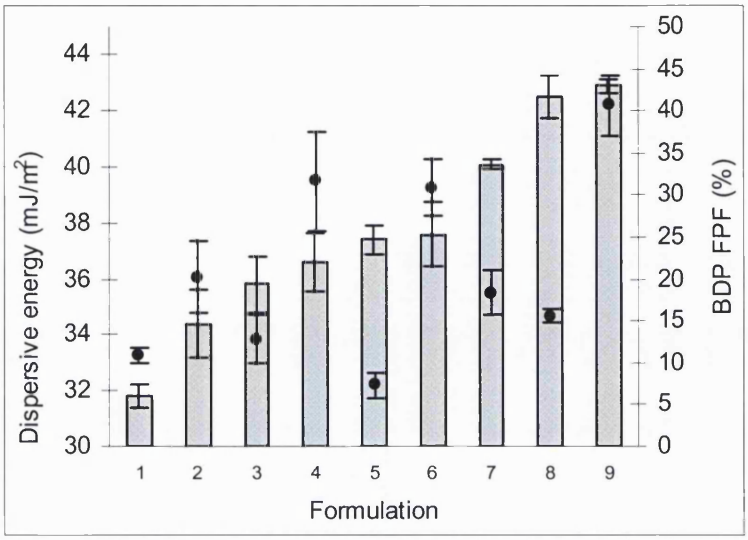

Figure 5.11. *Relationship between dispersive energy of the different carriers (grey columns) and BDP FPF (black points) using the Clickhaler®. Values are mean (n=3).*

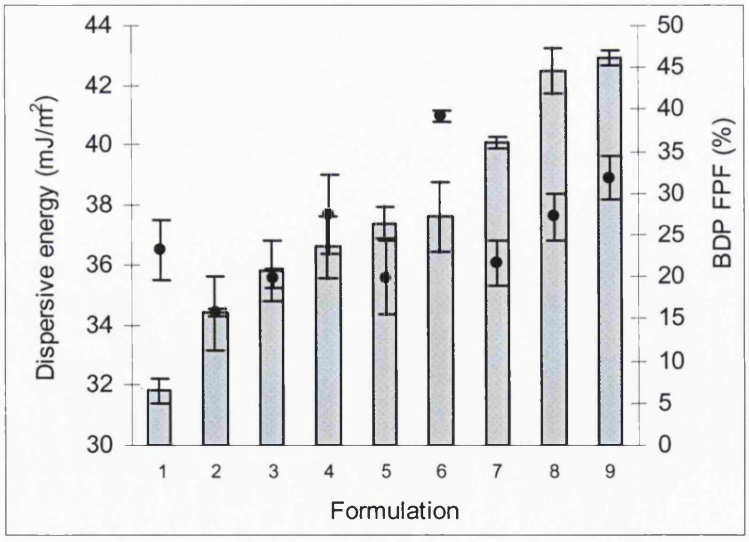

Figure 5.12. *Relationship between dispersive energy of the different carriers (grey columns)and BDP FPF (black points) using the Aerolizer®. Values are mean (n=3).*

No correlations between γ_s^d and BDP FPF could be found using the reservoir device (Figure 5.11). In Figure 5.12, the FPFs of Formulations 1 and 5 (corresponding to the air-jet sieved grades of lactose) did not fit in with the increasing trends between γ_s^d and BDP FPF using the Aerolizer®. Two increasing tendencies could be separated: one consisting of the original lactose batches (Formulations 7, 8 and 9) and the other consisting of the modified systems containing the lactose/PEG fines (Formulations 2, 3, 4 and 6).

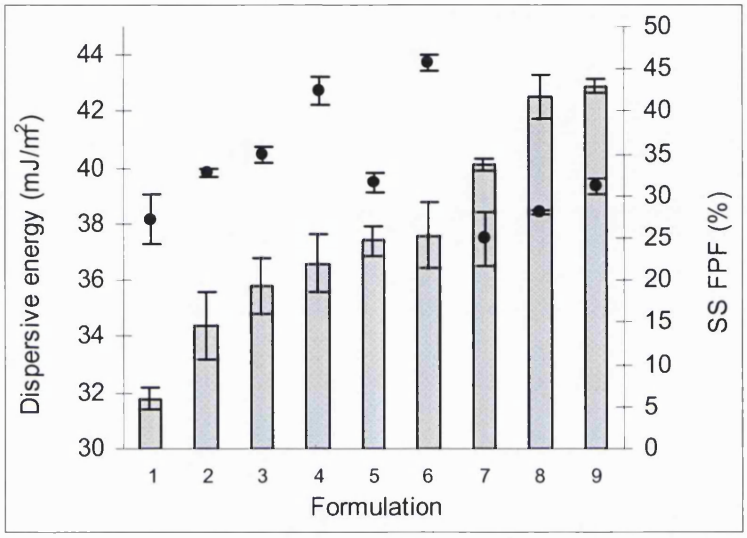

Figure 5.13. *Relationship between dispersive energy of the different carriers (grey columns) and SS FPF (black points) using the Clickhaler®. Values are mean (n=3).*

As previously described in chapter 3, an apparent correlation was found between the dispersive component of free energy of the commercially available lactose batches (Formulation 7, 8 and 9) and the deposition profile of SS using the Clickhaler® (Figure 5.13). Similarly, for Formulations 1 to 6 (excluding Formulation 5), an increase in γ_s^d was linked to an increase in SS FPF. However, these local trends could not be extrapolated to the entire set of formulations. Regarding a possible relationship using the Aerolizer®, no clear trend was detected, although most of the formulations with a low γ_s^d appeared to exhibit a lower FPF than those with a higher dispersive component value. This may be attributed to the reduced spread of FPFs using this particular device.

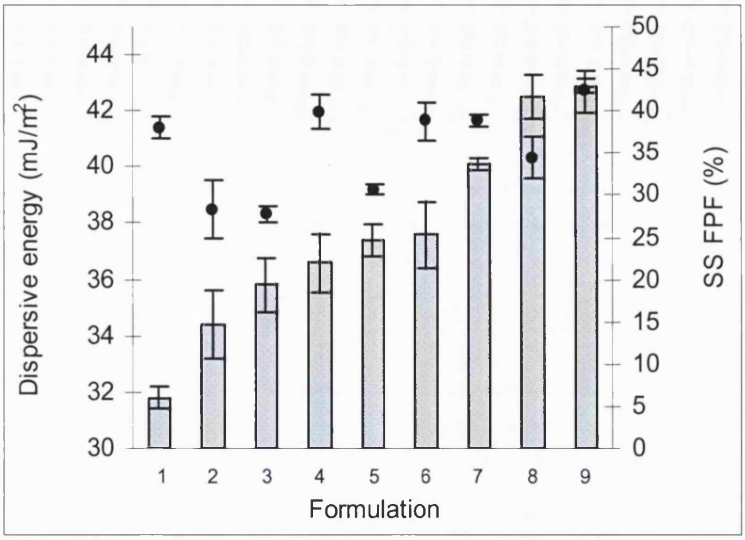

Figure 5.14. *Relationship between dispersive energy of the different carriers (grey columns) and SS FPF (black points) using the Aerolizer®. Values are mean (n=3).*

As a general conclusion, no obvious trends were established for BDP using the Clickhaler® and for SS using the Aerolizer®. However, both for BDP using the Aerolizer® and for SS using the Clickhaler®, trends were established each time for the same two groups of formulations. There was an increase in FPF with increasing γ_s^d for the marketed grades (Formulations 7, 8 and 9) and for the formulations containing the lactose/PEG systems (Formulations 2, 3, 4 and 6). No correlation including the air-jet sieved grades could be identified. As extensively described in chapter 2, γ_s^d and specific interaction parameters were used to quantify the properties of a material surface. The γ_s^d results were therefore not indicative of the true adhesion of the drug to the carrier. Moreover, attempts to correlate the dispersive energies of the carriers with FPF data did not take in consideration the intrinsic properties of the drugs.

5.5.7. Surface energy interaction theory

Due to difficulties in determining the acid-base contributions with the different methods described in chapter 2, a model developed by Cline and Dalby was instead evaluated. In their recent study (Cline and Dalby, 2002), the authors found a promising and convincing relationship between FPF and a parameter called surface energy interaction (SEI), which takes into account both the

dispersive component of surface energy and the acid-base properties of the different materials. Chloroform and tetrahydrofuran were respectively chosen as an acidic and a basic probe, in order to determine the Lewis acidity (K_A) and basicity (K_D). In this current study, tetrahydrofuran was replaced by ethyl acetate, which was not corrosive to the seals. The so-called SEI was obtained through harmonisation of the units of dispersive energy and the specific polar interactions. To do so, the specific interaction of each probe was converted to mJ/m^2 through Avogadro's number (molecule/mol) and the cross-sectional area of the probe (*a*, Å/molecule). This allowed the SEI to be calculated in the unit mJ/m^2 throughout.

$$SEI = 2\sqrt{\gamma^d{}_1 + \gamma^d{}_2} + 2\sqrt{K_{A1}K_{D2}} + 2\sqrt{K_{D1}K_{A2}} \qquad \text{[Equation 5.2]}$$

Another approach also described by Cline *et al.* was to calculate SEI in mJ/g. The specific surface areas (SSA) of the powder were determined in this study by IGC using the method described by Schultz *et al.* (Schultz *et al.*, 1987).

$$RT \ln V_n = 2Na\sqrt{\gamma_L{}^D \gamma_S{}^D} + RT \ln\left(\frac{Sg\pi_0}{P_0}\right) \qquad \text{[Equation 5.3]}$$

Where R is the gas constant; T is the absolute temperature; V_n is the net retention volume; P_0 is the partial pressure of the solute; π_0 is the bidimensional spreading pressure of the adsorbed film to a reference gas phase state; a is the surface area of the probe; S is the specific area of the sample; g is the specific weight of the sample; and $\gamma_S{}^d$ and $\gamma_L{}^d$ are the dispersive components of the surface tension of the solid and liquid probe respectively.

The calculation of SSA using IGC measurements nevertheless should be approached with caution since several problems may arise. The determination of the surface area of the different powders is based on the intercept term, obtained by linear extrapolation down to the y-axis over the alkane line (decane to hexane), as illustrated in Figure 2.16. This intercept is going to be affected by any change in the slope of the plot and therefore the calculated surface area might not be representative of the true surface area. Moreover, this approach assumes linearity of the relationship in the extrapolated region (i.e. C_0 to C_5) which may not be true (Chow *et al.*, 2004).

Prior to recalculating the different parameters (γ_s^d, K_A and K_D) in mJ/g, it was decided to compare the calculated surface IGC data to the one obtained from the BET nitrogen adsorption technique. Results are presented in Table 5.8.

Carrier	Material	SSA determined by BET (m^2/g)	SSA determined by IGC (m^2/g)
/	SS	6.001 (0.011)	3.84 (0.174)
/	BDP	4.656 (0.212)	3.73 (0.293)
1	Lactohale LH 100	0.133 (0.001)	0.127 (0.011)
2	A Aero Flo 65	0.186 (0.027)	0.498 (0.122)
3	A Pharmatose 325M	0.194 (0.008)	0.267 (0.017)
4	Pharmatose 325M	0.218 (0.009)	0.254 (0.011)
5	A Aero Flo 65 + fines	0.272 (0.001)	0.208 (0.013)
6	A Pharmatose 325M + fines	0.290 (0)	0.359 (0.017)
7	Aero Flo 65	0.291 (0.001)	0.226 (0.011)
8	A Pharmatose 325M + fused fines	0.333 (0.012)	0.723 (0.077)
9	A Aero Flo 65 + fused fines	0.337 (0.011)	0.389 (0.045)

Table 5.8. *Specific surface area of different materials determined by IGC and BET nitrogen adsorption. Values are mean (n=2).*

There was a large disagreement between the data sets obtained from the two methods. More essentially, there were no apparent parallel trends in the surface areas for the different materials. Specific surface area determination by IGC showed similar values for both drugs (3.84 (0.174) m^2/g and 3.73 (0.293) m^2/g for SS and BDP respectively), whereas differences in SSA were obvious when using the BET nitrogen adsorption technique (6.001 (0.011) m^2/g and 4.656 (0.212) m^2/g for SS and BDP respectively). This discrepancy was also pointed out by Chow *et al.* who concluded in the unsuitability of IGC for specific surface area determination. All calculations involving the SSA were therefore based on the data obtained from the BET nitrogen adsorption technique and the IGC calculations were disregarded.

Before calculating the SEI, it was decided to assess the relationship between the FPF and the SSA of the carriers, since preliminary work based on a limited amount of points (detailed in chapter 3) found a trend between BDP deposition and the latter parameter. Those results were dissimilar to the findings of Kawashima *et al.* (Kawashima *et al.*, 1998b) who came to the conclusion that carriers with a larger surface area separated fewer drug particles (in this case pranlukast hydrate) from their surface under shear force in the air stream. However, Cline and Dalby (Cline and Dalby, 2002) did conclude in an increased FPF with an increased SSA of the carrier. This observation could at first be difficult to understand, since a higher surface area may allow more contacts and interactions between the drug and carrier surfaces, which would lead to decreased DPI performances. The authors concluded in the need for a certain minimum interaction level between the drug particle and the carrier, especially during the mixing and aerosolisation process. This was stated to be particularly important for highly cohesive drugs, which have a general tendency to agglomerate. Figures 5.15 to 5.18 plotted the SSA of the different carriers against FPF of both drug models using the different devices. The different SSAs are represented by the grey columns, whereas the FPFs are represented by the black points.

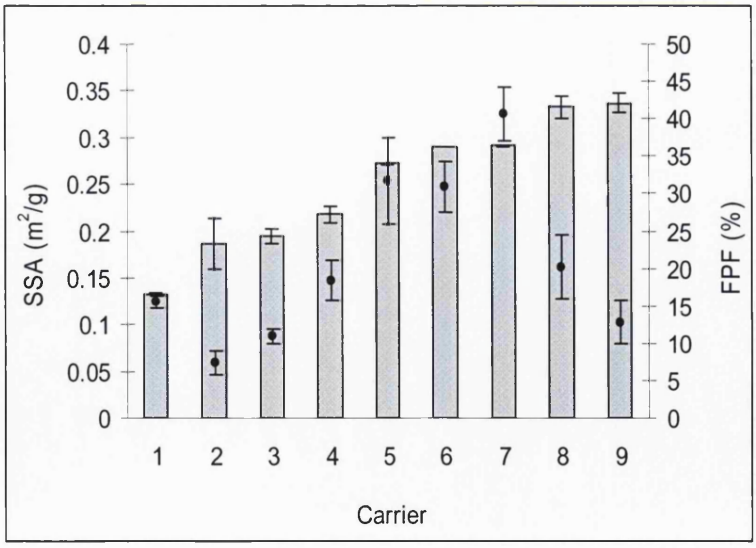

Figure 5.15. *FPF of BDP (black points) obtained with the Clickhaler® vs. SSA (m^2/g) of carrier (grey columns). Values are mean.*

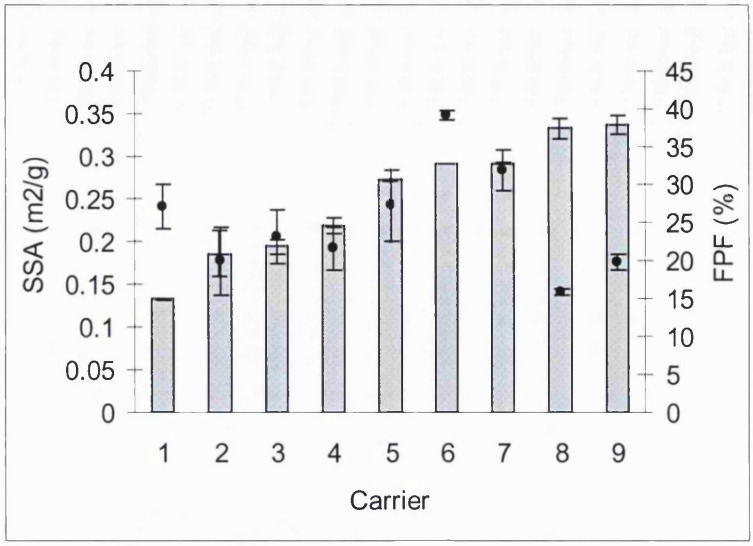

Figure 5.16. *FPF of BDP (black points) obtained with the Aerolizer® vs. SSA (m^2/g) of carrier (grey columns). Values are mean.*

Assessment of the relationship between specific surface area and BDP FPF revealed a certain correlation between the two factors. An increase in the SSA of the carrier resulted in an apparent increase in BDP FPF confirming the original observation established in chapter 3. This was particularly true when the Clickhaler® was used as the device (Figure 5.15). However, this SSA relationship would have predicted higher FPFs for the "fused" systems. This observation was not supported by the deposition data and the useful insight given by this parameter should therefore be treated with caution.

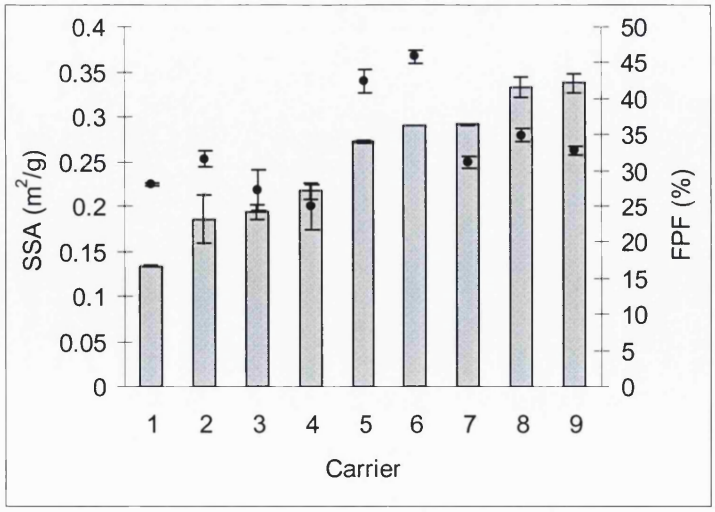

Figure 5.17. *FPF of SS (black points) obtained with the Clickhaler® vs. SSA (m^2/g) of carrier (grey columns). Values are mean.*

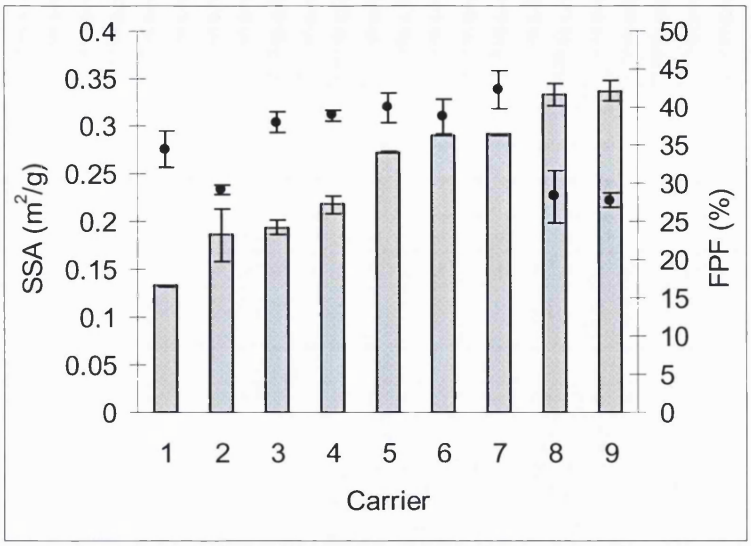

Figure 5.18. *FPF of SS (black points) obtained with the Aerolizer® vs. SSA (m^2/g) of carrier (grey columns). Values are mean.*

Overall, links between SSA and the hydrophilic drug model deposition were not very clear (Figure 5.18 and 5.19). This parameter did not therefore appear to be able to predict reliably the deposition of this drug.

5.5.7.1. Surface energy interaction (mJ/m^2)

5.5.7.1.1. SEI between the carrier and BDP

The data presented in Table 5.9 summarises *in vitro* BDP deposition patterns obtained with the different carriers using two different devices and the calculated SEI in mJ/m^2, in an attempt to assess a possible correlation between the two factors.

Formulation	Carrier	SEI (mJ/m^2)	FPF % Clickhaler®	FPF % Aerolizer®
1	A Aero Flo 65 + fines	110.6 (0.3)	31.6 (5.8)	27.3 (4.7)
2	A Aero Flo 65	111.8 (2.9)	7.3 (1.6)	19.9 (4.4)
3	Pharmatose 325M	112.5 (1.7)	18.4 (2.7)	21.6 (2.8)
4	A Pharmatose	112.7 (8.3)	10.9 (1.0)	23.1 (3.6)
5	A Pharmatose 325M + fused fines	117.9 (2.1)	20.2 (4.3)	15.7 (0.4)
6	A Pharmatose 325M + fines	122.8 (13)	30.9 (3.4)	39.1 (0.6)
7	A Aero Flo 65 + fused fines	123.4 (1.4)	12.8 (2.8)	19.8 (1.1)
8	Lactohale LH 100	148.6 (1.1)	15.6 (0.8)	27.1 (2.9)
9	Aero Flo 65	157.2 (0.8)	40.6 (3.5)	31.9 (2.6)

Table 5.9. *SEI (mJ/m^2) between BDP and the different carriers and FPF obtained by using the Clickhaler® and the Aerolizer®. Values are mean and (standard deviation).*

The SEIs between the hydrophobic drug model and the different carriers varied from 110.6 (0.3) mJ/m^2 to 157.2 (0.8) mJ/m^2. The highest value was found to correspond to the interaction between the Aero Flo 65 and BDP (Formulation 9). Interestingly, this carrier was found to produce the highest FPF with the reservoir device. This supports the idea that the stronger the adhesion, the higher the FPF produced. The information contained in the above table is represented as grey columns for SEI (mJ/m^2) and black points for the drug FPF in Figures 5.19 and 5.20. Based on those plots, no clear increasing trend between SEI and FPF was observed, irrespective of the device employed. The SEI theory in mJ/m^2 did not appear efficient in predicting the hydrophobic drug model deposition. Other factors such as electrostatic forces, particle shape and relative humidity of the environment would be expected to play an important role in the observed *in vitro* deposition pattern.

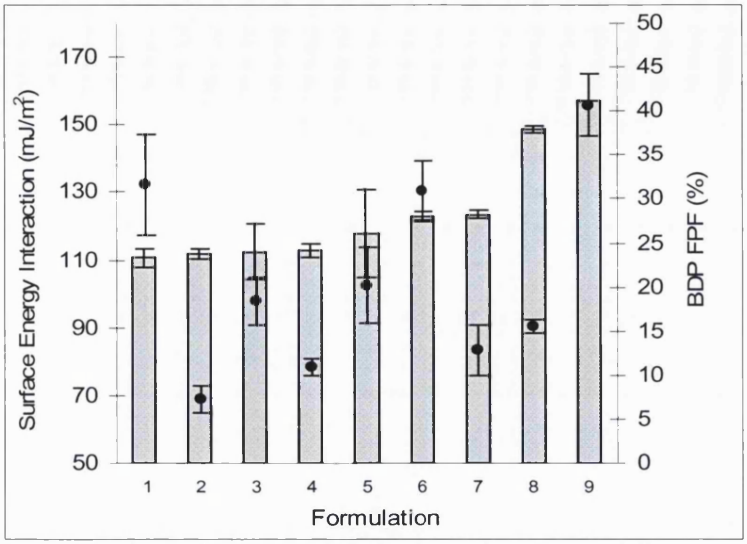

Figure 5.19. *SEI (mJ/m^2) of BDP with different lactose based carriers (grey columns) as a function of BDP FPF (black points) using the Clickhaler®. Values are mean (n=3)*

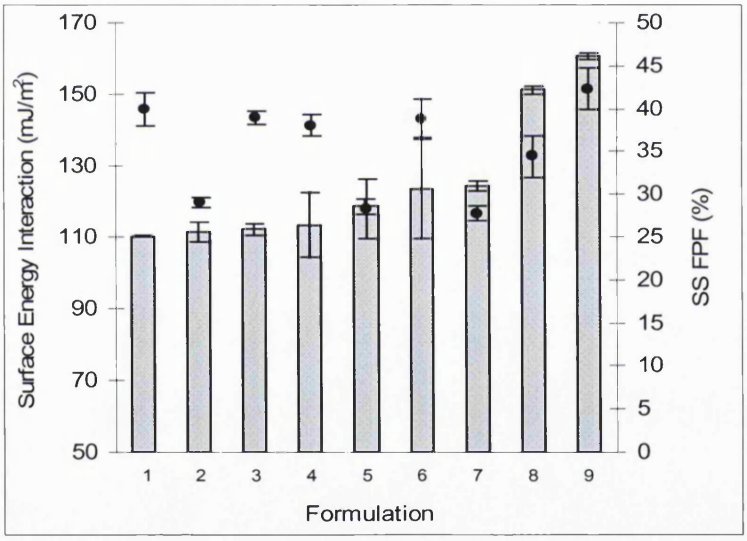

Figure 5.20. *SEI (mJ/m^2) of BDP with different lactose based carriers (grey columns) as a function of BDP FPF (black points) using the Aerolizer®.*

5.5.7.1.2. SEI between the carrier and SS

Analogous to BDP, the existence of a possible relationship between SEI (mJ/m^2) and FPF investigated for with the hydrophilic drug model. The data presented in Table 5.10 is represented in the corresponding Figures 5.21 and 5.22.

Formulation	Carrier	SEI (mJ/m^2)	FPF % Clickhaler®	FPF % Aerolizer®
1	A Aero Flo 65 + fines	110.2 (0.3)	42.4 (1.7)	39.9 (1.9)
2	A Aero Flo 65	111.4 (2.9)	31.7 (1.2)	29.1 (0.6)
3	Pharmatose 325M	112.1 (1.7)	24.9 (3.2)	38.9 (0.7)
4	A Pharmatose 325M	113.4 (9.0)	27.2 (2.8)	38.0 (1. 3)
5	A Pharmatose 325M + fused fines	118.8 (2.1)	34.9 (0.9)	28.3 (3.4)
6	A Pharmatose 325M + fines	123.7 (14.0)	45.8 (0.9)	38.7 (2.3)
7	A Aero Flo 65 + fused fines	124.6 (1.4)	32.8 (0.6)	27.8 (0.9)
8	Lactohale LH 100	151.3 (1.2)	28.1 (0.2)	34.4 (2.4)
9	Aero Flo 65	160.7 (0.8)	31.2 (0.9)	42.3 (2.4)

Table 5.10. *SEI (mJ/m^2) between SS and the different carriers and FPF obtained by using the Clickhaler® and the Aerolizer®. Values are mean and (standard deviation).*

The SEI values for SS were similar to those obtained for BDP. This can be explained by the similar surface energy properties exhibited by the two model drugs when the calculations were done in mJ/m^2 (Table 5.11). Although the SEI parameters for the different interactions were very similar between SS and BDP, the depositions remain profoundly different. As an example, while the SEI between an air-jet sieved Aero Flo 65 mixed with lactose/PEG fines and BDP (Formulation 1 in Table 5.9) was identical to the SEI between the same carrier and SS (Formulation 1 in Table 5.10) with values of 110.2 (0.3) mJ/m^2 and 110.6 (0.3) mJ/m^2, the corresponding FPFs were markedly less for BDP than SS whichever device was employed. This model did therefore not give a direct explanation for the differences seen between the two drug models.

Material	γ^d_s (mJ/m^2)	K_A (mJ/m^2)	K_D (mJ/m^2)	γ^d_s (mJ/g)	K_A (mJ/g)	K_D (mJ/g)
SS	50.0 (3.9)	51.8 (0.1)	3.8 (0.1)	300 (24)	314 (3.4)	23.8 (1.3)
BDP	53.1 ** (3)	42.6 (0.3)	3.1 (0.1)	246.8 (15)	198 (1.5)	14.5 (0.3)

Table 5.11. *IGC parameters for micronised SS and BDP. Values are mean and (standard deviation).*

** The results obtained from IGC of BDP were in accordance with the data obtained by Columbano (Columbano, 2000) who also studied this corticosteroid.

Furthermore, the data plotted in Figures 5.21 and 5.22 also indicated a lack of positive trend between the surface energy and the deposition. Therefore, this SEI concept required further evaluation, since differences between the drug models were more obvious in using mJ/g as a unit, because of differences in SSAs.

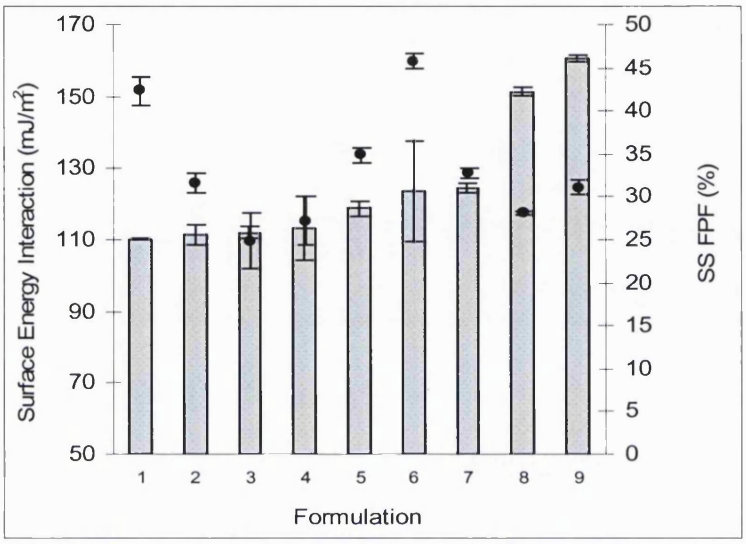

Figure 5.21. *SEI (mJ/m^2) of SS with different lactose based carriers (grey columns) as a function of SS FPF (black points) using the Clickhaler®. Values are mean (n=3)*

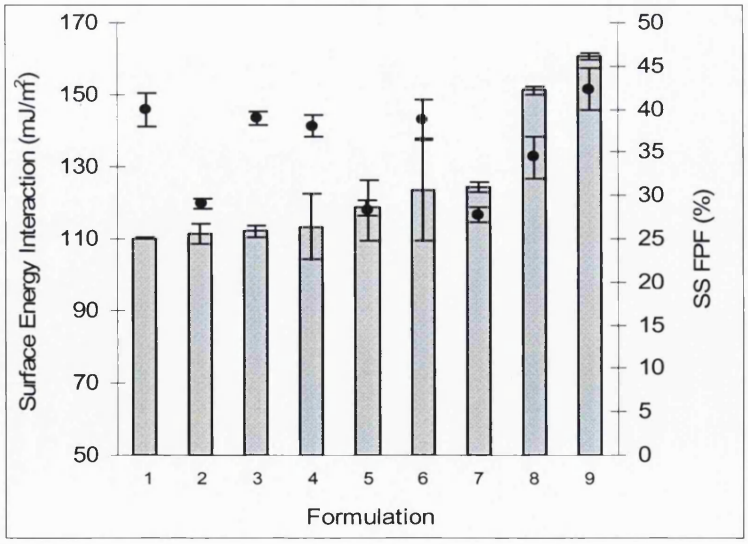

Figure 5.22. *SEI (mJ/m^2) of BDP with different lactose based carriers (grey columns) as a function of BDP FPF (black points) using the Aerolizer®. Values are mean (n=3)*

5.5.7.2. Surface energy interaction (mJ/g)

5.5.7.2.1. SEI between the carrier and BDP

The different carriers listed in Table 5.12 are represented by formulation numbers, which correspond to those in Figures 5.23 and 5.24. Those figures display the relationships between SEI in mJ/g and FPF of BDP determined using two different devices. An increase in SEI (mJ/g) was accompanied by an overall increase in BDP FPF for both devices. However, for the last two carriers (i.e Formulations 8 and 9 corresponding to the fused systems) this trend was not confirmed with high SEIs and low FPFs. The high SEI of the fused system may be attributed to their greater SSA. Interestingly, those systems also appeared to minimise the relationship between the FPF and the SSA as shown in Figure 5.15. As a general trend, it appeared that a certain minimum energy interaction between the carrier and the BDP particle was needed to pull the drug apart during the blending and the aerosolisation process.

Formulation	Carrier	SEI (mJ/g)	FPF % Clickhaler®	FPF % Aerolizer®
1	A Aero Flo 65	105.2 (2.8)	7.3 (1.6)	19.9 (4.4)
2	A Pharmatose	109.5 (7.9)	10.9 (1.0)	23.1 (3.6)
3	Pharmatose 325M	114.6 (1.7)	18.4 (2.7)	21.6 (2.8)
4	Lactohale LH 100	117.8 (0.9)	15.6 (0.8)	27.1 (2.9)
5	A Aero Flo 65 + fines	125.8 (0.3)	31.6 (5.8)	27.3 (4.7)
6	A Pharmatose 325M + fines	149.3 (6.7)	30.9 (3.4)	39.1 (0.6)
7	Aero Flo 65	184.4 (0.9)	40.6 (3.5)	31.9 (2.6)
8	A Pharmatose 325M + fused fines	186.7 (3.4)	20.2 (4.3)	15.7 (0.4)
9	A Aero Flo 65 + fused fines	189.2 (2.0)	12.8 (2.8)	19.8 (1.1)

Table 5.12. *SEI (mJ/g) between BDP and the different carriers and FPF obtained by using the Clickhaler® and the Aerolizer®. Values are mean and (standard deviation).*

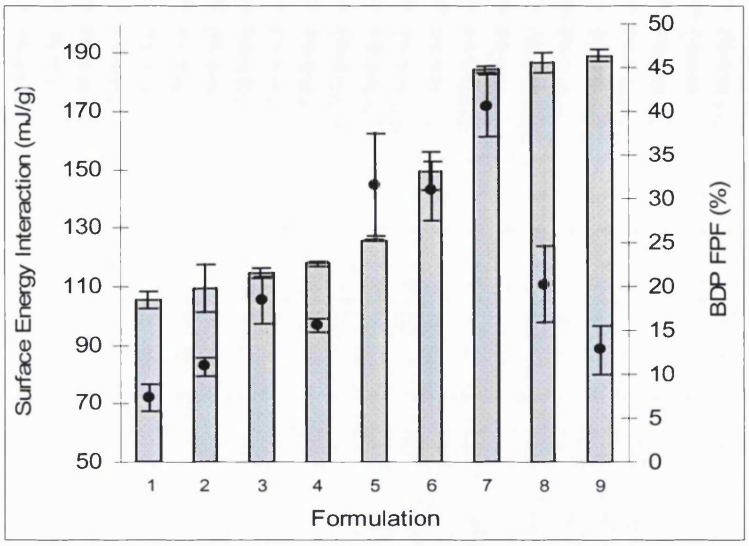

Figure 5.23. *SEI (mJ/g) of BDP with different lactose based carriers (grey columns) as a function of BDP FPF (black points) using the Clickhaler®. Values are mean (n=3)*

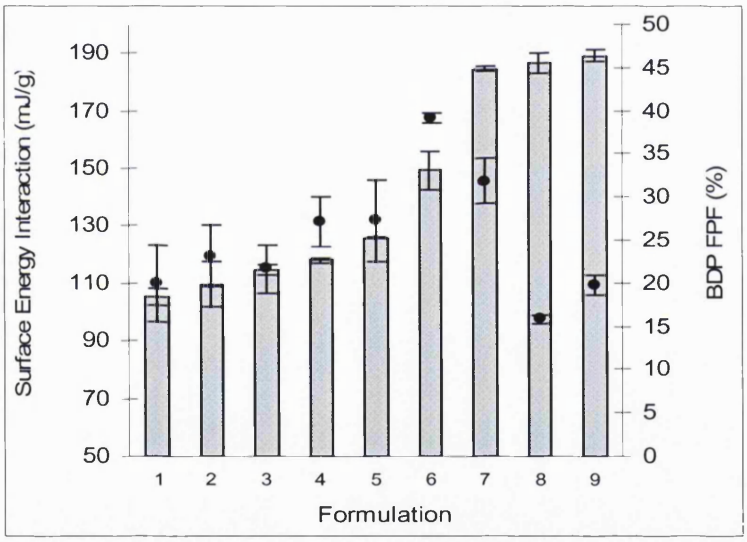

Figure 5.24. *SEI (mJ/g) of BDP with different lactose based carriers (grey columns) as a function of BDP FPF (black points) using the Aerolizer®. Values are mean (n=3)*

5.5.7.2.2. SEI between the carrier and SS

No direct relationship between SEI in mJ/g and FPF of SS could be identified (Figures 5.25 and 5.26). The theory developed by Cline and Dalby (Cline and Dalby, 2002), indicating that the greater the SEI between the drug and the carrier, the greater the drug FPF evolved, did not apply to this data set. For example, as seen in Table 5.13, Formulation 5 exhibited a SEI of 140.7 (0.3)

mJ/g with SS, whereas this value increased to 212 (1) mJ/g for Formulation 8. The model would have had predicted a higher FPF for the latter formulation. Unfortunately the earlier deposition study did not support this prediction, with FPF dropping from 42.4 % to 31.2 % using the Clickhaler® as the chosen device.

Formulation	Carrier	SEI (mJ/g)	FPF % Clickhaler®	FPF % Aerolizer®
1	A Aero Flo 65	117.7 (2.9)	31.7 (1.2)	29.1 (0.6)
2	A Pharmatose	123.7 (9.8)	27.2 (2.8)	38.0 (1.3)
3	Pharmatose 325M	128.2 (2.0)	34.9 (0.9)	38.9 (0.7)
4	Lactohale LH 100	139.3 (1.0)	28.1 (0.2)	34.4 (2.4)
5	A Aero Flo 65 + fines	140.7 (0.3)	42.4 (1.7)	39.9 (1.9)
6	A Pharmatose 325M + fines	169.5 (8.0)	45.8 (0.9)	38.7 (2.3)
7	A Pharmatose 325M + fused fines	209.9 (2.9)	34.9 (0.9)	28.3 (3.4)
8	Aero Flo 65	212.0 (1.0)	31.2 (0.9)	42.3 (2.4)
9	A Aero Flo 65 + fused fines	218.6 (2.3)	32.8 (0.6)	27.8 (0.9)

Table 5.13. *SEI (mJ/g) between SS and the different carriers and FPF obtained by using the Clickhaler® and the Aerolizer®. Values are mean and (standard deviation).*

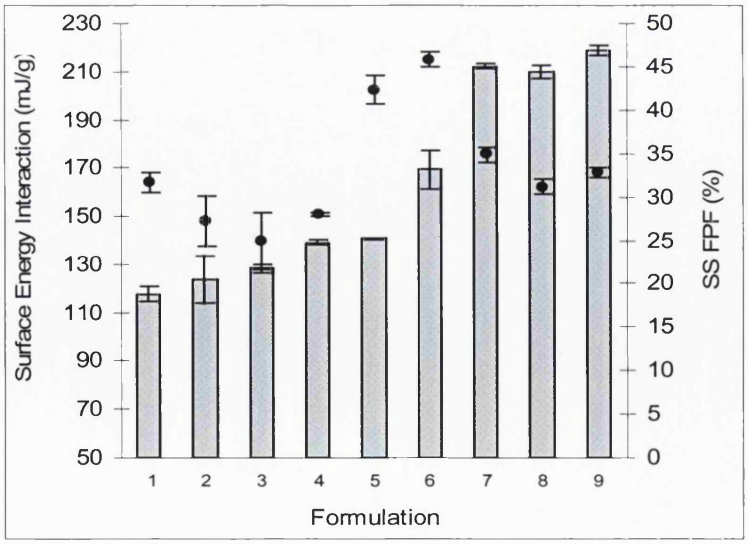

Figure 5.25. *SEI (mJ/g) of SS with different lactose based carriers (grey columns) as a function of SS FPF (black points) using the Clickhaler®. Values are mean (n=3)*

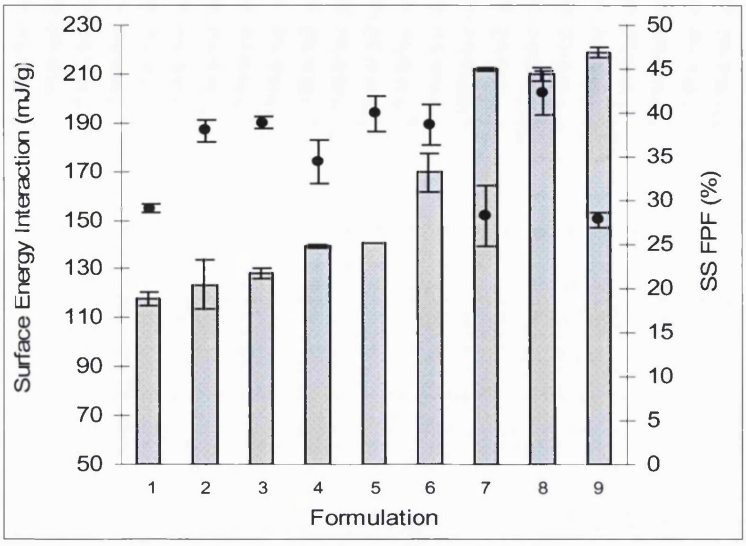

Figure 5.26. *SEI (mJ/g) of SS with different lactose based carriers (grey columns) as a function of SS FPF (black points) using the Aerolizer®. Values are mean (n=3)*

5.5.8. Spreading coefficient approach

Differences in drug deposition could not directly be related to the SEI either in mJ/m^2 or in mJ/g. A last attempt to correlate surface energy data to the TSI deposition pattern of the two drug models was done with the calculation of spreading coefficients. Ahfat *et al.* (Ahfat *et al.*, 1997) in an attempt to predict the mixing performance of binary and ternary systems, modelled the solid-solid interaction by calculating the spreading coefficients (λ) of two solid phases. In this current study, the spreading coefficients of the drugs over the carriers (λ_{sc} or λ_{bc}) were calculated by taking the difference between the work of adhesion between the two components and the work of cohesion of the drug. A positive result would show a tendency for the drug to spread over the carrier. The spreading coefficient of the carrier over the drug (λ_{cs} or λ_{cb}) could be similarly determined and would give an indication of the tendency of the carrier to spread over the drug. The spreading coefficients (in mJ/m^2) of the active particles over the different lactose-based carriers and that of the different carriers over the drugs are listed in Table 5.14.

	λ_{sc} (mJ/m^2)	λ_{cs} (mJ/m^2)	λ_{bc} (mJ/m^2)	λ_{cb} (mJ/m^2)
A Aero Flo 65+ fine	- 48.4 (2.1)	35.2 (0.8)	- 43.8 (4.6)	35.6 (0.7)
A Aero Flo 65	- 47.2 (4.2)	34.3 (5.7)	- 42.6 (5.5)	34.7 (5.7)
Pharmatose 325M	- 46.5 (3.0)	34.7 (3.6)	- 41.9 (4.9)	35.1 (3.4)
A Pharmatose 325M	- 45.2 (13.4)	33.1 (19.9)	- 41.7 (13.0)	32.4 (19.4)
A Pharmatose 325M + fused fines	- 39.8 (3.3)	- 30.5 (7.0)	- 36.5 (5.0)	- 31.4 (7.0)
A Pharmatose 325M + fines	- 34.9 (25.8)	18.3 (25.7)	- 31.6 (24.4)	17.4 (22.5)
A Aero Flo 65 + fused fines	- 34.0 (2.6)	- 24.1 (5.3)	- 31.0 (4.7)	- 25.3 (6.9)
Lactohale LH 100	- 7.3 (2.6)	4.3 (2.8)	- 5.8 (4.9)	1.6 (2.7)
Aero Flo 65	2.1 (2.2)	- 5.9 (2.2)	2.8 (4.8)	- 9.4 (2.2)

Table 5.14. *Spreading coefficients (mJ/m^2) of SS over lactose-based carriers (λ_{sc}), BDP over carriers (λ_{bc}), carriers over SS (λ_{cs}) and carriers over BDP (λ_{cb}). Values are mean and (standard deviation).*

Since the work of cohesion was very similar for both drugs (154.4 (3.7) mJ/m^2 for BDP and 158.6 (1.4) mJ/m^2 for SS), the corresponding calculated spreading coefficients were of identical extent. This was unexpected since it was thought that BDP would be more cohesive than SS (based on SEM pictures). Moreover, in a recent work by Begat *et al.* (Begat *et al.*, 2004), the cohesive-adhesive balances in DPI formulations have been quantified by atomic force microscopy (AFM). The measurements suggested that the BUD-BUD interactions were 3.84-fold greater that the BUD-lactose interactions, while lactose-lactose interactions were 2.36-fold greater that the BUD-lactose interactions. This suggested very strong BUD cohesive bonds that would result in the formulation exhibiting poor blend homogeneity and poor deposition. Regarding SS, the data indicated that the interactions between SS and lactose were 16.88 times and 1.22 times greater than the cohesive SS and lactose interactions. The IGC technique, utilized to measure the characteristics of the interparticulate forces, did not enable direct correlation with the *in vitro* observations.

The drugs were not easily spread over any carrier except the Aero Flo 65. In this case, the positive values indicated a favourable spreading. Interestingly, the deposition data for BDP showed a good deposition with this carrier, indicating that increased spreading led to a more efficient dispersion. However, the scanning electron micrograph (Figure 5.27) of a binary system consisting of BDP and Aero Flo 65 showed a different picture, with BDP particles appearing as drug agglomerates and binding with the carrier surface on a limited amount of contact points. Therefore, the spreading coefficient data did not seem to support the SEM observation. The spreading coefficients of the carriers over the drugs are also listed in Table 5.14. Except for the Aero Flo 65 and the fused systems, the spreading coefficients were positive, indicative of good spreading tendencies. This was expected to occur, since the work of cohesion for these systems was much less than that for the highly energetic micronised particles. The spreading of the fused systems was found to be less favourable than the spreading of other carriers over either drug.

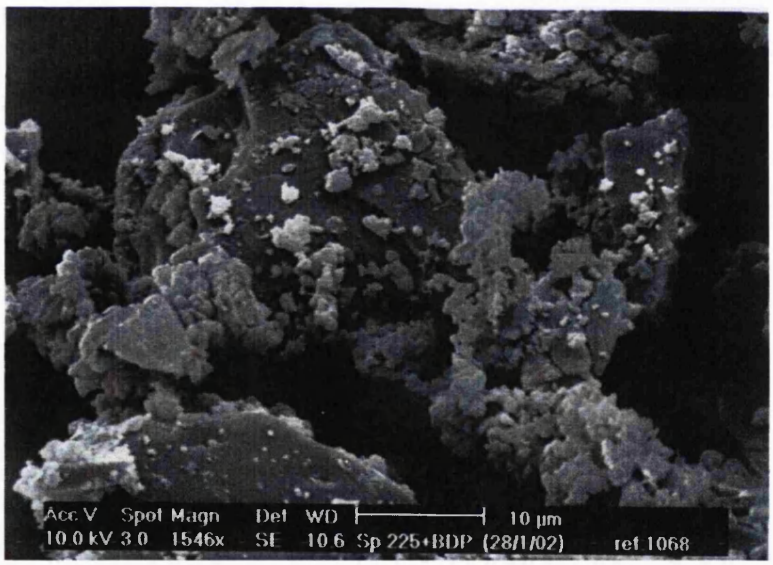

Figure 5.27. *Scanning electron micrograph of Aero Flo 65 mixed with BDP.*

Figures 5.28 and 5.29 show the plots of the *in vitro* deposition patterns of the two drugs obtained with the two inhalers (Clickhaler® and Aerolizer®) versus the spreading coefficients of the active models over the different carriers.

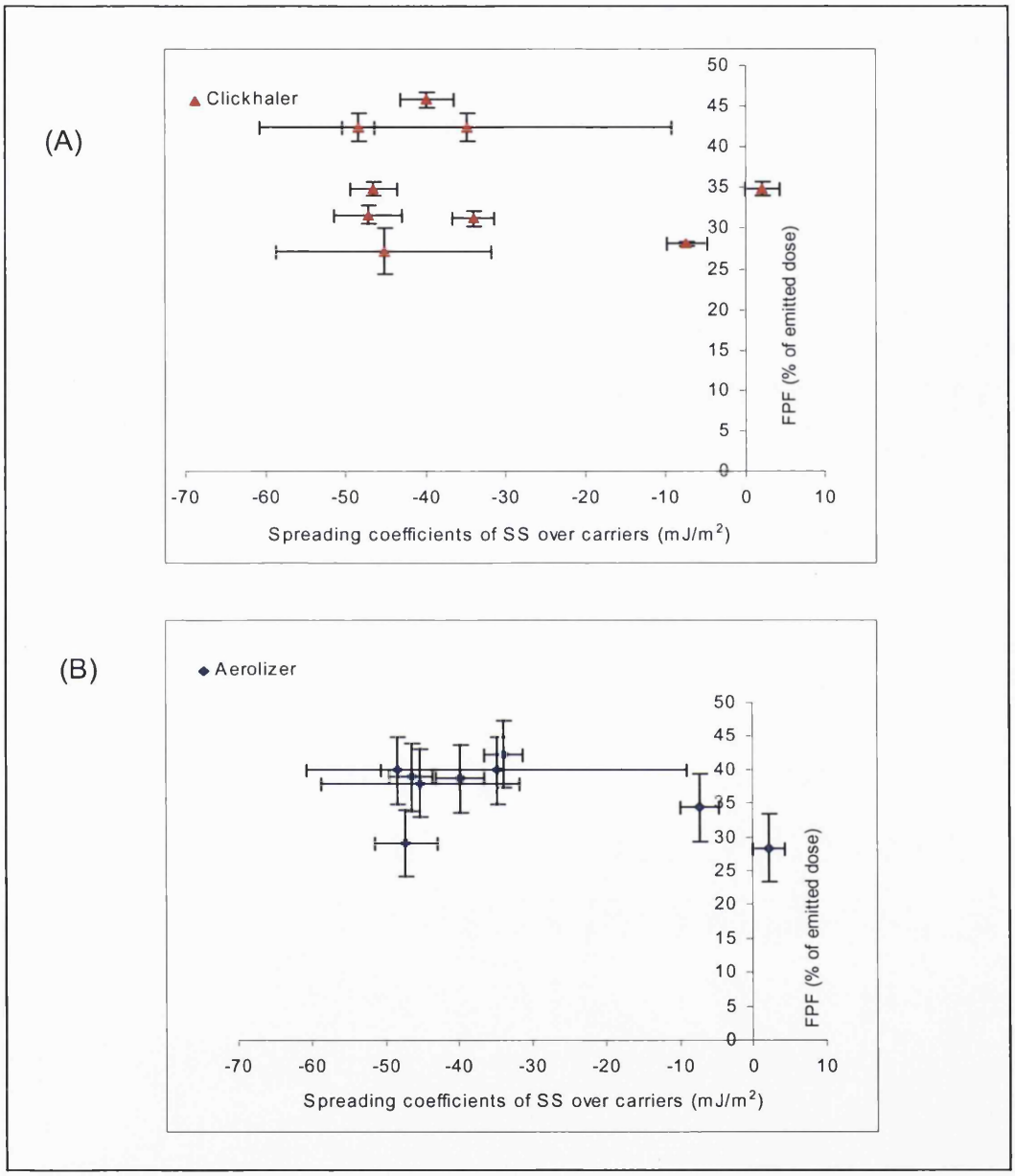

Figure 5.28. *FPF of SS using the clickhaler (A) or the Aerolizer (B) as a function of the spreading coefficients of SS over carriers (mJ/m²). Values are mean (n=3)*

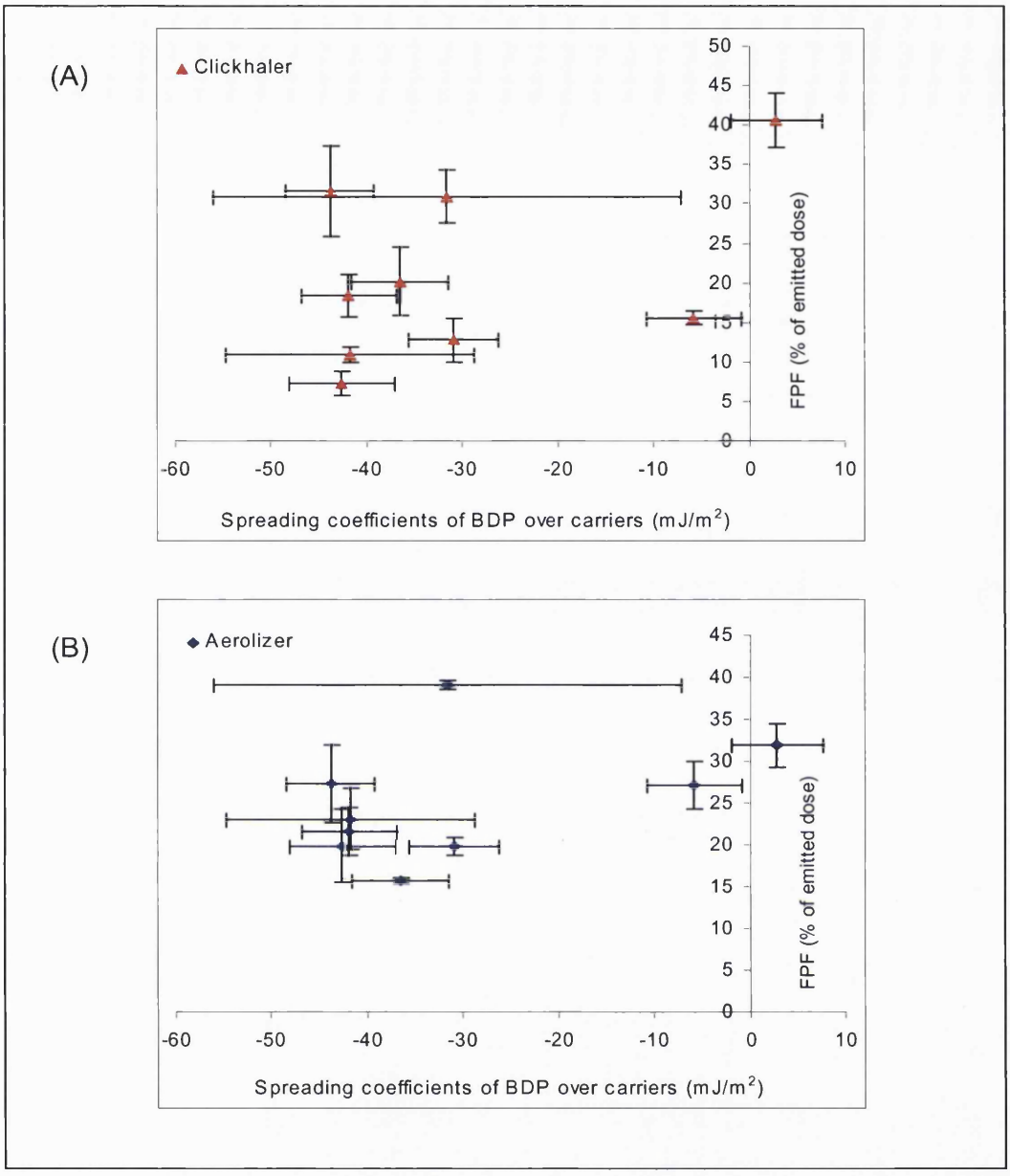

Figure 5.29. *FPF of BDP using the clickhaler (A) or the Aerolizer (B) as a function of the spreading coefficients of BDP over carriers (mJ/m^2). Values are mean (n=3)*

The major differences observed in the deposition pattern of the different drugs could not be directly explained by the spreading coefficients of the drugs over the different lactose-based carriers calculated in mJ/m^2.

Figures 5.30 and 5.31 show the FPFs obtained using the two inhalers versus the spreading coefficients of the carriers over the drugs. No overall direct correlation was found between both drugs and the corresponding spreading coefficients calculated in mJ/m^2, whichever device was used to perform the in vitro testing.

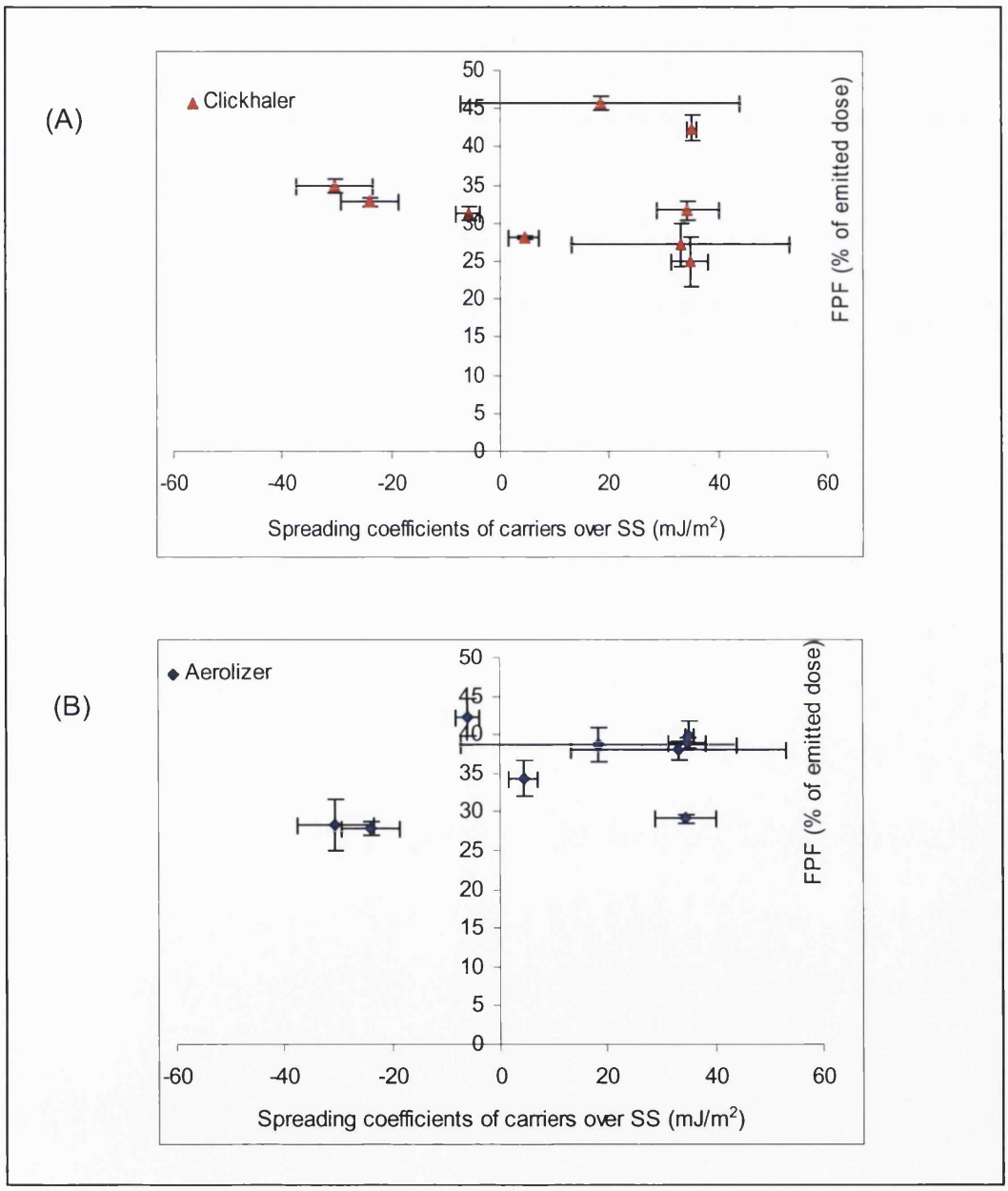

Figure 5.30. *FPF of SS using the clickhaler (A) or the Aerolizer (B) as a function of the spreading coefficients of carriers over SS (mJ/m^2). Values are mean (n=3)*

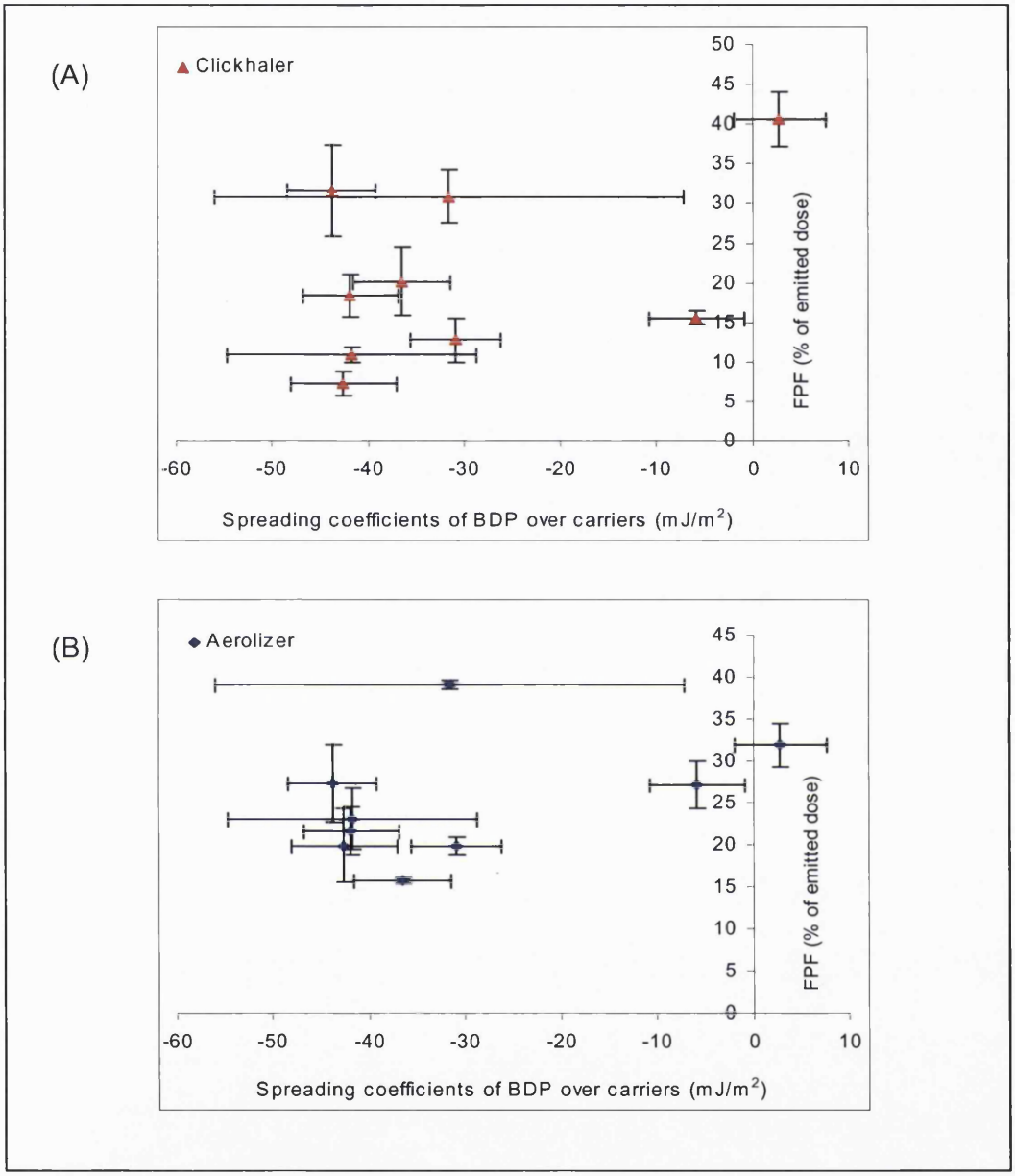

Figure 5.31. *FPF of BDP using the clickhaler (A) or the Aerolizer (B) as a function of the spreading coefficients of BDP over carriers (mJ/m^2). Values are mean (n=3)*

To further assess the usefulness of this approach to predict DPI performances, these coefficients were calculated in mJ/g by using the surface area of the materials. This offered a greater differentiation between the drugs, since the recalculated work of cohesion now varied from 718 (17.0) mJ/g for BDP to 949 (11.1) mJ/g for SS. Those values (Table 5.15) were unexpected since BDP appeared to be more cohesive than SS, leading to higher agglomeration tendency (confirmed by SEMs). As the deposition in stage 2 of the twin impinger depends, to a certain extent, on the ability of the drug to deaggregate when liberated into the air stream from the device, BDP deposition is usually lower than SS deposition.

Spreading coefficients of both drugs over the different carriers were all negative, indicating a difficult dispersion. The spreading coefficients of BDP were less negative than SS. This may suggest a higher adherence to the surface for the hydrophobic model compared to the hydrophilic active. However, this observation offers little explanation for the differences seen between the carrier efficiencies in liberating the hydrophobic drug.

	λ_{sc} (mJ/g)	λ_{cs} (mJ/g)	λ_{bc} (mJ/g)	λ_{cb} (mJ/g)
A Aero Flo 65	- 831.3 (14.4)	103.4 (7.3)	- 612.8 (21.6)	90.9 (7.1)
A Pharmatose 325M	- 825.3 (20.8)	113.0 (25.0)	- 608.5 (20.8)	98.8 (15.1)
Pharmatose 325M	- 820.8 (12.3)	111.3 (4.8)	- 603.4 (19.7)	97.7 (4.3)
Lactohale LH 100	- 809.7 (11.7)	119.8 (2.5)	- 600.2 (19.5)	98.3 (2.3)
A Aero Flo 65 + fines	- 808.3 (2.8)	120.3 (0.6)	- 592.2 (18.6)	105.4 (0.6)
A Pharmatose 325M + fines	- 779.5 (29.0)	146.5 (15.3)	- 568.7 (27.1)	126.2 (13)
A Pharmatose 325M + fused fines	- 737.0 (13.8)	162.3 (2.8)	- 533.6 (19.6)	133.9 (1.8)
Aero Flo 65	- 739.1 (12.3)	161.4 (5.3)	- 531.3 (21.8)	137.0 (5.4)
A Aero Flo 65 + fused fines	- 730.1 (13.1)	168.8 (4.7)	- 528.8 (21.4)	139.1 (3.4)

Table 5.15. *Spreading coefficients (mJ/g) of SS over lactose-based carriers (λ_{sc}), BDP over carriers (λ_{bc}), carriers over SS (λ_{cs}) and carriers over BDP (λ_{cb}). Values are mean and (standard deviation).*

Assesment of possible relationship between the different factors are presented in Figures 5.32 to 5.35. Firstly, as done for the calculations in mJ/m^2, the aerosol performances were plotted against the spreading coefficients of the drugs over the carriers (in mJ/g) (Figures 5.32 and 5.33).

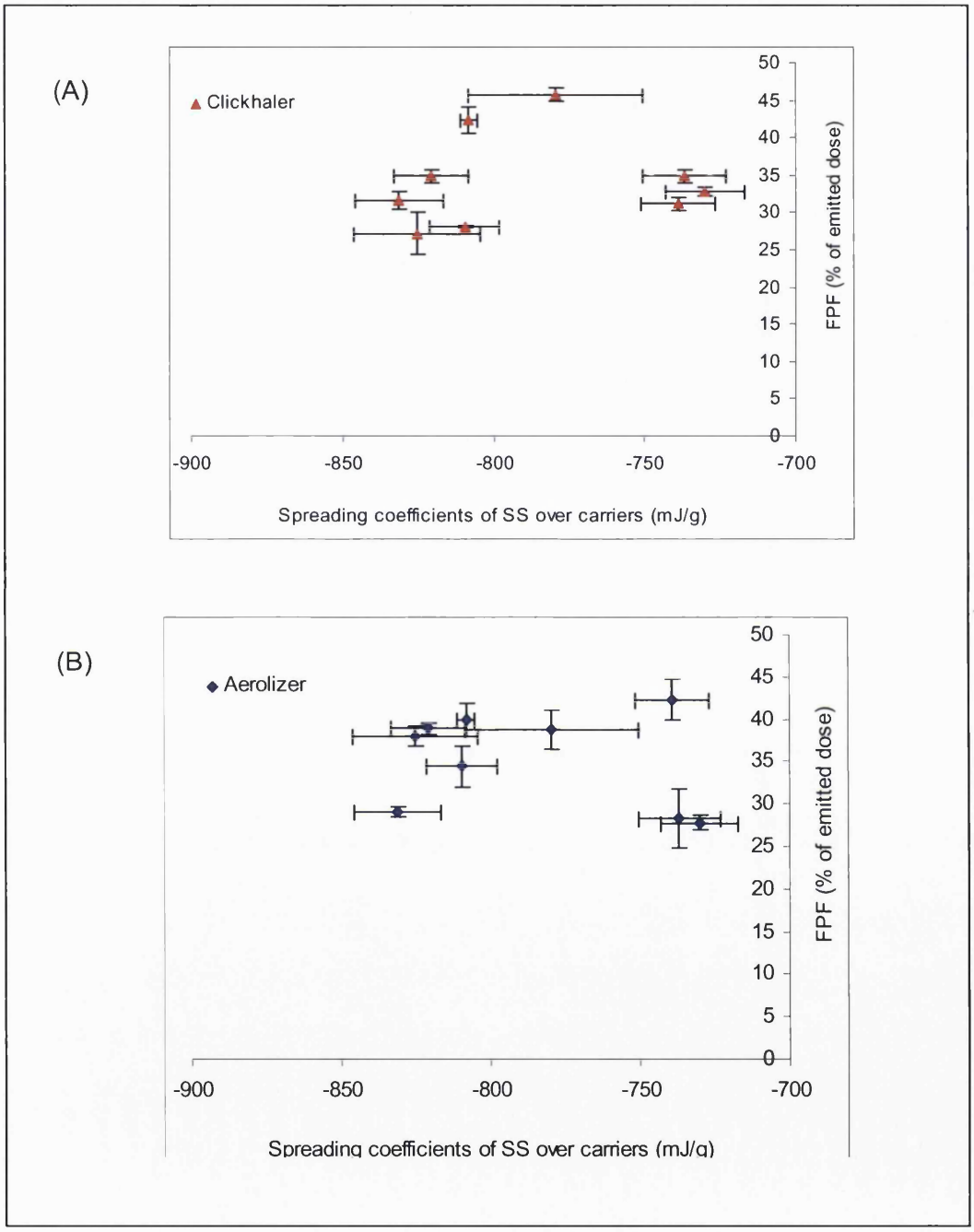

Figure 5.32. *FPF of SS using the clickhaler (A) or the Aerolizer (B) as a function of the spreading coefficients of SS over carriers (mJ/g). Values are mean (n=3)*

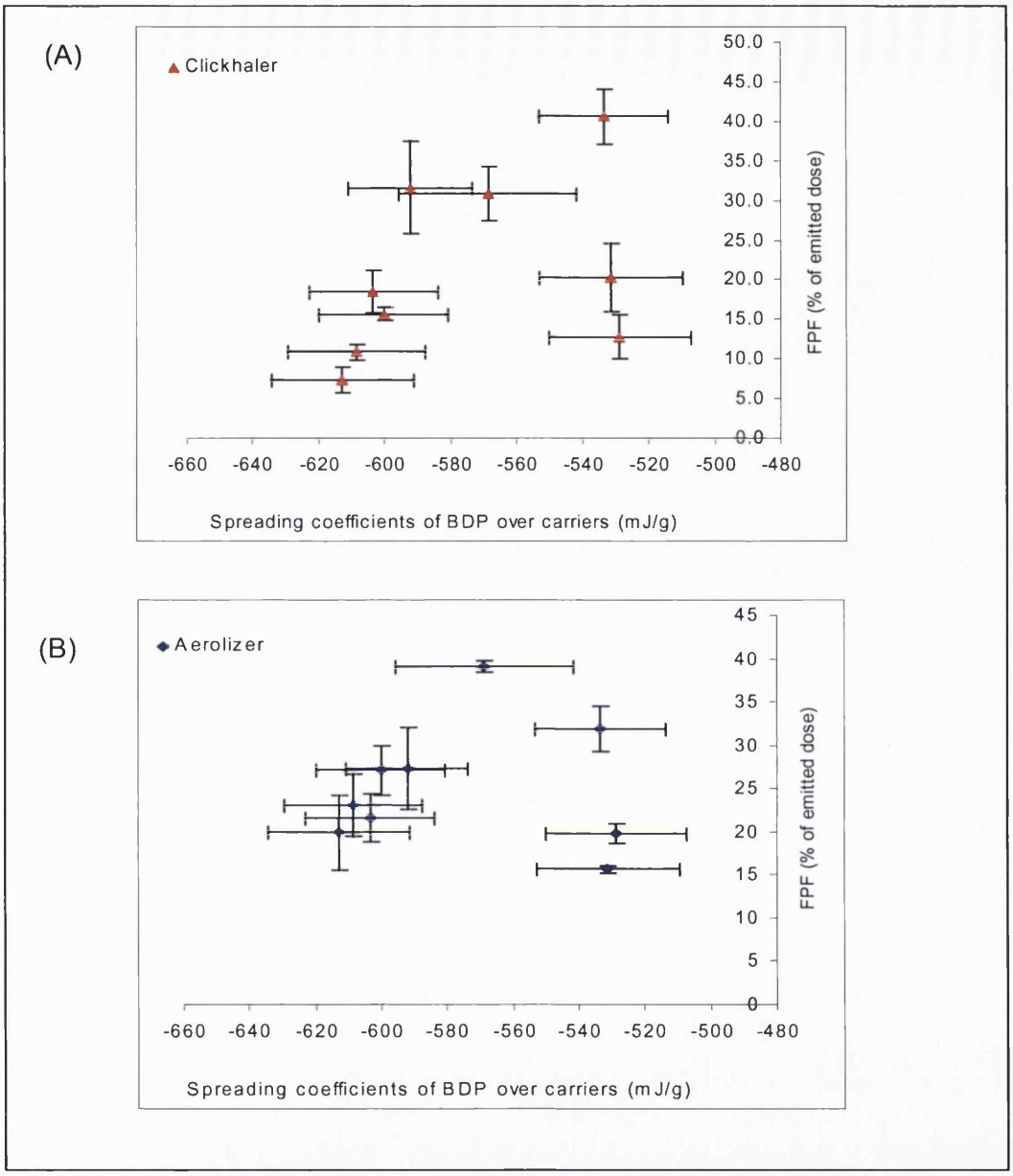

Figure 5.33. *FPF of BDP using the clickhaler (A) or the Aerolizer (B) as a function of the spreading coefficients of BDP over carriers (mJ/g). Values are mean (n=3)*

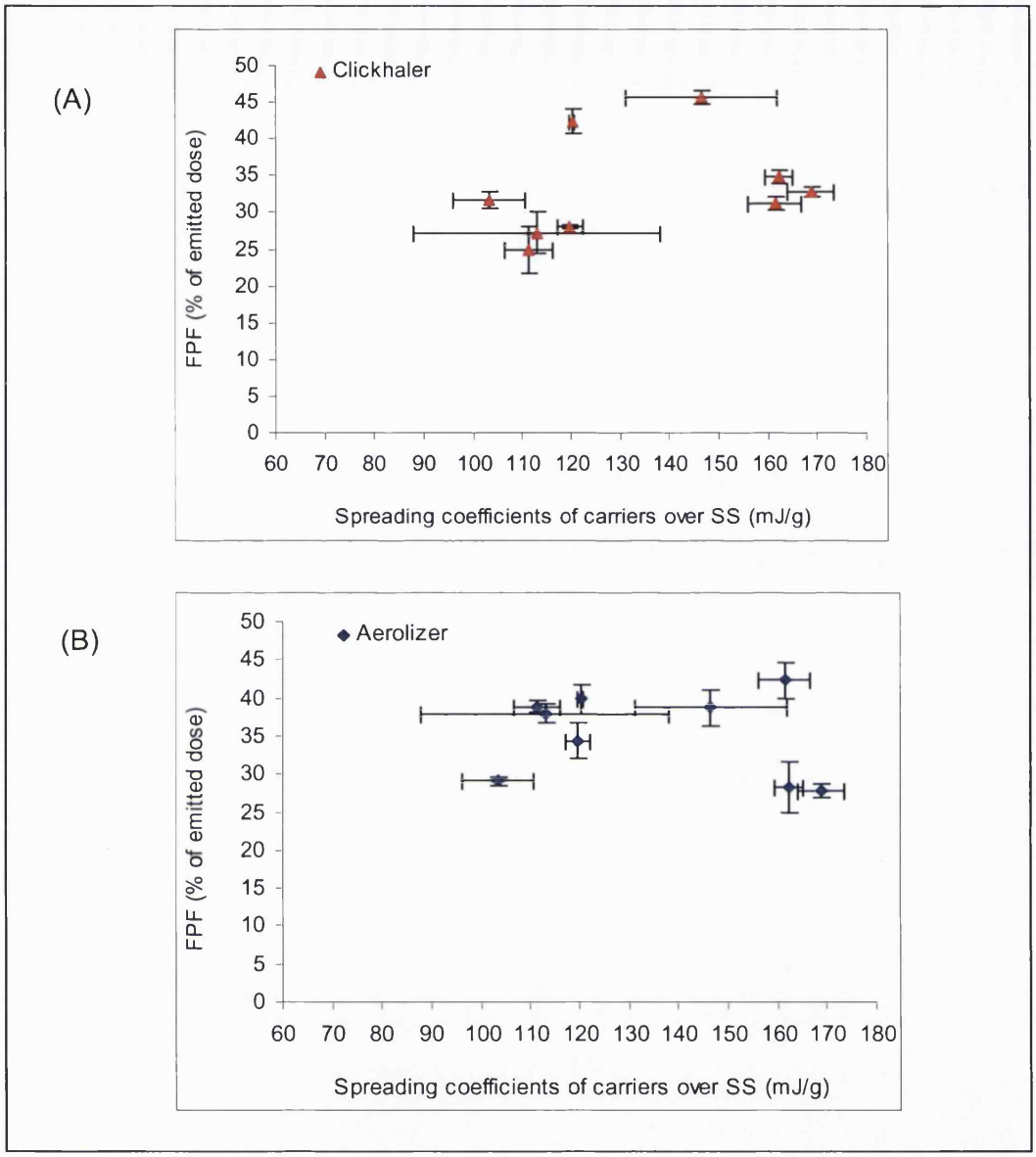

Figure 5.34. *FPF of SS using the clickhaler (A) or the Aerolizer (B) as a function of the spreading coefficients o carriers over SS (mJ/g). Values are mean (n=3)*

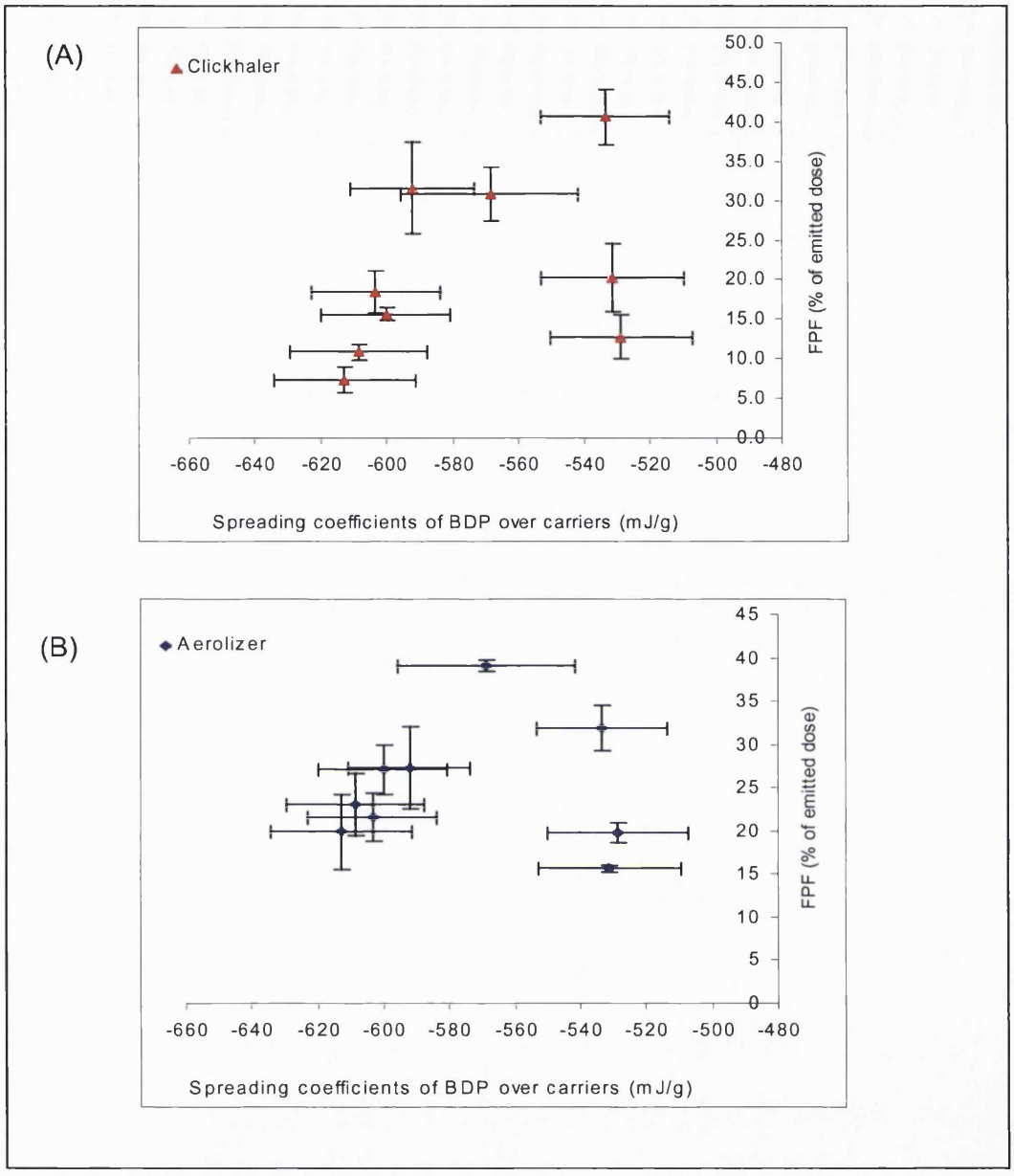

Figure 5.35. *FPF of BDP using the clickhaler (A) or the Aerolizer (B) as a function of the spreading coefficients of BDP over carriers (mJ/g). Values are mean (n=3)*

As an example, the Aero Flo 65 and a carrier composed of fused lactose/PEG fines on an Aero Flo 65 surface should, based on the calculated spreading coefficients, deliver BDP with the same efficiency. Here again, this was not supported by the aerosol deposition studies.

5.6. Conclusions

A partially amorphous lactose/PEG 4000 product was successfully generated by spray drying followed by spontaneous recrystallisation onto air-jet sieved lactose surfaces. The aims of this chapter were three-fold and the major findings are summarised below associated with the original objectives of the work carried out.

Investigation of the fusion of partially amorphous fines onto the surface of air-jet sieved coarse lactose and assessment of the impact on the DPI performance:

Partially amorphous lactose/PEG 4000 particles (containing 10 % PEG) were mixed with air-jet sieved grades of lactose and left to recrystallise for 24 hours. The final concentration of fines was equal to 10 % (w/w). The resulting crystalline products were analysed by IGC and it was found that the surface energy properties of the modified carriers were equivalent with regards to both the dispersive component of the free energy and the acid-base properties. These physical changes were seen to modify the surface interaction with the two asthma drugs and their subsequent deposition. It was shown that this new fused system was efficient in delivering SS respirable drug particles but was less appropriate for BDP (Table 5.3).

Examination of PEG 4000 [45-90] µm as a coarse carrier for DPI formulations:

PEG 4000 was found to be a useful model for investigation, although this polymer has not been approved for delivery to the lungs. It was found to be a good carrier for both SS and BDP when blended with 4 % drug using the Aerolizer® as a model device. To assess whether this deposition was not solely due to the type of device chosen, a comparative study between the reservoir device and the capsule based one was performed. The preponderant role played by the device was illustrated by differences in performances using the same formulation using the Aerolizer® or the Clickhaler® (Figures 5.9 and 5.10). Once again it is important to stress the importance of developing a formulation in combination with the design of the device.

Examination of the IGC application in predicting DPI performances:

In addition to early findings observed on a limited amount of points (n=3) and detailed in chapter 3, a recent work (Cline and Dalby, 2002) suggested a strong relationship between surface energy data and *in vitro* performance. The separate components of surface energy were converted from mJ/m^2 to mJ/g by taking in consideration the specific surface area of the material. The determination of SSA by IGC did not appear to be accurate, confirming the findings of Chow *et al.* (Chow *et al.*, 2004). Using the BET nitrogen adsorption technique, the SEIs in mJ/g were calculated and correlations with the hydrophobic drug deposition were promising. However, little insight for the SS deposition was possible with the calculation of this parameter, confirming the "fragility" of this theory to generally explain the deposition data of different drugs from different carriers.

Chapter 6

Surface modification of the drug substance

6.1. Summary

Dry powder formulations generally consist of mixtures of micronised drugs with larger carrier particles. To meet the particle size requirements for the respiratory drug delivery, the active ingredient is subjected to a micronisation process, usually carried out by air-jet milling. From the data presented in the previous chapters, it is clear that the deposition patterns are drug related. It seemed therefore appropriate to consider methods to make different drug particles with same aerosol efficiencies. In this study, spray drying was investigated as a potential method for the production of crystalline drug particles. SS was co-spray-dried with various proportions of PEG (300 or 4000) and lactose from a solution using the Büchi 191. Characterisation of their solid-state properties revealed the amorphous nature of the produced particles. Adding different proportions of lactose monohydrate to the solution to be spray dried did not affect the physical properties of the resulting particles. When mixed with a lactose-based carrier and tested *in vitro*, the deposition properties were poor compared to a formulation based on a crystalline SS. Further experiments were undertaken to co-spray dry drug substances (SS and BDP) and PEG 4000 from suspensions using both the Büchi 191 and the Niro SD MICRO™. Here again, depositions were lower than those observed with original drug models.

6.2. Introduction

The potential of spray drying to produce lactose/PEG fines for dry powder inhalers has been described in Chapters 4 and 5. Using an adequate process, spray drying may result in the direct preparation of crystalline products. The aim of the work described in the present chapter was to investigate this process with the active compounds in order to modify the physico-chemical characteristics of the drugs. Differences have been described about the aerosol performances of lactose-based formulations that were attributed to both the carrier and drug. The properties of the active have a significant impact on its deposition profile. Based on this previous work, BDP appeared to be far more sensitive to its environment than SS. This is probably due to the cohesive nature of the hydrophobic drug in a "hydrophilic environment, i.e. lactose".

The objectives of this chapter were two-fold: (1) to generate crystalline drug/PEG systems, with the required specifications for lung delivery, and (2) to evaluate these modified actives in terms of aerosolisation behaviour.

The surface modification of hydrophobic cohesive drug particles has been investigated by Kawashima *et al.* (Kawashima *et al.*, 1998a) who modified pranlukast hydrate (PH) surface properties with the incorporation of hydrophilic colloidal silica. Three different methods of silica incorporation were conducted: (1) mechanically sheared mixing, (2) freeze drying and (3) spray drying of aqueous dispersions of the drug and colloidal silica. The *in vitro* properties of the surface modified PH particles were evaluated using a Spinhaler® connected to a TSI. The spray drying method was found to improve the inhalation behaviour of the drug at high concentrations of silica (10 % (w/w)), with an FPF of 43.7 (3) % compared to 13.4 (1.7) % for the original PH formulation. The modification of the hydrophobic surface to a more hydrophilic one with silica particles was confirmed by a contact angle study. The contact angle of modified PH particles decreased in a linear fashion with increasing amount of the incorporated hydrophilic excipient, indicating that both components were mixed randomly on the surface. Figure 6.1 summarises this new particle design method.

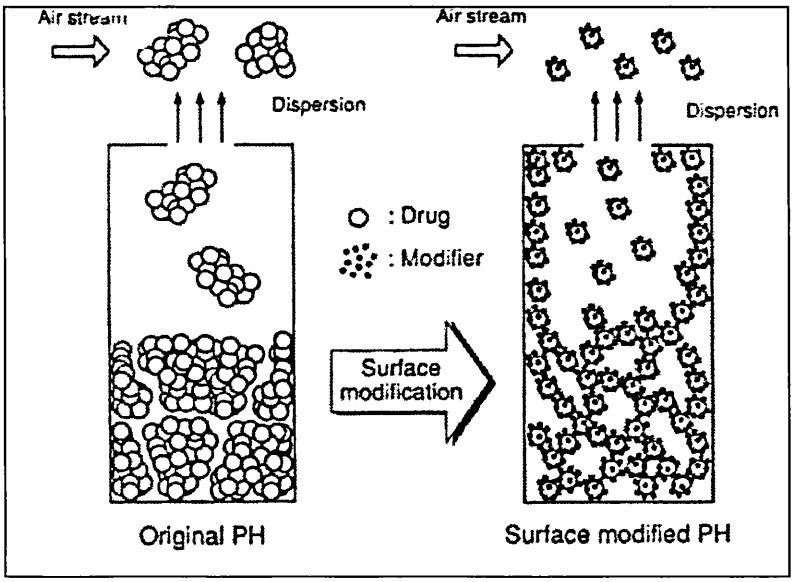

Figure 6.1. *Schematic representation of the effect of PH modifications on the aerosol properties, reproduced from Kawashima et al. (Kawashima et al., 1998a)*

Corrigan *et al.* also investigated the co-spray drying of drugs and different excipients (Corrigan *et al.*, 2003; Corrigan *et al.*, 2004). The authors spray-dried the thiazide diuretic drug bendroflumethiazide (BFMT), in the presence of PEG 4000 (10, 20 and 30 % (w/w) of polymer) to determine if amorphous BFMT/PEG systems with improved dissolution properties (compared to BFMT alone) could be formed. The co-spray-dried formulations were all amorphous, as determined by powder diffraction. However, the presence of the PEG polymer appeared to destabilise the amorphous BFMT at higher weight ratios causing faster recrystallisation.

In another study, the same authors spray-dried SS and lactose and/or PEG. Co-spray drying SS with two different PEGs (PEG 4000 and 20000) resulted in systems of varying crystallinity, whereas SS/lactose systems were all amorphous. The systems containing 20 or 40 % PEG 4000 did show some peaks indicative of crystallinity but to a lower extent compared to physical mixes. The SS/PEG 4000 (20 % PEG) appeared to consist of fused aggregates of spheres (25-30 µm in diameter), whereas the SS/PEG 4000 (40 % PEG) consisted of agglomerates of approximately 70 µm in diameter. Regarding the SS/PEG 20000, only the systems with 40 % of polymer proved to be partially crystalline. All other systems were entirely amorphous.

Based on this work, it appeared justified to further examine the influence of the PEG on the physicochemical properties of the resulting co-spray-dried systems, with the final goal being the formation of stable crystalline drug-PEG particle to probe the interaction with a lactose-PEG carrier.

6.3. Aims and objectives

As previously stated, the aims of this chapter were to investigate spray drying as a method for the production of modified drug particles for DPI formulation. Different SS/PEG systems were investigated as probes for a modified lactose/PEG carrier. The amount of polymer reaching the lungs is of concern and no direct clinical applications of these systems were considered at this stage of the research.

The objectives were:

- To spray dry the two drug models in the presence of PEG 4000, as solutions or suspensions using a Büchi 191 or a Niro SD MICRO^{TM};
- To characterise the physico-chemical properties of the resulting products and to use them as probes for modified lactose-based carriers.

6.4. Material and methods

6.4.1. Production of modified drug models

- Spray drying from a solution

Microparticles of SS/PEG 4000 consisting of 1, 5 and 10 % PEG 4000 by weight of total solid, were prepared by spray drying from solution in water using the Büchi 191. A 10% (w/v) solution was spray-dried under the experimental conditions (method M_1) described by Columbano *et al.* (Columbano *et al.*, 2003) and presented in Table 6.1.

Parameters	Settings (M_1)
Outlet temperature (°C)	145-150
Inlet temperature (°C)	75-80
Aspirator (%)	80
Pump (%)	15
Atomiser airflow rate (Normliter/h)	800

Table 6.1. *Parameters used to spray dry SS/PEG at different ratios.*

The physico-chemical properties of the resulting products were characterised by SEM, X-ray diffraction, DVS and IGC as described in Chapter 2 under each section heading for each instrument.

Spray drying conditions were further varied with the Büchi 191 (Table 6.2). In all experiments involving different methods (M_2, M_3 or M_4), the feed solution employed was a 10 % (w/v) solution. Different PEG molecular weights were tested (300 and 4000 g mol^{-1}). Regarding the SS/PEG 300 formulations, three polymer concentrations (5, 10, 20 % (w/w)) were prepared following the spray drying parameters corresponding to the methods M_3 and M_4.

Parameters	M_2	M_3	M_4
Outlet temperature (°C)	125	180	100
Inlet temperature (°C)	77	89	65
Aspirator (%)	12	20	15
Pump (%)	60	50	100
Atomiser airflow rate (Normliter/h)	600	600	550

Table 6.2. *Different spray drying parameters employed to generate SS/PEG particles.*

Additionnaly, SS was co-spray-dried with various proportions of lactose and PEGs. Two different sets of experiments were undertaken. In the first one, a solution comprising 1 % PEG 4000, 9 % lactose monohydrate and 90 % SS was spray dried following M_1 and M_3.

The effect of the addition of the sugar on the resulting particle characteristics was further studied using a low molecular weight PEG polymer (300 g mol^{-1}) following M_3 or M_1. The composition of the solution that was used was 9 % PEG 300, 1 % lactose monohydrate and 90 % SS. In all experiments involving lactose monohydrate, the amount of solids was 10 % w/v.

- Spray drying from a suspension

Spray drying the hydrophilic drug as a suspension was achieved on the Niro SD MICRO™ following the parameters previously described in Chapter 2, Section 2.2.1.2.10. Twenty percent PEG 4000 (by weight of total solids) was dissolved in ethanol (200 ml total volume) (HPLC grade). SS was suspended in the medium and sedimentation prevented by agitation using a magnetic stirrer. The material was spray-dried as a 1% (w/v) suspension.

Regarding BDP suspension, the active particles were dispersed into an aqueous PEG 4000 solution following the same conditions described for the preparation of the SS solution. The resulting preparation was spray-dried using the Büchi 191 following the operating conditions described in Table 6.3.

Parameters	Settings
Outlet temperature (°C)	145-150
Inlet temperature (°C)	85-90
Aspirator %	60
Pump %	15
Atomiser airflow rate (Normliter/h)	800

Table 6.3. *Spray drying parameters employed to spray-dry BDP/PEG from an aqueous solution using the Büchi 191.*

6.4.2. Evaluation of the aerosol properties

The modified drug particles were tested *in vitro* using the Clickhaler® coupled to a TSI as described in Chapter 2. The formulation tested consisted of the SS/PEG particles and a modified lactose carrier filled into the reservoir of the device. The lactose based carrier consisted of the airjet sieved Aero Flo 65 mixed with 10 % crystalline lactose/PEG fines (containing 10 % (w/w) PEG 4000) as described in Chapter 4. The final drug concentration was equal to 4 % (w/w) and the blending carried out using a Turbula mixer for 30 minutes at 42 rpm.

6.5. Results and discussion

6.5.1. Spray drying from a solution

Described in the following subsection are the the physico-chemical properties of the different co-spray dried formulations using the Buchi 191 and SS as a drug substance.

6.5.1.1. Characterisation of the particles

The scanning electron micrographs of spray-dried SS/PEG 4000 (prepared by M_1) at different ratios are shown in Figure 6.2. All solutions investigated were successfully spray dried, resulting in a transformation in the physical

appearance. Increasing the PEG proportion from 1 % (Figure 6.2 A) to 5 % (Figure 6.2 B) or even 10 % (Figure 6.2 C) did not seem to affect the morphology of the particles. All particles appeared to be spherical with a pitted surface and a diameter generally less than 5 µm, making them potentially good candidates for pulmonary delivery. This is consistent with prior work, where SS has been shown to produce microfine spherical particles in the respirable size range when spray dried on its own. (Chawla *et al.*, 1994).

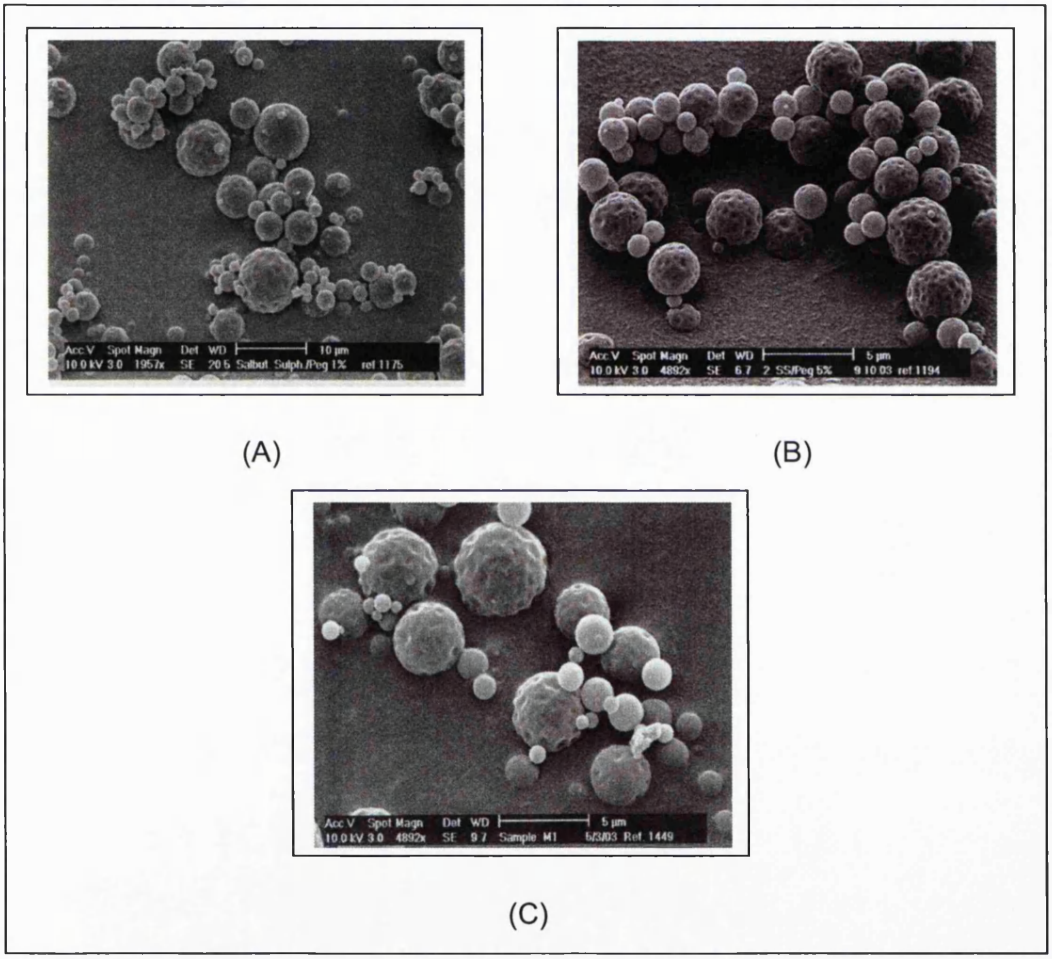

Figure 6.2. *Influence of the PEG 4000 concentration (1 % w/w = Figure A, 5 % w/w = Figure B, 10 % w/w = Figure C) on the resulting particle morphologies.*

The water sorption data (obtained by DVS) of the different co-spray-dried formulations and feed material (crystalline SS) are shown in Figures 6.3 and 6.4 respectively. As previously described, the different relative humidities are illustrated by the blue line, whereas the mass changes of the sample are represented by the red line. As a non hygroscopic nor hydrate forming drug

(Ward and Schultz, 1995), it was expected that SS would not absorb water to a large extent. Brodka-Pfeiffer *et al.* (Brodka-Pfeiffer *et al.*, 2003) could not measure the water uptake of crystalline SS by this method. However, Columbano *et al.* (Columbano *et al.*, 2002) reported a significant uptake of water when crystalline SS was exposed to 75 % RH. The small particle size (linked to an important surface area) was suggested as the reason for surface water adsorption.

To confirm these earlier observations by Columbano *et al.*, the DVS experiments were repeated. Rapid water uptake (up to 0.23 % (w/w)) was observed when the sample was exposed to 80 % RH. The water was then desorbed very quickly when the RH was reduced to 0 % (Figure 6.3).

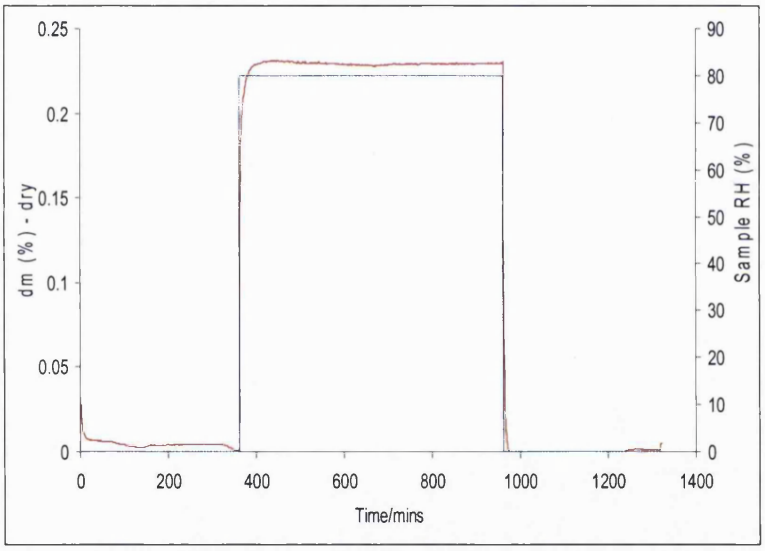

Figure 6.3. *Water sorption analysis of crystalline SS.*

From the water sorption data of the SS/PEG 4000 systems (Figure 6.4), it was clear that all systems were amorphous. Particles containing 5 or 10 % (w/w) PEG equilibrated to similar maximum water contents of approximately 11.3 % (w/w) when exposed to 80 % RH. The maximum water uptake for the sample containing 1 % (w/w) PEG (orange line) was slightly higher with around 12 % mass increase. The release of water from the SS/PEG particles at 80 % RH was characterised by two different desorption rates: the release of water was faster in the first part than in the second part of the desorption curve. Moreover, the system containing 1 % PEG was more efficient in releasing the water

compared to systems containing more PEG. The time for the onset of weight loss of the different SS/PEG systems was very similar at all ratios that were investigated.

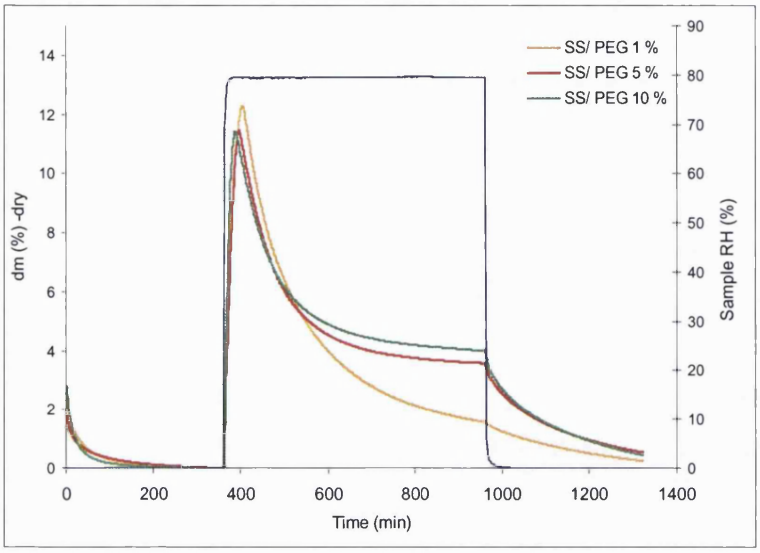

Figure 6.4. *DVS mass plot of SS/PEG 4000 systems as a function of time and % RH.*

When SS was spray-dried alone, a different DVS profile was observed (Figure 6.5, (Columbano *et al.*, 2002)). After exposure to 75 % RH, a rapid weight increase up to 13 % (w/w) was followed by a slow desorption process even when the RH was adjusted from 75 to 0 %. This indicated that the rate-limiting step was the diffusion of water through the solid and not the concentration difference between the particle surface and the vapour. After 65 hours at 75 % RH, the water content of the spray-dried SS was still 6 % (w/w). Some water could have been trapped between drug crystals explaining the water retention.

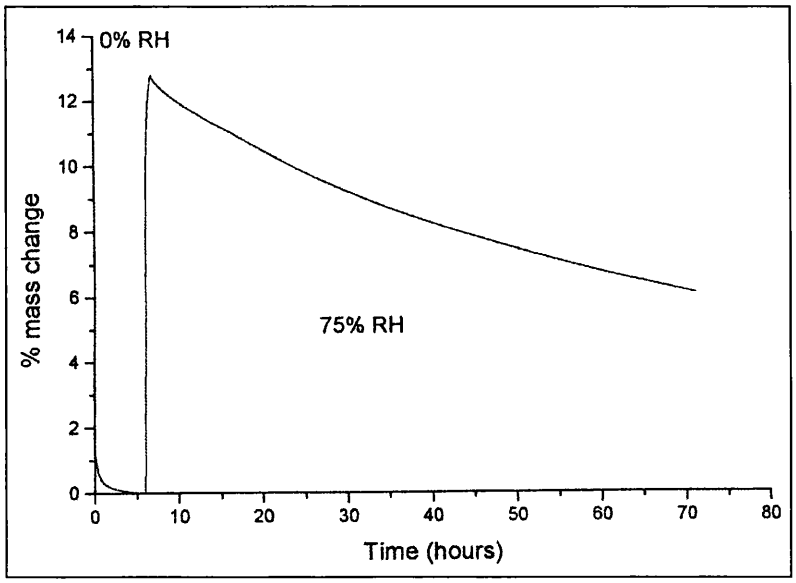

Figure 6.5. *Water vapour sorption of spray-dried SS at 25°C (Columbano et al., 2002).*

Following from gravimetrics studies, the surface energetics of the different spray dried formulations were evaluated (Table 6.4). The different co-spray-dried products were examined in terms of their dispersive surface energies (γ_s^d) (Figure 6.6) and their acid-base properties (Figure 6.7), calculated using the cross-sectional method as described in Chapter 2.

Materials	Specific polar interaction (kJ/mol)				Acid-base characteristics			γ_s^d (mJ/m^2)
	Acetone	Chloroform	Ethanol	Ethyl acetate	K_A	K_D	K_D/K_A	
SS	7980 (155)	1052 (58)	11506 (117)	10396 (112)	0.137	-0.011	-0.08	50 (3.9)
SS/PEG 1 %	5140 (136)	1743 (40)	7960 (117)	6943 (117)	0.089	0.019	0.22	35.7 (0.7)
SS/PEG 5 %	5381 (42)	2054 (64)	7934 (71)	7109 (48)	0.089	0.038	0.43	34.7 (1.6)
SS/PEG 10 %	5434 (68)	2121 (173)	7990 (176)	6788 (241)	0.085	0.050	0.60	32.8 (0.4)
PEG 4000	9821 (259)	7898 (252)	13286 (368)	10353 (209)	0.120	0.206	1.71	33.1 (0.2)

Table 6.4. *Surface energy data of spray-dried SS/PEG systems from solutions and PEG 4000. Values are mean (standard deviation).*

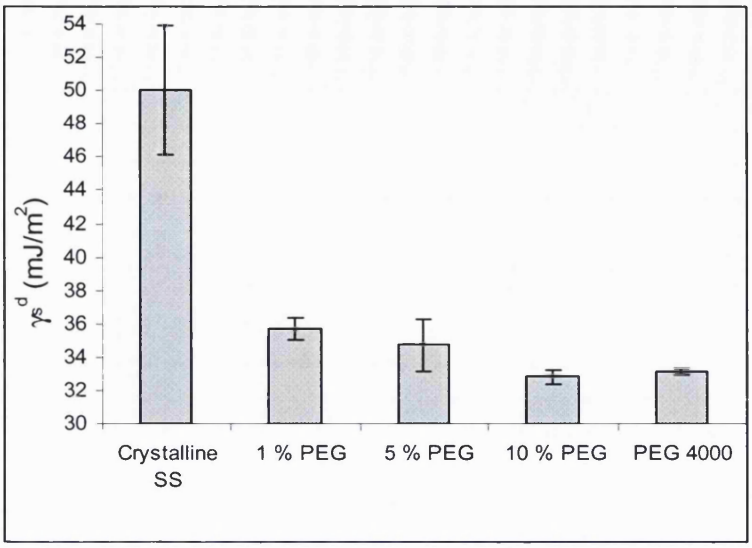

Figure 6.6. *Dispersive components of the crystalline SS, the different SS/PEG systems spray dried from a solution and PEG4000. Values are mean (n=3)*

The surfaces of the spray-dried systems in the presence of PEG were less energetic than those of purely crystalline SS. Decreasing γ_s^d whith increasing the PEG proportion was consistent with the data presented in Chapter 4, where the γ_s^d of lactose/PEG fines ranged from 34.7 (0.7) mJ/m^2 for a system containing 1% PEG to 38.4 (0.3) mJ/m^2 for a system containing 5 % PEG. Here again, the γ_s^d of the different co-spray-dried systems were closer to the γ_s^d of the PEG than the other component, indicating the presence of PEG at the surface of the particles (already seen in Chapter 4).

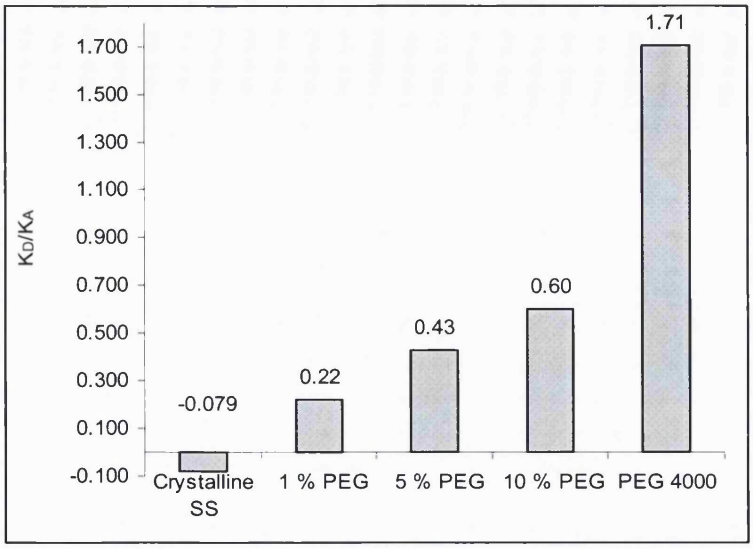

Figure 6.7. *Acid-base characteristics of the crystalline lactose, different lactose/PEG systems spray dried from a solution and PEG 4000.*

The addition of PEG at different concentrations in the spray-dried SS solution also had a substantial effect on the K_D/K_A values. The increase in the K_D/K_A ratio was mainly due to an increase in K_D values as K_A stayed almost constant for the formulations tested. This effect was linked to an increase in the amount of PEG present in the feed solution. Increasing the PEG concentration, may lead to more PEG molecules migrating to the surface of the particle causing a "PEG like effect". Those results were in accordance with earlier findings (Chapter 4) based on lactose/PEG co-spray-dried systems.

6.5.1.2. Deposition studies

The aerosol performances of the PEG modified formulations (Table 6.5) were determined using the TSI coupled to a Clickhaler®. The deposition data obtained for the unmodified SS (Formulation 1), used as a reference, was as reported in Chapter 4 (Formulation 3 in Table 4.6)

Formulation	active used	ED (µg)	RD (µg)	FPF (%)
1	SS	691 (14)	292 (16)	42.4 (1.7)
2	SS/PEG 1 %	723 (29)	146 (16)	20.2 (2.2)
3	SS/PEG 5 %	1119 (47)	214 (12)	19.1 (0.6)
4	SS/PEG 10 %	1076 (54)	152 (23)	14.1 (1.7)

Table 6.5. *Deposition of modified SS/PEG particles produced by spray drying from solutions. Values are mean (standard deviation).*

On analysing the RDs for these formulations, it was found that the aerosol properties of these systems were quite disappointing compared to the crystalline SS. As shown in Figure 6.8, the FPFs were indeed different in our study, with FPFs ranging from 42.4 (1.7) % for the formulation containing the micronised SS (Formulation 1) to 14.1 (1.7) % for the formulation containing the SS/PEG spray-dried active with 10 % PEG (Formulation 4). As a conclusion, data show a significant decrease in FPF for the PEG modified SS formulations, possibly due to their amorphous natures. Chawla *et al.* (Chawla *et al.*, 1994). reported similar *in vitro* behaviour for spray-dried and micronised SS from the Spinhaler® (FPF of 7.63 (3.02) % and 10.36 (6.76) % for the spray-dried and micronised materials respectively). A second explanation may be found in the presence of PEG which may cause those unstable particles to adhere to each other, increasing the MMAD values and therefore being too large for an efficient pulmonary application.

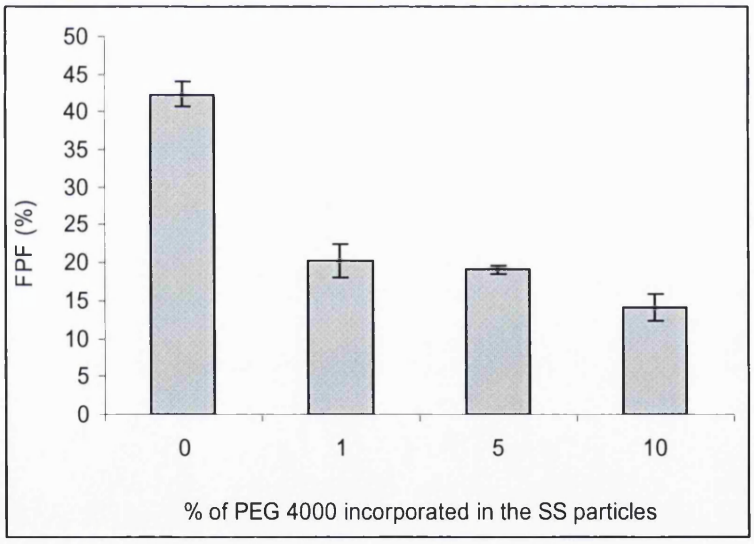

Figure 6.8. *Influence of the % of PEG 4000 contained in the SS particles on the obtained FPFs. Values are mean (n=3)*

Different options were considered to generate crystalline material following the spray drying of solutions. The first parameters that were varied were the spray drying conditions. Three new set-ups (Table 6.2) were investigated. A solution consisting of 10 % SS/PEG 4000 was employed in each case. Here again, varying the settings did not markedly affect the particle morphology or apparent

size. The systems under investigation consisted of smooth spherical particles with indentations (Figure 6.9).

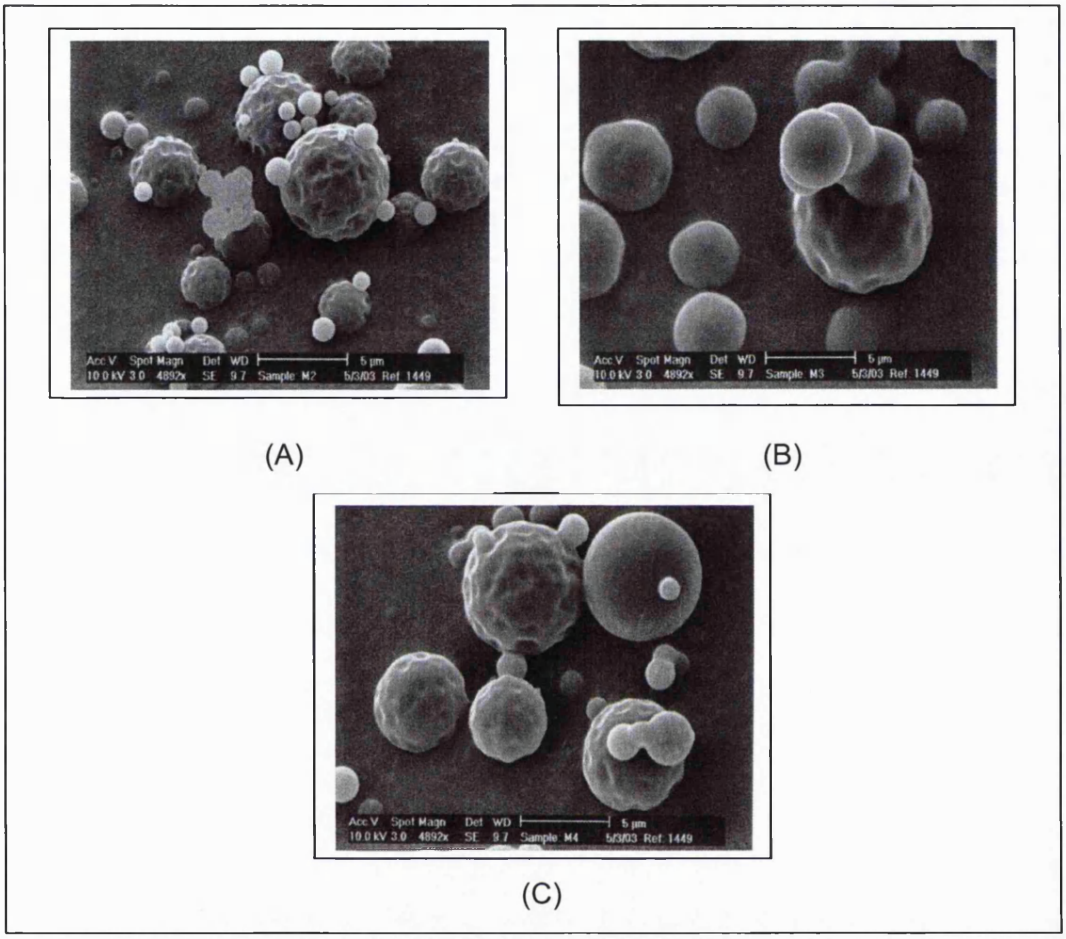

Figure 6.9. *SS/PEG 4000 systems containing 10 % PEG co-spray-dried following M_2 (A), M_3 (B) or M_4 (C).*

The amorphous nature of the spray-dried samples was confirmed and an example is shown in Figure 6.10. From the results it can be seen that the spray drying conditions did not cause retention of the crystalline material.

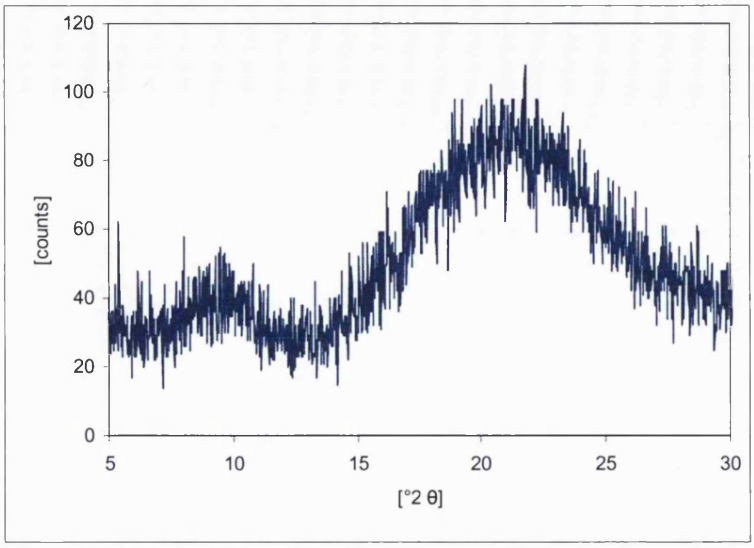

Figure 6.10. *X-ray diffraction scan of spray-dried SS/PEG 4000 10 % following* M_2.

The second parameter to be investigated was the PEG molecular weight. Liquid PEG 300 was used instead of PEG 4000 and different runs performed following M_3 or M_4 spray drying conditions. Three different solutions consisting of 5, 10 or 20 % PEG 300 were studied using each of the two methods. Varying the PEG grade did not affect either the particle morphology or the amorphous nature of the co-spray-dried systems. Examples of SEMs and X-ray patterns are shown in Figures 6.11 and 6.12 respectively.

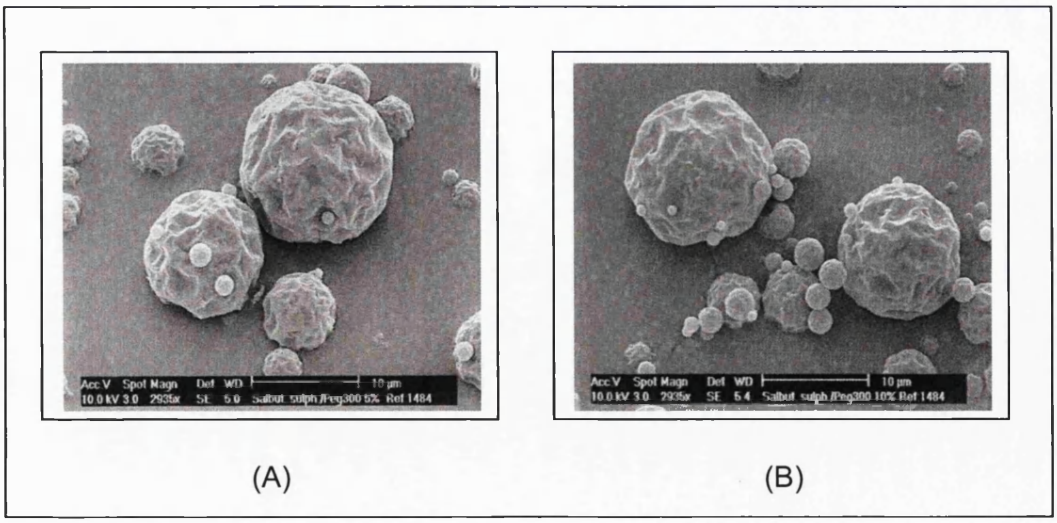

Figure 6.11. *Influence of the PEG 300 concentration (5 % (A) or 10 %(B)) on the resulting particle morphologies following* M_4.

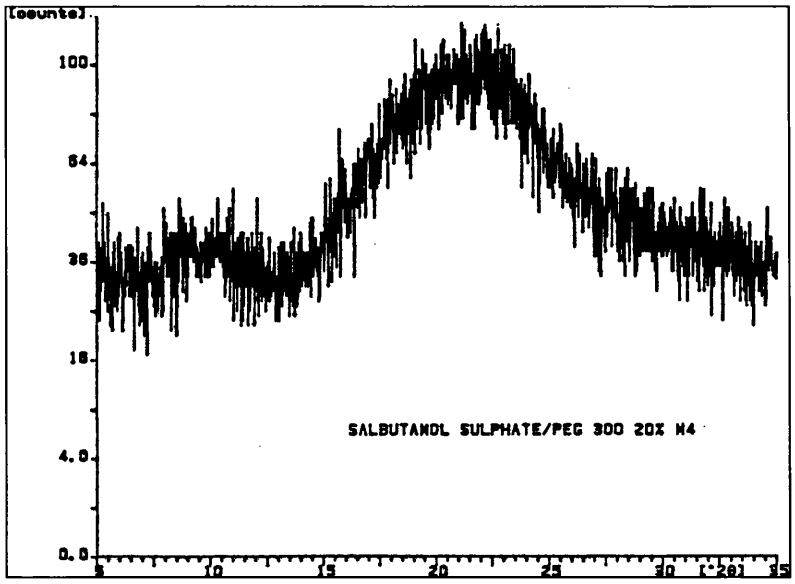

Figure 6.12. *X-ray diffraction scan of spray-dried SS/PEG 300 20 % following* M_4.

Amorphous material was also obtained when lactose monohydrate was added (Figure 6.13). Prior work had suggested that crystalline material could be obtained when lactose alone with PEG was spray dried. However, with these formulations only amorphous material was obtained.

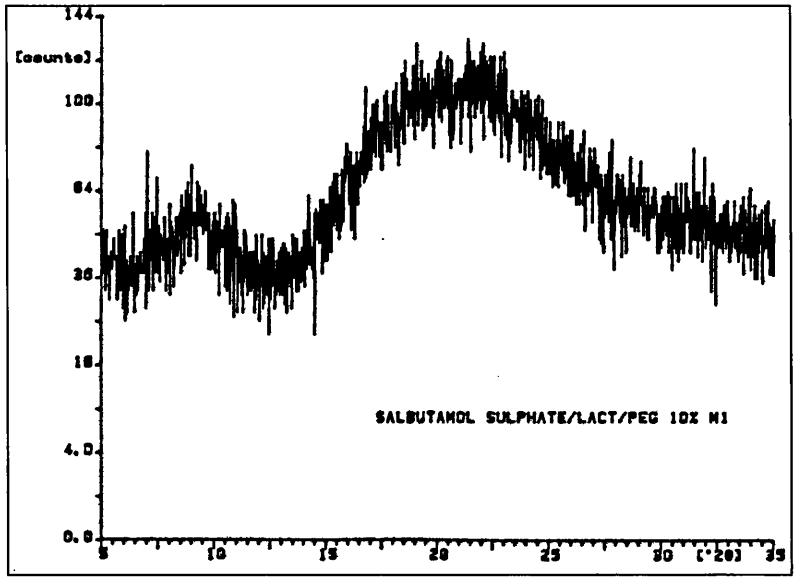

Figure 6.13. *X-ray diffraction for SS/PEG/lactose co- spray-dried product.*

The particle morphology was not influenced by the addition of lactose as ternary material (Figure 6.14).

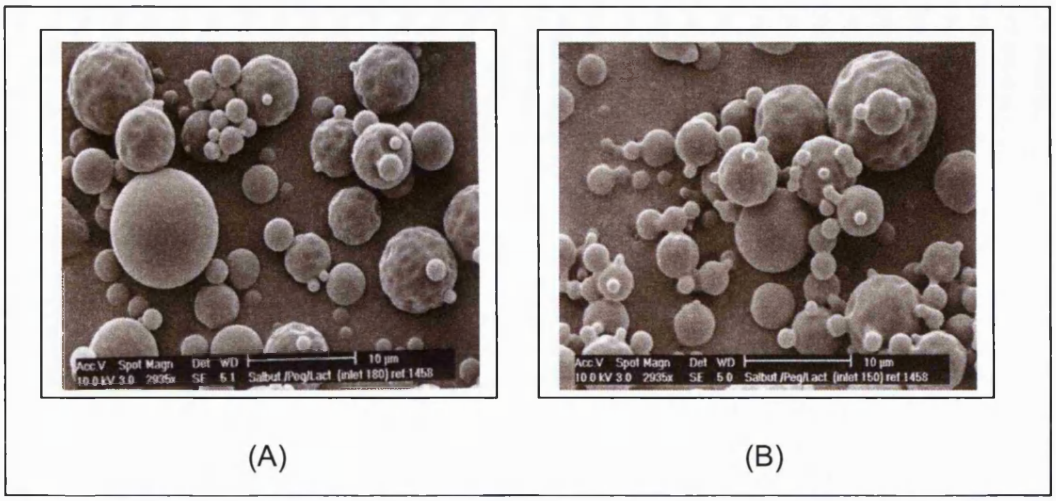

Figure 6.14. *Electron micrographs of lactose/PEG/SS systems; following M_3 (A), M_1 (B).*

Moreover, the recrystallisation process appears to be slowed by the presence of the PEG. Figure 6.15 shows the XRPD of a SS/PEG300/lactose system after 24 and 96 hours at room temperature. Partial crystallisation occurred, but the kinetic profile was slow with no total recrystallisation observed after 4 days. This effect was unexpected and is not fully understood since data presented in Chapter 4 showed that the presence of the polymer was responsible for the rapid crystallisation of the lactose/PEG system. The interactions between the sugar and the polymer would therefore be expected to differ from those existing between SS and the polymer. Further investigations are needed in order to have a better understanding on the specific interaction between the two excipients that could cause fast recrystallisation.

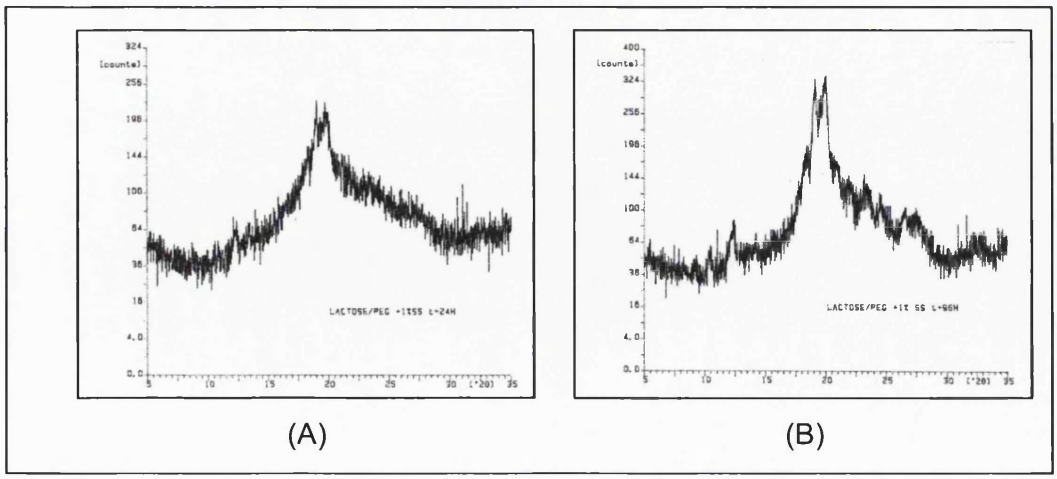

Figure 6.15. *X-ray diffraction for SS/PEG/lactose after 24 h (A) and 96 h (B) stored at ambient conditions.*

6.5.2. Spray drying from a suspension

6.5.2.1. Salbutamol sulphate

6.5.2.1.1. Characterisation of the particles

The main advantage of spray drying from a suspension is for the active to maintain its crystalline nature. Spray drying of the active in the presence of the polymer would result in a PEG coating onto the particle surface. Difficulties in ensuring homogenous particle size distributions and coating efficiencies are the principal disadvantages of this approach.

Characterisation of the resulting particles was essential to ensure that the spray drying process did not affect the physical properties of the drug. Assessment by SEM, X-ray diffraction, DVS and IGC were done for this purpose and the results are presented below. As seen in Figure 6.16, the modified SS/PEG particles kept the original shape and apparent size of the starting material indicating that the production of such systems was possible and non-destructive.

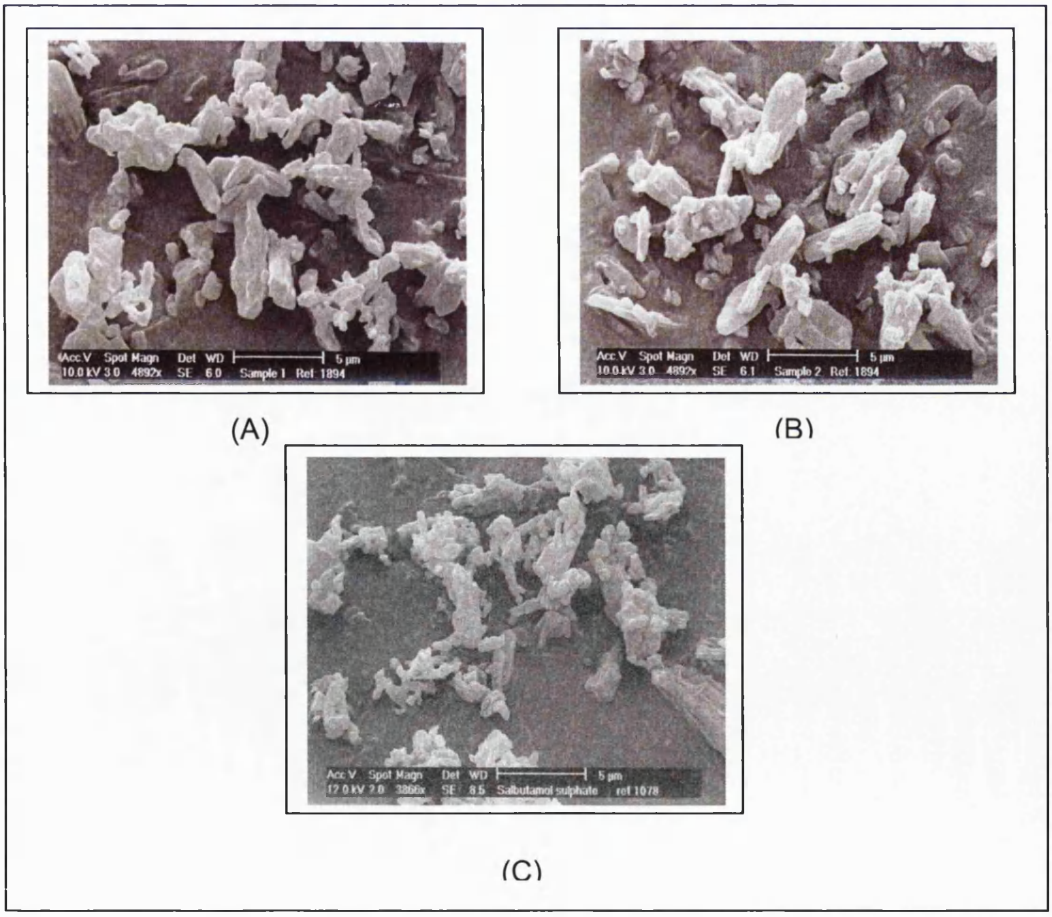

Figure 6.16. *Electron micrograph of (A) 10% suspension, (B) 20% suspension, (C) original.*

Confirmation of the crystallinity of the drug was further obtained by X-ray diffraction. The presence of the specific peaks of crystalline SS using different proportions of PEG 4000 was seen and an example shown in Figure 6.17.

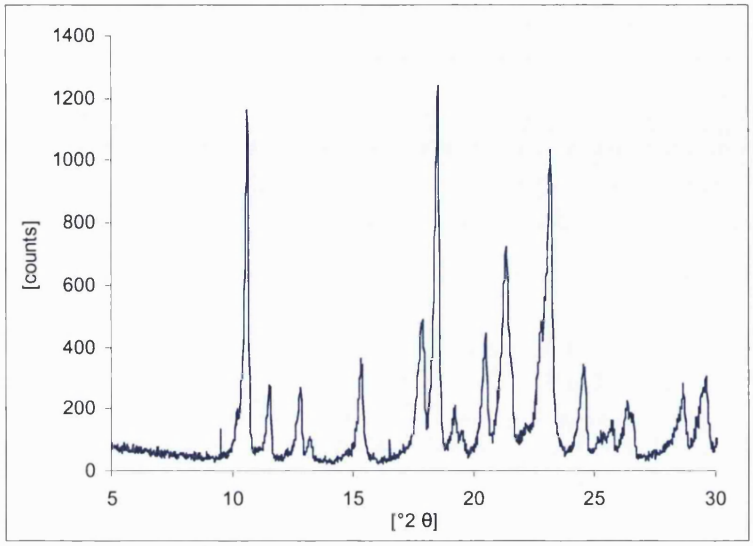

Figure 6.17. *XRPD of spray-dried SS/PEG (10 % PEG)*

DVS analysis was used to further characterise hygroscopicity and the results shown in Figures 6.18 and 6.19. The conditions employed were as described in Chapter 2.

The extent of water uptake when exposed at 80 % RH, depended on the amount of PEG added to the suspension. For a 10 % (w/w) PEG (Figure 6.18) the mass gain corresponded to approximately 0.35 % whereas this value increased to nearly 0.9 % for a 20 % PEG. This is consistent with the fact that the polymer is hydroscopic and therefore more water is taken up at higher ratios. No lag phases were observed and the desorption profiles were very similar indicating that the PEG was present at the surface of the formed particules.

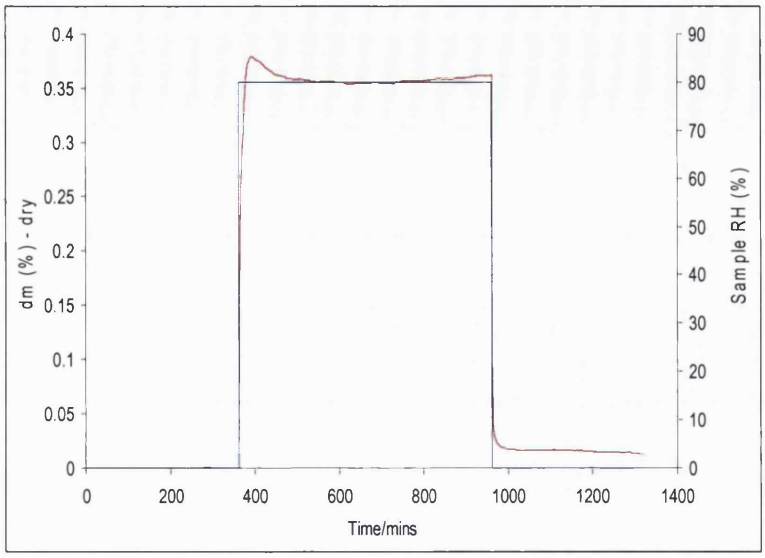

Figure 6.18. *Water sorption for SS/PEG 4000 (10 %).*

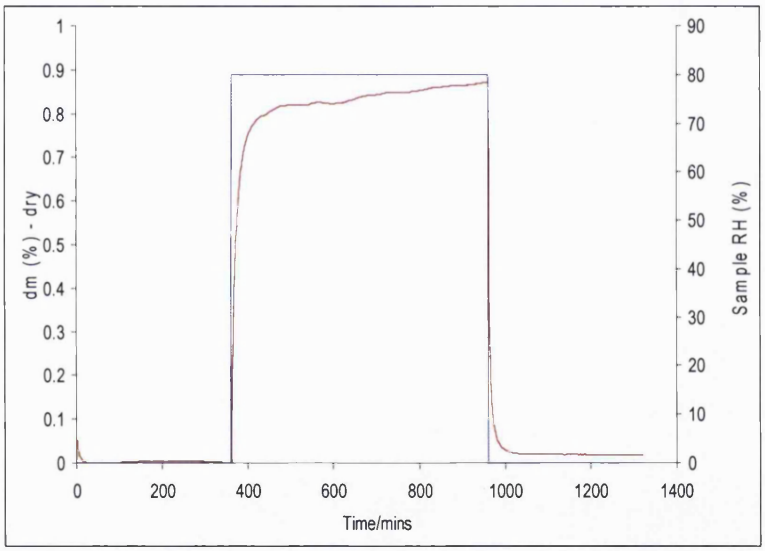

Figure 6.19. *Water sorption for SS/PEG 4000 (20 %).*

The surface energy of the co-spray dried SS (Table 6.6) shows a relatively low dispersive component and relatively high K_D/K_A ratios compared to the micronised sample. This indicates that the co-spray dried drugs present predominantly basic polar surfaces. The addition of PEG 4000 at different concentrations did not result in major changes (γ_s^d varying from 36.7 (0.3) to 37.3 (0.3) and K_D/K_A varying from 0.52 to 0.42).

This might be explained by considering that the droplet will go through rapid changes in concentration during the process, and therefore the final PEG 4000 concentration in the different systems might not be exactly 10 or 20 % (w/w).

Materials	Specific polar interaction (KJ/mol)				Acid-base characteristics			γ_s^d (mJ/m^2)
	Acetone	Chloroform	Ethanol	Ethyl acetate	K_A	K_D	K_D/K_A	
SS	7980 (155)	1052 (58)	11506 (117)	10396 (112)	0.137	-0.011	-0.08	50 (3.9)
10 % PEG	6050 (33)	3120 (45)	8330 (34)	7743 (30)	0.096	0.050	0.52	36.7 (0.3)
20 % PEG	6070 (87)	2696 (51)	8447 (87)	7724 (106)	0.097	0.041	0.42	37.3 (0.3)
PEG 4000	9821 (259)	7898 (252)	13286 (368)	10353 (209)	0.120	0.206	1.71	33.1 (0.2)

Table 6.6. *Surface energy data of the references and the spray-dried SS/PEG systems (10 or 20 % w/w of polymer) from suspensions. Values are mean (standard deviations).*

The IGC data indicates that spray drying SS, from a suspension, in the presence of PEG (Figures 6.20 and 6.21) did result in significant changes in the surface energetics. Interestingly, when compared to the surface energetics of SS/PEG particles obtained after spray drying from a solution (Table 6.4), the values are comparable with a decrease in γ_s^d and an increase in K_A/K_D values. The γ_s^d of SS/PEG co-spray dried (containing 10 % PEG) was 32.8 (0.4) when starting from a solution and 36.7 (0.3) when starting from a suspension. The lower value of the γ_s^d observed might be explained by the amorphous nature of the produced particle.

Moreover, the K_A/K_D values ranged from 0.52 to 0.60, indicating that in the case of a solution, the PEG is migrating to the surface of the particle.

It might be interesting to evaluate in more details those different systems in order to understand why an SS/PEG material, being amorphous and obtained after spray drying from a solution, exhibits dispersive and acid-base characteristics similar to that for crystalline SS/PEG obtained from a suspension.

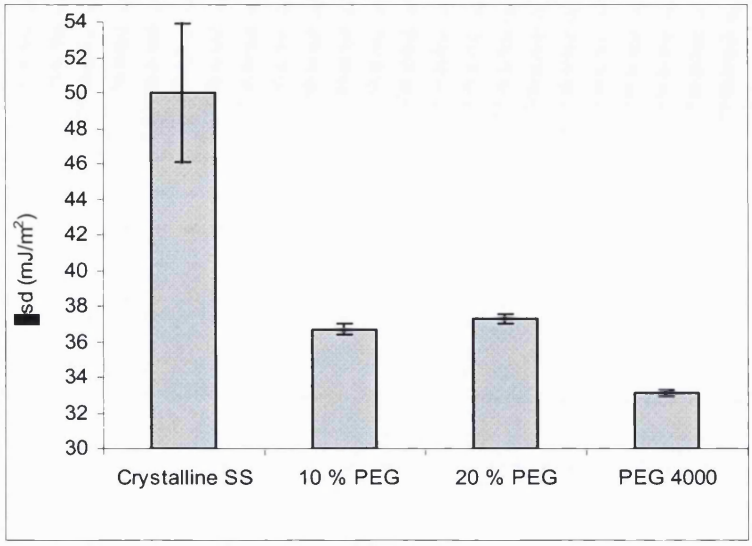

Figure 6.20. *Dispersive components of the crystalline SS, the different SS/PEG systems spray dried from a suspension and PEG4000. Values are mean (n=3)*

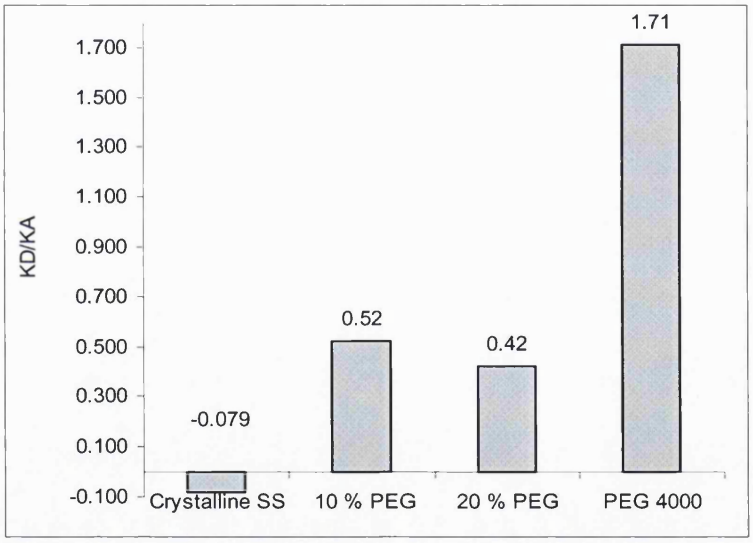

Figure 6.21. *Acid-base characteristics of the crystalline SS, different SS/PEG systems spray dried from a suspension and PEG 4000.*

6.5.2.1.2. Deposition study

Using the TSI and the Clickhaler®, there was little difference beween the EDs of the micronised and the SS spray dried from suspension (Table 6.7). Moreover, similar RDs lead to comparable FPFs (ranging from 34.9 (0.9) % for the micronised drug to 28.1 (1.2) % for the SS/PEG 20%) as seen in Table 6.7 below.

This study shows that modifying the surface of SS did not markedly affect the *in vitro* performance compared to a micronised active.

Formulation	Active used	ED (µg)	RD (µg)	FPF (%)
1	SS	1024 (37)	358 (21)	34.9 (0.9)
2	SS/PEG 10 %	1051 (148)	320 (30)	30.6 (2.9)
3	SS/PEG 20 %	983 (67)	276 (45)	28.1 (1.2)

Table 6.7. *Deposition of modified SS/PEG particles produced by spray drying from suspensions. Values are mean (standard deviations)*

6.5.2.2. Beclomethasone dipropionate

6.5.2.2.1. Charaterisation of the particles

Spray drying BDP/PEG suspensions produced a powder consisting of apparent agglomerated particles (Figure 6.22). A possible reason for this microscopic observation might be the absorption of moisture by these spherical particles. Nevertheless, no apparent degradation of the active was observable based on X-ray diffraction patterns (Figure 6.23). Gravimetric studies and surface energy measurements were undertaken to further characterise the modified BDP particles.

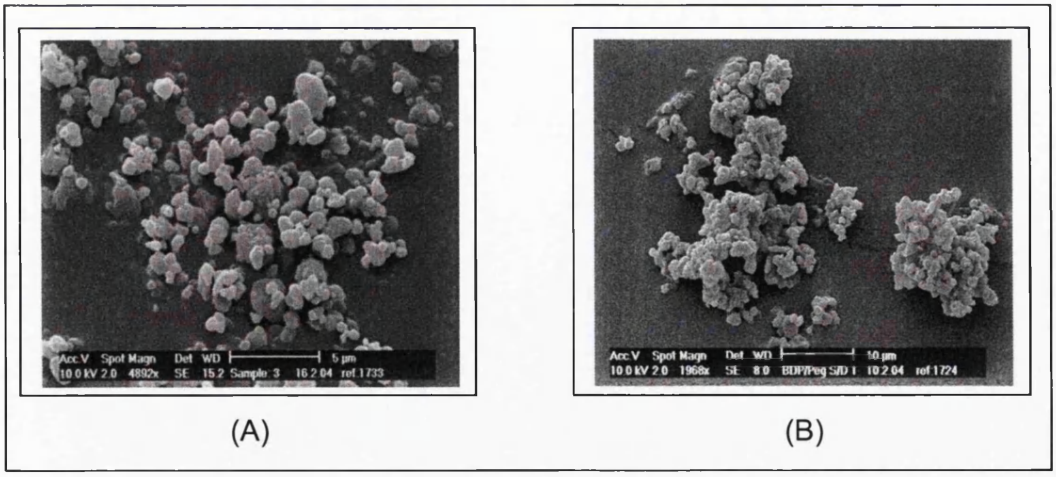

Figure 6.22. *Electron micrographs of (A) crystalline BDP,and (B) spray-dried BDP/PEG suspension.*

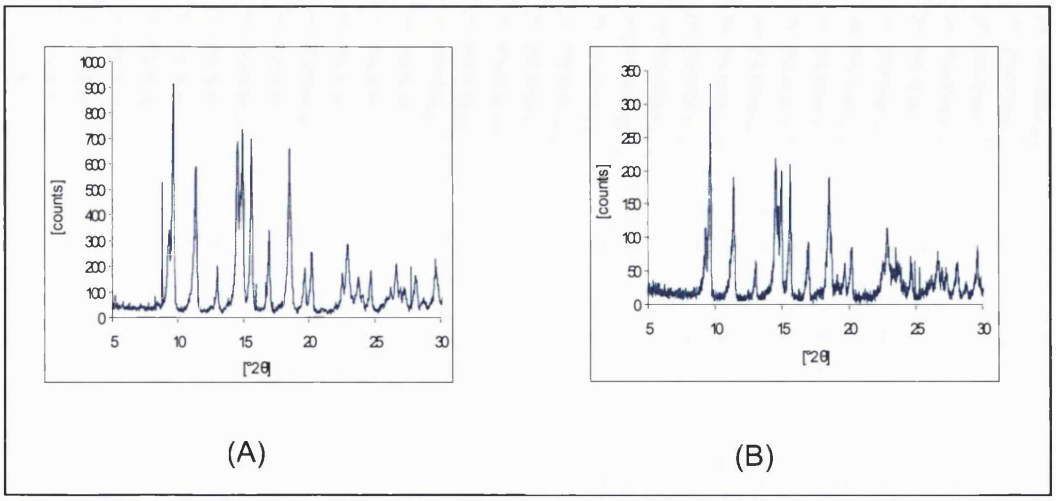

Figure 6.23. *X-ray diffraction patterns of BDP before (A) and after (B) spray drying on the Büchi 191.*

The water vapour sorption data of the crystalline BDP used throughout this dissertation is presented in Figure 6.24. The material was dried and subjected to the same RH as previously described. The sorption of water, illustrated by the increase in sample mass, reached a maximum before slightly dropping at 80 % RH. The increase in weight at the equilibrium corresponded to approximately 0.5 %. The rate of desorption when the sample was dried again was very fast with no final mass gain.

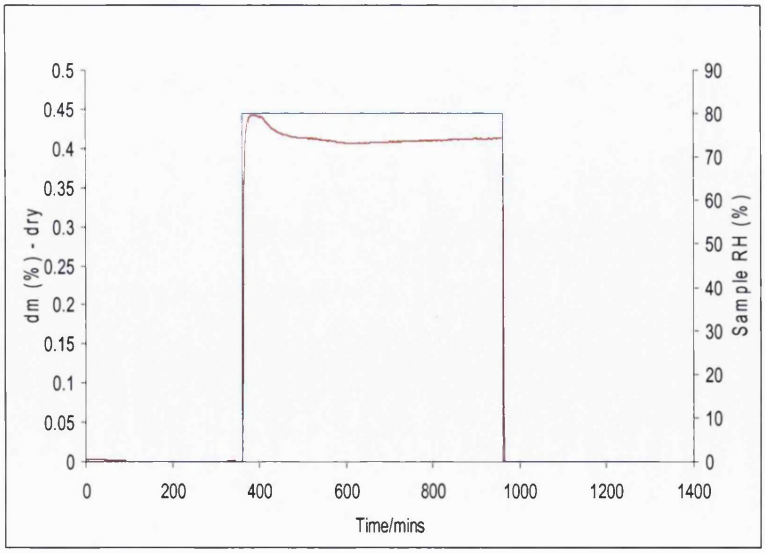

Figure 6.24. *DVS mass plot of crystalline BDP as a function of time and % RH.*

The sorption isotherms for the co-spray dried systems showed different profiles (Figures 6.25 and 6.26). The water uptake for those systems was higher when compared to crystalline BDP (Figure 6.24) due to the presence of the PEG at the surface of the particle. For the particles containing 10 % of polymer (Figure 6.25), the mass gain recorded was around 0.9 %, approximately twice as much as for crystalline BDP. This value went up to around 1.6 % when the PEG concentration was increased to 20 % (w/w). In both cases, comparable to what was observed for the control, a slight drop in the weight was detected when the samples were undertaking the humidification stages. No final mass gains were detected.

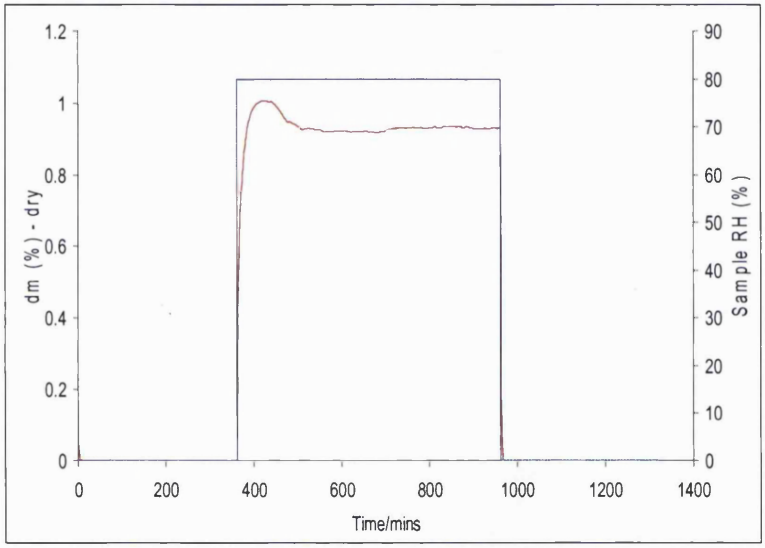

Figure 6.25. *DVS mass plot of spray-dried BDP/PEG 10 % from a suspension.*

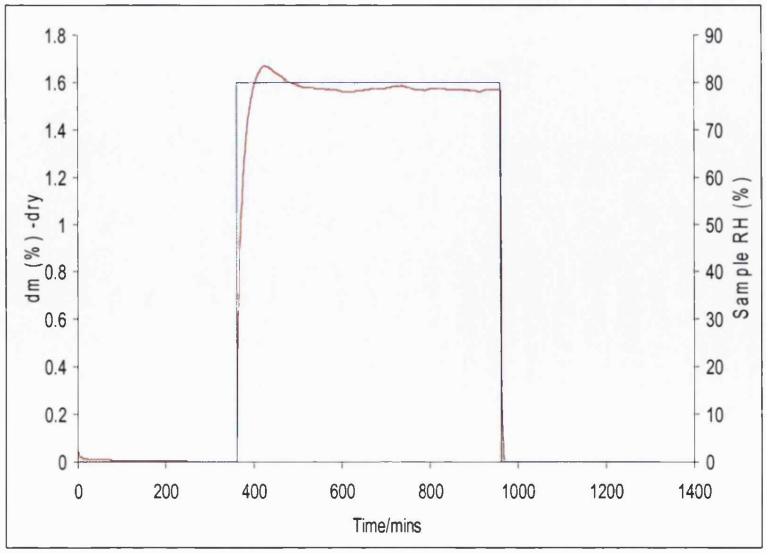

Figure 6.26. *DVS mass plot of spray-dried BDP/PEG 20% from a suspension.*

The surface energetics of the different particles produced were also studied and the data presented in Table 6.8. Comparable to the data obtained for SS/PEG co-spray dried systems, the γ_s^d were lower due to the incorporation of PEG (Figure 6.27). Here again, the γ_s^d of the different co-spray-dried systems were closer to the γ_s^d of the PEG than to that of BDP. In terms of polar properties, the presence of the PEG, presumably at the surface of the particles, had an effect (Figure 6.28). The surfaces became more basic mainly due to an increase of the K_D values. The effect of the PEG on the surface energy properties was comparable whether the starting material was lactose (Chapter 4), SS or BDP.

Materials	Specific polar interaction (kJ/mol)				Acid-base characteristics			γ_s^d (mJ/m^2)
	Acetone	Chloroform	Ethanol	Ethyl acetate	K_A	K_D	K_D/K_A	
BDP	6610 (48)	826 (14)	9194 (34)	8476 (66)	0.114	-0.011	-0.091	53.1 (0.3)
10 % PEG	6817 (217)	3129 (90)	7881 (83)	8737 (180)	0.096	0.098	1.01	39.7 (0.6)
20 % PEG	10779 (83)	8931 (21)	11624 (19)	11843 (7)	0.096	0.05	2.66	29.5 (0.1)
PEG 4000	9821 (259)	7898 (252)	13286 (368)	10353 (209)	0.12	0.206	1.71	33.1 (0.2)

Table 6.8. *Surface energy data of the crystalline references and the spray-dried BDP/PEG systems (10 or 20 % (w/w of polymer) from suspensions and PEG 4000. Values are mean (standard deviations).*

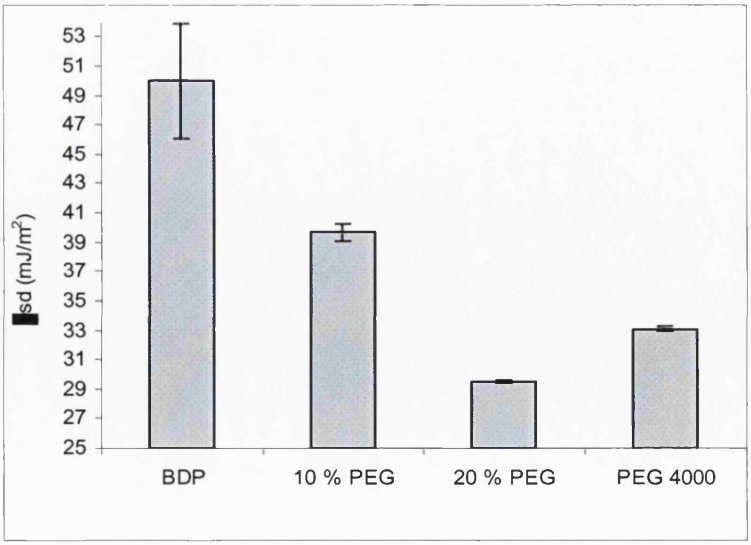

Figure 6.27. *Dispersive components of the crystalline BDP, the different BDP/PEG systems spray dried from a suspension and PEG4000. Values are mean (n=3)*

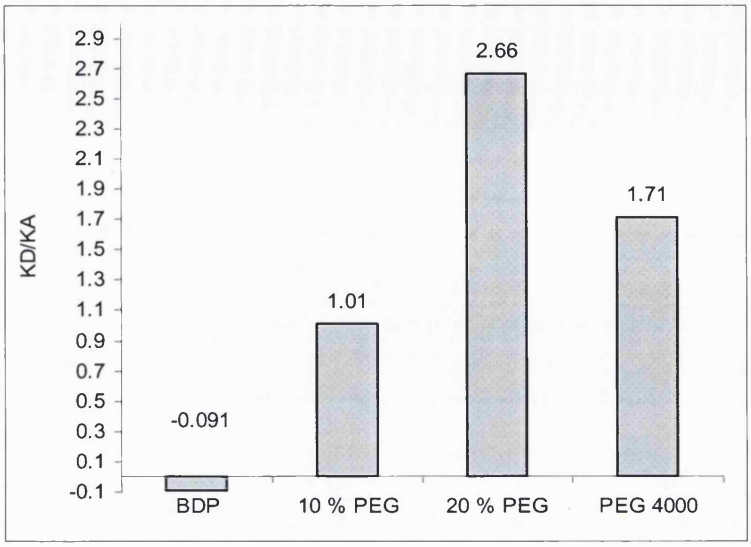

Figure 6.28. *Acid-base characteristics of the crystalline BDP, different BDP/PEG systems spray dried from a suspension and PEG 4000.*

The following figures (Figures 6.29 and 6.30) summarise the effect of the PEG on both the dispersive component and the acid base properties on the resulting co-spray dried systems. The crystalline drugs and PEG 4000 are also shown as controls.

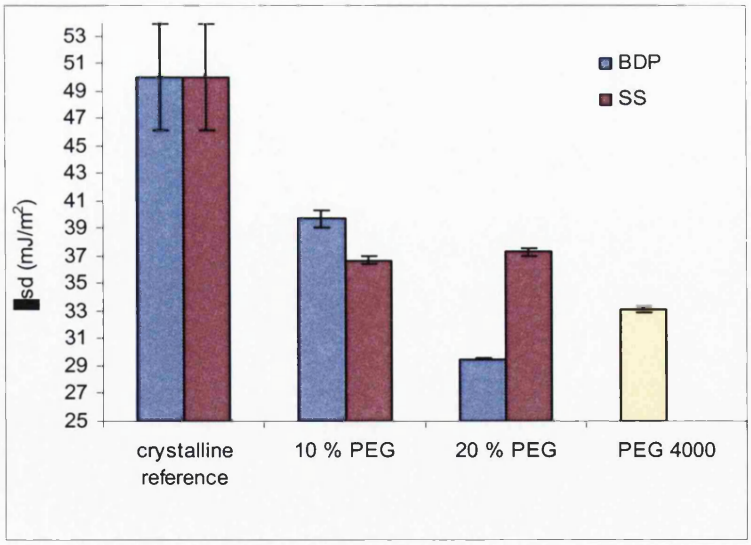

Figure 6.29. *Influence of the PEG concentration (in the suspension) on the dispersive component of the resulting SS or BDP co spray dried particles. Values are mean (n=3)*

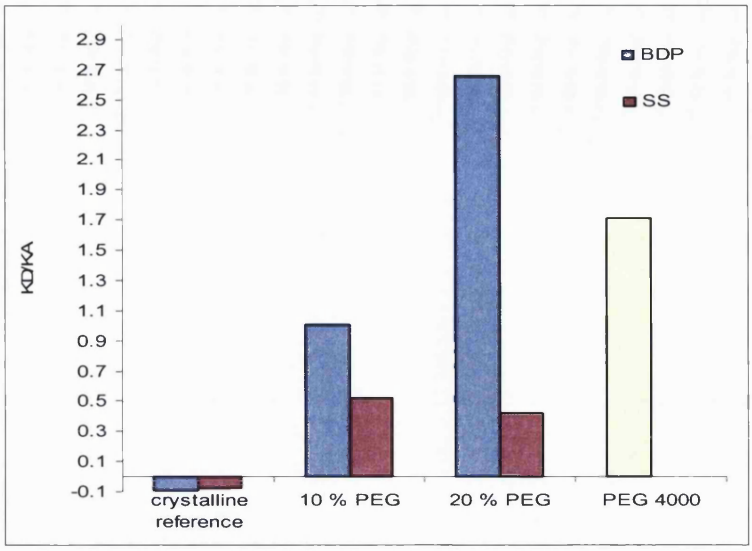

Figure 6.30. *Influence of the PEG concentration (in the suspension) on the acid base properties of the resulting SS or BDP co spray dried particles.*

Co-spray drying a suspension of either SS or BDP in the presence of PEG had an important effect on the dispersive component of the resulting particles. Adding 10 % (w/w) of polymer in the starting suspension resulted in particles exhibiting similar γ_s^d values for the two modified actives. From this data, it could be assumed that the "PEG treatment" of the surfaces resulted in similar dispersive interactions. However, when the polymer concentration was increased to 20 % (w/w), differences between the two systems were observed. Adding more PEG had little or no effect on the γ_s^d value of the SS/PEG product, whereas for BDP/PEG, a further decrease was observed (Figure 6.29).

Important differences were also seen for the acid-base properties of the modified drugs (Figure 6.30). Adding 10 % PEG to the starting suspension resulted in an increase in the K_A/K_D values. The effect was more prononced for BDP. Adding 20 % PEG marginally affected the acid-base properties of the SS/PEG system, whereas a sharp increase in the ratio of basic to acidic sites was observed for the BDP/PEG particles.

As a conclusion, in term of surface energetics, BDP seemed to be more affected by its surface modification than SS. This is in agreement with the work described elsewhere in this thesis showing the intrinsic differences between the two actives chosen as models.

6.5.2.2.2. Deposition study

The effect of modifying the surface properties of the BDP particles while keeping the general morphology (size and shape) and crystallinity was further investigated by undertaking deposition studies as previously described throughout this work.Table 6.9 shows the dispersion and deaggregation profiles of the modified particles. Unlike the hydrophilic model, these modifications influence the deposition data. The amounts of drug reaching the lower stage of the impinger were disappointing, with FPF values of 7.3 (2.6) % for the system containing 10 % of polymer and 3.7 (0.4) % for the system containing the highest proportion of PEG (Formulation 3). These values were mainly due to difficulties in deaggregation the particles since the drug emission was not particularly affected by the treatment. These results were unexpected since the surface properties described earlier would have suggested less cohesion between the micronised particles. A possible explanation could be the hydroscopic nature of these entities, which could lead to the generation of other types of forces such as capillary ones, which could increase the drug-drug interactions and therefore decrease the FPF values.

Formulation	Active used	ED (µg)	RD (µg)	FPF (%)
1	BDP	955 (172)	119 (07)	12.8 (2.8)
2	BDP/PEG 10 %	914 (27)	66 (22)	7.3 (2.6)
3	BDP/PEG 20 %	800 (34)	30 (01)	3.7 (0.4)

Table 6.9. *Deposition of modified BDP/PEG particles produced by spray drying from solutions. Values are mean (standard deviation).*

6.6. Conclusions

Chapters 4 and 5 focussed on the concept of modifying the carrier surface to examine approaches to "standardise" carriers to achieve carrier independent aerosol performances of both SS and BDP. This chapter aimed to modify the active to examine the potential to standardise the drug particulate properties of different actives. Particles were prepared by spray drying using different processing parameters. The major conclusions of this chapter are summarised below.

Investigation of the production of active/PEG systems by spray drying solutions or suspensions:

Spray drying a solution consisting of SS and PEG 4000 following the same processing parameters as used to produce crystalline lactose/PEG particles resulted in amorphous material. Varying the polymer to drug weight ratio, PEG molecular weight (PEG 300 instead of PEG 4000) or even the parameters of the spray dryer, was not followed by recrystallisation. Adding a ternary excipient such as lactose monohydrate did not affect the nature of the produced particles either. The particle morphologies were found to be independent of the different parameters investigated. They consisted of homogeneous spherical particles with clean surfaces having indentations. Next, the drug substances were spray dried from suspensions. The resulting particles were crystalline with no obvious alterations to their chemical properties (confirmed by XRPD). Their micron size made them good candidates for inhalation.

Characterisation of the physico-chemical properties of the newly modified drug models:

The amorphous nature of the SS/PEG particles obtained by spray drying of the solutions was confirmed by both XRPD and DVS. The surface energetics of those systems tended to be similar to the values obtained from crystalline SS, with a decrease in the dispersive component and an increase in the K_D/K_A values. Amorphous materials are described as more energetic than crystalline ones and thererefore it was expected that these SS/PEG systems would display

higher γ_s^d values. The crystalline nature of the SS/PEG spray dried from a suspension was also confirmed using gravimetric studies and X-ray diffraction. IGC data for the crystalline particles containing 10% PEG (Table 6.6) showed comparable results to those observed for the amorphous particles containing the same proportion of polymer (Table 6.4). This was particulary true for the acid-base contributions with values varying from 0.60 to 0.52 respectively. Regarding BDP/PEG systems, differences in the surface energetics were also important with a decrease in the dispersive van der Waals forces. Here again, the drug particles appear "coated" with a PEG film, responsible for this PEG like surface energy pattern.

Assessment of their deposition patterns:

The surface modifications of the actives were further investigated by *in vitro* measurements. The modified drugs were mixed with a modified carrier consisting or air-jet sieved Aero Flo 65 with 10 % lactose/PEG fines fused on its surface. This modified carrier was as described in Chapter 5 and the methodology employed as described in Chapter 2. Although it was possible to produce spray dried SS/PEG of suitable size for inhalation, the aerosol results obtained with the Clickhaler® proved to be disappointing with an inefficient aerosolisation for the amorphous SS/PEG systems and comparable FPFs of the crystalline SS/PEG particles to those obtained with the reference micronised SS. A possible explanation for such results is that the amorphous SS/PEG particles were present as strong self-agglomerates. The results agree with the work of Chawla *et al.* (1994) who found that a greater fraction of a micronised drug was delivered to the lower stage of a TSI compared to a spray dried form. They attributed such results to the effect of adhesion and cohesion forces. The hydrophobic drug deposition was even more affected by the surface treatment with an FPF value as low as 3.7 % for the particles containing 20 % of polymer. BDP/PEG particles may adhere more strongly to the modified coarse lactose than the crystalline reference. As a general conclusion, the aerosol results proved that having a "PEG like drug surface" mixed with a "PEG like coarse lactose" did not result in a equivalent performances for the two model drugs. Moreover, the micronised BDP performed better than the crystalline BDP/PEG.

Chapter 7

General discussion and future work

7.1. General Discussion

Inhalation technology has been widely acknowledged in the past decades for both local and potential systemic applications. Different types of devices namely pressurised metered dose inhalers, nebulisers and dry powder inhalers are used routinely for the pulmonary delivery of drugs for various respiratory indications. The issues faced by the transition from CFC to HFA propellants contributed to a renewed interest in DPI technologies over the past two decades. Standard DPI formulations generally consist of a micronised drug blended with a coarse α-lactose monohydrate carrier. The drug detachment from the carrier particle and its subsequent aerosolisation properties will depend on the formulation, the inhaler design and patient factors.

The main objective of this work was to gain a better understanding of aerosolisation behaviour of active particles from a binary powder mixture with different carrier systems. A number of different approaches were used in an attempt to understand the drug-carrier interactions. In this thesis, crystalline α-lactose monohydrate was used as the key carrier for both SS and BDP drug models. Here, three different commercially available grades of this disaccharide were used to prepare formulations which were subsequently filled and tested in the Clickhaler® DPI (chapter 3). This work brings to the fore the influence of the physico-chemical properties of the lactose tested on the BDP deposition profile, especially the presence of fine lactose particles (Figure 3.5 A). The aerosol performances of SS were less dependent on the choice of carrier (Table 3.4). Inverse gas chromatography was particularly important in differentiating between the various crystalline α-lactose monohydrate, especially in terms of specific interactions with polar probes (Figure 3.9). The method of K_A and K_D determination influenced the interpretation of the acid-base properties to *in vitro* deposition patterns correlations. As an example, using the boiling point approach a positive trend was established with SS deposition. The surface energy is one of the main factors influencing the adhesion of a particle onto a surface. For SS an increase in K_A values resulted in an increase in FPFs (Figure 3.16). The relationship was less pronounced for BDP, which tends to form particle aggregates and therefore does not adhere to the same extent to the coarse carrier surface as SS. Regarding the hydrophobic drug model, a

positive trend was found between the TSI deposition and the amount of fine lactose present in the different samples (Figure 3.5 A).

The role played by the fines and the surface energy of the carriers was further investigated by the introduction of crystalline lactose/PEG 4000 fines (produced by spray drying) to air-jet sieved grades of lactose (chapter 4). Different formulation parameters such as type (Tables 4.4 to 4.6) and proportion of added fines (Table 4.8), mixing sequence (Table 4.7) and drug concentration (Table 4.9) were investigated and all proved to affect the *in vitro* performance for both drug models.

The fines spray-dried following the parameters reported by Chidavaenzi *et al.* (Chidavaenzi *et al.*, 2001) were all crystalline, regardless of the lactose to PEG ratio. The particle size of the different systems, determined by the Mastersizer X (Table 4.1), confirmed the potential use of these fines for DPI formulations. The changes in surface energy of the particles were investigated using IGC. This helped to give an understanding of how the polymer interacted with the lactose. Moreover, the changes in both the dispersive surface energy and the acid-base properties reflected a change in the hydrophobicity of the particles. The presence of asperities on the particle surface was revealed by SEM. These asperities, corresponding to PEG crystals, seemed to play an important role in the dispersion profiles of BDP, as previously stated by Gilani *et al.* (Gilani *et al.*, 2004). The current work demonstrated that the addition of 10 % (w/w) crystalline lactose/PEG fines (containing 10 % PEG 4000) to air-jet sieved grades of lactose led to similar BDP deposition (Tables 4.4 and 4.5). In other words, differences between marketed lactose grades from different sources can be minimised. For SS, these modified carriers did not appear to be as effective (Table 4.6). However, adding 10 % fines had a detrimental effect on the ED, presumably due to bad flow properties for this particular formulation. The study (Table 4.8) of the impact of the fine concentration showed good linear relationships between FPF and fine content for both drugs. Furthermore, the steeper gradient for BDP compared to SS confirmed the hypothesis that BDP was more likely to be influenced than SS. In this section of the dissertation the necessity to balance the amount of ternary material (so that the improvement in FPF is not followed by a decrease in ED) was stressed.

The role of the added fines was further highlighted in the mixing sequence study (Figure 4.15). Regardless of the mixing sequence, ternary ordered mixes

exhibited higher FPFs than the corresponding binary mixes (without the addition of fines).

The mechanism of action of such fines is not yet clearly understood and different hypotheses are proposed: (1) coverage of active binding sites on the coarse lactose by the fines, affecting the particulate interaction between the drug and the carrier, (2) redistribution of BDP and fines between active and passive adhesion sites during the powder mixing, and (3) existence of small aggregates composed of lactose/PEG particles, acting as an alternative carrier.

Finally, the drug to carrier ratio (Table 4.9) also appeared to influence the FPF of the hydrophobic drug model, with an increase in the detachment from the carrier particles at high drug loading. The increased FPF observed at higher drug concentration could be attributed to the relatively low percentage of drug being adhered to high-energy binding sites. This study confirmed once again the differences between the drugs, with the hydrophilic drug model deposition not being affected by the drug loading.

To assess further the impact of the presence of free fines in the blend and also the importance of modifying a lactose surface, partially amorphous lactose/PEG fines were produced in chapter 5, following the parameters set by Corrigan *et al.* (Corrigan *et al.*, 2002). Those partially amorphous fines, whose nature was confirmed by XRPD and DVS experiments, were fused onto the surface of two air-jet sieved lactose grades. Based on IGC data (Tables 5.1 and 5.2) confirming that the surface energy properties of the modified surfaces were identical, it was hypothetised that the deposition patterns for the two drug models would be similar. The data presented in Table 5.3 confirmed that the modified carriers gave rise to similar deposition parameters (ED, RD and FPF) for the hydrophilic drug model. In contrast, BDP deposition in the second stage of the TSI was found to be lower than that from a carrier containing crystalline lactose/fines. This confirmed the importance of free fines in the possible mechanism of weakening the drug agglomerates.

The effect of chemical composition on carrier efficiency was evaluated using PEG [45-90] µm as a carrier probe. Despite poor content uniformity due to issues observed with the reservoir device, *in vitro* assessment was performed using the capsule-based Aerolizer®. This study also represented an opportunity to consider the device implication on the TSI deposition (Tables 5.5 and 5.6).

All aerosolisations were made at a flow rate of 60 L/min and the drug deposition tests (Table 5.4) showed good performances for both drug models. A possible explanation was found in the low van der Waals interactions as indicated by a low γ_s^d value of 33.1 mJ/m^2. The necessity to investigate a DPI formulation in combination with a particular device was illustrated by the data obtained from the two inhalers (Figures 5.9 and 5.10). Differences in deagglomeration efficiency of the hydrophobic drug model were highlighted by the different FPFs obtained from the same powder formulation, using the same inspiratory manoeuvre. Similarly, a given SS formulation performed differently, in terms of FPF, depending on the device chosen.

The different IGC studies confirmed the applicability of this technique to monitor differences in the crystalline lactose grades and in the spray-dried lactose/PEG particles, and to assess the surface modification after fusion of partially amorphous fines. A method developed by Cline and Dalby (2002) was applied to our data set for direct prediction of TSI deposition data. The strong relationship obtained by these researchers between the surface energy interactions (SEIs) and the aerosol properties of the different formulations could not always be confirmed with the carriers presented in this dissertation. The only positive trends were observable for BDP deposition when the SEI parameter was calculated in mJ/g (Figures 5.23 and 5.24). Little insight in the SS deposition was possible with the calculation of this parameter, confirming the lack of generality of this theory to reliably explain the deposition data of different drugs from different carriers.

In a shift away from the research focus of modifying the surface properties of the carriers, the surface of the drug models was modified by spray drying (chapter 6). Initial attempts to spray dry SS in the presence of PEG (300 or 4000) from a feed solution resulted in the production of amorphous products which did not lead to significant deposition in the stage 2 of the impinger. The agglomeration tendency of those particles was put forward to explain these disappointing deposition patterns. Spray drying suspensions, using the Niro SD Micro TM in the case of SS/PEG suspensions or the Büchi 191 for the BDP/PEG systems, led to crystalline products. No improvement of the aerosol properties of those modified actives when mixed with modified carriers were

obtained. The surface modifications of both actives and carriers have undoubtedly potential in optimising aerosol properties of the blends and the use of new polymers should be addressed.

In conclusion, this dissertation has shown that improvements through carrier surface modifications were drug specific and appeared to be dependent on many factors such as the device employed, the physico-chemical properties of the coarse particles and the surface energetics. Evaluation of drug surface modification by spray drying seems to be encouraging, even if time constraints did not allow for totally efficient investigation of the spray drying conditions.

7.2. Suggested future work

- Water sorption analysis coupled with near-infrared spectroscopy could be used to probe the lactose/PEG crystallisation process. Further studies are also required to evaluate the effect of the PEG molecular weight and concentration on the physicochemical properties and stabilities of the spray-dried lactose/PEG systems;

- The work relating to SS/PEG systems could be expanded with the aim to understand the differences in crystallisation behaviour observed with the lactose/PEG systems;

- This dissertation introduced the concept of a universal carrier which would lead to performance equivalency between different lactose sources. Additional modifications of the active surface by spray drying could be investigated in order to minimise the drug to drug variability. This may involve the use of solutions or suspensions and a new range of polymers. IGC studies could be extended to monitor the surface modification of the drugs;

- In this work, surface energy parameters were used to predict DPI performance. The different materials tested were found to have similar surface energetics and it would be interesting to examine new materials exhibiting higher differences in surface energetics.

References

References

2002. European Pharmacopoeia. 4th Edition Ed., Strasbourg, France.

Agu, R.U., Ugwoke, M.I., Armand, M., Kinget, R., Verbeke, N., 2001. The lung as a route for systemic delivery of therapeutic proteins and peptides. Respiratory Research 2, 198-209.

Ahfat, N.M., Buckton, G., Burrows, R., Ticehurst, M.D., 1997. Predicting mixing performance using surface energy measurements. International Journal of Pharmaceutics 156, 89-95.

Ahlneck, C., Zografi, G., 1990. The molecular basis of moisture effects on the physical and chemical stability of drugs in the solid state. International Journal of Pharmaceutics 62, 87-95.

Al-Hadithi, D. Carrier surface modifications to improve aerosol performance of dry powder inhalation delivery. 2004. PhD thesis, University of London.

Allen,T., 1997. Particle size measurement. 5th Edition Ed., London.

Aulton,M.E., 2002. Pharmaceutics: the science of dosage form design. 2 Ed..

Bailey, A.G., 1984. Electrostatic phenomena during powder handling. Powder Technology 37, 71-85.

Barry, P.W., O'Callaghan, C., 2003. The influence of inhaler selection on efficacy of asthma therapies. Advanced Drug Delivery Reviews 55, 879-923.

Begat, P., Morton, D.A.V., Staniforth, J.N., Price, R., 2004. The cohesive-adhesive balances in dry powder inhaler formulations I: direct quantification by atomic force microscopy. Pharmaceutical Research 21, 1591-1597.

Bennet, F.S., Carter, P.A., Rowley, G., Dandiker, Y., 1999. Modification of electrostatic charge on inhaled carrier lactose particles by addition of fine particles. Drug Development and Industrial Pharmacy. 25, 99-103.

Berard, V., Lesniewska, E., Andres, C., Pertuy, C., Laroche, C., Pourcelot, Y., 2002. Dry powder inhaler: influence of humidity on topology and adhesion studied by AFM. International Journal of Pharmaceutics 232, 213-224.

Brain, J.D., Valberg, P.A., 1979. Deposition of aerosols in the respiratory tract. American Review of Respiratory Disease 120, 1325-1373.

Braun, M.A., Oschmann, R., Schmidt, P.C., 1996. Influence of excipients and storage humidity on the deposition of disodium cromoglycate (DSCG) in the Twin Impinger. International Journal of Pharmaceutics 135, 53-62.

British National Formulary, 2004. London.

Brittain, H.G., Bogdanowich, S.J., Bugay, D.E., Devincentis, J., Lewen, G., Newman, A.W., 1991. Physical characterization of pharmaceutical solids. Pharmaceutical Research 8, 963-973.

Brodka-Pfeiffer, K., Langguth, P., Graß, P., Häusler, H., 2003. Influence of mechanical activation on the physical stability of salbutamol sulphate. European Journal of Pharmaceutics and Biopharmaceutics 393-400.

Buckton,G., 1995. Interfacial phenomena in drug delivery and targeting. Harwood Academic Publishers, Switzerland.

Buckton, G., 1997. Characterisation of small changes in the physical properties of powders of significance for dry powder inhaler formulations. Advanced Drug Delivery Reviews 26, 17-27.

Buckton, G., Darcy, P., 1995. The use of gravimetric studies to assess the degree of crystallinity of predominantly crystalline powders. International Journal of Pharmaceutics 123, 265-271.

Byron, P. R., Miller, N. C., Blondino, F. E., Visich, J. E., and Ward, G. H. Some aspects of alternative propellant solvency. Proceedings of Respiratory Drug Delivery IV 1, 231-242. 1994.

Byron, P. R., Naini, V., and Phillips, E. M. Drug carrier selection-important physicochemical characteristics. Proceedings of Respiratory Drug Delivery VI , 103-113. 1996.

Byron, P.R., Peart, J., Staniforth, J.N., 1999. Aerosol electrostatics. I: Properties of fine powders before and after aerosolization by dry powder inhalers. Pharmaceutical Research 14, 698-705.

Carter, P.A., Rowley, G., Fletcher, E.J., Hill, E.A., 1992. An experimental investigation of triboelectrification in cohesive and non-cohesive pharmaceutical powders. Drug Development and Industrial Pharmacy. 18, 1505-1526.

Carter, P.A., Rowley, G., Fletcher, E.J., Stylianopoulos, V., 1998. Measurement of electrostatic charge decay in pharmaceutical powders and polymer materials used in dry powder inhaler devices. Drug Development and Industrial Pharmacy. 24, 1083-1088.

Chatham, S. M. Characterisation of molten filled hard gelatin capsules. 1985. PhD thesis, Chelsea College, University of London.

Chawla, A., Taylor, K.M.G., Newton, J.M., Johnson, M.C.R., 1994. Production of spray dried salbutamol sulphate for use in dry powder inhaler formulation. International Journal of Pharmaceutics 108, 233-240.

Chehimi, M.M., Pigois-Landureau, E., 1994. Determination of acid-base properties of solid materials by inverse gas chromatography at infinite dilution. Journal of Material Chemistry 4, 741-745.

Chew, N. Y. K and Chan, H-K. In vitro performance of Foradile Aerolizer® and Oxis Turbuhaler®. [VII], 623-624. 2000. Proceeding of Respiratory Drug Delivery VII.

Chidavaenzi, O.C., Buckton, G., Koosha, F., 2001. The effect of co-spray drying with polyethylene glycol 4000 on the crystallinity and physical form of lactose. International Journal of Pharmaceutics 216, 43-49.

Chow, A.H.L., Tong, H.H.Y., Shekunov, B.Y., York, P., 2004. Use of inverse gas chromatography (IGC) to determine the surface energy and surface area of powdered materials. Pharmaceutical Research 21, 1718-1720.

Clark, A.R., 1995. Medical aerosol inhalers: past, present and future. Aerosol Science and Technology 22, 374-391.

Clark, T.J., 1972. Effect of beclomethasone dipropionate delivered in patients with asthma. The Lancet 7765, 1361-1364.

Clarke, M.J., Tobyn, M.J., Staniforth, J.N., 2001. Formulation of powder inhalation systems containing a high mass of nedocromil sodium trihydrate. Journal of Pharmaceutical Sciences 90, 213-223.

Clarke, S.W., Newman, S.P., 1984. Therapeutic aerosols 2-Drugs available by the inhaled route. Thorax 39, 1-7.

Clay, M.M., Pavia, D., Newman, S.P., Lennard-Jones, T., Clarke, S.W., 1983. Assessment of jet nebulisers for lung aerosol therapy. Lancet 2, 592-594.

Cline, D., Dalby, R., 2002. Predicting the quality of powder for inhalation from surface energy and area. Pharmaceutical Research 19, 1274-1277.

Columbano, A. Modification of microparticle surfaces by use of alkylpolyglycoside surfactants. 2000. PhD thesis, University of London.

Columbano, A., Buckton, G., Wikeley, P., 2002. A study of the crystallisation of amorphous salbutamol sulphate using water vapour sorption and near infrared spectroscopy. International Journal of Pharmaceutics 237, 171-178.

Columbano, A., Buckton, G., Wikeley, P., 2003. Characterisation of surface modified salbutamol sulphate-alkylpolyglycoside microparticles prepared by spray drying. International Journal of Pharmaceutics 253, 61-70.

Corrigan, D.O., Corrigan, O.I., Healy, A.M., 2004. Predicting the physical state of spray dried composites: salbutamol sulphate/lactose and salbutamol

sulphate/polyethylene glycol co-spray dried systems. International Journal of Pharmaceutics 273, 171-182.

Corrigan, D.O., Healy, A.M., Corrigan, O.I., 2002. The effect of spray drying solutions of polyethylene glycol (PEG) and lactose/PEG on their physiochemical properties. International Journal of Pharmaceutics 235, 193-205.

Corrigan, D.O., Healy, A.M., Corrigan, O.I., 2003. The effect of spray drying solutions of bendroflumethiazide/polyethylene glycol on the physicochemical properties of the resultant materials. International Journal of Pharmaceutics 262, 125-137.

Courrier, H.M., Butz, N., Vandamme, T.F., 2002. Pulmonary drug delivery systems: recent developments and prospects. Critical Reviews in Therapeutic Drug Carrier Systems 19, 425-498.

Craig, D.Q.M., 1995. A review of thermal methods used for the analysis of the crystal form, solution thermodynamics and glass transition behaviour of polyethylene glycols. Thermochimica Acta 248, 189-203.

Craig, D.Q.M., Royall, P.G., Kett, V.L., Hopton, M.L., 1999. The relevance of the amorphous state to pharmaceutical dosage forms: glassy drugs and freeze dried systems. International Journal of Pharmaceutics 179, 179-207.

Crompton, G.K., 1990. The adult patient's difficulties with inhalers. Lungs 168, 658-662.

D'Souza, S., 1995. The Montreal protocol and essential use exceptions. Journal of Aerosol Medicine 8, S13-S17.

Dalby,R.N., Hickey,A.J., Taino,S.L., 1996. Medical devices for the delivery of therapeutic aerosols to the lungs. In: Hickey A.J. (Ed.), Marcel Dekker,Inc, New York.

Dove, J.W., Buckton, G., Doherty, C., 1996. A comparison of two contact angle measurement methods and inverse gas chromatography to assess the surface

energies of theophylline and caffeine. International Journal of Pharmaceutics 138, 199-206.

Drapier-Beche, N., Fanni, J., Parmentier, M., Vilasi, M., 1997. Evaluation of lactose crystalline forms by non destructive analysis. Journal of Dairy Science 80, 457-463.

Effros, R.M., Mason, G.R., 1983. Measurements of pulmonary epithelial permeability in vivo. American Review of Respiratory Disease 127, S59-S65.

Eilbeck, J., Rowley, G., Fletcher, E., and Smith, I. An investigation of the effects of contact surface on triboelectrification in pharmaceutical powder systems. [Proceeding of 11th Pharm Tech Conference], 2358-2366. 1992.

Elversson, J., Millqvist-Fubery, A., Alderborn, G., Elofsson, U., 2003. Droplet and particle size relationship and shell thickness of inhalable lactose particles during spray drying. Journal of Pharmaceutical Sciences 92, 900-910.

Enna, S.J., Schanker, L.S., 1972. Absorption of saccharides and urea from the rat lung. American Journal of Physiology 222, 409-414.

Fan,L.S., Zhu,C., 1998. Interparticle forces and field forces. In: Fan,L.S., Zhu,C. (Eds.), Cambridge University Press, Cambridge, 101-106.

Farber, L., Tardos, G.I., Michaels, J.N., 2003. Evolution and structure of drying material bridges of pharmaceutical excipients: studies on a microscope slide. Chemical Engineering Science 58, 4515-4525.

Farid, M., 2003. A new approach to modelling of single droplet drying. Chemical Engineering Science 58, 2985-2993.

Feeley, J.C., York, P., Sumby, B.S., Dicks, H., 1998. Determination of surface properties and flow characteristics of salbutamol sulphate, before and after micronisation. International Journal of Pharmaceutics 172, 89-96.

Ferron, G.A., 1977. The size of soluble aerosol particles as a function of the humidity of the air. Application to the human respiratory tract. Journal of Aerosol Science 8, 251-267.

Fiegel, J., Fu, J., Hanes, J., 2004. Poly(ether-anhydride) dry powder aerosols for sustained drug delivery in the lungs. Journal of Controlled Release 96, 411-423.

Finot, E., Lesniewska, E., Mutin, J.C., Goudonnet, J.P., 1996. Contact force dependence on relative humidity: investigations using atomic force microscopy. Scanning Microscopy 10, 697-708.

Foster, W.M., Langenback, E.G., Bergofsky, E.H., 1985. Dissociation in the mucociliary function of the central and peripheral airways of asymptomatic smokers. American Review of Respiratory Disease 132, 633-639.

Fowkes, F.M., 1964. Attractive forces at interfaces. Industrial and Engineering Chemistry 56, 40-52.

French, D.L., Edwards, D.A., Niven, R.W., 1996. The influence of formulation on emission, deaggregation and deposition of dry powders for inhalation. Journal of Aerosol Science 27, 769-783.

Fu, J., Fiegel, J., Krauland, E., Hanes, J., 2002. New polymeric carriers for controlled drug delivery following inhalation or injection. Biomaterials 23, 4425-4433.

Fukunaga, Y., Nishibayashi, T., Odomi, M., and Shott, M. Evaluation of a novel ß2 agonist dry powder inhaler formulation using the Clickhaler: an initial feasibility study. Proceeding of Respiratory Drug Delivery VII. 2, 425-428. 2000.

Ganderton, D., 1992. The generation of respirable clouds from coarse powder aggregates. Journal of Biopharmaceutical Sciences 3, 101-105.

Gao, D., Rytting, J.H., 1997. Use of solution calorimetry to determine the extent of crystallinity of drugs and excipients. International Journal of Pharmaceutics 151, 183-192.

Geuns, E.R.M., Toren, J.S., Barends, D.M., Bult, A., 1997. Decrease of the stage-2 deposition in the twin impinger during storage of beclomethasone dipropionate dry powder inhalers in controlled and uncontrolled humidities. European Journal of Pharmaceutics and Biopharmaceutics 44, 187-194.

Gilani, K., Najafabadi, A.R., Barghi, M., Rafiee-Tehrani, M., 2004. Aerosolisation of beclomethasone dipropionate using spray dried lactose/polyethyleneglycol carriers. European Journal of Pharmaceutics and Biopharmaceutics 58, 596-606.

Gordon, M., Taylor, J.S., 1952. Ideal copolymers and the second-order transitions of synthetic rubbers.I. Non-crystalline copolymers. Journal of Applied Chemistry 2, 493-500.

Grimsey, I.M., Sunkersett, M., Osborn, J.C., York, P., Rowe, R.C., 1999. Interpretation of the differences in the surface energetics of two optical forms of mannitol by inverse gas chromatography and molecular modelling. International Journal of Pharmaceutics 191, 43-50.

Guardani, R., Nascimento, C.A.O., Onimaru, R.S., 2002. Use of neural networks in the analysis of particle distribution by laser diffraction: tests with different particle systems. Powder Technology 126, 42-50.

Gutmann,V., 1978. The donor-acceptor approach to molecular interactions. New York.

Hallworth, G.W., Clough, D., Newnham, T., Andrews, U.G., 1978. A simple impinger device for rapid quality control of the particle size of inhalation aerosols delivered by pressurised aerosols and powder inhalers. Journal of Pharmacy and Pharmacology 30, 39P.

Hallworth, G.W., Westmoreland, D.G., 1987. The twin impinger: a simple device for assessing the delivery of drugs from metered dose pressurized aerosol inhalers. Journal of Pharmacy and Pharmacology 39, 966-972.

Harjunen, P., Lankinen, T., Salonen, H., Lehto, V., Järvinen, K., 2003. Effects of carriers and storage of formulation on the lung deposition of a hydrophobic and hydrophilic drug from a DPI. International Journal of Pharmaceutics 263, 151-163.

Hersey, J.A., 1975. Ordered mixing a new concept in powder mixing practice. Powder Technology 11, 41-44.

Hiestand, E.N., 1966. Powders: particle-particle interactions. Journal of Pharmaceutical Sciences 55, 1325-1344.

Hogan, S.E., Buckton, G., 2000. The quantification of small degrees of disorder in lactose using solution calorimetry. International Journal of Pharmaceutics 207, 57-64.

Hogan, S.E., Buckton, G., 2001. Water sorption/desorption - near IR and calorimetric study of crystalline and amorphous raffinose. International Journal of Pharmaceutics 227, 57-69.

Ikegami, K., Kawashima, Y., Takeuchi, H., Yamamoto, H., Isshiki, N., Momose, D., Ouchi, K., 2002. Primary crystal growth during spherical agglomeration in liquid: designing an ideal dry powder inhalation system. Powder Technology 126, 266-274.

Islam, N., Stewart, P., Larson, I., Hartley, P., 2004. Lactose surface modification by decantation: are drug-fine lactose ratios the key to better dispersion of salmeterol xinafoate from lactose-interactive mixtures? Pharmaceutical Research 21, 492-499.

Jashnani, R.N., Byron, P.R., 1996. Dry powder generation in different environments: performance comparisons of albuterol, albuterol sulphate,

albuterol adipate and albuterol stearate. International Journal of Pharmaceutics 130, 13-24.

Jashnani, R.N., Byron, P.R., Dalby, R.N., 1995. Testing of dry powder aerosol formulations in different environmental conditions. International Journal of Pharmaceutics 113, 123-130.

Johari, G.P., Hallbrucker, A., Mayer, E., 1987. The glass transition of hyperquenched glassy water. Nature 330, 552-553.

Kawashima, Y., Serigano, T., Hino, T., Yamamoto, H., Takeuchi, H., 1998a. Design of inhalation dry powder of pranlukast hydrate to improve dispersibility by the surface modification with light anhydrous silicic acid (Aerosil 200). International Journal of Pharmaceutics 173, 243-251.

Kawashima, Y., Serigano, T., Hino, T., Yamamoto, H., Takeuchi, H., 1998b. Effect of surface morphology of carrier lactose on dry powder inhalation property of pranlukast hydrate. International Journal of Pharmaceutics 172, 179-188.

Kibbe,A.H., 2000. Handbook of pharmaceutical excipients. third edition Ed., American Pharmaceutical Association and Pharmaceutical Press.

Kim, K.J., Matsukawa, Y., Yamahara, H., Kalra, V.K., Lee, V.H.L., Crandall, E.D., 2003. Absorption of intact albumin across rat alveaolar epithelial cell monolayers. American Journal of Physiology-Lung Cellular and Molecular Physiology 284, 465.

Kovacs, A.J., Giothier, A., Straupe, C., 1975. Isothermal growth, thickening and melting of poly (ethylene oxide) single crystals in the bulk. Journal of Polymeric Science 50, 283-325.

Lankinen, T., Harjunen, P., Järvinen, K., Paronen, T. P., and Lehto, V. Conversion of amorphous material to a corresponding crystalline material by spray drying and utilization of the crystalline spray dried material in drug formulations. [WO 03/094892 A1]. 2003.

Larhrib, H., Martin, G.P., Prime, D., Marriott, C., 2003. Characterisation and deposition studies of engineered lactose crystals with potential for use as a carrier for aerosolised salbutamol sulphate from dry powder inhalers. European Journal of Pharmaceutical Sciences 19, 211-221.

Larhrib, H., Zeng, X.M., Martin, G.P., Marriott, C., Pritchard, J., 1999. The use of different grades of lactose as a carrier for aerosolised salbutamol sulphate. International Journal of Pharmaceutics 191, 1-14.

Lenney, J., Innes, J.A., Crompton, G.K., 2000. Inappropriate inhaler use: assessment of use and patient preference of seven inhalation devices. Respiratory Medecine 94, 496-500.

Lopez-Vidriero,M.T., 1984. Lungs secretions. In: Clarke S.W.,P.D. (Ed.), Butterworths, London, 19-45.

Louey, M.D., Razia, S., Stewart, P.J., 2003. Influence of physico-chemical carrier properties on the in vitro aerosol deposition from interactive mixtures. International Journal of Pharmaceutics 252, 87-98.

Louey, M.D., Stewart, P.J., 2002. Particle interactions involved in aerosol dispersion of ternary interactive mixtures. Pharmaceutical Research 19, 1524-1531.

Lucas, P., Anderson, K., Potter, U.J., Staniforth, J.N., 1999. Enhancement of small particle size dry powder aerosol formulation using an ultra low density additive. Pharmaceutical Research 16, 1643-1647.

Lucas, P., Anderson, K., Staniforth, J.N., 1998a. Protein deposition from dry powder inhalers: fine particle multiplets as performance modifiers. Pharmaceutical Research 15, 562-569.

Lucas, P., Clarke, M. J., Anderson, K., Tobyn, M. J., and Staniforth, J. N. The role of fine particle excipients in pharmaceutical dry powder aerosols. Proceeding of Respiratory Drug Delivery VI , 243-250. 1998b.

Maa, Y.F., Costantino, H.R., Nguyen, P.A., Hsu, C.C., 1997. The effect of operating and formulation variables on the morphology of spray-dried protein particles. Pharmaceutical Development and Technology 2, 213-223.

Masters,K., 2002. Spray drying in practice. SprayDryConsult International Aps., Charlottenhund.

Masuda,H., Gotoh,K., 1997. Adhesive force of a single particle. In: Gotoh,K., Masuda,H., Higashitani,K. (Eds.), Marcel Dekker Inc, New York, 133-142.

McDonald, K.J., Martin, G.P., 2000. Transition to CFC-free metered dose inhalers- into the new millenium. International Journal of Pharmaceutics 201, 89-107.

Miller, N.C., Marple, V.A., Schultz, R.K., Poon, W.S., 1992. Assessment of the twin impinger for size measurement of metered-dose inhaler sprays. Pharmaceutical Research 9, 1123-1127.

Mohammad, H.A.H., Fell, J.T., 1982. Contact angles of powder mixtures consisting of spherical particles. International Journal of Pharmaceutics 11, 149-154.

Morén, F., 1981. Pressurised aerosols for oral inhalation. International Journal of Pharmaceutics 8, 1-10.

Morice, A.H., Adler, L.M., Ellis, S., Hewitt, A., 2002. Do patients prefer dry powder inhalers or metered-dose inhalers? a retrospective, combined analysis. Current Therapeutic Research 63, 496-506.

Mukhopadhyay, P., Schreiber, H.P., 1995. Aspects of acid-base interactions and use of inverse gas chromatography. Colloids and surfaces A: Physicochemical and Engineering Aspects 100, 47-71.

Nantel, N.P., Newhouse, M.T., 1999. Inspiratory flow rates through a novel dry powder inhaler (Clickhaler) in pediatric patients with asthma. Journal of Aerosol Medicine 12, 55-58.

Nardin, M., Papirer, E., 1990. Relationship between vapor pressure and surface energy of liquids: application to inverse gas chromatography. Journal of Colloid and Interface Science 137, 534-545.

Neville, A., Palmer, J.B., Gaddie, J., May, C.S., Palmer, K.N., Murchison, L.E., 1977. Metabolic effects of salbutamol: comparison of aerosol and intravenous administration. British Medical Journal 1, 413-414.

Newell, H.E., Buckton, G., Butler, D.A., Thielmann, F., Williams, D.R., 2001a. The use of inverse gas chromatography to measure the surface energy of crystalline, amorphous and recently milled lactose. Pharmaceutical Research 18, 662-666.

Newell, H.E., Buckton, G., Butler, D.A., Thielmann, F., Williams, D.R., 2001b. The use of inverse gas chromatography to study the change of surface energy of amorphous lactose as a function or relative humidity and the processes of collapse and crystallisation. International Journal of Pharmaceutics 217, 45-56.

Newhouse, M.T., Nantel, N.P., Chambers, C.B., Pratt, B., Parry-billings, M., 1999. Clickhaler (a novel dry powder inhaler) provides similar bronchodilation to pressurized metered-dose inhaler, even at flow rates. Chest 115, 952-956.

O'Callaghan, C., Barry, P.W., 1997. The science of nebulised drug delivery. Thorax 52, S31-S44.

O'Donohue, W.J.Jr., 1996. Guidelines for the use of nebulizers in the home and domicilary sites.Report of a consensus conference. NAMDRC Consensus Group. Chest 109, 814-820.

Oberdorster, G., 1988. Lung clearance of inhaled insoluble and soluble particles. Journal of Aerosol Medicine 289-330.

Ohta, M., Buckton, G., 2004. Determination of the changes in surface energetics of cefditoren pivoxil as a consequence of processing induced disorder and equilibration to different relative humidities. International Journal of Pharmaceutics 269, 81-88.

Olano, A., Corzo, N., Martinez-Castro, I., 1983. Studies on β–lactose crystallization. Milchwissenchaft 38, 471-474.

Parmar, R. The interaction of a model steroid with phospholipds structures. 1997. PhD thesis, University of London, UK.

Parry-billings, M., Boyes, R.N., Clisby, L.M., Braithwaite, P., Williams, S., Harper, A.E., 1999. Design, development and performance of a novel multidose dry-powder inhaler. Pharmaceutical Technology 23, 70-81.

Patton, J., 1996. Mechanisms of macromolecule absorption by the lungs. Advanced Drug Delivery Reviews 19, 3-36.

Pavia, D., Thomson, M.L., Clarke, S.W., Shannon, H.S., 1977. Effect of lung function and mode of inhalation on penetration of aerosol into the human lung. Thorax 32, 194-197.

Pierson, D.J., 2000. Consensus statement on aerosols and delivery devices. Respiratory Care 45, 589-596.

Planinsek, O., Buckton, G., 2003. Inverse gas chromatography: considerations about appropriate use for amorphous and crystalline powders. Journal of Pharmaceutical Sciences 92, 1286-1294.

Planinsek, O., Trojak, A., Srcic, S., 2001. The dispersive component of the surface free energy of powders assessed using inverse gas chromatography and contact angle measurements. International Journal of Pharmaceutics 221, 211-217.

Podczeck, F., 1998. The relationship between physical properties of lactose monohydrate and the aerodynamic behaviour of adhered drug particles. International Journal of Pharmaceutics 160, 119-130.

Rabinovich, Y., Adler, J.J., Esayanur, M.S., Ata, A., Singh, R.K., Moudgil, B.M., 2002. Capillary forces between surfaces with nanoscale roughness. Advances in Colloid and Interface Science 96, 213-230.

Riddle, F.L., Fowkes, F.W., 1990. Spectral shifts in acid-base chemistry. 1. Van der Waals contributions to acceptor numbers. Journal of American Chemical Society 112, 3259-3264.

Saleki-Gerhardt, A., Ahlneck, C., Zografi, G., 1994. Assessment of disorder in crystalline solids. International Journal of Pharmaceutics 101, 237-247.

Savaiano, D.A., Levitt, M.D., 1987. Milk intolerance and microbe-containing dairy foods. Journal of Dairy Science 70, 397-406.

Sawyer, D.T., Brookman, D.J., 1968. Thermodynamically based gas chromatographic retention index for organic molecules using salt-modified aluminas and porous silica beads. Analytical Chemistry 40, 1847-1853.

Schanker, L.S., Less, M.J., 1977. Lung pH and pulmonary absorption of nonvolatile drugs in the rat. Drug Metabolism and Disposition 5, 174-178.

Schlesinger, R.B., 1985. Clearance from the respiratory tract. Fondamental Applied Toxicology 5, 435-450.

Schultz, J., Lavielle, L., Martin, C., 1987. The role of the interface in carbon fibre-epoxy composites. Journal of Adhesion 23, 45-60.

Schulz, H., 1998. Mechanisms and factors affecting intrapulmonary particle deposition:implications for efficient inhalation therapies. Pharmaceutical Science and Technology Today 1, 336-344.

Sing, K., 2001. The use of nitrogen adsorption for the characterisation of porous materials. Colloids and surfaces A: Physicochemical and Engineering Aspects 187-188, 3-9.

Smith, I.J., Parry-billings, M., 2003. The inhalers of the future? A review of dry powder devices on the market today. Pulmonary Pharmacology and Therapeutics 16, 79-95.

Smith, P.L., 1997. Peptide delivery via the pulmonary route: a valid approach for local and systemic delivery. Journal of Controlled Release 46, 99-106.

Smyth, H.D.C., 2003. The influence of formulation variables on the performance of alternative propellant-driven metered dose inhalers. Advanced Drug Delivery Reviews 55, 807-828.

Srichana, T., Martin, G.P., Marriott, C., 1998. Dry powder inhalers: The influence of device resistance and powder formulation on drug and lactose deposition in vitro. European Journal of Pharmaceutical Sciences 7, 73-80.

Staniforth, J. N. Improvements in dry powder inhaler performance: surface passivation effects. [Proceeding of Drug delivery to the lungs VII.], 86-89. 1996a.

Staniforth, J. N. Pre-formulation aspects of dry powder aerosols. [Proceeding of Respiratory Drug Delivery V.], 65-73. 1996b.

Staniforth, J. N. Carrier particles for use in dry powder inhalers. [US6153224]. 2000.

Staniforth, J.N., Rees, J.E., Lai, F.K., Hersey, J.A., 1982. Interparticle forces in binary and ternary ordered powder mixes. Journal of Pharmacy and Pharmacology 34, 141-145.

Steckel, H., Bolzen, N., 2004. Alternative sugars as potential carriers for dry powder inhalations. International Journal of Pharmaceutics 270, 297-306.

Steckel, H., Borowski, M., Eskandar, F., 2004a. Selecting Lactose for a capsule-based dry powder inhaler. Pharmaceutical Technology Europe 23-35.

Steckel, H., Brandes, H.G., 2004. A novel spray drying technique to produce low density particles for pulmonary delivery. International Journal of Pharmaceutics 278, 187-195.

Steckel, H., Markefka, P., te Wierik, H., Kammelar, R., 2004b. Functionality testing of inhalation grade lactose. European Journal of Pharmaceutics and Biopharmaceutics 57, 495-505.

Steckel, H., Müller, B.W., 1997. In vitro evaluation of dry powder inhalers II: influence of carrier particle size and concentration on in vitro deposition. International Journal of Pharmaceutics 154, 31-37.

Steckel, H., Pichert, L., Müller, B.W., 2004c. Influence of process parameters in the ASES process on particle properties of budesonide for pulmonary delivery. European Journal of Pharmaceutics and Biopharmaceutics 57, 507-512.

Stewart, P.J., 1986. Particle interaction in pharmaceutical systems. Pharmacy International 146-149.

Svartengren, K., Ericsson, C.H., Svartengren, M., Mossberg, B., Philipson, K., Camner, P., 1996. Deposition and clearance in large and small airways in chronic bronchitis. Experimental Lung Research 22, 555-576.

Taylor, K.M.G., McCallion, O.N.M., 1997. Ultrasonic nebulisers for pulmonary drug delivery. International Journal of Pharmaceutics 153, 93-104.

Tee, S.K., Marriott, C., Zeng, X.M., Martin, G.P., 2000. The use of different sugars as fine and coarse carriers for aerosolised salbutamol sulphate. International Journal of Pharmaceutics 208, 111-123.

Thermometric AB. The calorimeter for additions during an on-going experiment, whole titration series and dissolution experiments. 1997.

Ticehurst, M.D., Basford, P.A., Dallman, C.I., Lukas, T.M., Marshall, P.V., Nichols, G., Smith, D., 2000. Characterisation of the influence of micronisation on the crystallinity and physical stability of revatropate hydrobromide. International Journal of Pharmaceutics 193, 247-259.

Ticehurst, M.D., Rowe, R.C., York, P., 1994. Determination of the surface properties of two batches of salbutamol sulphate by inverse gas chromatography. International Journal of Pharmaceutics 111, 241-249.

Ticehurst, M.D., York, P., Rowe, R.C., Dwivedi, S.K., 1996. Characterisation of the surface properties of α– lactose monohydrate with inverse gas chromatography,used to detect batch variation. International Journal of Pharmaceutics 141, 93-99.

Velaga, S.P., Bergh, S., Carlfors, J., 2004. Stability and aerodynamic behaviour of glucocorticoid particles prepared by a supercritical fluids process. European Journal of Pharmaceutical Sciences 21, 501-509.

Vidgren, M.T., Vidgren, P.A., Paronen, T.P., 1987. Comparison of physical and inhalation properties of spray-dried and mechanically micronized disodium cromoglycate. International Journal of Pharmaceutics 35, 139-144.

Visser, J., 1989. Van der Waals and other cohesive forces affecting powder fluidization. Powder Technology 58, 1-10.

Wanner, A., Salathe, M., O'Riordan, T.G., 1996. Mucociliary clearance in the airways. American Journal of Respiratory Critical Care Medecine 154, 1868-1902.

Ward, G.H., Schultz, R.K., 1995. Process-induced crystallinity changes in albuterol sulphate and its effect on powder physical stability. Pharmaceutical Research 12, 773-779.

Washington,N., Washington,C., Wilson,C.G., 2001. Physiological pharmaceutics: barriers to drug absorption. second edition Ed., Taylor and Francis, London.

Weibel, E. R. Morphometry of the human lung. 1963. Berlin: Springer-Verlag.

Willard,H.H., Merritt,L.L., Dean,J.A., Settle,F.A., 1988. Instrumental methods of analysis. Seventh edition Ed., Wadsworth.

Williams, G. and Tcherevatchenkoff, A. Moisture transport into CFC-free metered dose inhalers. [Proceedings of Drug Delivery to the Lungs VIII.], 91-94. 1998.

XU, R., Di Guida, O.A., 2003. Comparison of sizing small particles using different technologies. Powder Technology 132, 145-153.

York, P., Ticehurst, M.D., Osborn, J.C., Roberts, R.J., Rowe, R.C., 1998. Characterisation of the surface energetics of milled dl-propranolol hydrochloride using inverse gas chromatography and molecular modelling. International Journal of Pharmaceutics 174, 179-186.

Young, P.M., Price, R., Tobyn, M.J., Buttrum, M., Dey, F., 2003. Investigation into the effect of humidity on drug-drug interactions using the atomic force microscope. Journal of Pharmaceutical Sciences 92, 815-822.

Yu, L., 2001. Amorphous pharmaceutical solids: preparation, characterization and stabilization. Advanced Drug Delivery Reviews 48, 27-42.

Yue, Y., Angell, C.A., 2004. clarifying the glass-transition behaviour of water by comparison with hyperquenched inorganic glasses. Nature 427, 717-720.

Zanen, P., Van Spiegel, P.I., Van der Kolk, H., Tushuizen, E., Enthoven, R., 1992. The effect of the inhalation flow on the performance of a dry powder inhalation system. International Journal of Pharmaceutics 81, 199-203.

Zeegers-Huyskens,T., Huyskens,P., 1991. Intermolecular forces. In: Huyskens P.L.,L.W.A.P.Z.T. (Ed.), Springer-Verlag Berlin, Heidelberg, 1-30.

Zeng, X.M., Martin, G.P., Marriott, C., Pritchard, J., 2000a. The influence of carrier morphology on drug delivery by dry powder inhalers. International Journal of Pharmaceutics 200, 93-106.

Zeng, X.M., Martin, G.P., Tee, S.K., Ghoush, A.A., Marriott, C., 1999. Effects of particle size and adding sequence of fine lactose on the deposition of

salbutamol sulphate from a dry powder formulation. International Journal of Pharmaceutics 182, 133-144.

Zeng, X.M., Martin, G.P., Tee, S.K., Marriott, C., 1998. The role of fine lactose on the dispersion and deaggregation of salbutamol sulphate in an air stream in vivo. International Journal of Pharmaceutics 176, 99-110.

Zeng, X.M., Pandhal, K.H., Martin, G.P., 2000b. The influence of lactose carrier on the content homogeneity and dispersibility of beclomethasone dipropionate from dry powder aerosols. International Journal of Pharmaceutics 197, 41-52.

Zheng, Y., Marsh, K.C., Bertz, R.J., El-Shourbagy, T., Adjei, A.L., 1999. Pulmonary delivery of a dopamine D-1 agonist, ABT-431, in dogs and humans. International Journal of Pharmaceutics 191, 131-140.